

Performance-Based Evaluation of Cost-Effective Aggregate Options for Granular Roadways

Final Report
October 2019



IOWA STATE UNIVERSITY
Institute for Transportation

Sponsored by
Iowa Highway Research Board
(IHRB Project TR-704)
Iowa Department of Transportation
(Intrans Project 16-570)

About the Institute for Transportation

The mission of the Institute for Transportation (InTrans) at Iowa State University is to develop and implement innovative methods, materials, and technologies for improving transportation efficiency, safety, reliability, and sustainability while improving the learning environment of students, faculty, and staff in transportation-related fields.

Iowa State University Nondiscrimination Statement

Iowa State University does not discriminate on the basis of race, color, age, ethnicity, religion, national origin, pregnancy, sexual orientation, gender identity, genetic information, sex, marital status, disability, or status as a US veteran. Inquiries regarding nondiscrimination policies may be directed to the Office of Equal Opportunity, 3410 Beardshear Hall, 515 Morrill Road, Ames, Iowa 50011, telephone: 515-294-7612, hotline: 515-294-1222, email: eooffice@iastate.edu.

Disclaimer Notice

The contents of this report reflect the views of the authors, who are responsible for the facts and the accuracy of the information presented herein. The opinions, findings and conclusions expressed in this publication are those of the authors and not necessarily those of the sponsors.

The sponsors assume no liability for the contents or use of the information contained in this document. This report does not constitute a standard, specification, or regulation.

The sponsors do not endorse products or manufacturers. Trademarks or manufacturers' names appear in this report only because they are considered essential to the objective of the document.

Iowa DOT Statements

Federal and state laws prohibit employment and/or public accommodation discrimination on the basis of age, color, creed, disability, gender identity, national origin, pregnancy, race, religion, sex, sexual orientation or veteran's status. If you believe you have been discriminated against, please contact the Iowa Civil Rights Commission at 800-457-4416 or the Iowa Department of Transportation affirmative action officer. If you need accommodations because of a disability to access the Iowa Department of Transportation's services, contact the agency's affirmative action officer at 800-262-0003.

The preparation of this report was financed in part through funds provided by the Iowa Department of Transportation through its "Second Revised Agreement for the Management of Research Conducted by Iowa State University for the Iowa Department of Transportation" and its amendments.

The opinions, findings, and conclusions expressed in this publication are those of the authors and not necessarily those of the Iowa Department of Transportation.

Technical Report Documentation Page

1. Report No. IHRB Project TR-704	2. Government Accession No.	3. Recipient's Catalog No.	
4. Title and Subtitle Performance-Based Evaluation of Cost-Effective Aggregate Options for Granular Roadways		5. Report Date October 2019	
		6. Performing Organization Code	
7. Author(s) Bora Cetin (orcid.org/0000-0003-0415-7139), Sajjad Satvati (orcid.org/0000-0002-2129-7953), Jeremy C. Ashlock (orcid.org/0000-0003-0677-9900), and Charles Jahren (orcid.org/0000-0003-2828-8483)		8. Performing Organization Report No. InTrans Project 16-570	
9. Performing Organization Name and Address Institute for Transportation Iowa State University 2711 South Loop Drive, Suite 4700 Ames, IA 50010-8664		10. Work Unit No. (TRAIS)	
		11. Contract or Grant No.	
12. Sponsoring Organization Name and Address Iowa Highway Research Board Iowa Department of Transportation 800 Lincoln Way Ames, Iowa 50010		13. Type of Report and Period Covered Final Report	
		14. Sponsoring Agency Code IHRB Project TR-704	
15. Supplementary Notes Visit www.intrans.iastate.edu for color pdfs of this and other research reports.			
16. Abstract <p>The goal of this project was to investigate the cost-benefits of using high-quality clean (large size) aggregates for construction and maintenance of granular roadways located in areas with low-quality aggregates. Granular road surface aggregates were collected from four different quarries to build seven test sections. Three of these sections were built with typical granular roadway aggregates (Class A) and four sections were built by mixing locally available Class A material with high-quality clean (large size) aggregates.</p> <p>Test sections were constructed in Decatur County on a relatively stiff subgrade. This site was also selected since its locally available material deteriorates significantly when subjected to freezing and thawing during the winter and spring seasons. Construction and maintenance procedures are detailed, and the costs of aggregate, hauling, and equipment for construction and maintenance are documented in this report.</p> <p>Extensive laboratory and field tests were performed after construction, as well as before and after three seasonal freeze/thaw periods from 2016 to 2019, to monitor the performance of the demonstration sections. Temperature sensors were embedded at 1 ft increments in the subgrade to monitor ground temperatures up to a depth of 7 ft. These sensors were used to determine the duration and depths of ground freezing and thawing in addition to the number of freeze/thaw cycles at the test site.</p> <p>A benefit-cost analysis was performed using the documented construction and maintenance costs for service life scenarios of 20, 30, 40, and 50 years. The benefit-cost ratio was calculated for each test section for different scenarios based on the performance measures including surface material and thickness loss, gravel-size material loss, average fines content, total breakage, gravel-to-sand ratio, stiffness, shear strength, surface roughness, and dust production. Performance measures were categorized into three overall mechanistic performance-based groups and their benefit-cost ratios were compared.</p> <p>Overall, results of this study showed that the test sections constructed with a mixture of local Class A and Lime Creek Formation (LCF) and of local Class A and Crushed River Gravel (CRG) Clean aggregate were the most cost-effective ones. Moreover, sections consisting of aggregate mixtures had better performance under freeze/thaw cycles than that of the locally available Class A material and the mixtures of locally available Class A and clean aggregates. Depending on the distance to higher quality clean aggregate sources, mixing locally available Class A materials with lower quality aggregates can improve the performance of local materials and result in less frequent maintenance.</p>			
17. Key Words aggregates—benefit cost analyses—gradation—granular roadways—stiffness		18. Distribution Statement No restrictions.	
19. Security Classification (of this report) Unclassified.	20. Security Classification (of this page) Unclassified.	21. No. of Pages 298	22. Price NA

PERFORMANCE-BASED EVALUATION OF COST-EFFECTIVE AGGREGATE OPTIONS FOR GRANULAR ROADWAYS

Final Report
October 2019

Principal Investigator

Bora Cetin, Assistant Professor
Civil and Environmental Engineering, Michigan State University

Co-Principal Investigator

Jeremy C. Ashlock, Richard L. Handy Associate Professor of Geotechnical Engineering
Civil, Construction, and Environmental Engineering, Iowa State University

Charles T. Jahren, W. A. Klinger Teaching Professor
Civil, Construction, and Environmental Engineering, Iowa State University

Research Assistant

Sajjad Satvati

Authors

Sajjad Satvati, Bora Cetin, Jeremy C. Ashlock, and Charles Jahren

Sponsored by
Iowa Highway Research Board
and Iowa Department of Transportation
(IHRB Project TR-704)

Preparation of this report was financed in part
through funds provided by the Iowa Department of Transportation
through its Research Management Agreement with the
Institute for Transportation
(InTrans Project 16-570)

A report from
Institute for Transportation
Iowa State University
2711 South Loop Drive, Suite 4700
Ames, IA 50010-8664
Phone: 515-294-8103 / Fax: 515-294-0467
www.intrans.iastate.edu

TABLE OF CONTENTS

ACKNOWLEDGMENTS	xv
EXECUTIVE SUMMARY	xvii
CHAPTER 1. INTRODUCTION	1
1.1 Problem Statement	1
1.2 Research Objectives	2
1.3 Site Selection	2
1.4 Significance of the Research	4
1.5 Organization of the Report	4
CHAPTER 2. BACKGROUND	5
2.1 Aggregate Deterioration	5
2.2 Multichannel Analysis of Surface Waves	6
2.3 Falling Weight Deflectometer	6
2.4 Life-Cycle Cost Analysis	7
2.5 Benefit-Cost Analysis	8
CHAPTER 3. METHODS	10
3.1 Laboratory Tests	10
3.2 Field Tests	19
CHAPTER 4. MATERIALS	34
4.1 Geomaterials	34
4.2 Gradation	37
4.3 Compaction Test Results	41
4.4 California Bearing Ratio Test Results	43
4.5 Abrasion Test Results	45
4.6 C-Freeze Test Results	46
4.7 Gyratory Compaction Test Results	47
CHAPTER 5. CONSTRUCTION AND MAINTENANCE	57
5.1 Site Description	57
5.2 Construction	58
5.3 Maintenance	60
5.4 Quality Assurance and Quality Control	63
CHAPTER 6. RESULTS AND DISCUSSION	64
6.1 Gradation Change	64
6.2 Nuclear Density Gauge Tests	73
6.3 DCP Test Results	77
6.4 MASW Test Results	87
6.5 FWD Test Results	98
6.6 APLT Results	105
6.7 IRI Results	110
6.8 LWD Results	114

6.9 Dustometer Test Results	119
6.10 Ground Temperature Monitoring Results	122
CHAPTER 7. COST ANALYSIS	129
7.1 Construction Costs	130
7.2 Maintenance Costs	134
7.3 Hauling Costs.....	138
7.4 Benefit-Cost Analysis	139
7.5 Base Case and Alternatives.....	139
7.6 Defining the Benefits	139
7.7 NPV Calculation for Benefit-Cost Calculation.....	140
7.8 Results and Discussion	140
CHAPTER 8. CONCLUSIONS AND RECOMMENDATIONS	170
8.1 Field Observations	170
8.2 Laboratory Test Results	170
8.3 Field Test Results.....	171
8.4 Cost Analysis Results	172
8.5 Recommendations.....	173
REFERENCES	175
APPENDIX A. IMAGE LOG OF GRAVEL ROAD IN DECATUR COUNTY, IOWA– CONSTRUCTION, MAINTENANCE, AND FIELD SURVEYING	183
Equipment.....	183
Section 1. LCF Class A.....	185
Section 2. OFD Class A	186
Section 3. BFL Class A.....	188
Section 4. 80% BFL Class A + 20% BFL Clean	190
Section 5. 70% BFL Class A + 30% OFD Clean	191
Section 6. 70% BFL Class A + 30% LCF Clean	193
Section 7. 70% BFL Class A + 30% CRG Clean	195
Image Log of Gravel Road in Decatur County, Iowa–December 2016	197
Image Log of Gravel Road in Decatur County, Iowa–February 2017	201
Image Log of Gravel Road in Decatur County, Iowa–August 2017	204
Image Log of Gravel Road in Decatur County, Iowa–January 2018	208
Image Log of Gravel Road in Decatur County, Iowa–February 2018	212
Image Log of Gravel Road in Decatur County, Iowa–April 2018	219
Image Log of Gravel Road in Decatur County, Iowa–May 2018.....	226
Image Log of Gravel Road in Decatur County, Iowa–April 2019	233
APPENDIX B. PARTICLE-SIZE ANALYSIS RESULTS	241
APPENDIX C. DCP TEST RESULTS	249
APPENDIX D. AUTOMATED PLATE LOAD TEST (APLT) RESULTS	263
APPENDIX E. THERMOCOUPLE INSTALLATION.....	271
APPENDIX F. BENEFIT-COST ANALYSIS SPREADSHEET	279

LIST OF FIGURES

Figure 1. Location of the project.....	3
Figure 2. CR J22 before construction	3
Figure 3. Shaker for sieve analysis	11
Figure 4. Liquid limit test device.....	11
Figure 5. LA abrasion test device	13
Figure 6. C-Freeze test device	14
Figure 7. Hobart mixer, left, and automated mechanical rammer, right.....	15
Figure 8. California bearing ratio device	16
Figure 9. Brovold gyratory compactor, left, and PDA device, right	17
Figure 10. Falling weight deflectometer overview	19
Figure 11. FWD device.....	20
Figure 12. MASW general view	23
Figure 13. Experimental dispersion of the results of MASW.....	24
Figure 14. Experimental dispersion and theoretical dispersion in inversion process	24
Figure 15. Procedure to get the elastic modulus from FWD and MASW in situ tests	25
Figure 16. Lightweight deflectometer device	27
Figure 17. Dynamic cone penetrometer device	28
Figure 18. Cumulative blows vs. cumulative depth.....	29
Figure 19. APLT setup mounted on a trailer	30
Figure 20. Real-time APLT results of load pulse and deformation	30
Figure 21. Dustometer setup, top, and dust production measurement paper, bottom.....	32
Figure 22. Nuclear density gauge test device	33
Figure 23. Location of the aggregate quarries for this project.....	34
Figure 24. Class A surface aggregate materials.....	35
Figure 25. Clean surface aggregate materials	36
Figure 26. Mixture of clean and BFL Class A surface aggregate materials.....	37
Figure 27. Particle-size distribution of the surface aggregate materials	38
Figure 28. Particle-size distribution curve of clean aggregate materials	39
Figure 29. Dry density vs. water content graphs from standard Proctor tests for all materials	43
Figure 30. Penetration depth vs. stress on piston during CBR test.....	44
Figure 31. CBR values for all sections	45
Figure 32. LA abrasion and Micro-Deval test results.....	46
Figure 33. C-Freeze results	47
Figure 34. Height changes in the specimens after 500 gyrations	48
Figure 35. Dry unit weight (γ_{dry}) changes in the specimens after 500 gyrations	49
Figure 36. Comparison of the γ_{dMax} obtained from gyratory and Proctor compaction tests.....	50
Figure 37. Change in the void ratio vs. shear resistance during gyratory test	51
Figure 38. The change in particle-size distribution of materials after 500 gyrations	52
Figure 39. Fines content change in the materials after 500 gyrations	53
Figure 40. Sand content change of the materials after 500 gyrations	54
Figure 41. Gravel content change in the materials after 500 gyrations	55
Figure 42. Total breakage calculated for each material after 500 gyrations.....	56
Figure 43. Directions to the project location from I-35 south	57

Figure 44. Schematic diagram of the locations of the test sections	57
Figure 45. Schematic diagram of the test sections.....	58
Figure 46. CR J22 before construction	59
Figure 47. Scraped surface of the roadway.....	59
Figure 48. Construction steps	60
Figure 49. Distress types on surface materials: (a) big pothole in middle of BFL Class A, (b) severe rutting in 80% BFL Class A + 20% BFL Clean, (c) scattered potholes in 70% BFL Class A + 30% LCF Clean, and (d) material movement 70% BFL Class A + 30% CRG	61
Figure 50. Equipment used: (a) motor grader for blading, (b) dump trucks, (c) loader for collection the existing chip seal layer, and (d) vibratory roller for compaction	62
Figure 51. Fines content change of materials over time	64
Figure 52. Gravel-to-sand ratio changes of all materials over time.....	65
Figure 53. Total breakage change of all materials over time.....	66
Figure 54. Wet density results of nuclear gauge test	74
Figure 55. Dry density results of nuclear gauge test.....	74
Figure 56. Water content results of nuclear gauge test.....	75
Figure 57. Cumulative blows, DCPI, and correlated CBR versus cumulative depth for the first section	79
Figure 58. Surface DCP-CBR results over the course of the project.....	86
Figure 59. Subgrade DCP-CBR results for different times	87
Figure 60. Surface elastic modulus of MASW–large hammer	88
Figure 61. Surface elastic modulus ranges of MASW–large hammer.....	89
Figure 62. Surface elastic modulus of MASW–small hammer	89
Figure 63. Surface elastic modulus ranges of MASW–small hammer.....	90
Figure 64. Subgrade elastic modulus of MASW–large hammer	90
Figure 65. Subgrade elastic modulus ranges of MASW–large hammer.....	91
Figure 66. Subgrade elastic modulus of MASW–small hammer	91
Figure 67. Subgrade elastic modulus ranges of MASW–small hammer.....	92
Figure 68. Surface elastic modulus of FWD.....	98
Figure 69. Subgrade elastic modulus of FWD.....	99
Figure 70. Surface elastic modulus ranges of FWD	99
Figure 71. Subgrade elastic modulus ranges of FWD	100
Figure 72. In situ M_{r-Comp} results at each test point.....	106
Figure 73. Permanent deformation (δ_p) results at each test point	107
Figure 74. cIRI values over the length of the road	111
Figure 75. Average values of cIRI for each section over time	112
Figure 76. Average LWD composite elastic modulus results for each section over time	114
Figure 77. Dustometer results for each section over time	120
Figure 78. Data loggers to record the temperature changes.....	123
Figure 79. Sketch details of the center and shoulder thermocouples and the data loggers.....	123
Figure 80. Temperature variations recorded for the center of the road	124
Figure 81. Temperature variations recorded for the shoulder of the road	125
Figure 82. Freeze/thaw periods for three consecutive years, recorded at the center of the road.....	126

Figure 83. Freeze/thaw periods for two consecutive years, recorded at the shoulder of the road.....	127
Figure 84. Locations of the aggregate resources and the site in Iowa	129
Figure 85. Construction, top, and maintenance, bottom, costs for materials and hauling (truck).....	141
Figure 86. Material loss for each section before maintenance.....	143
Figure 87. Thickness loss from initial thickness (4 in.) for each section before maintenance ...	144
Figure 88. BCR values for material and thickness loss	145
Figure 89. Gravel percentage change from construction to maintenance.....	146
Figure 90. BCR values for gravel loss	147
Figure 91. Classification of the laboratory and field results for BCA	148
Figure 92. Total breakage average values over the length of project	149
Figure 93. BCR values for average total breakage	150
Figure 94. Average fines content values over the length of project	151
Figure 95. BCR values for average fines content	152
Figure 96. Average gravel-to-sand ratio values over the length of project	153
Figure 97. BCR values for average gravel-to-sand ratio	154
Figure 98. Average back-calculated surface elastic moduli during the project.....	156
Figure 99. BCR values for average back-calculated surface elastic modulus	157
Figure 100. Average surface shear strength values over the length of project.....	158
Figure 101. BCR values for average surface shear strength.....	159
Figure 102. Average dust production over the length of project	160
Figure 103. BCR values for average dust production.....	161
Figure 104. Average surface roughness (cIRI) over the length of project.....	163
Figure 105. BCR values for average surface roughness conditions	164
Figure 106. Weighted average of the BCR values based on the mechanical properties	165
Figure 107. BCR values for weighted performance measures	165
Figure 108. Weighted average of the BCR values based on the mechanical properties and material/thickness loss	166
Figure 109. BCR values for weighted performance measures and material/thickness loss	167
Figure 110. Weighted average of the BCR values based on the mechanical properties and gravel loss	168
Figure 111. BCR values for weighted performance measures and gravel loss	168
Figure A.1. Subgrade elastic modulus of FWD test in May 2017	183
Figure A.2. Drum roller used to compact the shaped surfaces	184
Figure A.3. Loader.....	184
Figure A.4. First section before construction.....	185
Figure A.5. Materials dumped for the first sections	185
Figure A.6. Compacted surface of the first section after construction	186
Figure A.7. OFD Class A materials dumped on the second section.....	186
Figure A.8. Second section during the construction	187
Figure A.9. Wheel compacted OFD Class A materials in second section.....	187
Figure A.10. Second section during drum roller compaction.....	188
Figure A.11. BFL Class A materials on the third section.....	188
Figure A.12. Wheel compacted surface of the third section.....	189
Figure A.13. Final compacted surface of the third section.....	189

Figure A.14. The mixture of the BFL Class A and Clean on the fourth section	190
Figure A.15. Compacted surface of the fourth section	190
Figure A.16. Scraped surface of the fifth section before construction during drum roller compaction	191
Figure A.17. OFD Clean	191
Figure A.18. BFL Class A	192
Figure A.19. Compacted surface of the fifth section	192
Figure A.20. LCF Clean	193
Figure A.21. BFL Class A and LCF Clean mixture	193
Figure A.22. 70% BFL Class A + 30% LCF Clean under compaction	194
Figure A.23. Wheel compacted surface of 70% BFL Class A + 30% LCF Clean	194
Figure A.24. Prepared surface of 70% BFL Class A + 30% LCF Clean	195
Figure A.25. Round shape CRG Clean materials	195
Figure A.26. CRG Clean materials on the surface	196
Figure A.27. Compacted surface of 70% BFL Class A + 30% CRG Clean	196
Figure A.28. Shaped and compacted surface of 70% BFL Class A + 30% CRG Clean	197
Figure A.29. LCF Class A	197
Figure A.30. OFD Class A	198
Figure A.31. BFL Class A	198
Figure A.32. 80% BFL Class A + 20% BFL Clean	199
Figure A.33. 70% BFL Class A + 30% OFD Clean	199
Figure A.34. 70% BFL Class A + LCF Class A	200
Figure A.35. 70% BFL Class A + CRG Clean	200
Figure A.36. LCF Class A	201
Figure A.37. OFD Class A	201
Figure A.38. BFL Class A	202
Figure A.39. 80% BFL Class A + 20% BFL Clean	202
Figure A.40. 70% BFL Class A + 30% OFD Clean	203
Figure A.41. 70% BFL Class A + 30% LCF Clean	203
Figure A.42. 70% BFL Class A + 30% CRG Clean	204
Figure A.43. LCF Class A	204
Figure A.44. OFD Class A	205
Figure A.45. BFL Class A	205
Figure A.46. 80% BFL Class A + 20% BFL Clean	206
Figure A.47. 70% BFL Class A + 30% OFD Clean	206
Figure A.48. 70% BFL Class A + 30% LCF Clean	207
Figure A.49. 70% BFL Class A + 30% CRG Clean	207
Figure A.50. LCF Class A	208
Figure A.51. OFD Class A	208
Figure A.52. BFL Class A	209
Figure A.53. 80% BFL Class A + 20% BFL Clean	209
Figure A.54. 70% BFL Class A + 30% OFD Clean	210
Figure A.55. 70% BFL Class A + 30% LCF Clean	210
Figure A.56. 70% BFL Class A + 30% CRG Clean	211
Figure A.57. LCF Class A	212
Figure A.58. OFD Class A	213

Figure A.59. BFL Class A	214
Figure A.60. 80% BFL Class A + 20% BFL Clean.....	215
Figure A.61. 70% BFL Class A + 30% OFD Clean.....	216
Figure A.62. 70% BFL Class A + 30% LCF Clean.....	217
Figure A.63. 70% BFL Class A + 30% CRG Clean.....	218
Figure A.64. LCF Class A	219
Figure A.65. OFD Class A.....	220
Figure A.66. BFL Class A	221
Figure A.67. 80% BFL Class A + 20% BFL Clean.....	222
Figure A.68. 70% BFL Class A + 30% OFD Clean.....	223
Figure A.69. 70% BFL Class A + 30% LCF Clean.....	224
Figure A.70. 70% BFL Class A + 30% CRG Clean.....	225
Figure A.71. LCF Class A	226
Figure A.72. OFD Class A.....	227
Figure A.73. BFL Class A	228
Figure A.74. 80% BFL Class A + 20% BFL Clean.....	229
Figure A.75. 70% BFL Class A + 30% OFD Clean.....	230
Figure A.76. 70% BFL Class A + 30% LCF Clean.....	231
Figure A.77. 70% BFL Class A + 30% CRG Clean.....	232
Figure A.78. LCF Class A	233
Figure A.79. OFD Class A.....	234
Figure A.80. BFL Class A	235
Figure A.81. 80% BFL Class A + 20% BFL Clean.....	236
Figure A.82. 70% BFL Class A + 30% OFD Clean.....	237
Figure A.83. 70% BFL Class A + 30% LCF Clean.....	238
Figure A.84. 70% BFL Class A + 30% CRG Clean.....	239
Figure B.1. Particle-size distributions of the first section over time	241
Figure B.2. Particle-size distributions of the second section over time.....	242
Figure B.3. Particle-size distributions of the third section over time	243
Figure B.4. Particle-size distributions of the fourth section over time	244
Figure B.5. Particle-size distributions of the fifth section over time	245
Figure B.6. Particle-size distributions of the sixth section over time	246
Figure B.7. Particle-size distributions of the seventh section over time.....	247
Figure C.1. DCP results for changes in the blows, DCPI, and DCP-CBR with cumulative depth for October 2016	251
Figure C.2. DCP results for changes in the blows, DCPI, and DCP-CBR with cumulative depth for November 2016	253
Figure C.3. DCP results for changes in the blows, DCPI, and DCP-CBR with cumulative depth for April 2017.....	255
Figure C.4. DCP results for changes in the blows, DCPI, and DCP-CBR with cumulative depth for June 2017	257
Figure C.5. DCP results for changes in the blows, DCPI, and DCP-CBR with cumulative depth for May 2018.....	259
Figure C.6. DCP results for changes in the blows, DCPI, and DCP-CBR with cumulative depth for April 2019.....	261
Figure D.1. APLT test results for the first section.....	263

Figure D.2. APLT test results for the second section	264
Figure D.3. APLT test results for the third section.....	265
Figure D.4. APLT test results for the fourth section.....	266
Figure D.5. APLT test results for the fifth section	267
Figure D.6. APLT test results for the sixth section.....	268
Figure D.7. APLT test results for the seventh section	269
Figure D.8. APLT test results for the control section.....	270
Figure E.1. Borehole digging with auger at center and shoulder of the road	271
Figure E.2. Painting the thermocouple path.....	272
Figure E.3. Digging the thermocouple path with auger.....	273
Figure E.4. Digging the surface for the thermocouple installation.....	274
Figure E.5. Thermocouples at PVC tubes.....	275
Figure E.6. Connecting the thermocouples to the data logger	276
Figure E.7. Locking the data loggers	277
Figure F.1. BCR calculator Excel sheet.....	279

LIST OF TABLES

Table 1. Gyratory device operational parameters	18
Table 2. FWD configuration	20
Table 3. MASW configuration	23
Table 4. Index properties	40
Table 5. Optimum moisture content and the maximum dry density results of the Proctor test	41
Table 6. Labor and equipment hours for the construction	60
Table 7. Labor and equipment hours for the maintenance.....	62
Table 8. Fine content change for all section over time	66
Table 9. Gravel-to-sand ratio changes for all sections over time	67
Table 10. Total breakage changes for all sections over time.....	68
Table 11. Fines content, gravel-to-sand ratio, and breakage potential changes of all sections in April 2017	69
Table 12. Fines content, gravel-to-sand ratio, and breakage potential changes in May 2017	69
Table 13. Fines content, gravel-to-sand ratio, and breakage potential changes in June 2017	70
Table 14. Fines content, gravel-to-sand ratio, and breakage potential changes in April 2018.....	71
Table 15. Fines content, gravel-to-sand ratio, and breakage potential changes in May 2018	71
Table 16. Mean value and the standard deviations of fines content, gravel-to-sand ratio, breakage potential and total breakage of all sections.....	72
Table 17. Fines content, gravel-to-sand ratio, and breakage potential changes in April 2019.....	73
Table 18. Nuclear gauge results for dry density, wet density, and water content	76
Table 19. Relative ratings of subbase and subgrade layers based on CBR values	78
Table 20. DCP results of thickness for the surface, surface and subgrade CBR, and rating in October 2016.....	78
Table 21. DCP results of thickness for the surface, surface and subgrade CBR and rating in November 2016.....	79

Table 22. DCP results of change in surface thickness and subgrade and surface CBR from October 2016.....	80
Table 23. DCP results of thickness for the surface, surface and subgrade CBR, and rating in April 2017	81
Table 24. DCP results of change in thickness for the surface and surface and subgrade CBR between October 2016 and April 2017	81
Table 25. DCP results of thickness for the surface, surface and subgrade CBR and rating in June 2017	82
Table 26. DCP results of change in thickness for the surface and surface and subgrade CBR between October 2016 and June 2017	82
Table 27. DCP results of thickness for the surface, surface and subgrade CBR, and rating in May 2018	83
Table 28. DCP results of change in thickness for the surface and surface and subgrade CBR between October 2016 and May 2018	84
Table 29. DCP results of thickness for the surface, surface and subgrade CBR, and rating in April 2019	84
Table 30. DCP results of change in thickness for the surface and surface and subgrade CBR between October 2016 and April 2019	85
Table 31. Surface elastic modulus of MASW small and large hammer tests in October 2016.....	93
Table 32. Subgrade elastic modulus of MASW small and large hammer tests in October 2016.....	93
Table 33. Surface elastic modulus of MASW small and large hammer tests in April 2017	95
Table 34. Subgrade elastic modulus of MASW small and large hammer tests in April 2017	95
Table 35. Surface elastic modulus of MASW small and large hammer tests in May 2018	97
Table 36. Subgrade elastic modulus of MASW small and large hammer tests in May 2018	97
Table 37. Surface elastic modulus of FWD test in October 2016	101
Table 38. Subgrade elastic modulus of FWD test in October 2016.....	101
Table 39. Surface elastic modulus of FWD test in May 2017	102
Table 40. Subgrade elastic modulus of FWD test in May 2017	102
Table 41. Surface elastic modulus of FWD test in June 2017	103
Table 42. Subgrade elastic modulus of FWD test in June 2017	103
Table 43. Surface elastic modulus of FWD test in May 2018	104
Table 44. Subgrade elastic modulus of FWD test in May 2018	104
Table 45. Surface elastic modulus of FWD test in May 2019	105
Table 46. Subgrade elastic modulus of FWD test in May 2019	105
Table 47. Comparison of in situ M_{r-comp} and δ_p at the end of the test results (cyclic stress = 90 psi).....	107
Table 48. Summary of permanent deformation prediction parameters (cyclic stress = 90 psi).....	109
Table 49. IRI classification	111
Table 50. Average IRI values for each section over time.....	113
Table 51. LWD composite elastic modulus values (ksi) for all sections over time.....	114
Table 52. Surface elastic modulus of LWD test in October 2016	115
Table 53. Surface elastic modulus of FWD test in November 2016	116
Table 54. Surface elastic modulus of FWD test in December 2016.....	116

Table 55. Surface elastic modulus of FWD test in February 2017	117
Table 56. Surface elastic modulus of FWD test in April 2017	117
Table 57. Surface elastic modulus of FWD test in June 2017	118
Table 58. Surface elastic modulus of FWD test in May 2018	118
Table 59. Surface elastic modulus of FWD test in April 2019	119
Table 60. LWD composite elastic modulus mean values and the standard deviations for each section	119
Table 61. Dust production (E-03 lb/mile) for all sections over time	120
Table 62. Average dust production for each section.....	122
Table 63. The number of the freeze/thaw periods that each layer experienced.....	128
Table 64. Aggregate and hauling time costs for each material	129
Table 65. Labor and equipment unit costs	130
Table 66. Weight of the surface aggregate materials required for each section for construction	131
Table 67. Gravel and labor cost of hauling the gravel for each section for construction	132
Table 68. Labor and equipment required times for construction.....	132
Table 69. Equipment costs for each section for construction	133
Table 70. Labor costs of the sections for construction	133
Table 71. Equipment, gravel, and labor total costs for each section per square yard.....	133
Table 72. Weight of the surface gravel materials required for each section for maintenance....	135
Table 73. Aggregate and labor cost of hauling the gravel for each section for maintenance	136
Table 74. Labor and equipment required times for maintenance	136
Table 75. Equipment costs for each sections for maintenance	137
Table 76. Labor costs for each section for maintenance.....	137
Table 77. Equipment, gravel, and labor total costs for each section per square yard.....	137
Table 78. Comparisons between the labor costs of hauling materials for railway and roadway	138
Table 79. Total costs of construction for each section.....	139
Table 80. Hauling costs of OFD materials per mile with rail and truck.....	142
Table 81. Scenarios for maintenance frequency based on the thickness and aggregate loss.....	144
Table 82. Scenarios for maintenance frequency based on the gravel loss for each section	147
Table 83. Scenarios for maintenance frequency based on the average total breakage	150
Table 84. Scenarios for maintenance frequency based on the average fines content	152
Table 85. Scenarios for maintenance frequency based on the average gravel-to-sand ratio	154
Table 86. Scenarios for maintenance frequency based on the average surface elastic modulus	156
Table 87. Scenarios for maintenance frequency based on the average surface shear strength...	159
Table 88. Scenarios for maintenance frequency based on the average dust production.....	161
Table 89. Scenarios for maintenance frequency based on the average surface roughness.....	163
Table B.1. Percentage of change in fines content (%).....	247
Table B.2. Percentage of change in gravel-to-sand ratio (%).....	248
Table B.3. Percentage of change in breakage potential (%).....	248

ACKNOWLEDGMENTS

The authors gratefully acknowledge sponsorship for this project from the Iowa Department of Transportation (DOT) and the Iowa Highway Research Board (IHRB), who used research funds as part of their funding for this study.

The project technical advisory committee (TAC) members, Vanessa Goetz (Iowa DOT), Malcom Dawson (Iowa DOT), Brian Gossman (Iowa DOT), Kevin Jones (Iowa DOT), Danny Waid (County Engineers Service Bureau), Zachary A. Gunsolley (Union County), Daniel Doerfler (Decatur County), Dillon Davenport (Decatur County), Wade Weiss (Greene County), Jacob Thorius (Washington County), and Paul Assman (Crawford County) are gratefully acknowledged for their guidance, support, and direction throughout the research.

Technical guidance from Terry Cozad (Decatur County) is sincerely appreciated. Kyle Frame (Iowa DOT) is acknowledged for his generous help and sharing information and experience. The authors would also like to sincerely thank graduate research assistants Cheng Li, Yijun Wu, Haluk Sinan Coban, Masrur Mahedi, Derya Genc, Ali Nahvi, and Leela Sai Praveen Gopiseti for their valuable assistance with the field investigations.

EXECUTIVE SUMMARY

The goal of this project was to examine the performance of granular roadways constructed with aggregates of varying quality used alone and in mixtures, and determine whether it was cost-effective to haul high-quality aggregates from greater distances to locations with relatively low-quality aggregate sources nearby. Aggregate materials were collected from four different locations in Iowa and used to build test sections on the same stretch of granular road. Several series of laboratory and field tests were conducted to characterize the materials and assess their performance in service through three seasonal freeze/thaw periods, from 2016 to 2019. Laboratory tests included sieve and hydrometer analyses, Atterberg limits, compaction tests, gyratory compaction tests, and California bearing ratio (CBR) tests. Field performance was evaluated via abrasion resistance, freeze/thaw resistance, density, material loss, modulus, gradation change, dust production, ride quality, and shear strength. Field tests include dynamic cone penetrometer (DCP), International Roughness Index (IRI), dust measurement, multichannel analysis of surface waves (MASW), lightweight deflectometer (LWD), and falling weight deflectometer (FWD) tests.

Overall, two main types of materials were used: Class A, which is a common aggregate type used for granular roadways, and clean large-sized aggregates. Seven test sections were built for this project. The test site consisted of three Class A sections (Lime Creek Formation [LCF] Class A, Oneota Formation Dolomite [OFD] Class A, and local Bethany Falls Limestone [BFL] Class A) and four test sections built with mixtures of local BFL Class A and different clean aggregates: LCF Clean, OFD Clean, local BFL Clean, and Crushed River Gravel (CRG) Clean. The length of each test section was 500 ft except for one section at 300 ft long, and each was 30 ft wide and 4 in. thick. The sections with mixtures contained Class A and clean aggregates at the following ratios by weight: 70% BFL Class A + 30% LCF Clean, 80% BFL + 20% BFL Clean, 70% BFL Class A + 30% OFD Clean, and 70% BFL Class A + 30% Clean CRG.

The construction and maintenance procedures were documented in detail and are presented in this report. Extensive laboratory and field tests were performed before and after the three freeze/thaw seasons in order to monitor and evaluate the performance of the different surface aggregate materials alone and when mixed with local Class A materials. In order to monitor changes in ground temperature, thermocouples were installed to a depth of 7 ft at the center and one shoulder of the road, in the middle of the first test section.

A benefit-cost analysis (BCA) was conducted based on the construction and maintenance costs extrapolated to estimate cumulative costs per mile. Accordingly, the benefit-cost ratio, user cost savings, and maintenance cost savings values were calculated based on the BCA and different service lives, discount rates, and maintenance frequencies were compared to continuing the current maintenance practices.

Laboratory test results of the virgin materials used in construction showed that Class A aggregates hauled from long distances and mixtures of local Class A and clean aggregates had higher abrasion resistances than those of local Class A (BFL) materials and local Class A (BFL) + clean aggregate (BFL) mixtures. Compared to the local aggregates, the higher quality

aggregates hauled from longer distances exhibited relatively smaller changes in gradation and total breakage in laboratory gyratory compaction tests.

Field DCP test results showed that the performance of all test sections were classified as excellent to very good throughout the project duration. While gradation characteristics (fines content, gravel-to-sand ratio, and gravel content) of all test sections changed over time, it was clearly observed that the addition of LCF Clean, OFD Clean, and CRG Clean aggregates to the local BFL Class A resulted in less degradation as evidenced by relatively smaller changes in gradation compared to the test sections built with local aggregates. Among the sections with aggregate mixtures, the ones exhibiting the lowest changes in these characteristics were the 70% BFL Class A + 30% LCF Clean and 70% BFL Class A + 30% CRG Clean mixtures. Based on the stiffness values computed from MASW, LWD, and FWD test results, all test sections performed similar to each other over the project duration. No clear trend was observed between the index properties and stiffnesses of the test sections. It was concluded that these stiffness tests require modification in order to be suitable for granular roadway performance testing. IRI results showed that the maximum roughness value was observed for the mixture of 70% BFL Class A + 30% CRG Clean.

The BCA showed that hauling LCF Clean and CRG Clean to be mixed with local BFL Class A material resulted in the most cost-effective method when considering the following performance criteria: change in fines content, gravel-to-sand ratio, gravel content, total breakage, and material and thickness loss. Benefit-cost analyses were also made for both truck and rail hauling, and the results showed that rail hauling was highly dependent on the locations of quarries, construction sites, and transition points of the railways.

Overall observations, challenges, and recommendations are summarized based on the results of this project as follows:

- Changes in gradation and increases in fines contents in particular had a significant impact on the performance of the granular roadways.
- The spreadsheet developed in this study can be utilized to assess the benefit-cost analysis of a variety of granular roadway construction and maintenance alternatives.
- Currently available stiffness tests were required to be modified to evaluate the performance of granular roadways.
- Labor costs and equipment time do not vary significantly between test sections that are built at 500 ft in length. It is recommended that test sections in future studies be at least 0.25 mile in length to produce discernable differences between them.

CHAPTER 1. INTRODUCTION

1.1 Problem Statement

Approximately 68,400 miles of granular roadways exist in the 114,000 mile road network in the state of Iowa. Operation and maintenance of these granular roadways costs roughly \$270 million annually. The sustainability of granular roadways is very important to the rural economy, since these roads provide access to rural land and enable the transportation of agricultural products. The timing of the transportation of these products is often tightly constrained by economic and weather considerations. Any interruption in access via these granular roadways can, thus, have a significant impact on agricultural productivity and the economy of Iowa. Heavy traffic loads and freeze/thaw cycles during the winter and spring seasons can cause extensive damage to granular roads. Such damage leads to many problems such as material loss, gradation change, loss of crown, surface erosion, rutting, and potholes. The rate of deterioration (or damage) is directly correlated to the quality of the granular aggregate materials used in the design of granular roads.

Performance and long-term sustainability of granular roadways are dependent to a considerable degree on the quality of the aggregate materials used, which varies considerably from one source to another across Iowa. There are a wide range of granular material sources in Iowa, each producing different qualities, supply amounts, and prices. County engineers and Iowa Department of Transportation (DOT) personnel have observed considerable differences between regions of the state with respect to the level of performance that granular materials are able to provide. They have reported that quarries located in certain counties have higher quality granular materials offered at prices similar to others of lesser quality. For instance, materials in northeast Iowa (e.g., Ordovician and Silurian bedrock) perform better and degrade more slowly than those in the southern regions of the state (e.g., Pennsylvanian bedrock). Thus, roads in some counties require more maintenance efforts and therefore, higher costs in comparison to other counties. A similar contrast occurs for the cost of new construction of granular roads.

County engineers and their employees invest considerable effort in managing and maintaining granular roads. However, to date there are no readily available tools to evaluate the costs versus field performance of granular road materials. When maintenance and construction of granular roadways is costly due to use of low-quality materials, it is necessary for counties to spend a considerable portion of their budget (sometimes up to 28% of the total county budget) just to purchase granular materials (excluding placement and maintenance) to replace those lost during the service life of a granular road. The problems commonly encountered with granular roads are: (1) unsuitable material usage, (2) inadequate material distribution, (3) surface deterioration through aggregate loss, (4) surface abrasion, (5) ineffective drainage, and (6) insufficient road maintenance. This study aims to test the problems associated with unsuitable material usage and surface abrasion.

In this project, the research team conducted laboratory and field tests to examine the link between quality and performance of granular aggregate materials used in granular road designs, using materials collected from various quarries in Iowa. Field test sections were constructed using materials with different aggregates collected from different locations in the state. The field

performance (abrasion resistance, freeze/thaw resistance, density, material loss, modulus, and gradation change) of sections built with different quality materials were compared. Then, a comprehensive cost-performance analysis was conducted to evaluate the cost-effectiveness of the different materials to determine whether it was economically advantageous to transport high-quality aggregate materials from quarries located at different locations in the state.

1.2 Research Objectives

The overall goal of this project was to determine the cost-effectiveness of hauling high-quality coarse (clean) aggregates to improve the performance and reduce the maintenance frequency of granular roadways in regions with low-quality aggregates. The specific objectives of this project were as follows:

1. Evaluate the quality of aggregate materials collected from various sources around Iowa
2. Monitor the change in material properties over time and the impact of these changes on granular roadway performance
3. Determine the relationships between the material properties and performance of granular roadway materials
4. Conduct a comprehensive cost analysis for each test section

1.3 Site Selection

A 3,600 ft stretch of granular roadway was selected in Decatur County, Iowa. It is located at County Road (CR) J22 (Popcorn Road) off of US 69 extending approximately a mile east. Figure 1 shows the location of the project.

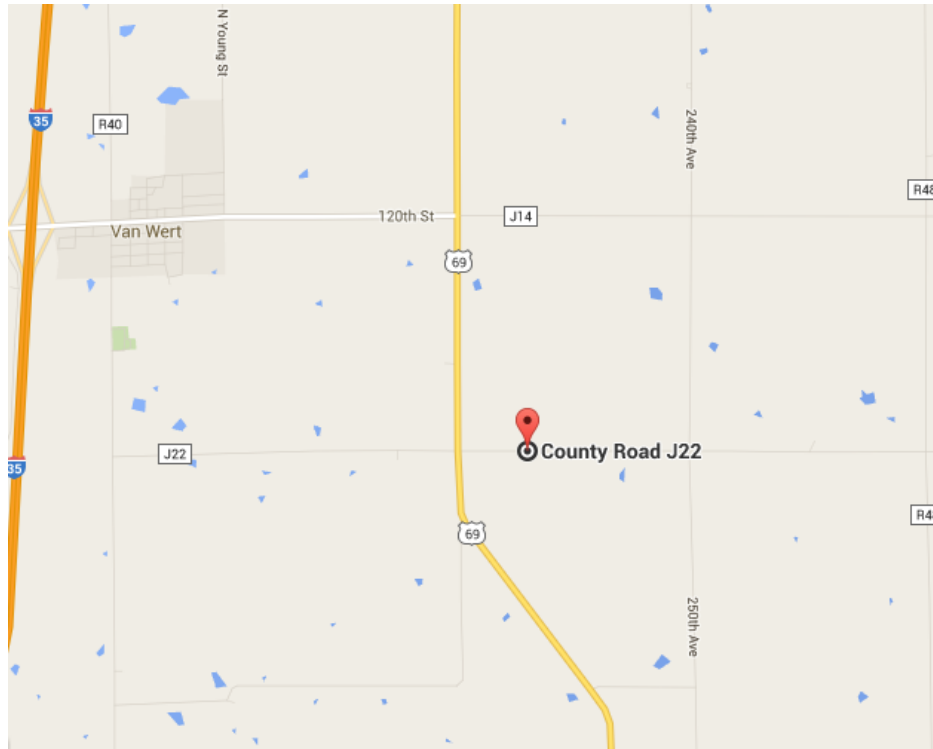


Figure 1. Location of the project

This site was selected for several reasons. Annual average daily traffic (AADT) for this location was 80. Daily traffic load and the percentage of trucks were slightly above average compared to other granular roads in Iowa (Iowa DOT 2012). The surface level of the road was reasonably higher than the ground surface around the road. This provides better conditions for drainage. In addition, the site was three miles away from an interstate, which provided reasonable accessibility. Furthermore, the subgrade was very strong (California bearing ratio [CBR] >5). Figure 2 shows the site prior to construction.



Figure 2. CR J22 before construction

1.4 Significance of the Research

The purpose of this research was to investigate the surface aggregate materials' mechanistic properties over time and develop a cost-benefit analysis methodology to compare the benefits of utilizing aggregates from different resources based on the construction and maintenance costs over the three years of this project.

1.5 Organization of the Report

This report includes eight chapters:

- Chapter 1 (Introduction) explains the problem statement, objectives, site selection, and the significance of the research
- Chapter 2 (Background) consists of a review of previous studies on granular roads and briefly summarizes the methods of field testing and cost analysis
- Chapter 3 (Methods) presents different methods of laboratory and field tests that were conducted in this project
- Chapter 4 (Materials) provides information about the geomaterials and the preliminary results of the laboratory tests, which presents the index properties, compaction characteristics, strength, abrasion, and freeze/thaw resistance
- Chapter 5 (Construction and Maintenance) describes the site, sections, and the construction and maintenance procedures
- Chapter 6 (Results and Discussion) provides the results of the field tests over the three-year period of the project
- Chapter 7 (Cost Analysis) contains the results of the economic analysis on all different test sections
- Chapter 8 (Conclusions and Recommendations) presents the conclusions of this project and recommendations
- Appendices present supporting materials for the project

CHAPTER 2. BACKGROUND

2.1 Aggregate Deterioration

Aggregate deterioration is described as progressive worsening of aggregate conditions, and it depends on the index properties of the aggregates themselves, subgrade soils, drainage conditions, traffic load, and environmental effects (Alzubaidi and Magnusson 2002, Paterson 1987, Provencher 1995, Strombom 1987). The performance of a granular road is highly dependent on gradation characteristics, plasticity index (PI), abrasion resistance, morphology, and mineral composition. In addition, other conditions such as traffic loads, moisture contents, and degree of compaction during construction are other very important factors that could impact the gravel loss and deterioration of gravel roads (Fathi et al. 2019, Hardin 1985, Lade et al. 1996, Lees and Kennedy 1975, Marsal 1967, Nurmikolu 2005, Paterson 1991, White et al. 2004, Zeghal 2009).

It is well-known that abrasion and freeze/thaw resistances of granular roads are highly dependent on the aggregate quality (Alzubaidi and Magnusson 2002). Traffic flow affects the gravel deterioration due to the removal and breakage of surface aggregates. This depends on traffic volume, speed, and traffic loads (Dobson and Postill 1983, Isemo and Johansson 1976). Under heavy traffic loads (especially during spring seasons), gravel particles are either scattered or are broken into finer-sized particles, which may result in general loss of stability in the granular roadways. Moreover, aggregates with low abrasion resistances tend to experience considerable increases in fines contents. Thus, it causes a significant decrease in the overall performances of granular roadways and requires more frequent maintenance. Freeze/thaw durability of surface aggregate materials is also another factor that could influence the performance of granular roads. (Li et al. 2015a; Vallejo et al. 2006; White and Vennapusa 2013, 2014a).

Li et al. (2015a) investigated the use of several stabilization methods including use of cement, fly ash, bentonite, macadam stone base, and geosynthetics to improve the serviceability of granular roadways. The results showed that macadam stone base, fly ash, and cement stabilized sections concluded the highest elastic modulus values immediately after construction. However, macadam stone base can be more cost-effective to implement (Li et al. 2017a). Vallejo et al. (2006) reported that particle crushing in the base and subbase layers of paved roads occurs in unfavorable conditions such as the use of low-quality aggregates, high loads, and unfavorable weather (Vallejo et al. 2006). Nurmikolu (2005) investigated the important factors in frost susceptibility of aggregates. The results of this study showed that higher porosity and water content were disadvantageous in case of frost susceptibility (Nurmikolu 2005). Freezing and thawing and the effects of high traffic loads cause a lack of drainage for the melt water and capillary water trapped in the surface course and top of the subgrade of unpaved roads. Consequently, saturation of the materials leads to a loss of strength and stiffness in the road layers. Blading the surface aggregates and dumping virgin aggregates typically are practices for repairing freeze/thaw damage instead of improving frost susceptibility of aggregates (White and Vennapusa 2013, 2014b).

2.2 Multichannel Analysis of Surface Waves

Multichannel analysis of surface waves (MASW) is one of the wave-propagation methods that is commonly used to calculate the elastic moduli of different layers of the roads. Elastic modulus of roadway layers is one of the main important parameters that is used in roadway design.

Wave-propagation methods have been used in determining the properties of soils. These properties include soil structure, stiffness, and strength (Gheibi and Hedayat 2018). MASW is used to measure the surface wave velocities and the stiffness properties of the soil by matching the experimental and theoretical dispersion curves (Lin and Ashlock 2012, 2015; Nazarian and Stokoe 1985; Park et al. 2001; Park et al. 1995; Ryden 2009). In recent years, the MASW method has been used to evaluate the moduli of pavement layers (Li et al. 2018c, Lin and Ashlock 2015, Lin et al. 2016, Park et al. 2001). Studies on surface wave testing to measure the properties of pavement layers started by conducting the continuous surface wave (CSW) method developed by Van der Poel (1951) and improved over the years (Heukelom and Foster 1962; Jones 1955, 1958, 1962; Vidale 1964). Afterward, spectral analysis of surface waves (SASW) was developed and widely used (Heisey et al. 1982a, Nazarian and Stokoe 1985, Rix et al. 1991, Stokoe et al. 1994).

Yusoff et al. (2015) found a satisfactory match between the results of the elastic modulus of the subgrade layer from falling weight deflectometer (FWD) and SASW tests on a paved road system. However, it is speculated that moduli values calculated from MASW can be more precise than those calculated from FWD, due to a higher number of geophones, the lower distances between them, and their unique method of calculating the elastic modulus compared to the back- and forward-calculations (Lin et al. 2016).

2.3 Falling Weight Deflectometer

The FWD was developed in the 1960s and has been one of the most common non-destructive tests to evaluate the elastic modulus (stiffness) of roadway layers in the US for more than three decades (Akbariyeh 2015). The FWD method simulates the traffic load by obtaining the roadway deflection data and uses the concept of “deflection bowl” to measure the modulus of the layers (Brown et al. 1987, Hadidi and Gucunski 2010, Hudson 1997, Kuo et al. 2016, Uddin 2000, Uddin et al. 1985, Ullidtz 1987). This method applies to static and dynamic loads. Many studies have been conducted to back-calculate the elastic modulus of roadway layers from FWD test data (Sebaaly et al. 1986; Xu et al. 2002a, 2002b), and these studies concluded that FWD back-calculation methods are mainly dependent on the seed value (100 to 200 ksi for the surface layer and 5 to 15 ksi for subsurface layers) of the elastic modulus and error minimization techniques (Tarefder and Ahmed 2013).

The majority of the FWD back-calculation methods apply the linearly static theory that ignores the static loading mode and duration, assumes material properties are homogenous and isotropic, and layers are infinite in the horizontal direction (Uddin 2000). The combination of the modulus values for each roadway layer, even assuming a semi-infinite subgrade depth and an infinite horizontal extent of roadway layers are non-unique in the calculation of the same deflection

basin on the surface due to its dependence on the thickness of the layers and the temperature. This creates uncertainty about the results of the modulus from the iterative method of back-calculation of the FWD results (Nega et al. 2016, Uddin et al. 1985). Static-based analysis of the FWD data without considering the existence of sources of nonlinearity, consideration of stress hardening for surface and stress softening for the subgrade layers, and dynamic response analysis, can cause unreliable results for roadway performances (Ceylan et al. 2005, Nega et al. 2016, Uddin 2000). Chang et al. (1992a) showed the importance of considering the dynamic deflection basin on the back-calculated moduli of surface and subgrade layers. However, considering nonlinearity and dynamic loading effects in back-calculation methods has its own complexity. These methods included large number of variables and dynamic motion while evaluating the pavement responses in modulus values (Nega et al. 2016; Xu et al. 2002a, 2002b).

Heisey et al. (1982b) stated that the FWD test was better suited for deflection measurements in roadways due to its capacity to apply high loads compared to the wave propagation methods such as SASW. SASW uses Rayleigh waves to measure the shear wave velocity through layers of the roadway (Heisey et al. 1982a). FWD is a dynamic method involving wave propagation. However, static loading is assumed in the analysis, which causes considerable differences in their actual and calculated stress distributions. On the other hand, wave-propagation methods follow a unique solution to find the moduli and thickness of the layers (Nazarian 1983). Moreover, the nonlinear elasto-plastic response of materials on deflections under dynamic loading in the FWD test is related to subgrade stiffness, and the subgrade participates in 60 to 80% of the central deflection. Therefore, errors in the subgrade moduli back-calculation can be a source of significant errors in the back-calculated moduli of the other layers (Appea 2003, Chang et al. 1992b, Ghadimi et al. 2015, Nega et al. 2016). The FWD is insensitive to the modulus of the surface layer if the thickness of the surface layer is a few centimeters (Yusoff et al. 2015). In addition, the temperature variation can cause difficulties in getting accurate results from back-calculation (Nega et al. 2016).

2.4 Life-Cycle Cost Analysis

Every project is a combination of different alternatives, and selecting the most cost-effective option is important in asset management of the project. Life-cycle cost analysis (LCCA) is a common cost analysis method that considers the costs of construction, maintenance, rehabilitation, service life, and discount rates to find the most cost-effective option in the service life of any project. LCCA was first used by state agencies in the 1950s for cost evaluations to compare proposed pavement systems (AASHTO 1960). Different pavement types, qualities of pavement, effects on the motoring public, and maintenance and rehabilitation costs should be considered in this type of analysis (Wilde et al. 1999). It evaluates overall long-term costs including initial, maintenance, rehabilitation, user, and salvage costs (Walls and Smith 1998). The LCCA period is the period over which future costs are evaluated. This period should be long enough to reflect long-term cost differences associated with reasonable design strategies. After determining the construction and probable maintenance costs, future costs including any maintenance procedures are discounted to the current year and added to the construction costs to calculate the net present value (NPV) for the LCCA alternatives (equation 1).

$$NPV = \text{Initial Costs} + \sum_{k=1}^n \text{Rehabilitation Cost}_k \left[\frac{1}{(1+i)^{n_k}} \right] - \text{Salvage Value} \left[\frac{1}{(1+i)^{n_k}} \right] \quad (1)$$

Routine annual maintenance costs including regular blading for granular roads usually are not different for different alternative sections and do not change significantly annually and thus, have negligible effects on the total NPV compared to initial construction or maintenance costs, particularly with high service life values (over 20 years). Moreover, salvage value represents the value of an investment alternative at the end of the service life. (Vosoughi et al. 2017).

2.5 Benefit-Cost Analysis

Cost analyses are helpful to determine whether transporting materials from high-quality sources to replace low-quality local materials in granular roadway construction. Cost calculations include different possible routes and transportation modes between high-quality aggregate sources and construction sites lacking nearby high-quality sources. This project presents a case study of a benefit-cost analysis (BCA) of a gravel road constructed in a rural road system. The findings could help the Iowa DOT and Iowa county engineers to determine the most beneficial material alternatives with lower costs of hauling, material, labor, and equipment for construction and maintenance of granular roadways.

Conducting a BCA is very important before any investment in transportation infrastructure to find out the efficiency of the project in utilizing resources, due to the need to facilitate social and economic activities (Carlsson et al. 2015, Dharmadhikari et al. 2016, Prest and Turvey 1965). Deterministic BCA is considered a traditional decision-making approach in pavement management (Nahvi et al. 2018, Walls and Smith 1998). Prest and Turvey (1965) presented four main criteria prior to performing any benefit-cost analysis: (1) enumeration of costs and benefits, (2) valuation of costs and benefits, (3) choice of interest rate, and (4) relevant constraints. Dharmadhikari et al. (2016) presented four main steps to perform a life-cycle benefit-cost analysis: (1) determining the project base case and alternatives, (2) defining the benefits, (3) costs and benefits calculation, and (4) determining the current value of costs and benefits. The base case is defined as the condition where no alternatives are suggested, and the alternatives are the other options to be considered in order to make the project beneficial. In this case, the minimum value of the construction cost was considered as the base case. The determination of the base case and benefits should be done with extreme care to have a solid and trustable cost analysis.

Moreover, agencies should avoid using the BCA framework of a project on another project because of the differences in various considerations and assumptions in each project (Gibson and Wallace 2016). The values of the annual costs and benefits and the project's present value considering the properly suggested discount rate are included in the overall approaches to the BCA (Layard and Glaister 1994). Jones et al. (2014) called traffic forecast, cost estimation, discount rate, value of life, safety, value of time, regional impacts, local impacts, equity, environmental impacts, and residual use as the major challenges in performing BCA for transportation infrastructure. The main factor in deterministic BCA is the benefit-cost ratio

(BCR), which is the ratio of the NPV of the benefits divided by the NPV of the costs of a project (Walls and Smith 1998).

Hauling and placing aggregate are the most costly processes. Therefore, it may prove beneficial to construct granular roads using higher quality materials that can sustain their performance for longer durations with less maintenance. However, there is a lack of high-quality aggregate sources in certain regions of Iowa. It has been reported that sources in certain parts of Iowa, such as the northeast, have higher quality aggregates than other regions, such as the west and south, possibly enabling the use of half as much aggregate for the same roadway performance. Li et al. (2018c) observed similar findings from field tests on granular roads in southwestern Iowa.

CHAPTER 3. METHODS

This chapter includes the methods for both laboratory and field tests. Laboratory tests were conducted to determine the classification and soil index properties, abrasion resistance, and compaction behavior of the surface and subgrade materials, while field tests were performed to investigate the mechanistic properties of the surface and subgrade layers such as strength, stiffness, in situ water content and dry density, the amount of dust, surface roughness, and friction.

3.1 Laboratory Tests

Laboratory tests such as particle-size analysis, Atterberg limits, Proctor, California bearing ratio, and gyratory compaction tests were conducted in the laboratory to acquire the particle-size distribution, plasticity of soil, maximum dry density (γ_{dmax}), optimum water content (w_{opt}), shear strength, and compaction characteristics. The Los Angeles (LA) abrasion, C-Freeze, and Micro-Deval tests were conducted at the Iowa DOT Central Materials Laboratory to determine the abrasion and freeze/thaw resistance of the aggregate materials.

3.1.1 Particle-Size Analysis

Particle-size analyses were performed in accordance with ASTM D422 Standard Test Method for Particle-Size Analysis of Soils. Sieve sizes were in the range of 1 ½ in. (75 mm) to sieve #200 (75 μ m). In addition, to determine the size distribution of fine particles (i.e., particles that pass through a #200 sieve), hydrometer tests were conducted on the materials passed through sieve #10 (2 mm). To test a representative sample, the sampling method ASTM D75-13 Standard Practice for Sampling Aggregates was followed. Figure 3 shows the sieve test setup used during sieve analysis.

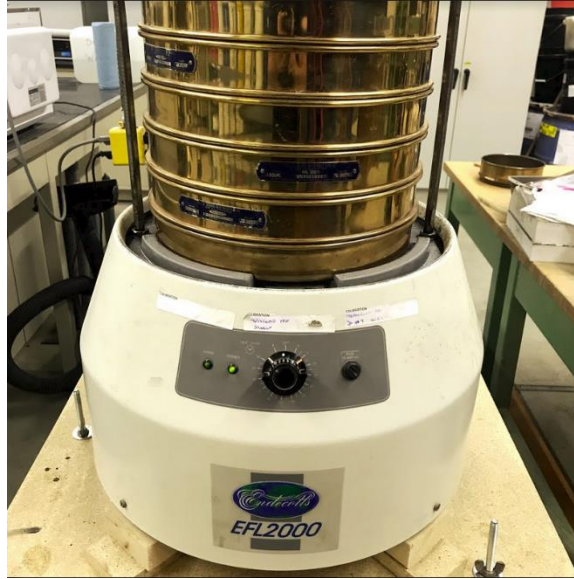


Figure 3. Shaker for sieve analysis

3.1.2 Atterberg Limits

Atterberg limits tests were performed on the surface aggregate and subgrade materials to determine the liquid limit (LL), plastic limit (PL), and the plasticity index (PI) of materials. The wet preparation-multiple point test method was conducted on materials after they were sieved through a #40 (425 μm) sieve. ASTM D4318-10e1 Standard Test Methods for Liquid Limit, Plastic Limit, and Plasticity Index of Soils were followed for these analyses. A standard brass cup and a glass plate were used to find the liquid and plastic limits, respectively (Figure 4).



Figure 4. Liquid limit test device

3.1.3 Soil Classification

The results of the sieve analyses and Atterberg limits were used to classify the materials. Materials were classified in accordance with ASTM D2487-11 Standard Practice for Classification of Soils for Engineering Purposes (Unified Soil Classification System [USCS]) and ASTM D3282-15 Standard Practice for Classification of Soils and Soil-Aggregate Mixtures for Highway Construction Purposes, which uses the American Association of State Highway and Transportation Officials (AASHTO) classification system.

3.1.4 Abrasion Tests

Abrasion is a common phenomenon that geomaterials experience especially in cold regions during the winter and spring seasons due to the freeze/thaw effect. Abrasion can be observed more severely in spring (during the thawing season), when granular roads are subjected to heavy traffic loads, which are transporting large amounts of agricultural/poultry products and construction/maintenance supplies. Therefore, abrasion resistance of the granular surface materials should be scrutinized as a main factor for evaluation of different surface aggregate materials. In this regard, the abrasion resistance of the aggregates were measured using several abrasion tests including the LA abrasion and Micro-Deval.

3.1.5 Los Angeles Abrasion

The LA abrasion test was performed on aggregate particles over $\frac{3}{4}$ in. in size to evaluate their degradation. It was conducted in accordance with ASTM C535-12 Standard Test Method for Resistance to Degradation of Large-Size Coarse Aggregate by Abrasion and Impact in the Los Angeles Machine. Soil samples were placed into the LA abrasion machine's steel drum alongside 12 steel spheres, and the drum was rotated at 30–33 rpm for 500 revolutions. The change in the weight of the washed and dried aggregate materials above sieve #12 is reported as the percentage of loss (Iowa DOT 2018). This test was performed on granular road surface aggregate materials from all sections to determine the degradation resistance of each material. Figure 5 shows the LA abrasion equipment.



Figure 5. LA abrasion test device

3.1.6 Micro-Deval

The Micro-Deval abrasion test measures the degradation of the granular road surface aggregate materials of all sections in the presence of water, steel balls, and rotation. It was conducted in accordance with ASTM D6928-10 Resistance of Coarse Aggregate to Degradation by Abrasion in the Micro-Deval Apparatus. The abrasion loss is the difference between the masses of the original sample and the washed and oven-dried sample after performing the test.

3.1.7 C-Freeze Test

A set of seven C-freeze tests was performed on the aggregate samples for materials from all sections to determine the soundness of the aggregates during freeze/thaw cycles. It was conducted in accordance with Iowa 211-B Method of Tests for Determining the Soundness of Coarse Aggregates by Freezing and Thawing. This method is similar to the AASHTO T 103 Soundness of Aggregates by Freezing and Thawing (Procedure A Total Immerse in Water). AASHTO T-103-Method C of freezing and thawing is usually used to measure the change in the percentage of the materials that are passed through a US #8 sieve before and after the test. This is supposed to represent the potential of materials to have gravel loss when used in granular roads. In this method, 25 freeze/thaw cycles were applied on specimens that were soaked in water (Iowa DOT 2018). Figure 6 shows the equipment for freezing control during this test.



Figure 6. C-Freeze test device

3.1.8 Proctor Test

Standard Proctor tests, ASTM D698-12e1 Standard Test Methods for Laboratory Compaction Characteristics of Soil Using Standard Effort (12 400 ft-lbf/ft³ (600 kN-m/m³)), were conducted on all materials (both surface aggregates and subgrade) to determine their optimum water content (w_{opt}) and the maximum dry density (γ_{dmax}). Figure 7 shows the equipment used for compaction tests.



Figure 7. Hobart mixer, left, and automated mechanical rammer, right

3.1.9 California Bearing Ratio

The CBR test was performed to evaluate the shear strength of the granular road surface aggregate and subgrade materials. It was conducted in accordance with ASTM D1883-16 Standard Test Method for California Bearing Ratio (CBR) of Laboratory-Compacted Soils. Each specimen was compacted at optimum moisture content with standard Proctor energy. CBR tests were performed on both unsoaked and soaked specimens to simulate the optimum and saturated conditions in the field, respectively. Figure 8 shows the CBR equipment.



Figure 8. California bearing ratio device

3.1.10 Moisture Determination

The moisture contents of all materials from each section were measured in the laboratory in accordance with ASTM D2216–10 Standard Test Methods for Laboratory Determination of Water (Moisture) Content of Soil and Rock by Mass.

3.1.11 Gyratory Compaction Test

Granular road surface aggregate materials undergo significant deterioration due to steadily increasing traffic loads and volumes. The durability of surfacing aggregates has been determined via LA abrasion and Micro-Deval tests for many years. However, these two tests do not simulate the effects of normal and shear stresses applied from the traffic loads on a roadway and do not test the actual full gradation and resulting particle packing of the material used in the field. The gyratory compaction test has been developed to determine the maximum density of asphalt materials by applying specific values of normal pressure while inducing shear stresses by applying specified degrees of gyration (Bozorgzad and Lee 2017). The effects of gyratory compaction in reducing the void ratio of asphalt specimens has been investigated for many years (Ghasemi et al. 2016, 2018; Notani et al. 2019). Gyratory compaction has also been used for granular materials by applying certain vertical loads with a specific degree and number of

gyrations, which enable shear distortions and particle reorientations, to simulate traffic loading of granular roadway materials.

While conducting the gyratory test, the shear resistance, void ratio, and applied gyratory energy can be determined in addition to the dry unit weight of the material for each gyration. The gyratory compaction test usually applies a greater energy than other common compaction tests such as the standard and modified Proctor tests. Therefore, conducting gyratory compaction (gyration number) to obtain optimum void ratio, resistive shear strength, and dry unit weight values could be important for proportionally large size surface aggregate materials such as those used in granular roadways. Such values could help improve the efficiency of field compaction operations by determining the required number of compaction passes beyond which little improvement is obtained.

Gyratory compaction test was conducted in accordance with AASHTO T 312 Standard Method of Test for Preparing and Determining the Density of Hot-Mix Asphalt (HMA) Specimens by Means of the Superpave Gyratory Compactor. A Brovold gyratory compactor was used to perform the gyrations and a pressure distributor analyzer (PDA) was used on top of the molds to record the load applied on top of the surface and the eccentricity of the cumulative load (Figure 9).



Figure 9. Brovold gyratory compactor, left, and PDA device, right

The gyratory mold had a 150 mm diameter and a 200 mm internal height. The vertical pressure applied to the top of the specimens was held constant at 600 kPa for all of the tests. The maximum number of gyrations that the device could deliver was 299. Due to this limitation, tests were performed in two stages of 250 gyrations to reach a total of 500 gyrations for each specimen. Two dwell gyrations were performed to square each specimen after the first 250

gyrations. The gyration angle during testing was set to 1.25° , and the rate of gyration was set to 30 rpm. The specimen height was recorded by the device to the nearest 0.1 mm after each gyration. The operational parameters used in the gyratory compaction tests are summarized in Table 1.

Table 1. Gyratory device operational parameters

Parameters	Value
Vertical pressure	600 ± 10 kPa
Gyration angle	$1.25 \pm 0.02^\circ$
Number of gyrations	500
Gyration rate	30 ± 0.5 rpm
Number of dwell gyrations	2

The PDA was used to calculate the undrained shear strength of the specimens by measuring the resultant gyratory force (R) and eccentricity while performing the gyratory test, where R is the summation of forces from three load cells (P_1 , P_2 , and P_3) at any time. The eccentricity (e_R) of the resultant force relative to the center of the PDA plate can be calculated based on the general moment equilibrium equations along two perpendicular axes (equations 2–5), in which the distance between each pair of load cells for the PDA used in this study was 100 mm.

$$\sum M_y = 0 \rightarrow e_x(R) = P_3 \left(\frac{100 \text{ mm}}{2} \right) - P_1 \left(\frac{100 \text{ mm}}{2} \right) \quad (2)$$

$$\sum M_x = 0 \rightarrow e_y(R) = P_2(100. \cos 30^\circ) \quad (3)$$

$$e_R = \sqrt{e_x^2 + (r_y - e_y)^2} \quad (4)$$

$$\tau_G = \frac{R_i e_i}{A h_i} \quad (5)$$

where, τ_G is the bulk frictional shear resistance of the specimen (kPa), e_R is the eccentricity of the resultant ram force (mm), R_i is the magnitude of the resultant ram force (kN), e_i is the eccentricity for each gyration, A is the constant sample cross-section area (m^2), and h_i is the sample height (m), all at the same gyration number.

The total compaction energy of the gyratory compactor is the sum of the work per unit volume due to the resultant force (P) and the work per unit volume due to the moment caused by the eccentricity of the applied force (equation 6):

$$\text{Energy}_{\text{gyratory}} = \frac{\sigma_{\text{vertical}} A (h_0 - h_i) + 4\theta \sum_{i=0}^n (\tau_{G_i} V_i)}{V_i} \quad (6)$$

where, $\sigma_{vertical}$ is the applied vertical pressure (600 kPa), h_0 is the initial specimen height before compaction (m), θ is the gyration angle (radians), and V_i is the specimen volume (m^3) for each gyration (DelRio-Prat et al. 2011, Li et al. 2015a).

3.2 Field Tests

FWD, MASW, lightweight deflectometer (LWD), dynamic cone penetrometer (DCP), and nuclear gauge tests were performed on five points for each test section as a preliminary assessment of the difference in support capacity of the different sections related to the different aggregate sources utilized on the surface. For all sections, the spacing between the test points were 100 ft, except the section two (OFD Class A), where the length of the section was smaller than others and the spacing between the testing points was 50 ft. In addition, International Roughness Index (IRI) and dustometer tests were performed on each test section. On the other hand, a ground temperature monitoring system was placed in the midpoint of the first test section to investigate the frost depth and number of freeze/thaw cycles per year.

3.2.1 Falling Weight Deflectometer

An SN121 JILS model FWD was used for this project (Figures 10 and 11).

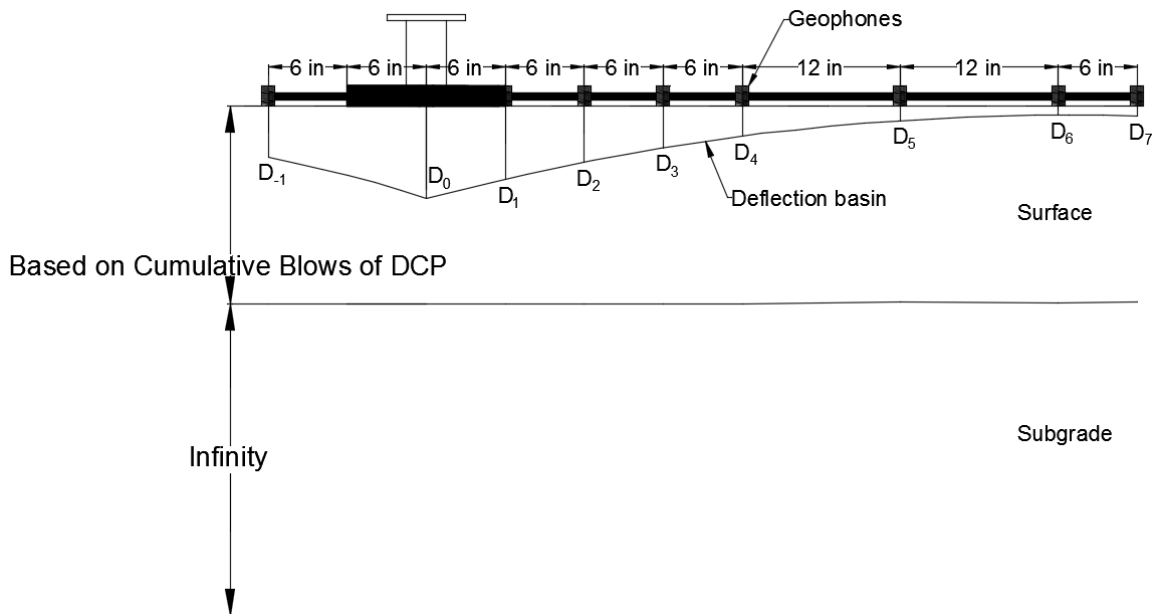


Figure 10. Falling weight deflectometer overview



Figure 11. FWD device

The loading plate is segmented into two parts to make the pressure distribution uniform under the loading plate. This model of FWD has nine sensors with 6 in. to 12 in. horizontal spacing to measure the deflections on the road and to provide a measured deflection basin. The schematic diagram of the FWD test setup, deflection bowl, and the granular road layers are shown in Figure 10. Before performing the test, a static load equal to 5.3 kN was applied to the plate to achieve a good contact between the plate and the surface materials. Then, three different dynamic pressures (36 psi, 40 psi, and 44 psi) were applied on the plate. Table 2 describes the FWD configuration.

Table 2. FWD configuration

Parameter	FWD
Number of geophones	9
Geophone spacing (in.)	6 to 12 ^a
Total length (in.)	66
Distance from the source to the first geophone (in.)	0
Static load (lb)	1,200
Dynamic loads (lb)	4,000; 4,500; 5,000

^a Distance between the transducers in FWD are -12, 0, 6, 12, 18, 24, 36, 48 and 54 in.

Boussinesq's solution was utilized to obtain the stress, strains, and deformation at every given depth and radius in a homogeneous, linear-elastic half-space, and Odemark's theory was used to assume equivalent layer thickness and match the measured surface deflections with the calculated deflections over the equivalent single layer (Li et al. 2018a). According to this combined theory, back-calculation was done based on the dynamic loads and peak deflections that were observed under the geophones on the two-layered system (Boussinesq 1885, Grasmick

et al. 2013, Li et al. 2017a, Odemark 1949, Saltan et al. 2013, Stokoe et al. 1994). In addition, the BAKFAA and Modulus 7.0 programs were used for back-calculation analyses to evaluate the accuracy and consistency of the results obtained from the combination of Boussinesq's solution and Odemark's equivalent layer thickness assumption. The bedrock depth was assumed to be equal to 158 ft below the ground surface based on the bedrock geology of south-central Iowa (Iowa Geological Survey 2002).

FWD data are generally followed by a back-calculation procedure to acquire the results of the elastic modulus for surface and subgrade layers. In that regard, AASHTO's Guide for the Design of Pavement Structures approach (AASHTO 1993) was used for the back-calculation by using combined Boussinesq's and Odemark's theories for a homogeneous, linear-elastic two-layered system of pavement. Boussinesq's method is helpful to find the stress, strain, and deformation values in different depths and horizontal distances from the loading point as shown in equation 7. Moreover, an integrated Boussinesq's solution to find the vertical deflection beneath the center of the circular loading plate is shown in equation 8.

$$d_{r,z} = \frac{(1+\nu)F_{Max}}{2\pi E\nu\sqrt{z^2+r^2}} \left[2(1-\nu) + \frac{z^2}{z^2+r^2} \right] \quad (7)$$

$$d_{0,z} = \frac{f(1-\nu^2)F_{Max}}{\pi a E} \frac{1}{\sqrt{1+(\frac{z}{a})^2}} \quad (8)$$

where,

$d_{r,z}$ = vertical deflection at depth z and radius r

$d_{0,z}$ = vertical deflection beneath the loading plate at the surface

ν = Poisson's ratio, which is assumed 0.4 and 0.3 for surface and subgrade, respectively

F_{Max} = vertical force

E = elastic modulus

z = depth

r = radius from the center of the loading plate

f = shape factor, which is assumed equal to 2 for uniformly distributed stress condition

a = radius of the circular loading plate

For the points with the horizontal distances greater than $2a$, the measured surface deflection is almost the same and is mainly developed due to the subgrade deflection (Ullidtz 1998).

Therefore, using equation 7 and based on the surface deflection at $r > 2a$, the subgrade elastic modulus is calculated by using equation 9.

$$E_{SG} = \frac{(1-\nu^2)F_{Max}}{\pi r d_{r,0}} \quad (9)$$

According to Odemark's theory, an equivalent thickness (h_e) was assumed for the calculation of the surface elastic modulus in a two-layered system under loading point as it is shown in equation 10. Moreover, the measured surface deflection for horizontal distances greater than the

stress bulb's effective radius (a_e) should be taken into consideration for calculation of the subgrade elastic modulus. However, at relatively greater distances from the loading point, the error in the measured deflection can be significant. Accordingly, a radius greater than $0.7a_e$ should be considered to be placed in equation 9 to calculate the elastic modulus of the subgrade layer (AASHTO 1993). The radius of the stress bulb (a_e) is shown in equation 11.

$$h_e = h^3 \sqrt{\frac{E_{AGG}}{E_{SG}}} \quad (10)$$

$$a_e = \sqrt{a^2 + \left(h^3 \sqrt{\frac{E_{AGG}}{E_{SG}}}\right)^2} \quad (11)$$

where,

h_e = equivalent thickness

h = thickness of the surface layer

E_{AGG} = elastic modulus of the surface layer

E_{SG} = elastic modulus of the subgrade layer

a_e = is the radius of the stress bulb

The back-calculation procedure to determine the elastic modulus of the surface materials is followed by a combined Boussinesq's and Odemark's solution, as it is shown in equation 12. The formula follows a matching procedure between the calculated and measured surface deflections beneath the loading point by minimizing the value of the error between those values with the change in the surface elastic modulus values (E_{AGG}) (Grasmick 2013).

$$d_{0,0} = \frac{f(1-\nu^2)F_{Max}}{\pi a} \left\{ \frac{1}{E_{SG} \sqrt{1 + \left(\frac{h^3 \sqrt{E_{AGG}}}{a \sqrt{E_{SG}}}\right)^2}} + \frac{\left[1 - \frac{1}{\sqrt{1 + \left(\frac{h}{a}\right)^2}}\right]}{E_{AGG}} \right\} \quad (12)$$

3.2.2 Multichannel Analysis of Surface Waves

The MASW device used for this project had 24 vertical geophones (4.5 Hz) that were fixed in steel land streamers to ensure a good contact with the granular road surface. The geophones on the land streamer have a higher quality of data in a shorter period of time, compared to the ones with spikes to fix the geophones into the ground surface. Heisey et al. (1982b) suggested that the spacing between the geophones should be less than two wavelengths and greater than one-third of a wavelength. The spacing between the geophones for the device used in this study was 6 in. All receivers were connected to a 24-channel Geometrics Geode seismograph. Figure 12 shows the schematic diagram of the MASW test setup used in the current study.

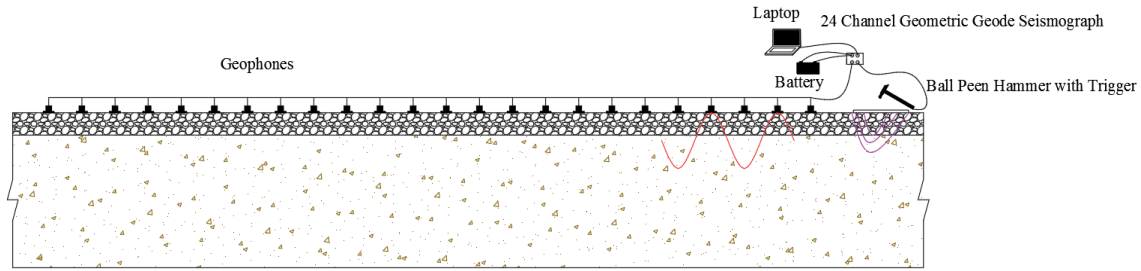


Figure 12. MASW general view

Table 3 shows that the number of geophones in the MASW is greater than those of FWD.

Table 3. MASW configuration

Parameters	MASW
Number of receivers	24
Receiver spacing (in.)	6
Total length (in.)	138
Distance from the source to the first receiver (in.)	12 and 72 ^a

^a Distance from source to the first geophone in MASW is 12 in. for small hammer and 72 in. for large hammer

The spacing of geophones in MASW is less, and they record the velocity as a unique value (Park et al. 1999a) compared to the FWD, which only records the maximum deflection beneath the geophones.

MASW presents the change in the Rayleigh wave velocity (V_R) with the change of frequency as the dispersion curve (Park et al. 1999a). Figure 13 shows the dispersion curve generated based on the field data by recording the phase velocity and the frequency by using a small hammer as the active source for one of the test points.

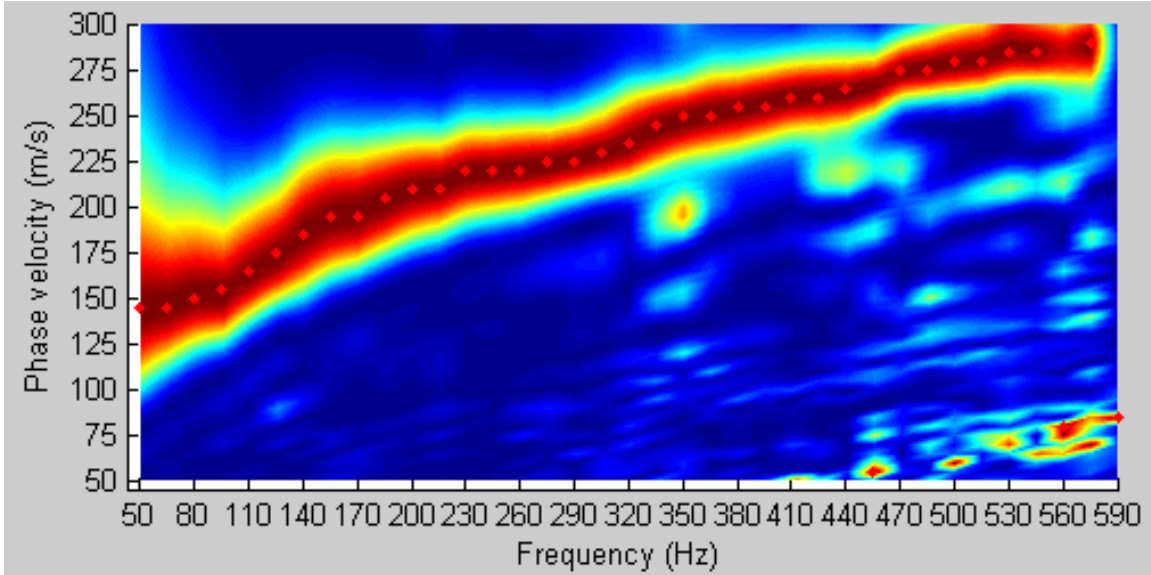


Figure 13. Experimental dispersion of the results of MASW

A new hybrid genetic-simulated annealing (GSA) inversion procedure (Lin 2014) was used in this study by employing the thickness (m), dry unit weight (kg/cm^3), and Poisson's ratio values for the surface and subgrade layers beside the dispersion curve, as the inputs, to back-calculate the actual shear wave velocity. Figure 14 represents the final match between the results of the change in phase velocity and the change in frequency for dispersion and inversion.

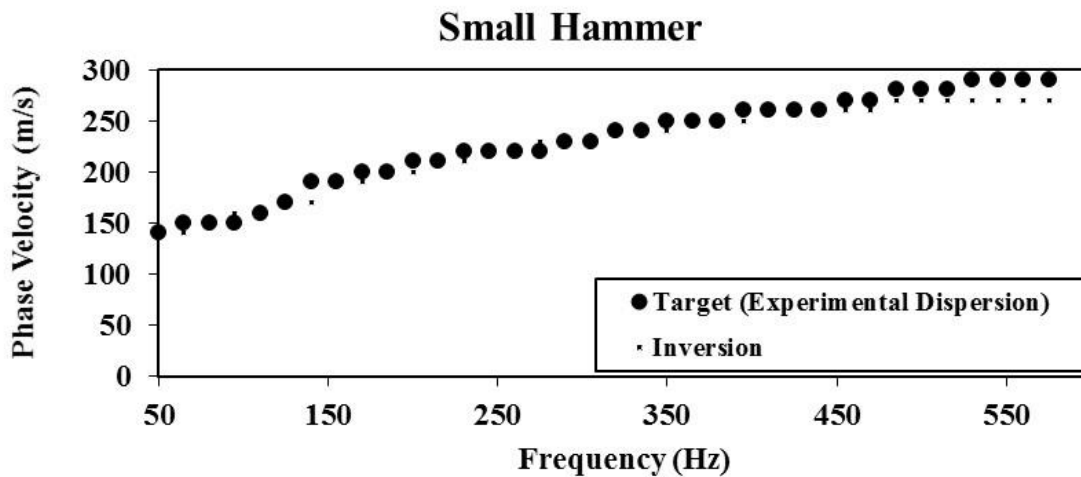


Figure 14. Experimental dispersion and theoretical dispersion in inversion process

Shear wave velocity is directly related to the elastic modulus (Li et al. 2015b). In this regard, equations 13–15 were used to calculate the elastic modulus of the surface and subgrade layers as follows:

$$V_S = V_R \times (1.13 - 0.16\nu) \quad (13)$$

$$G = V_S^2 \times \rho \quad (14)$$

$$E = 2 \times G \times (1 + \nu) \quad (15)$$

where, V_S is shear wave velocity, V_R is the Rayleigh wave velocity, ν is the Poisson's ratio, G is the shear modulus, and E is the elastic modulus.

Figure 15 summarizes the elastic modulus calculation procedures for the FWD and MASW tests.

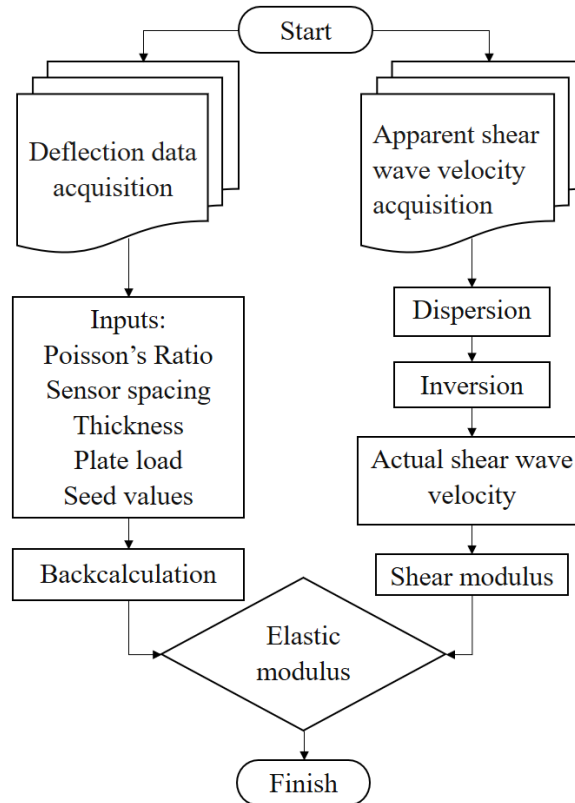


Figure 15. Procedure to get the elastic modulus from FWD and MASW in situ tests

The triggering load applied for the MASW test was much smaller than that applied during the FWD test and was produced by hitting a 2 lb (small) and a 12 lb (large) hammer on an inch thick 2.3 in.² aluminum plate to couple the impact energy from the hammer with the underlying layers. The base plate as a coupler mechanism improves the conversion of the impact energy of the hammer into the seismic wave energy (Mereu et al. 1963). The change in the shear wave velocity due to the change in the frequency is called dispersion (Park et al. 1999b). The resolution of the dispersion curve depends on the number of geophones (Mahvelati and Coe 2018). After getting the dispersion curve from the field tests, the inversion curve was matched with the dispersion curve to obtain the results for the actual shear wave velocity. Poisson's ratios, as the inputs for the surface and subgrade layers were assumed to be 0.3 and 0.4, respectively. The thickness values of the surface layers were determined from DCP tests and the subgrade layer thickness

was assumed to be infinite for a two-layered system. Then, the shear and elastic modulus of the surface and subgrade layers were calculated using equations 13–15.

3.2.3 Lightweight Deflectometer

The LWD equipment as a non-destructive test was specifically developed to perform rapid field testing of pavement materials, and LWD tests in this study were conducted to determine the maintenance frequency required for the test sections. The tests were performed on five points within each test section to evaluate the in situ composite elastic modulus (E_{Comp}) (stiffness) of the granular surfaces and subgrades, as a measure of road serviceability. This stiffness is a function of several factors, including compaction quality, packing structure of the various particle sizes (Tirado et al. 2017, Xiao et al. 2012), density of the road layers, water content, and temperature (Oloo et al. 1997). Any changes in these factors can result in severe distresses (e.g., potholes, rutting, etc.), creating a need for road maintenance. Therefore, along with the E_{comp} data for each test section, the surface layer temperature and water content are presented. The ambient temperature of the surface course was measured using a thermocouple installed in the middle of the first section, and the same ambient temperature was assumed for all the sections. The water content values were measured from samples collected during field testing. The LWD device used for testing in this study features a 22 lb hammer with a drop height of 19.69 in., and a base plate diameter of 11.81 in. Figure 16 shows the LWD test setup used in this study.



Figure 16. Lightweight deflectometer device

The in situ elastic modulus then was calculated based on the average vertical deflection as shown in equation 16.

$$E_{LWD} = \frac{(1-\nu^2)\sigma_0 A f}{d_0} \quad (16)$$

where, E_{LWD} is elastic modulus, as the result of LWD test, σ_0 is vertical stress applied on top of the plate, ν is Poisson's ratio (assumed as 0.4), d_0 is applied stress, A is plate radius, and f is shape factor (assumed to be 2 for a uniform stress distribution) (Vennapusa and White 2009).

3.2.4 Dynamic Cone Penetrometer

DCP was used to determine the shear strength and thicknesses of the granular surface and subgrade layers for each test section. DCP tests were conducted in accordance with ASTM

D6951 (D6951M-09 2015). A DCP cone with a 0.79 in. base diameter was used to penetrate to the soil up to 23 in. by using a 17.6 lb hammer. Figure 17 shows the DCP setup.



Figure 17. Dynamic cone penetrometer device

Using the DCP index (DCPI) (in./blow) as the rate of penetration and empirical correlations based on the ASTM standard, the CBR values for each layer were calculated, as noted in equations 17 and 18.

$$\text{CBR} = \frac{292}{\text{DCPI}^{1.12}} \quad (17)$$

where, $\text{CBR} > 10$

$$\text{CBR} = \frac{1}{(0.017019 \times \text{DCPI})^2} \quad (18)$$

where, $CBR < 10$

Sudden changes in the cumulative blows versus depth is identified as the change in the layer characteristics. Therefore, the depth of the penetration to the transition zone is the thickness of the surface layer, as shown in Figure 18.

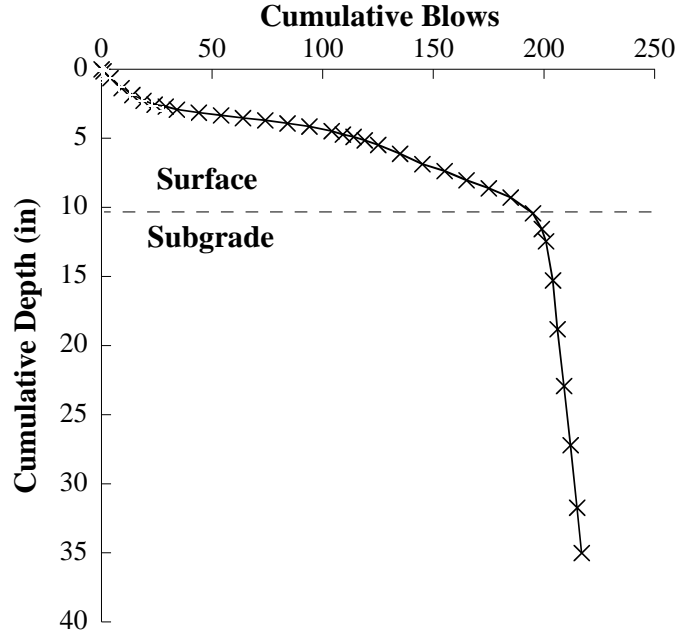


Figure 18. Cumulative blows vs. cumulative depth

The weighted average of the surface and subgrade CBR values then were calculated as shown in equations 19 and 20.

$$CBR_{AGG} = \frac{\sum_{i=1}^n CBR_i \times D_i}{\text{Surface thickness}} \quad (19)$$

$$CBR_{SG} = \frac{\sum_{i=n+1}^m CBR_i \times D_i}{\text{Final depth measurement} - \text{Surface thickness}} \quad (20)$$

where, CBR_{AGG} and CBR_{SG} are the weighted average CBR values for the surface and subgrade, CBR_i is the CBR value calculated by (equations 17–18) formulas for each reading in the surface or subgrade layer, D_i is the reading of the depth of penetration in each layer, n is the number of readings in the surface layer, and m is the total number of readings.

3.2.5 Automated Plate Load Testing

Automated plate load test (APLT) was performed on the surface of each testing point to provide the stiffness, based on the load-deformation response in accordance with ASTM D1195 Standard Test Method for Repetitive Static Plate Load Tests of Soils and Flexible Pavement Components, for Use in Evaluation and Design of Airport and Highway Pavements. The results of the APLT field testing are to provide the long-term loading performance of the road layers by applying a target cyclic stress of 90 psi as a static load for 1,000 cycles on a 12 in. circular flat plate at each point for vehicle-loading conditions simulation. Figure 19 shows the plate load test mounted on a trailer unit.



Figure 19. APLT setup mounted on a trailer

The cyclic loading process uses a load pulse during and a dwell time beside the deformation, which can be monitored by the operator as shown in Figure 20.

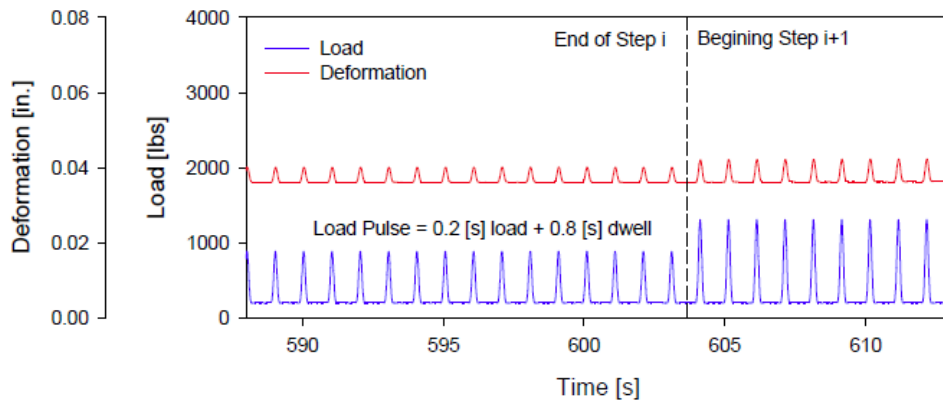


Figure 20. Real-time APLT results of load pulse and deformation

Permanent deformation (δ_p) as the result of the cumulative plastic shear strain, compaction, and consolidation (White and Vennapusa 2017) and the composite resilient modulus (M_r) are calculated as shown in equations 21 and 22.

$$M_{r\text{-comp}} = \frac{(1-\nu^2)\sigma_0 a f}{\delta_r} \quad (21)$$

$$\delta_p = C N^d \quad (22)$$

where,

$M_{r\text{-comp}}$ = in situ composite resilient modulus

ν = Poisson's ratio (assumed to be 0.4)

σ_0 = cyclic stress

a = radius of the plate (6 in.)

f = shape factor (assumed to be 8/3)

δ_p = permanent deformation

C = the plastic deformation after the first cycle of repeated loading

N = number of load cycles

d = scaling exponent

3.2.6 International Roughness Index

Roughness of the road surface as representative of ride quality is an important factor to evaluate the granular roadway performance, and lower IRI values reflect higher ride quality, lower fuel consumption, and longer service life (Jia et al. 2018). In the current study, the collection of road roughness measurements representative of road condition was done using a smartphone application named Roadroid. This software used a built-in smartphone accelerometer to evaluate roughness index of the different surfaces in a rapid and cost-effective manner (Akinmade et al. n.d.). In this method, the smartphone was mounted on the windshield of a one-ton truck and, after adjustments, the calculated International Roughness Index (cIRI) values were measured and stored in the phone while driving between 40 and 50 mph. Moreover, photos are taken during the survey. In addition, the software has the ability to do a friction survey. To accomplish the friction survey, the driver should reach to above 30 mph and then push the break until the car completely stops. The friction value (μ) and a photo of the stop point are stored to the phone. The data in addition to the location of the test are uploaded and available on the Roadroid website.

3.2.7 Dustometer

The dustometer test is another road-performance measure used in this study to estimate the appropriate granular road maintenance frequency. To evaluate the dust production of each test section in relation to the different aggregate sources utilized in the surface layers, dustometer tests were performed several times over the length of the project. Figure 21 shows the setup of the dustometer device attached by a steel bracket to the bumper of a one-ton truck.



Figure 21. Dustometer setup, top, and dust production measurement paper, bottom

The dustometer has a 12 in. × 12 in. steel mesh with a 0.0079 in. mesh size sieve to prevent large particles from damaging the tightly held filter paper. A 1/3 horsepower suction pump is connected to the mounted dustometer with a 2 in. diameter flexible hose to collect dust behind the rear wheel while driving at a speed of 45 mph. A 4,400 watt gasoline-powered generator provides power for the suction pump. The filter paper was removed after performing the test over a section, and the mass of the dust on the paper is divided by the length of the sections to determine the amount of dust per unit length.

3.2.8 Nuclear Gauge Test

A nuclear gauge test is a fast and non-destructive test and was performed by Iowa DOT to measure the in situ density and the moisture content of the surface material by attenuation of the gamma radiation at a known depth. It is conducted in accordance with ASTM D6938-15 Standard Test Methods for In-Place Density and Water Content of Soil and Soil-Aggregate by Nuclear Methods (Shallow Depth). In this test, the setup should be placed in a good contact to the surface of the granular roadway. The device recorded the wet density and the water content. Then, the dry density (γ_{dry}) was calculated by using equation 23.

$$\gamma_{dry} = \frac{\gamma_{wet}}{1+WC/100} \quad (23)$$

where, the γ_{dry} is the dry density, γ_{wet} is the wet density, and WC is the water content.

Figure 22 shows the nuclear density gauge device.



Figure 22. Nuclear density gauge test device

CHAPTER 4. MATERIALS

Results of the sieve analysis, Atterberg limits, compaction, abrasion, and C-Freeze tests for the geomaterials used for this project are summarized in this chapter.

4.1 Geomaterials

Surface aggregate materials for this study were collected from quarries featuring four different Iowa bedrock types: Lime Creek Formation (LCF), Oneota Formation Dolomite (OFD), Bethany Falls Limestone (BFL), and Crushed River Gravel (CRG) (Figure 23).

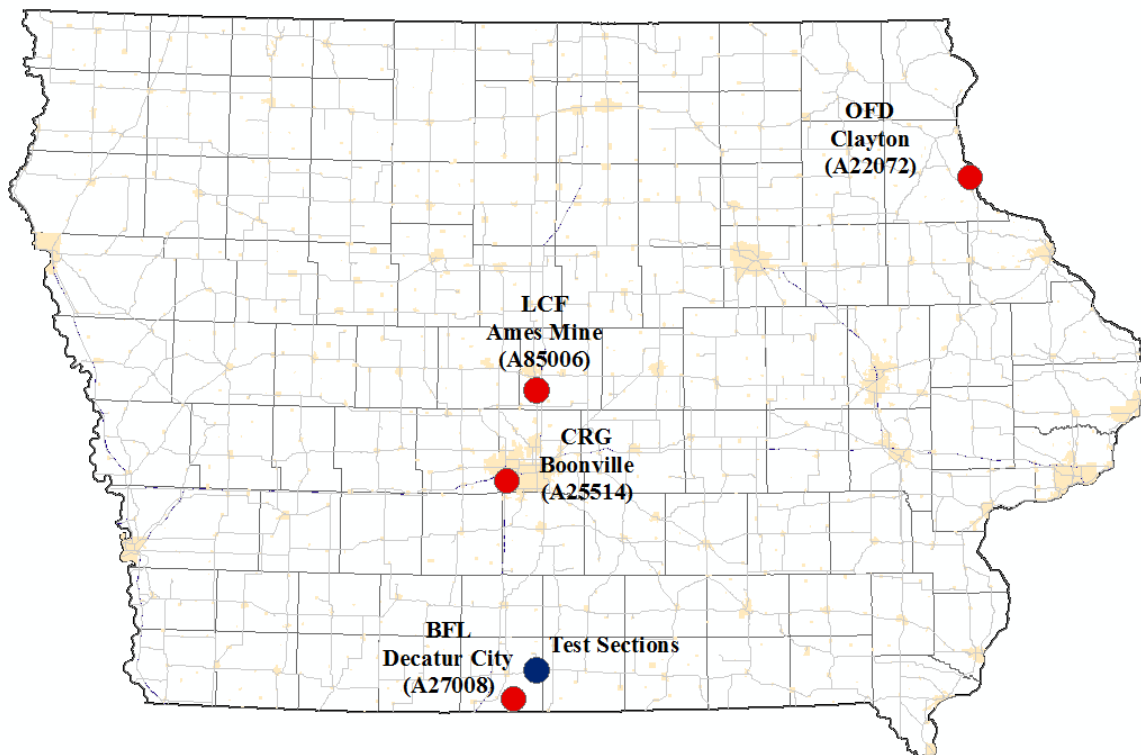


Figure 23. Location of the aggregate quarries for this project

The first three quarries provided both conventional (Class A) and coarse clean aggregate materials, while the CRG quarry provided crushed coarse clean gravel materials. The main difference between the Class A and clean materials was their particle sizes, whereby the Class A materials had higher fines contents and lower percentages of coarse aggregates than the clean materials. Figures 24 to 26 show the samples of the Class A, clean, and the mixture of the Class A and clean materials.

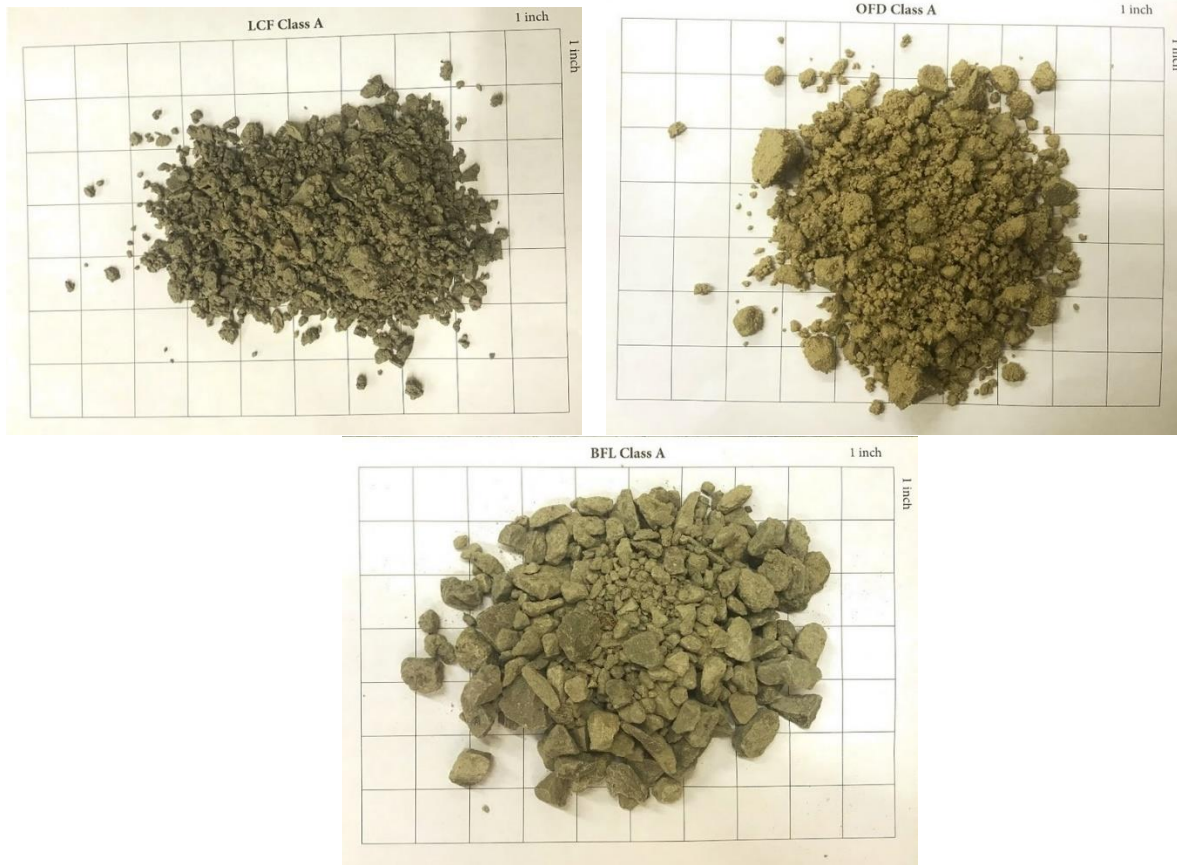


Figure 24. Class A surface aggregate materials



Figure 25. Clean surface aggregate materials



Figure 26. Mixture of clean and BFL Class A surface aggregate materials

Seven field test sections were built in Decatur County, Iowa. The first three sections consisted of Class A materials: LCF Class A, OFD Class A, and BFL Class A, while the local BFL Class A material was also mixed with clean aggregate materials collected from all four quarries for the final four sections. Therefore, the local BFL Class A material was the only one mixed with the four clean materials to examine the mechanistic performance of such mixtures. To achieve the best performance and durability for the mixture sections, the optimum target particle-size distribution (PSD) curves of the mixtures were determined via the gradation optimization method described in (Li et al. 2018b). According to the optimization analyses, it was determined that the mixing ratios by weight for the last four test sections should be as follows: 80% BFL Class A + 20% BFL Clean, 70% BFL Class A + 30% OFD Clean, 70% BFL Class A + 30% LCF Clean, and 70% BFL Class A + 30% CRG Clean aggregate.

4.2 Gradation

Figures 27 and 28 show the particle-size distribution of Class A aggregates and clean aggregates that were collected from each test site during construction, as well as the subgrade.

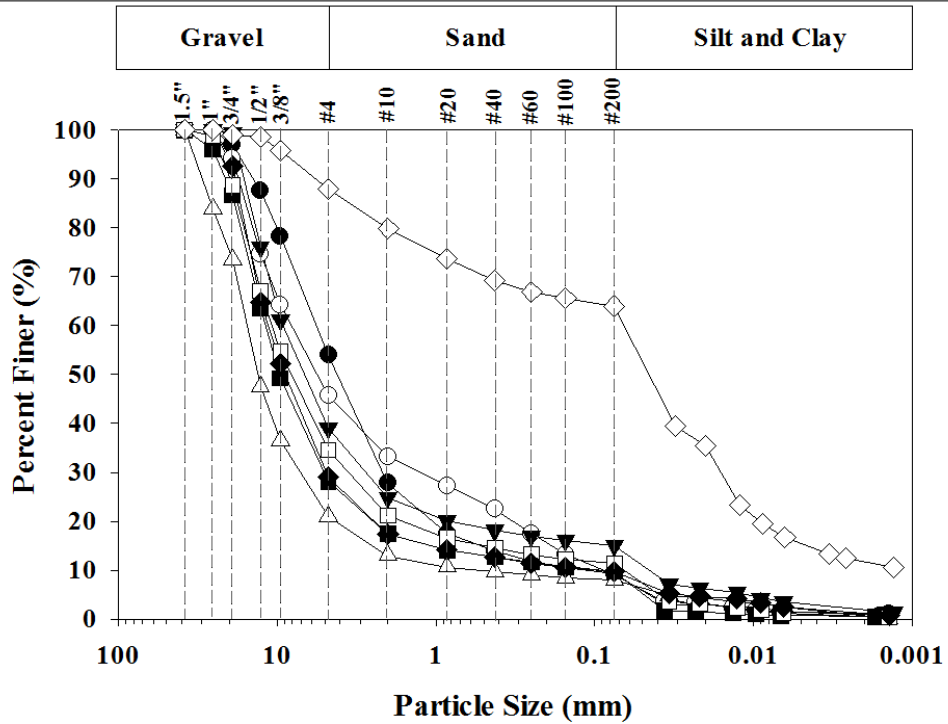
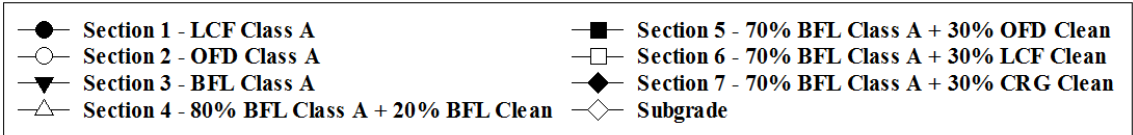


Figure 27. Particle-size distribution of the surface aggregate materials

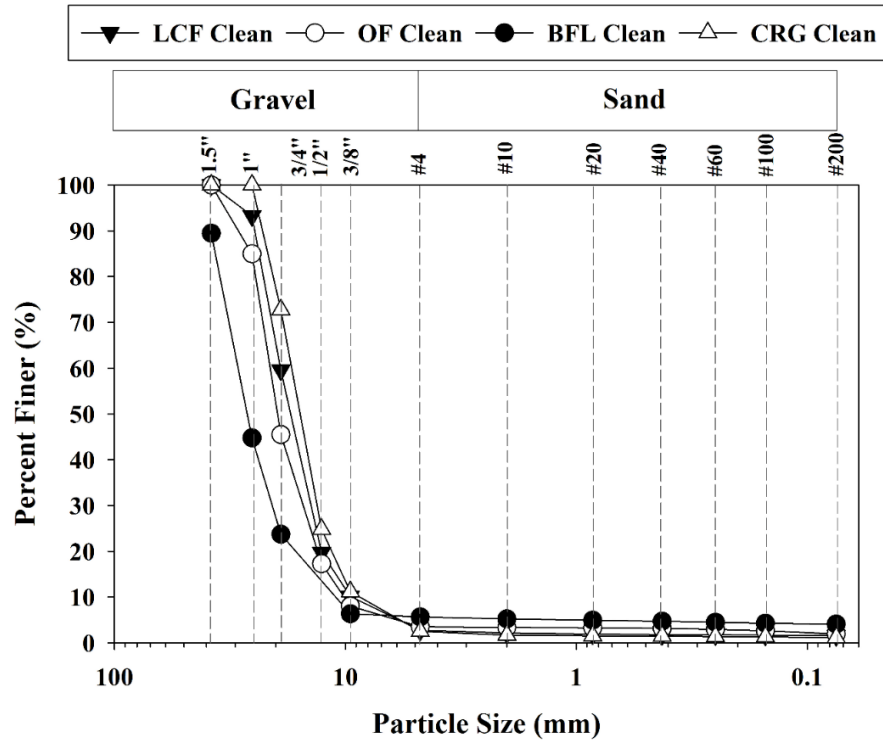


Figure 28. Particle-size distribution curve of clean aggregate materials

Table 4 also summarizes the soil index properties.

Table 4. Index properties

Parameter	LCF Class A	OFD Class A	BFL Class A	80%	70%	70%	70%	Subgrade	LCF Clean	OFD Clean	BFL Clean	CRG Clean
				BFL Class A +	BFL Class A +	BFL Class A +	BFL Class A +					
				20% BFL Clean	30% OFD Clean	30% LCF Clean	30% CRG Clean					
Particle-size analysis results (ASTM D422-03)												
Gravel content (%) (>4.75 mm)	46	54	61	79	72	65	71	12	97	97	94	98
Sand content (%) (4.75 mm–75 µm)	45	37	24	13	18	23	19	24	1	2	2	1
Silt content (%) (75 µm–2 µm)	8	8	14	8	8	11	9	53	2	2	4	1
Clay content (%) (< 2 µm)	1	1.3	2	0	2	0	0	11				
D10 (mm)	0	0	0	1	0	0	0	0	10	10	14	9
D30 (mm)	2	1	3	7	5	4	5	0	14	15	20	13
D60 (mm)	6	8	9	15	12	11	11	0	19	21	29	17
Coefficient of uniformity, C _u	48	91	185	25	111	154	103	0	2	2	2	2
Coefficient of curvature, C _c	7	2	17	5	19	17	19	7	1	1	1	1
Atterberg limits test results (ASTM D4318-10e1)												
Liquid limit (%)	15	NA	20	20	19	17	19	31	-	-	-	-
Plasticity index	1	NA	4	5	4	3	5	12	-	-	-	-
AASHTO and USCS soil classifications (ASTM D2487-11 and D3282-09)												
AASHTO	A-1-a	A-6	A-1-a	A-1-a	A-1-a	A-1-a						
USCS group symbol	GW	CL	GP	GP	GP	GP						
USCS group name	Well-Graded Gravel	Sandy Lean Clay	Poor-Graded Gravel	Poor-Graded Gravel	Poor-Graded Gravel	Poor-Graded Gravel						

Table 4 shows the gravel, sand, and fines content of the Class A materials, and they ranged from 46 to 61%, 26 to 45%, and 9 to 15%, respectively. In addition, the gravel, sand, and fines contents for the clean aggregate materials ranged from 94 to 98%, 1 to 2%, and 1 to 4%, respectively. BFL Clean and CRG Clean have the aggregate top size of 1 ½ in. and ¾ in., respectively. However, LCF Clean and OFD Clean have the aggregate top size of 1 in.

Sections with LCF Class A, OFD Class A, BFL Class A, and the mixture of 70% BFL Class A + 30% CRG Clean have the aggregate top size of ¾ in. for their surface aggregate. On the other hand, sections with 80% BFL Class A + 20% BFL Clean, 70% BFL Class A + 30% OFD Clean, and 70% BFL Class A + 30% LCF Clean have the aggregate top size of 1 in. All of the granular road surface aggregate materials are classified as well-graded gravel (GW), or A-1-a, while the subgrade is classified as sandy lean clay (CL), or A-6, by USCS and AASHTO classification systems, respectively. All clean materials are classified as poor-graded gravel (GP) and A-1-a by USCS and AASHTO classification systems, respectively. OFD Class A did not show any plasticity. On the other hand, the liquid limit and plasticity index of materials collected from other sections ranged from 15 to 20 and 1 to 5, respectively.

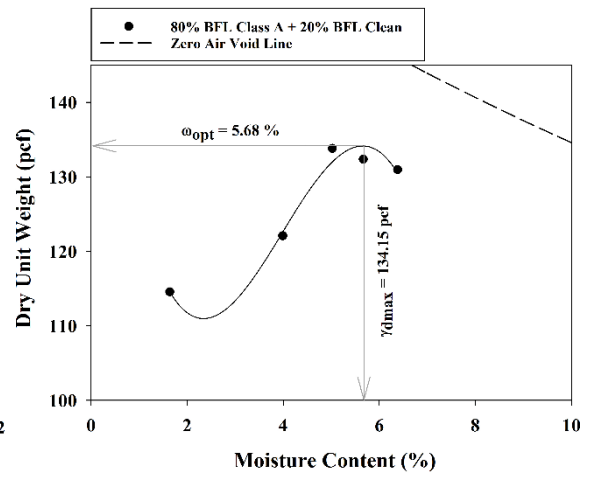
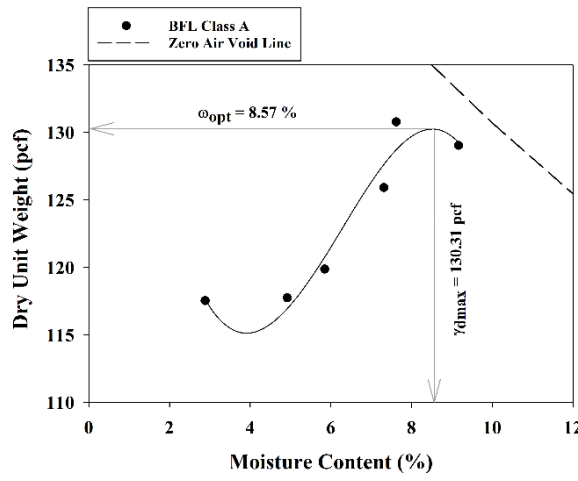
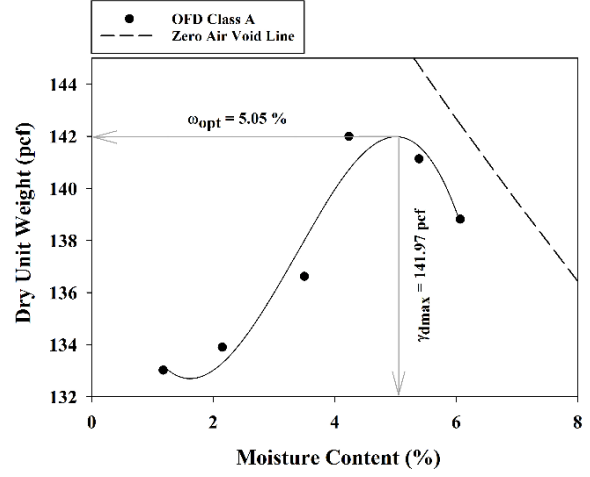
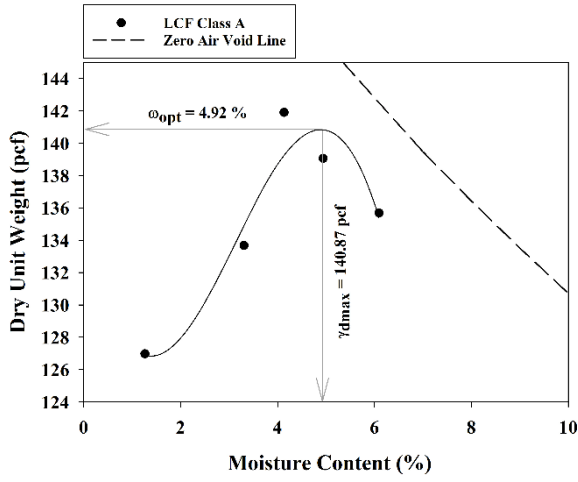
4.3 Compaction Test Results

The standard Proctor test was performed on the surface aggregate materials and subgrade to determine the optimum moisture content (w_{opt}) and the maximum dry density (γ_{dmax}) of each material (ASTM D698-12e1). A summary of the results is shown in Table 5.

Table 5. Optimum moisture content and the maximum dry density results of the Proctor test

Materials	Optimum moisture content (%)	Maximum dry density (pcf)
LCF Class A	5	141
OFD Class A	5	142
BFL Class A	9	130
80% BFL Class A + 20% BFL Clean	6	134
70% BFL Class A + 30% OFD Clean	9	135
70% BFL Class A + 30% LCF Clean	5	134
70% BFL Class A + 30% CRG Clean	10	132
Subgrade	13	113

Moreover, the eight graphs in Figure 29 show the compaction curves obtained for all materials along with zero air void lines.



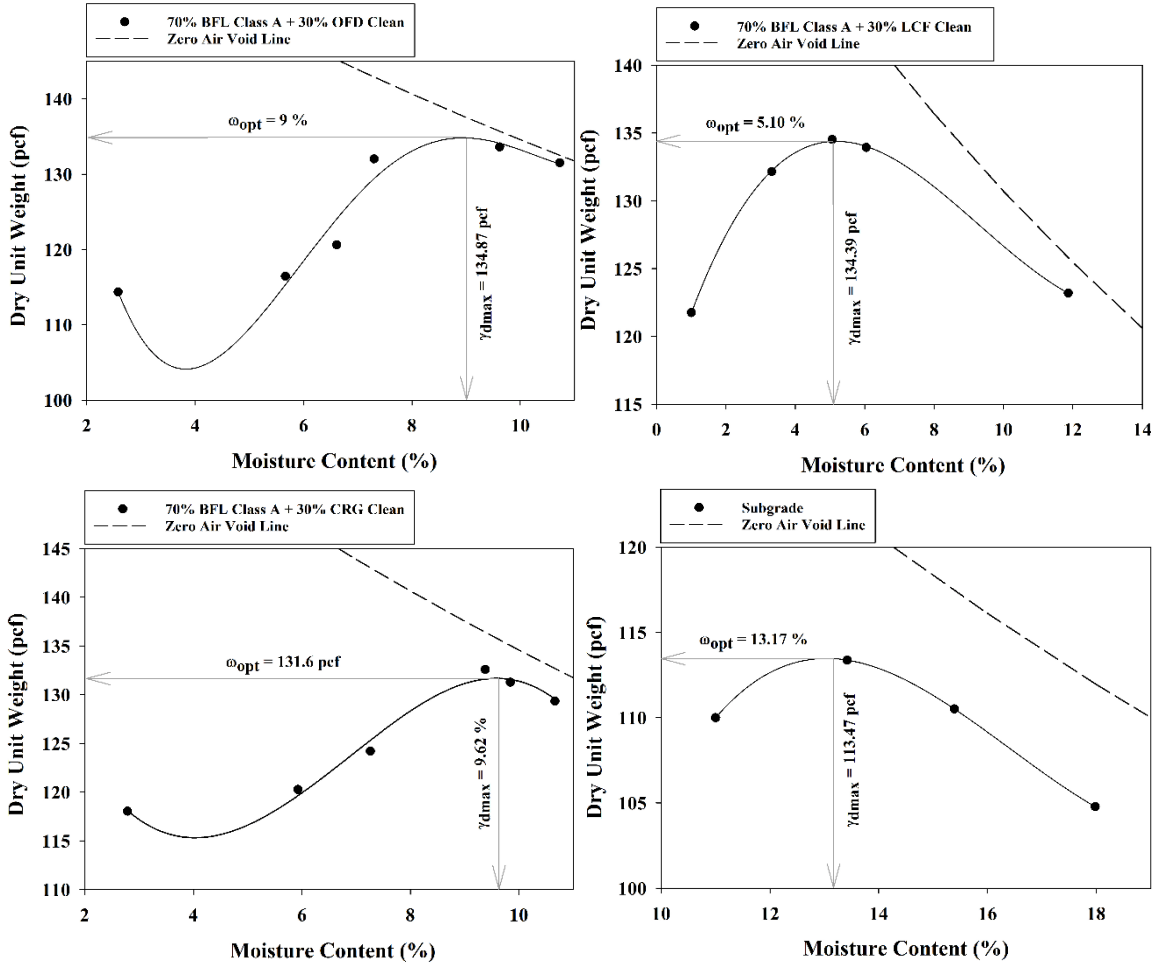


Figure 29. Dry density vs. water content graphs from standard Proctor tests for all materials

The zero-air-void lines (100% degree of saturation line) were also drawn for all materials to check the accuracy of the compaction test results. The γ_{dmax} of the subgrade was lower than those of all granular road surface aggregates (113 pcf) and its w_{opt} was the highest (13%). The w_{opt} of granular road surface aggregates were between 4.9% and 9.6%.

4.4 California Bearing Ratio Test Results

Figure 30 shows the results of the laboratory CBR tests that were performed on the surface aggregate and subgrade materials.

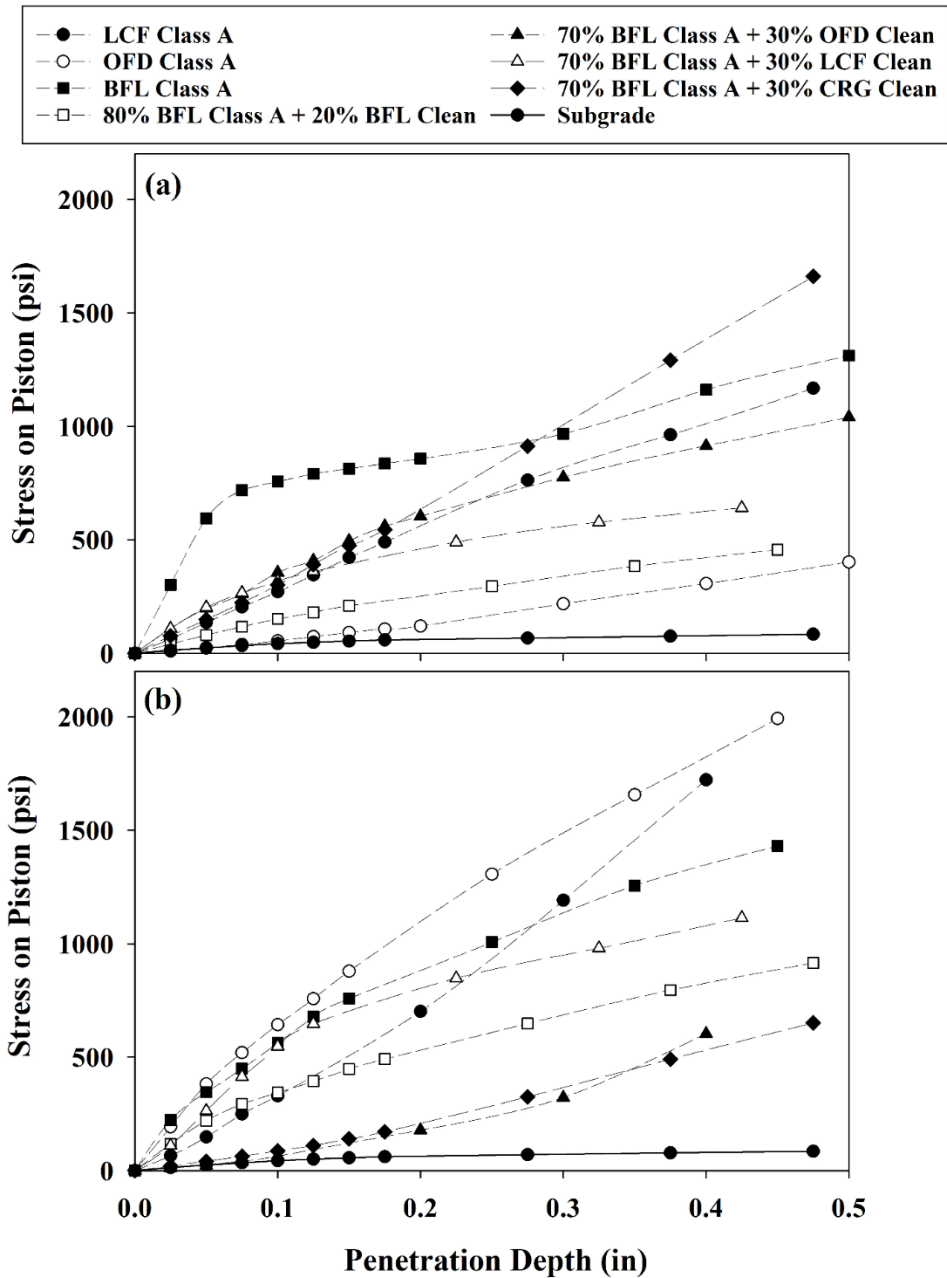


Figure 30. Penetration depth vs. stress on piston during CBR test

The CBR specimens were prepared at their w_{opt} with standard Proctor energy. In this project, the CBR tests were performed under both soaked and unsoaked conditions.

Figure 31 shows the CBR values for each specimen, which are measured using the corrected stress values for 0.1 in. depth of penetration.

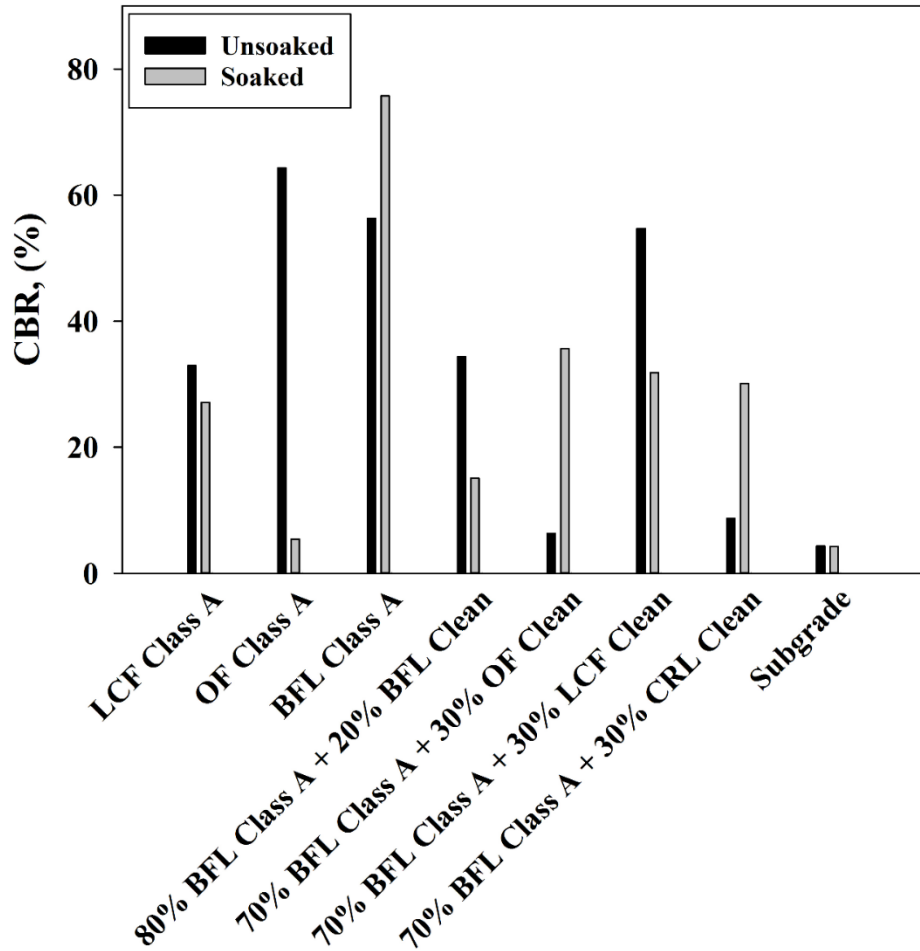


Figure 31. CBR values for all sections

Duplicate tests were conducted, and the average of these duplicates were presented as the CBR of each granular road surface aggregate and subgrade soil.

4.5 Abrasion Test Results

The results of the LA abrasion and Micro-Deval tests performed on all of the surface materials are presented in Figure 32.

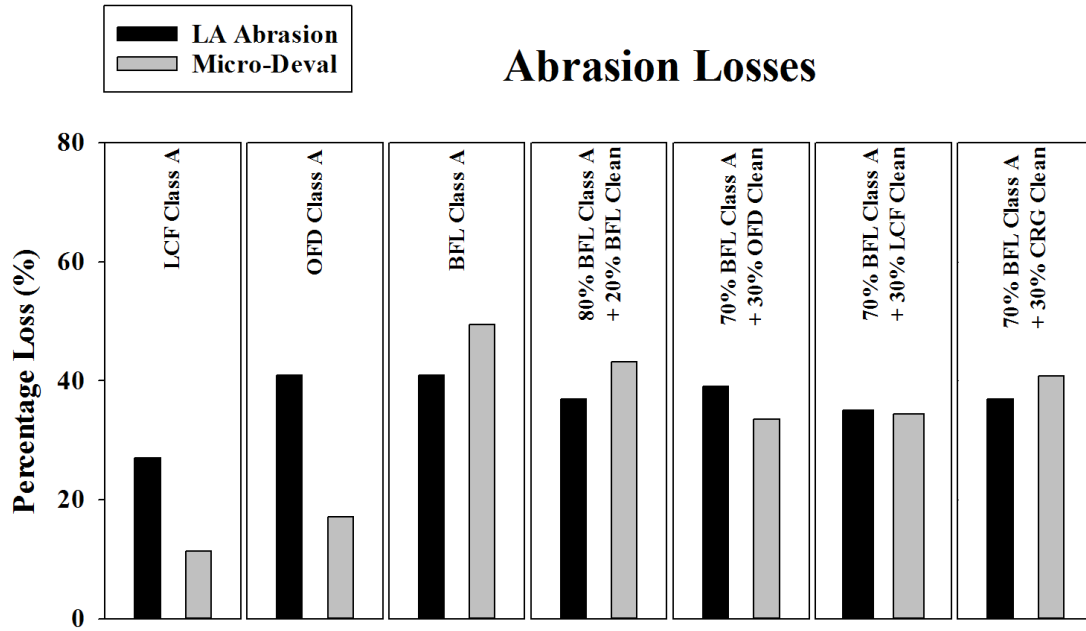


Figure 32. LA abrasion and Micro-Deval test results

The Micro-Deval test results showed that the LCF Class A experienced the least material loss (11%) while local BFL Class A had the highest material loss (49%). This indicates that the BFL Class A does not have high durability under wet conditions. After LCF Class A, OFD Class A had the second lowest Micro-Deval material loss (17%). Material loss for the mixtures of BFL Class A with the four clean aggregates were between 33% and 43% according to the Micro-Deval tests. These results indicate that inclusion of BFL Class A in the surface mixtures will yield a significant decrease in the resistance to abrasion.

The results of LA abrasion tests were similar to those of the Micro-Deval tests. LCF Class A experienced the lowest material loss of 27%, while the rest of the materials have similar losses ranging from 36%–40%. All of the granular road surface aggregates used in this study met the Iowa DOT specification for Class A surface materials, which requires an LA abrasion loss below 45%.

4.6 C-Freeze Test Results

Figure 33 shows the results of C-Freeze test, which was performed on all surface materials.

C-Freeze Results

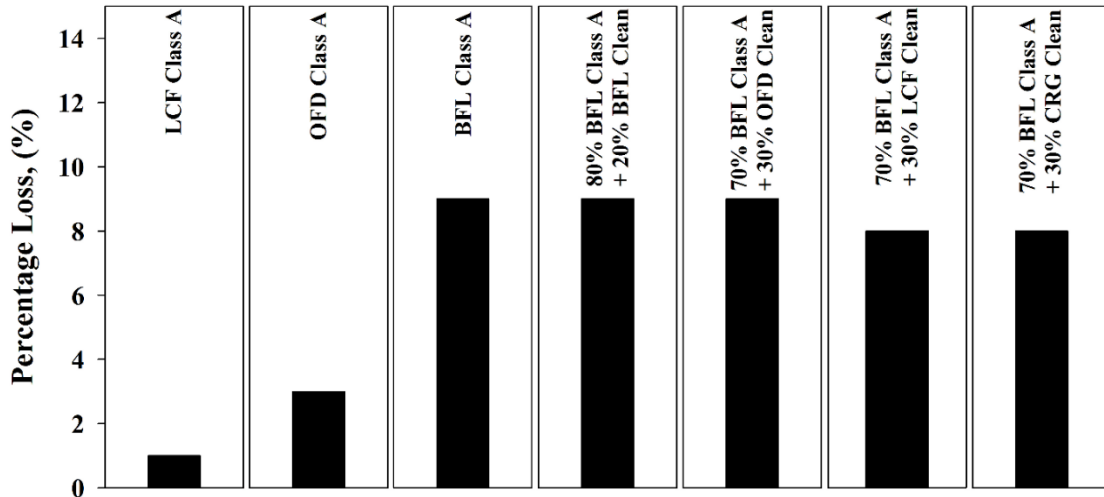


Figure 33. C-Freeze results

LCF Class A and OFD Class A had 1% and 3% loss, respectively, during the test. Loss of other surface materials were between 8% and 9%. BFL Class A had the highest loss (9%) indicating that local material had the least durability under freeze/thaw conditions. As a result, inclusion of BFL Class A in the surface materials makes the roadways more prone to abrasion during freezing and thawing. Overall, the results of C-Freeze tests showed that all surface materials met the Iowa DOT specification for granular roadways (<15%).

4.7 Gyrotory Compaction Test Results

Gyrotory compaction tests were conducted on the geomaterials of all seven granular road surfaces to evaluate the changes in dry unit weight (γ_{dry}) and shear resistance. Figure 34 shows the changes in the height of the specimens after 500 gyrations.

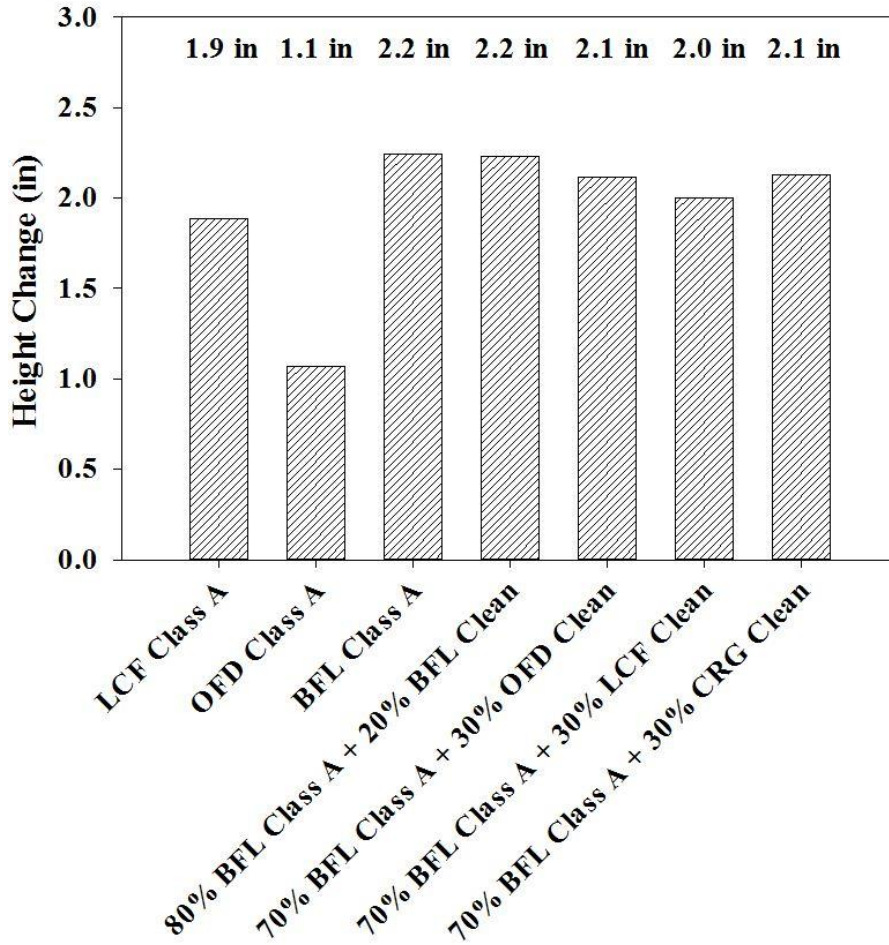


Figure 34. Height changes in the specimens after 500 gyrations

LCF Class A followed by OFD Class A had the minimum changes in the height, 1.1 in. and 1.9 in., respectively. However, the rest of the specimens, which have BFL Class A, had higher amounts of height loss (2 in. to 2.2 in.).

Figure 35 shows the increase in the γ_{dry} of the specimens after 500 gyrations.

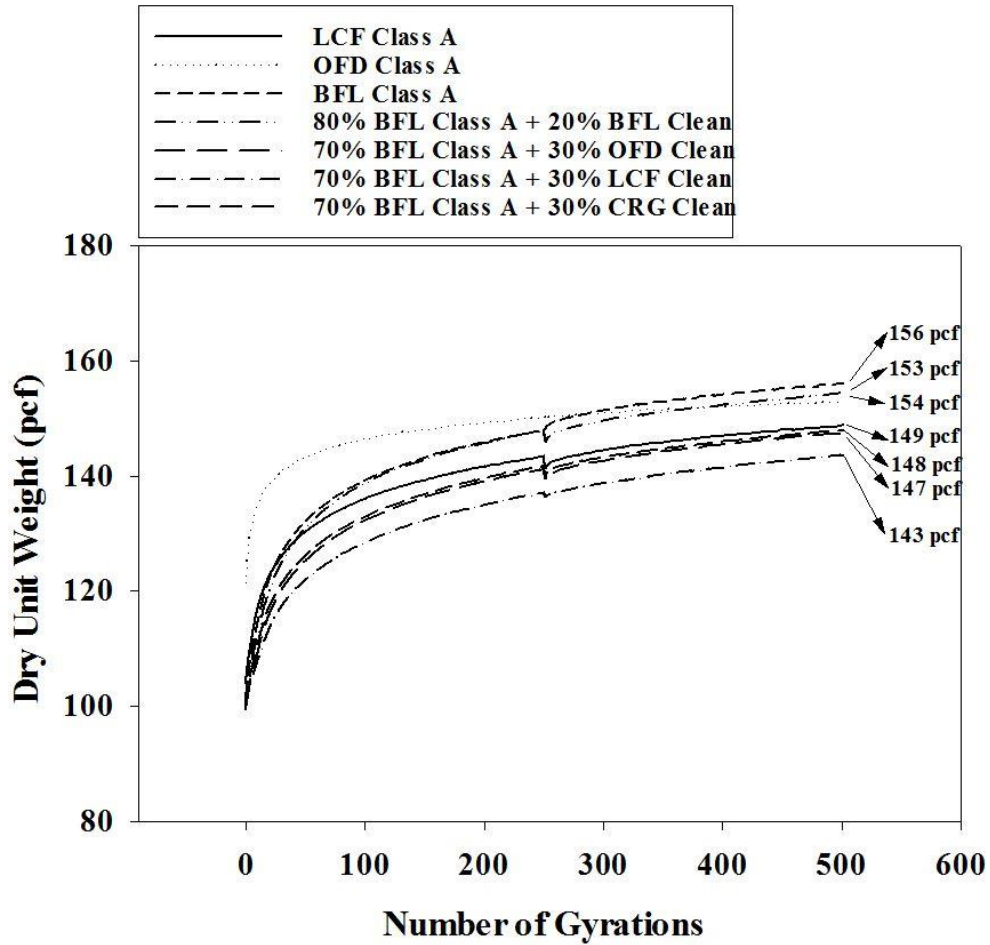


Figure 35. Dry unit weight (γ_{dry}) changes in the specimens after 500 gyrations

BFL Class A with 156 pcf had the maximum and 70% BFL Class A + 30% LCF Clean with 143 pcf had the minimum γ_{dry} . The increase in γ_{dry} was observed to be faster for OFD Class A while the decrease rate slowed down after 20 gyrations.

Figure 36 compares the γ_{dry} obtained from the Proctor test and gyratory tests.

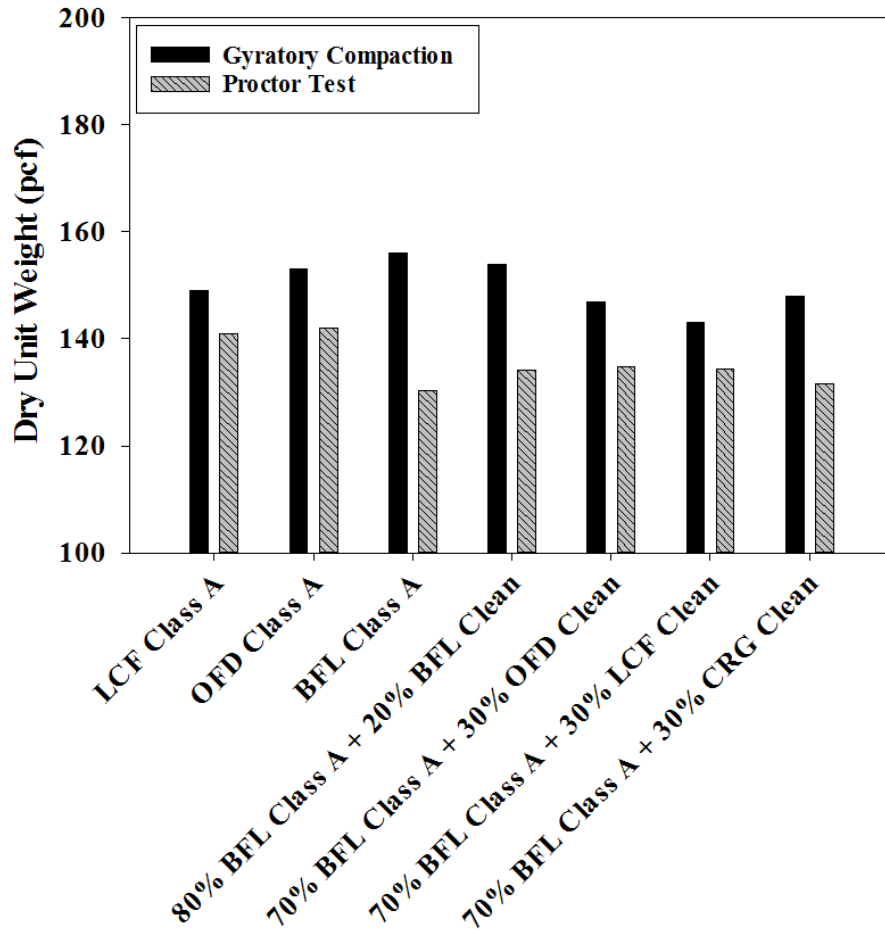


Figure 36. Comparison of the γ_{dMax} obtained from gyrotory and Proctor compaction tests

Results showed that the γ_{dmax} obtained through gyrotory compaction were higher for all materials than those determined via the Proctor compaction test. The reason for these results could be due to the higher energy levels applied on the specimens during gyrotory compaction process.

Figure 37 shows the change in the shear resistance (τ_G , pcf) and void ratio (e) in the specimens after 500 gyrations.

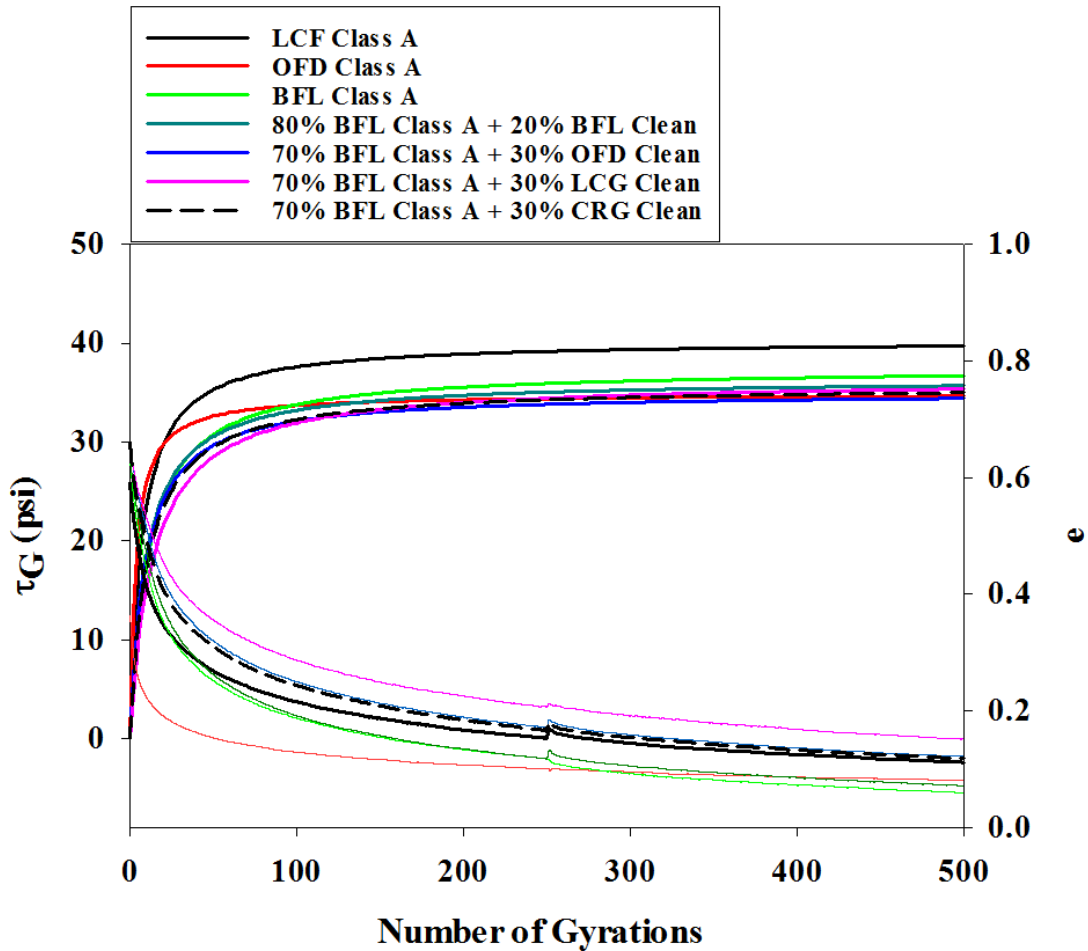


Figure 37. Change in the void ratio vs. shear resistance during gyratory test

The results showed that there was always a fluctuation in the shear resistance while the void ratio follows a gradual change. The reason for this behavior was reported to be the kneading-shearing mechanism induced by the gyratory test due to the change in aggregate coordinates and point-to-point contact between the aggregates during the test (Li et al. 2017b). Moreover, a small change in the void ratio after the first 250 gyrations (while the test was stopped) caused a tremendous change in the shear resistance for all materials.

Figure 38 shows the change in the particle-size distribution of each material after 500 gyrations.

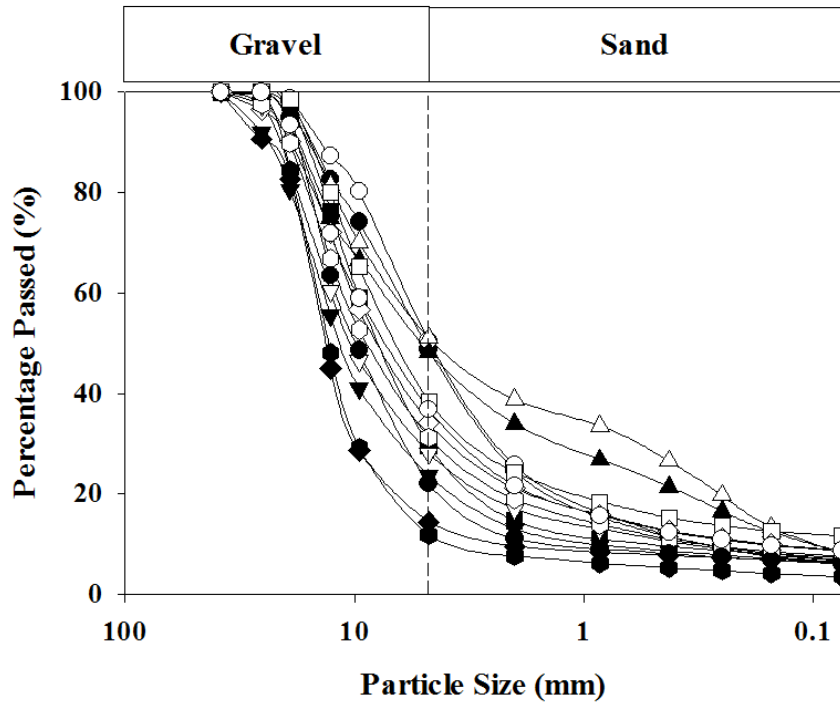
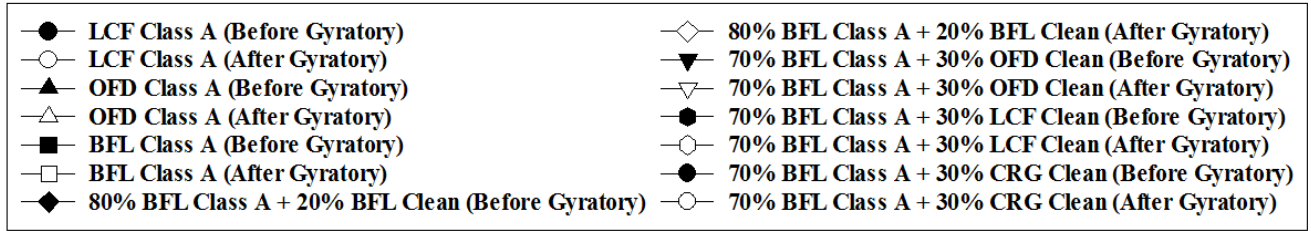


Figure 38. The change in particle-size distribution of materials after 500 gyrations

Results showed that the minimum change in particle-size distribution was observed for LCF Class A, followed by OFD Class A and 70% BFL Class A + 30% OFD Clean. The maximum changes in particle-size distributions were observed for 80% BFL Class A + 20% BFL Clean and 70% BFL Class A + 30% LCF Clean indicating that local BFL Class A has the worst resistance under gyratory loads.

Figure 39 shows the changes in the fines content of each granular roadway surface material after being subjected to 500 gyrations.

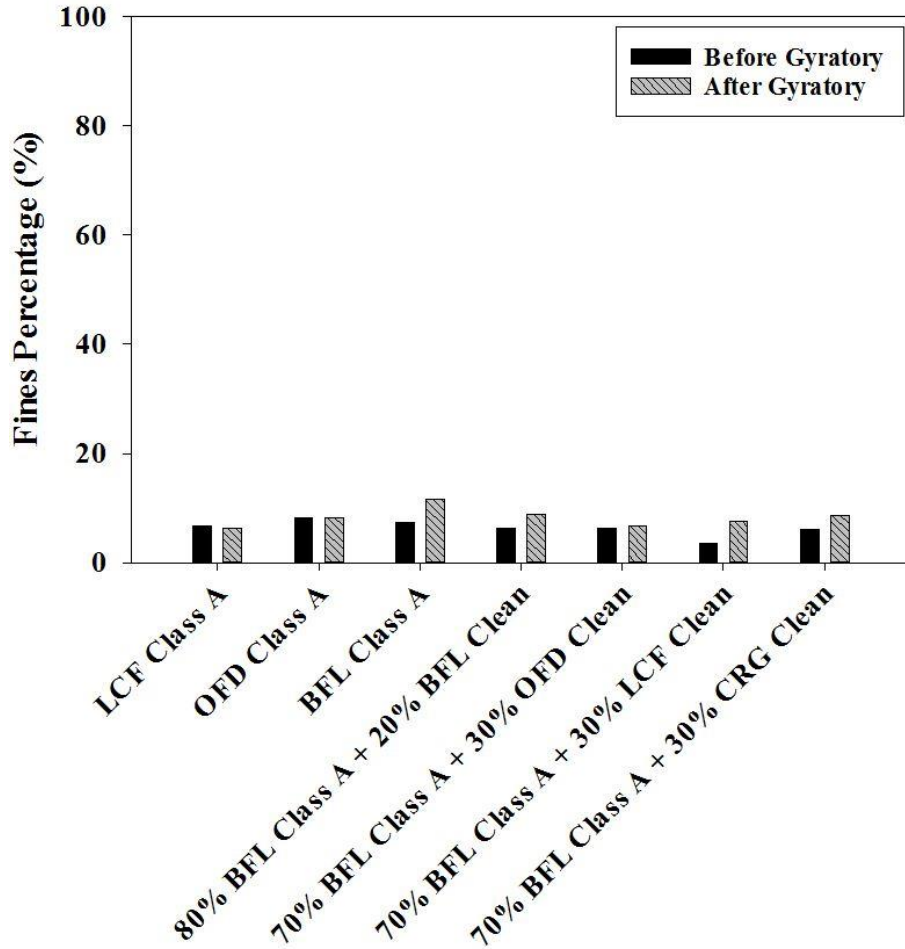


Figure 39. Fines content change in the materials after 500 gyrations

Results showed that the LCF Class A and OFD Class A had the smallest decrease in fines content, while the rest of the materials with BFL Class A inclusion experienced an increase in their corresponding fines content. The maximum increase in fines content was observed for the BFL Class A and 70% BFL Class A + 30% LCF Clean mixture.

Results showed that sand content of each material was increased after 500 gyrations. The maximum sand content increase was observed for 80% BFL Class A + 20% BFL Clean and 70% BFL Class A + 30% LCF Clean while the minimum increase was observed for LCF Class A and OFD Class A (Figure 40).

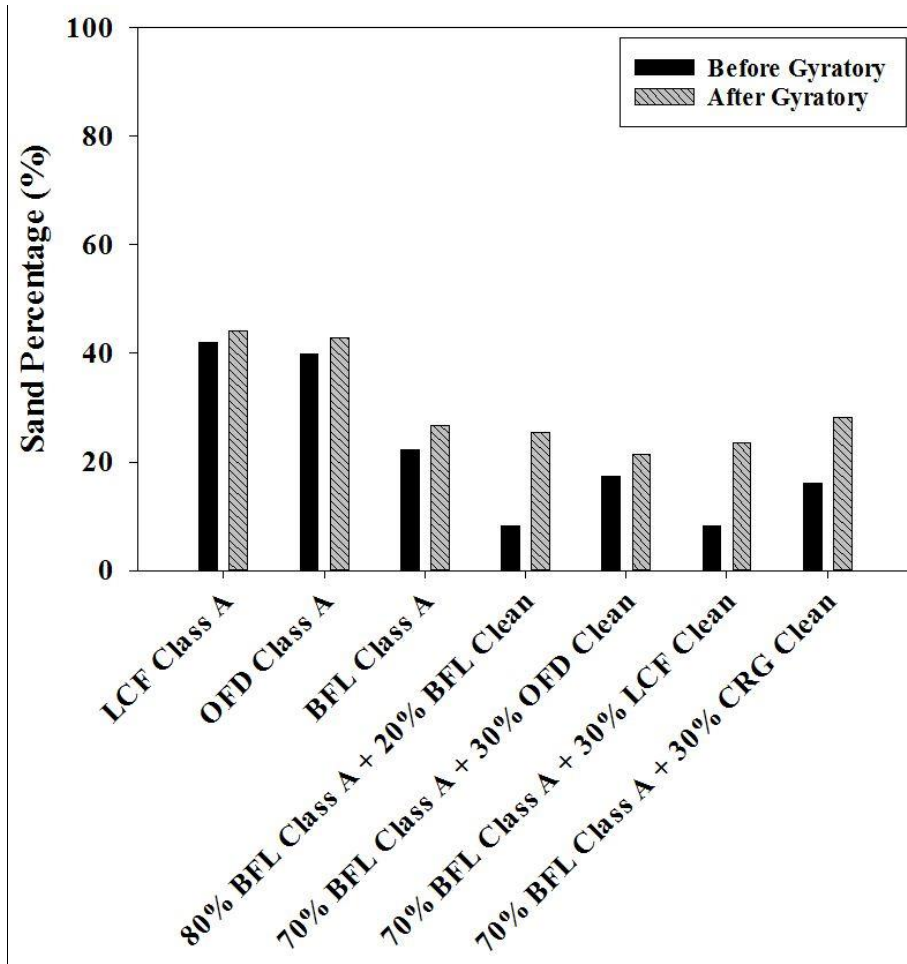


Figure 40. Sand content change of the materials after 500 gyrations

Gravel content was also decreased for all materials after being subjected to 400 gyrations. The maximum gravel content decrease was also observed for the 80% BFL Class A + 20% BFL Clean and the 70% BFL Class A + 30% LCF Clean, the same results as for the sand content. The minimum increase in gravel content was observed for LCF Class A, OFD Class A, and 70% BFL Class A + 30% OFD Clean (Figure 41).

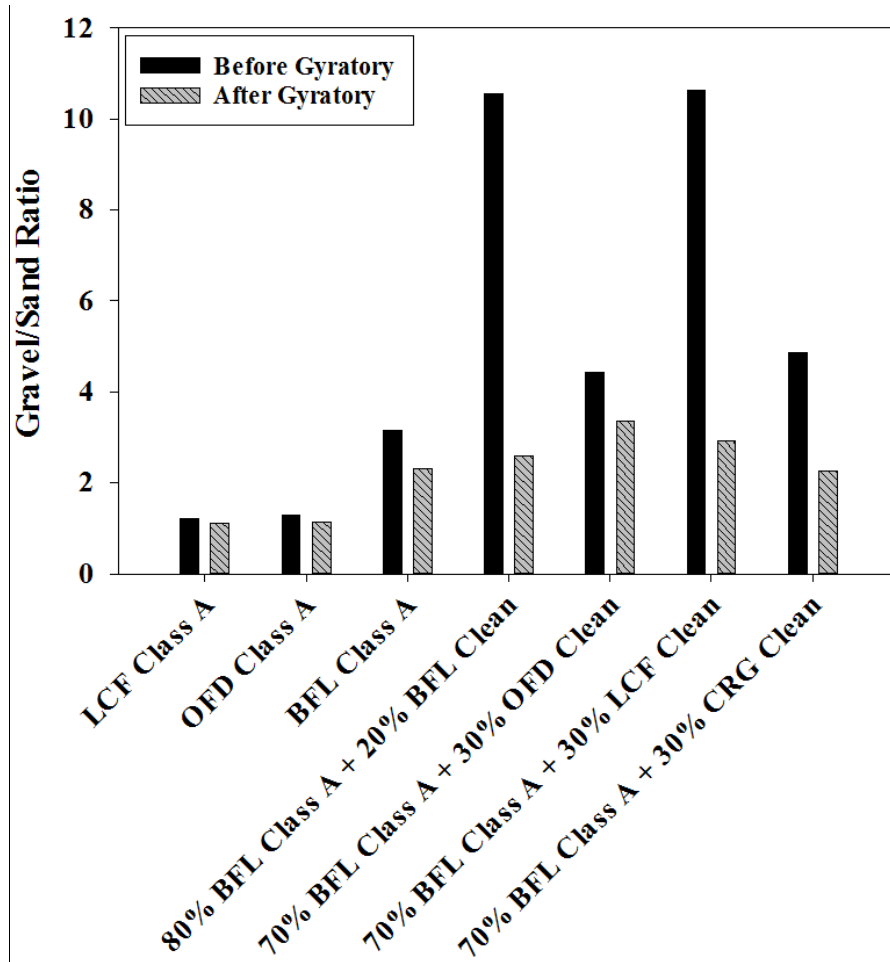


Figure 41. Gravel content change in the materials after 500 gyrations

Figure 42 shows the total breakage of the aggregate materials after 500 gyrations.

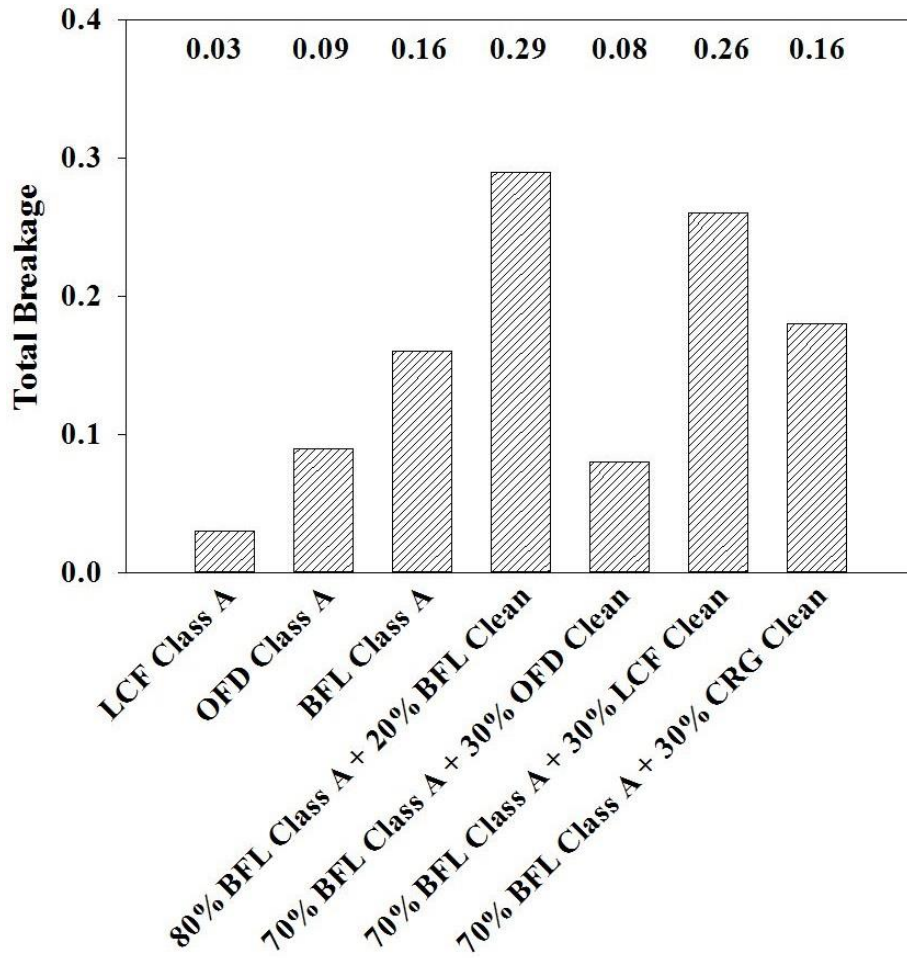


Figure 42. Total breakage calculated for each material after 500 gyrations

The maximum total breakage was observed for the 80% BFL Class A + 20% BFL Clean (0.29) and the 70% BFL Class A + 30% LCF Clean (0.26), while the minimum total breakage was observed for LCF Class A (0.03), OFD Class A (0.09), and 70% BFL Class A + 30% OFD Clean (0.08).

CHAPTER 5. CONSTRUCTION AND MAINTENANCE

5.1 Site Description

The test sites were located on CR J22 Popcorn Road, Decatur County, Iowa. Figure 43 represents the accessibility of the project location from I-35 south.



Figure 43. Directions to the project location from I-35 south

Figure 44 shows the schematic diagram of the locations of the test sections. Sections aimed to avoid being near private properties. Therefore, there was some distance between sections 2 and 3, 4 and 5, 5 and 6, and 6 and 7. The BFL Class A section was selected as a control section.

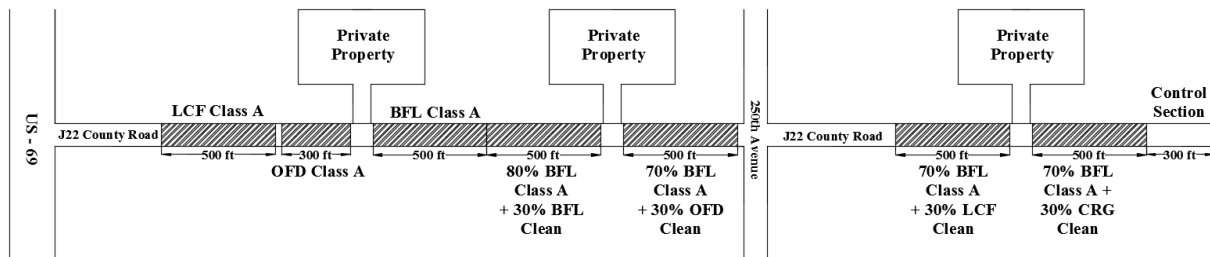


Figure 44. Schematic diagram of the locations of the test sections

The road width was 30 ft and built in seven sections. The granular road surface aggregate materials were compacted to achieve a final thickness of 4 in. (Figure 45).

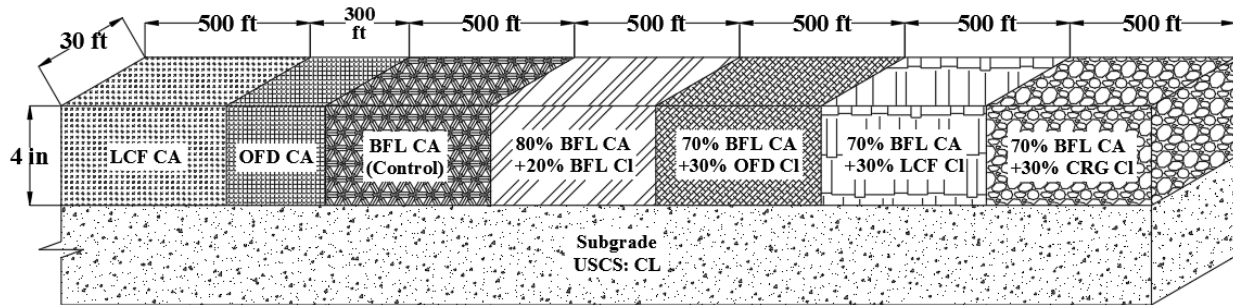


Figure 45. Schematic diagram of the test sections

The length of each section was 500 ft, while the second section length was 300 ft, due to the lack of material (OFD Class A). The research team conducted the field tests on five points for the seven sections. The first testing point was placed 50 ft from the beginning of the section, and the spacing between each point was 100 ft. However, due to the shorter length of the second section (OFD Class A), 50 ft was considered as the interval between the testing points.

DCP, FWD, MASW, APLT, and nuclear gauge tests were conducted at each testing point, and samples of the granular road surface materials were collected to monitor the changes in the gradation characteristics (fines content, gravel-to-sand ratio) and the breakage indices over time. Test sites were monitored from fall 2016 to spring 2019.

5.2 Construction

The existing (original) surface of the granular road was a chip seal layer (Figure 46), which was ripped off from the surface before the construction of test sections (Figure 47).



Figure 46. CR J22 before construction



Figure 47. Scraped surface of the roadway

In this regard, the scarifier blades, which were attached to the motor grader, were used to remove the existing materials from the surface. The removed materials then were dumped into trucks by a loader. Afterward, the top of the surface was compacted using a drum roller in order to have a uniform subgrade layer. Then, the specific aggregate materials for each section were brought by tandem-dump and bottom-dump trucks. The blading and compaction were performed to achieve a smooth road surface by using the motor grader and drum roller, respectively. Figure 48 summarizes the five steps of the construction.

Step 1	Hauling from quarry to piles	Truck
Step 2	Scraping the existing surface	Motor Grader
Step 3	Hauling from pile to site	Loader and Truck
Step 4	Blading	Motor Grader
Step 5	Compacting	Drum Roller

Figure 48. Construction steps

Photographs of the construction process are shown for each section in Appendix A. Details of the time spent for the labor and equipment for all sections are reported in Table 6.

Table 6. Labor and equipment hours for the construction

Sections	Labor (hr)	Grader (hr)	Tandem dump (hr)	Bottom dump (hr)	Drum roller (hr)
LCF Class A	66	16	21	7	5
OFD Class A	46	11	15	5	4
BFL Class A	66	16	21	7	5
80% BFL Class A + 20% BFL Clean	66	16	21	7	5
70% BFL Class A + 30% OFD Clean	66	16	21	7	5
70% BFL Class A + 30% LCF Clean	66	16	21	7	5
70% BFL Class A + 30% CRG Clean	66	16	21	7	5

5.3 Maintenance

Granular roadways in cold regions, such as Iowa, are prone to harsh surface deteriorations and distresses due to freezing and thawing. Figure 49 shows a few examples of these distresses, including potholes, rutting, and wash boarding.



Figure 49. Distress types on surface materials: (a) big pothole in middle of BFL Class A, (b) severe rutting in 80% BFL Class A + 20% BFL Clean, (c) scattered potholes in 70% BFL Class A + 30% LCF Clean, and (d) material movement 70% BFL Class A + 30% CRG

Blading is a common maintenance procedure for county engineers to make the roadway surface smooth and as convenient as possible for the drivers.

In order to determine the ride quality on the road surface after the freeze/thaw seasons (spring 2017 and spring 2018), a field survey was conducted in April 2017 and May 2018 to monitor the aggregate deteriorations. After the survey, samples from 10 different locations from each test section were collected for gradation analyses, and surface layer thickness measurements were conducted. The weight of the newly added materials were calculated based on the existing surface of the test sections to ensure that surface thickness went back to initial construction thickness (4 in.).

The maintenance procedure started with scraping the surface of each test section with the motor grader. Scarifier blades were used for the second section (OFD Class A) to scrape the surface, due to the stiffer surface of this section than the others. The new aggregate materials were brought from the piles and placed on each section accordingly. Then, the existing and new

aggregate materials were bladed to get the optimum mixture, and then the motor grader shaped the surface. In order to wheel compact the surfaces, the motor grader passed several times on the road surfaces. Table 7 shows a summary of the labor and equipment hours for the maintenance.

Table 7. Labor and equipment hours for the maintenance

Sections	Labor (hr)	Grader (hr)	Tandem dump (hr)	Loader (hr)
LCF Class A	10	3	6	2
OFD Class A	7	2	4	1
BFL Class A	10	3	6	2
80% BFL Class A + 20% BFL Clean	10	3	6	2
70% BFL Class A + 30% OFD Clean	10	3	6	2
70% BFL Class A + 30% LCF Clean	10	3	6	2
70% BFL Class A + 30% CRG Clean	10	3	6	2

Figure 50 shows the equipment used for construction and maintenance.



Figure 50. Equipment used: (a) motor grader for blading, (b) dump trucks, (c) loader for collection the existing chip seal layer, and (d) vibratory roller for compaction

5.4 Quality Assurance and Quality Control

Quality assurance (QA) and quality control (QC) were performed on the sections during and after construction and maintenance. In that regard, the required thickness, moisture content, and the quality of the compaction were monitored and controlled by visual observation and the experience of the county engineers and crew.

The thickness of the surfaces was checked immediately after dumping the aggregate materials, blading, and compacting the granular roadway surface. Accordingly, a ruler was pushed to the surface at several points of each section in the middle and the shoulders of the road to ensure that the thickness of the compacted granular road surface was 4 in. Moisture contents were measured via nuclear density gauge and adjusted accordingly.

To ensure adequate compaction, a drum roller and wheel compaction with a motor grader were used, respectively, for construction and maintenance.

CHAPTER 6. RESULTS AND DISCUSSION

6.1 Gradation Change

In order to monitor the material deterioration over time, samples were collected at different times, and sieve analysis was performed on each sample. The materials were collected from between the surface and the top of the subgrade layer from five points in each section. Then, the samples were combined and one sample was used to perform sieve analyses per each section. Particle-size distribution curves of each surface material sample collected from seven sections over time are shown in Appendix B. The change in fines content, gravel-to-sand ratio, and total breakage, were calculated to evaluate the change in each surface material over time from September 2016 to May 2019 (Figures 51–53).

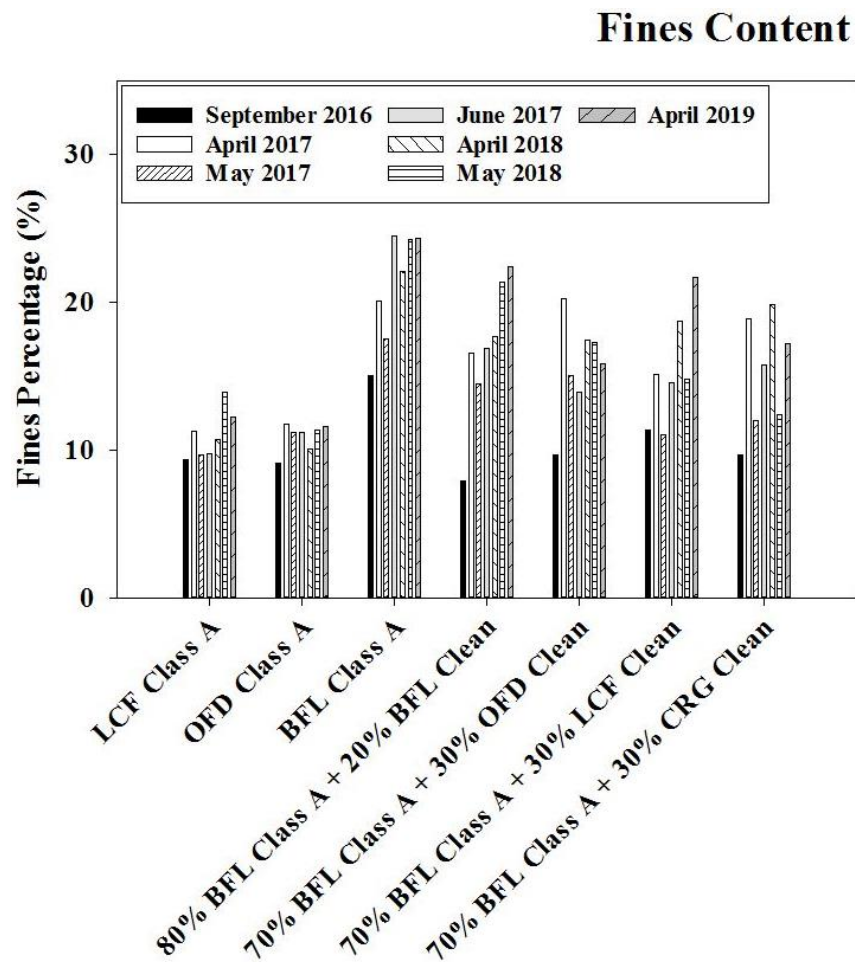


Figure 51. Fines content change of materials over time

Gravel to Sand Ratio

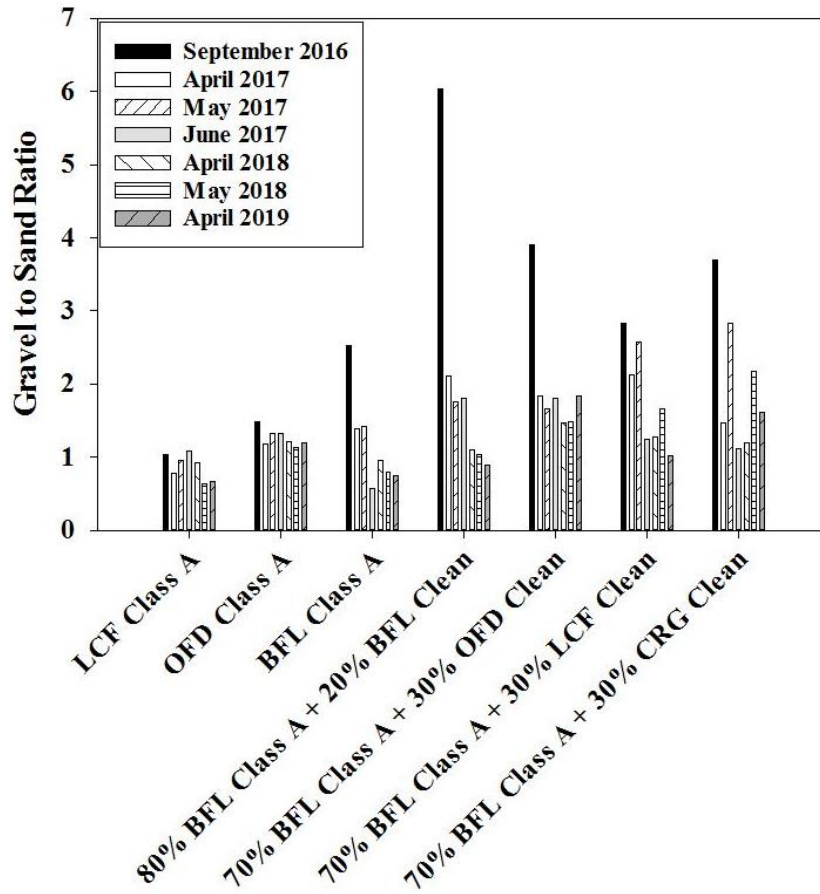


Figure 52. Gravel-to-sand ratio changes of all materials over time

Total Breakage

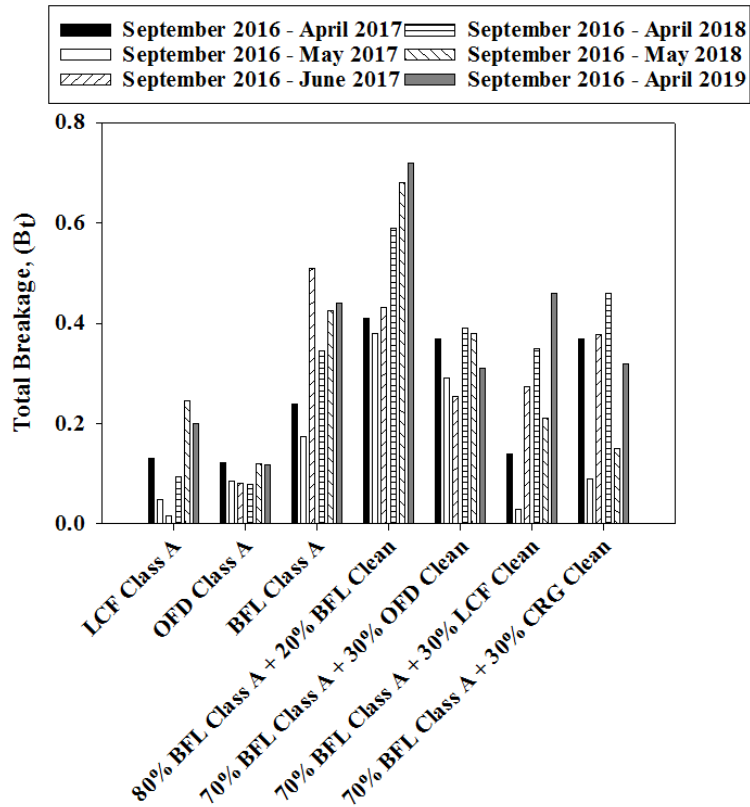


Figure 53. Total breakage change of all materials over time

Moreover, the changes in the values of the fines content and gravel-to-sand ratio, from September 2016 to April 2019, are also shown in detail in Tables 8 and 9.

Table 8. Fine content change for all section over time

Sections	Fines content						
	Sep-16	Apr-17	May-17	Jun-17	Apr-18	May-18	Apr-19
LCF Class A	9	11	10	10	11	14	12
OFD Class A	9	12	11	11	10	11	12
BFL Class A	15	20	18	24	22	24	24
80% BFL Class A + 20% BFL Clean	8	17	14	17	18	21	22
70% BFL Class A + 30% OFD Clean	10	20	15	14	17	17	16
70% BFL Class A + 30% LCF Clean	11	15	11	15	19	15	22
70% BFL Class A + 30% CRG Clean	10	19	12	16	20	12	17

Table 9. Gravel-to-sand ratio changes for all sections over time

Sections	Gravel-to-sand ratio						
	Sep-16	Apr-17	May-17	Jun-17	Apr-18	May-18	Apr-19
LCF Class A	1.0	0.8	1.0	1.1	0.9	0.6	0.7
OFD Class A	1.5	1.2	1.3	1.3	1.2	1.1	1.2
BFL Class A	2.5	1.4	1.4	0.6	1.0	0.8	0.7
80% BFL Class A + 20% BFL Clean	6.0	2.1	1.8	1.8	1.1	1.0	0.9
70% BFL Class A + 30% OFD Clean	3.9	1.8	1.7	1.8	1.5	1.5	1.8
70% BFL Class A + 30% LCF Clean	2.8	2.1	2.6	1.3	1.3	1.7	1.0
70% BFL Class A + 30% CRG Clean	3.7	1.5	2.8	1.1	1.2	2.2	1.6

The variations in the fines content for LCF Class A (9 to 14%) and the OFD Class A (9 to 12%) were the lowest. However, the rest of the sections, which were built with BFL Class A, showed higher variations in fines content over time (Figure 52 and Table 8). Moreover, the lowest fines content change was observed for LCF Class A and OFD Class A. Within the mixtures, the 80% BFL Class A + 20% BFL Clean mixture experienced the highest increase in fines content over the three-year period, while the 70% BFL Class A + 30% Clean OFD had the lowest fines content increase.

Figure 52 and Table 9 show the changes of the gravel-to-sand ratio values over time. Gravel-to-sand ratios of all materials were the highest right after construction, when none of the sections had been exposed to high volume of traffic yet. The minimum variations in the gravel-to-sand ratio were observed for OFD Class A (1.2 to 1.5) and LCF Class A (0.6 to 1.1). However, the rest of the sections, which included BFL Class A, experienced a decrease in their gravel-to-sand ratios over time (Figure 52 and Table 9). Moreover, the highest gravel-to-sand ratio was observed for 80% BFL Class A + 20% BFL Clean after the construction where the maximum size of the aggregate was 1.5 in., while for the rest of the sections this value was 1 in. Figure 52 shows that 80% BFL Class A + 20% BFL Clean experienced the highest decrease in gravel-to-sand ratio. The mixture of 70% BFL Class A + 30% OFD Clean seemed to be the most stable in terms of keeping the gravel-to-sand ratio constant over time.

Figure 53 and Table 10 show the total breakage changes of the aggregate materials over the time of the project. The maximum total breakage was observed for the 80% BFL Class A + 20% BFL Clean, where the top size aggregate material was higher than those of others (1.5 in.). The minimum total breakage change was observed for OFD Class A (0.08 to 0.12), while the maximum change in total breakage was observed for 70% BFL Class A + 20% BFL Clean.

Table 10. Total breakage changes for all sections over time

Sections	Total breakage					
	Sep-16– Apr-17	Sep-16– May-17	Sep-16– Jun-17	Sep-16– Apr-18	Sep-16– May-18	Sep-16– Apr-19
LCF Class A	0.13	0.05	0.02	0.10	0.25	0.20
OFD Class A	0.12	0.09	0.08	0.08	0.12	0.12
BFL Class A	0.24	0.17	0.51	0.35	0.43	0.44
80% BFL Class A + 20% BFL Clean	0.41	0.38	0.43	0.59	0.68	0.72
70% BFL Class A + 30% OFD Clean	0.37	0.29	0.25	0.39	0.38	0.31
70% BFL Class A + 30% LCF Clean	0.14	0.03	0.27	0.35	0.21	0.46
70% BFL Class A + 30% CRG Clean	0.37	0.09	0.38	0.46	0.15	0.32

6.1.1 September 2016 (Construction)

The sample collection started in September 2016, immediately after the construction of test sections. Sieve analyses were performed on the samples. Based on the results of the sieve analyses, the fines content of the surface aggregate materials were in the range of 8 to 15%, where the minimum fines content was for the 80% BFL Class A + 20% BFL Clean section and the BFL Class A had the highest fines content. In addition, the gravel-to-sand ratio values ranged from 1 to 6 for LCF Class A and 80% BFL Class A + 20% BFL Clean, respectively. The breakage potential values ranged from 1.56 to 2, where the minimum breakage potential is for OFD Class A, and the maximum breakage potential is for 80% BFL Class A + 20% BFL Clean.

6.1.2 April 2017

The second sample collection was carried out after the first winter season, in April 2017, in order to monitor the effects of freezing and thawing on the surface materials. Fines contents for all test sections increased in the range of 21 to 109%, where the minimum increase was observed for the LCF Class A section, and the maximum increase for the 80% BFL Class A + 20% BFL Clean section. However, gravel-to-sand ratios for all surface materials decreased from 21% to 65%. The maximum gravel-to-sand ratio decrease was observed for 80% BFL Class A + 20% BFL Clean, and the minimum change was observed for OFD Class A. The breakage potential values for all sections decreased from 8% to 20% for OFD Class A and 80% BFL Class A + 20% BFL Clean, respectively (Table 11).

Table 11. Fines content, gravel-to-sand ratio, and breakage potential changes of all sections in April 2017

Sections	April 2017		
	Fines content (%)	Gravel/Sand (%)	Breakage potential (%)
LCF Class A	21	-25	-8
OFD Class A	29	-21	-8
BFL Class A	33	-45	-15
80% BFL Class A + 20% BFL Clean	109	-65	-20
70% BFL Class A + 30% OFD Clean	109	-53	-20
70% BFL Class A + 30% LCF Clean	33	-25	-8
70% BFL Class A + 30% CRG Clean	95	-60	-20

6.1.3 May 2017 (Maintenance)

Maintenance was first conducted in May 2017 to reshape the surfaces and arrange the PSD of the surface materials as close as possible to the target gradation. Accordingly, new aggregate materials were placed on top of the surfaces and were mixed and compacted with the existing aggregate materials by the motor grader. The fines contents of test sections only decreased by 3% for the 70% BFL Class A + 30% LCF Clean after the addition of coarser aggregates. Fines contents of all other sections were higher than their initial fines contents (September 2016). Gravel-to-sand ratio change was between 0.96 and 2.58 for LCF Class A and 70% BFL Class A + 30% CRG Clean, respectively. The percent change in gravel-to-sand ratio was between -7% for the LCF Class A and -71% for the 80% BFL Class A + 20% LCF Clean. Gravel-to-sand ratios changed between 1.52 and 1.72 for the LCF Class A, the 70% BFL Class A + 30% LCF Clean, and the 70% BFL Class A + 30% CRG Clean. The lowest change in gravel-to-sand ratio from initial condition was for the 70% BFL Class A + 30% LCF Clean, with -2% and the highest change in gravel-to-sand ratio was for the 80% BFL Class A + 20% BFL Clean with -19%. Breakage potentials of the surface materials after the first maintenance were also lower than those for all sections after construction.

Table 12 shows the results of the sample testing in May 2017.

Table 12. Fines content, gravel-to-sand ratio, and breakage potential changes in May 2017

Sections	May 2017		
	Fines content (%)	Gravel/Sand (%)	Breakage potential (%)
LCF Class A	3	-7	-3
OFD Class A	23	-11	-6
BFL Class A	16	-44	-11
80% BFL Class A + 20% BFL Clean	83	-71	-19
70% BFL Class A + 30% OFD Clean	56	-58	-16
70% BFL Class A + 30% LCF Clean	-3	-9	-2
70% BFL Class A + 30% CRG Clean	24	-23	-5

6.1.4 June 2017

In order to monitor changes in the gradation properties of surface materials one month after the maintenance, another sample collection was performed in June 2017. The fines content for the BFL Class A section, the 70% BFL Class A + 30% LCF Clean, and the 70% BFL Class A + 30% CRG Clean changed significantly since maintenance, where it increased 40%, 31%, and 31%, respectively. Likewise, the gravel-to-sand ratios decreased significantly for the BFL Class A section (60%), the 70% BFL Class A + 30% LCF Clean (51%), and the 70% BFL Class A + 30% CRG Clean (61%), while the changes in the gravel-to-sand ratio for other sections was negligible. Moreover, the breakage potential was notably changed just for the aforementioned sections, where the breakage potential decreased 23% for the BFL Class A section, 14% for the 70% BFL Class A + 30% LCF Clean, and 17% for the 70% BFL Class A + 30% CRG Clean.

Table 13 shows the results of the sample testing in June 2017.

Table 13. Fines content, gravel-to-sand ratio, and breakage potential changes in June 2017

Sections	June 2017		
	Fines content (%)	Gravel/Sand (%)	Breakage potential (%)
LCF Class A	1	13	2
OFD Class A	0	1	0
BFL Class A	40	-60	-23
80% BFL Class A + 20% BFL Clean	16	2	-3
70% BFL Class A + 30% OFD Clean	-7	10	3
70% BFL Class A + 30% LCF Clean	31	-51	-14
70% BFL Class A + 30% CRG Clean	31	-61	-17

6.1.5 April 2018

In order to monitor the changes in the material properties after the second freeze/thaw period, samples were collected from the sections in April 2018, and sieve analyses were performed. The fines contents of the 70% BFL Class A + 30% LCF Clean (69%) and the 70% BFL Class A + 30% CRG Clean (65%) changed significantly after maintenance. However, the OFD Class A had a decrease in its fines content. The gravel-to-sand ratios of all materials decreased since the first maintenance, ranging from 4% to 58%. The minimum and maximum changes in the gravel-to-sand ratios for this period were observed for LCF Class A and 70% BFL Class A + 30% CRG Clean, respectively. The breakage potentials for all sections decreased with the exception of OFD Class A. The maximum decrease in the breakage potential was observed for 70% BFL Class A + 30% CRG Clean.

Table 14 shows the results of the sample testing in April 2018.

Table 14. Fines content, gravel-to-sand ratio, and breakage potential changes in April 2018

Sections	April 2018		
	Fines content (%)	Gravel/Sand (%)	Breakage potential (%)
LCF Class A	11	-4	-3
OFD Class A	-10	-8	1
BFL Class A	26	-32	-12
80% BFL Class A + 20% BFL Clean	22	-38	-13
70% BFL Class A + 30% OFD Clean	16	-12	-6
70% BFL Class A + 30% LCF Clean	69	-50	-18
70% BFL Class A + 30% CRG Clean	65	-58	-22

6.1.6 May 2018

Another sample collection was implemented in May 2018 after maintenance completed in April 2018. The results of the sieve analyses showed that the fines contents of all sections since spring 2017 (maintenance) increased while the gravel-to-sand ratios and the breakage potentials decreased as expected. OFD Class A had the minimum and 80% BFL Class A + 20% BFL Clean had the maximum changes in the fines content, gravel-to-sand ratios, and the breakage potentials among all of the sections.

Table 15 shows the results of the sample testing in May 2018.

Table 15. Fines content, gravel-to-sand ratio, and breakage potential changes in May 2018

Sections	May 2018		
	Fines content (%)	Gravel/Sand (%)	Breakage potential (%)
LCF Class A	44	-35	-13
OFD Class A	1	-14	-2
BFL Class A	39	-43	-17
80% BFL Class A + 20% BFL Clean	48	-41	-19
70% BFL Class A + 30% OFD Clean	15	-10	-5
70% BFL Class A + 30% LCF Clean	34	-36	-11
70% BFL Class A + 30% CRG Clean	3	-23	-4

6.1.7 Comparisons between the Sections over Time

Table 16 shows the comparison between the mean values and the standard deviations of the results of the fines contents, gravel-to-sand ratios, breakage potentials, total breakages, and breakage ratios over the three years during which samples were collected.

Table 16. Mean value and the standard deviations of fines content, gravel-to-sand ratio, breakage potential and total breakage of all sections

Sections	Fines content (%)		Gravel/Sand		Breakage potential		Total breakage	
	Mean	SD	Mean	SD	Mean	SD	Mean	SD
LCF Class A	11	1.65	0.87	0.18	1.47	0.09	0.13	0.09
OFD Class A	11	0.96	1.27	0.12	1.47	0.04	0.10	0.02
BFL Class A	21	3.73	1.20	0.67	1.32	0.18	0.36	0.13
80% BFL Class A + 20% BFL Clean	17	4.79	2.11	1.79	1.54	0.25	0.54	0.15
70% BFL Class A + 30% OFD Clean	16	3.32	1.99	0.86	1.55	0.13	0.33	0.06
70% BFL Class A + 30% LCF Clean	15	3.80	1.82	0.70	1.54	0.17	0.24	0.15
70% BFL Class A + 30% CRG Clean	15	3.83	2.01	0.96	1.55	0.17	0.30	0.14

6.1.8 Fines Content

The maximum average fines content change was observed for BFL Class A (21%), while the minimum average fines content change was observed for LCF Class A and OFD Class A (11%). The presence of BFL Class A was the main reason for higher fines content changes in other sections. The maximum standard deviation of the fines content was observed for 80% BFL Class A + 20% BFL Clean, while the minimum standard deviation was observed for OFD Class A (4.79). Sections with BFL Class A generally had higher standard deviations compared to the first two sections without BFL Class A. This may be due to the deterioration of BFL Class A, which showed lower abrasion resistance (Table 16).

6.1.9 April 2019

In order to monitor the changes in the material properties after the third freeze/thaw period, samples were collected from the sections in April 2019, and sieve analyses were performed on them. The fines content of all sections increased significantly, especially for 70% BFL Class A + 30% LCF Clean (96%). The minimum change in the fines content was observed for OFD Class A (3%). The gravel-to-sand ratios decreased for all sections since the last maintenance (spring 2018) in the range of 9% to 60%, except for 70% BFL Class A + 30% OFD Clean, which had an 11% increase in the gravel-to-sand ratio. The minimum and maximum changes in the gravel-to-sand ratios since the first maintenance (May 2017) were for OFD Class A (-9%) and 70% BFL Class A + 30% LCF Clean (-60%), respectively. The breakage potentials for all of the sections decreased, where the maximum decrease was observed for 70% BFL Class A + 30% LCF Clean (25%), and the minimum decrease was observed for 70% BFL Class A + 30% OFD Clean (1%).

Table 17 shows the results of the sample testing in April 2019.

Table 17. Fines content, gravel-to-sand ratio, and breakage potential changes in April 2019

Sections	April 2019		
	Fines content (%)	Gravel/Sand (%)	Breakage potential (%)
LCF Class A	27	-31	-10
OFD Class A	3	-9	-2
BFL Class A	39	-48	-18
80% BFL Class A + 20% BFL Clean	55	-49	-21
70% BFL Class A + 30% OFD Clean	5	11	-1
70% BFL Class A + 30% LCF Clean	96	-60	-25
70% BFL Class A + 30% CRG Clean	43	-43	-13

6.1.10 Gravel-to-Sand Ratio

The maximum average gravel-to-sand ratio changes were observed for the 80% BFL Class A + 20% BFL Clean (2.11), which had the highest aggregate top size. On the other hand, the minimum gravel-to-sand ratio change was for the LCF Class A (0.87). The mixture of 80% BFL Class A + 20% BFL Clean had the highest standard deviation (1.79). This could be due to the breakage of the BFL Class A and BFL Class A + BFL Clean mixture over time. On the other hand, the lowest standard deviation was observed for the OFD Class A (0.12) (Table 16).

6.1.11 Breakage Potential

The average breakage potential values for the mixture sections (1.54~1.55) were higher than those with Class A aggregates (1.32 to 1.47). BFL Class A had the minimum breakage potential (1.32) due to the presence of the higher fines content. The 80% BFL Class A + 20% BFL Clean mixture had the highest (0.25) and the OFD Class A had the lowest (0.04) standard deviation of breakage potential over the past three years.

The maximum and minimum average total breakages were observed, respectively, for the 80% BFL Class A + 20% BFL Clean (0.54) and the OFD Class A (0.10). The 80% BFL Class A + 20% BFL Clean and 70% BFL Class A + 30% LCF Clean mixtures had the highest (0.15) and OFD Class A had the lowest (0.02) standard deviation of the total breakage over the project period (Table 16).

6.2 Nuclear Density Gauge Tests

In order to determine the in situ wet and dry densities and water content of the surface materials, nuclear gauge tests were performed in October 2016, May 2018, and April 2019 on 38 testing points in total, and the results are shown in Figures 54–56.

Table 18. Nuclear gauge results for dry density, wet density, and water content

Sections	October 2016			May 2018			April 2019		
	γ_w (pcf)	γ_d (pcf)	ω (%)	γ_w (pcf)	γ_d (pcf)	ω (%)	γ_w (pcf)	γ_d (pcf)	ω (%)
LCF Class A	128	131	4	127	122	5	138	133	4
OFD Class A	130	136	5	122	116	7	137	131	4
BFL Class A	123	131	7	128	121	6	137	129	6
80% BFL Class A + 20% BFL Clean	124	131	6	129	123	5	141	135	5
70% BFL Class A + 30% OFD Clean	122	130	6	127	120	6	140	133	6
70% BFL Class A + 30% LCF Clean	120	126	5	137	131	5	140	133	5
70% BFL Class A + 30% CRG Clean	117	123	5	134	127	6	140	132	6

The nuclear gauge test results are discussed in the following sections.

6.2.1 October 2016

The first set of nuclear gauge tests was performed after construction in October 2016. The maximum dry density (140 pcf) and wet density (132 pcf) were observed on the OFD Class A section. On the other hand, the minimum dry density (123 pcf) and wet density (117 pcf) were measured for the 70% BFL Class A + 30% CRG Clean. The water content values ranged between 4% (LCF Class A) and 7% (BFL Class A).

6.2.2 May 2018

The second set of nuclear gauge tests was conducted after the second freeze/thaw season in May 2018. The highest dry density (131 pcf) and wet density (137 pcf) were observed on the 70% BFL Class A + 30% LCF Clean section. The lowest dry (116 pcf) and wet (122 pcf) densities were for the OFD Class A. The water content values ranged between 5% (LCF Class A) and 7% (OFD Class A).

6.2.3 April 2019

The third set of nuclear gauge tests was conducted after the second freeze/thaw season in April 2019. The highest dry density (135 pcf) and wet density (141 pcf) were observed on 80% BFL Class A + 20% BFL Clean. The lowest dry (129 pcf) and wet (137 pcf) densities were for the BFL Class A. The water content values ranged between 4% (LCF Class A and OFD Class A) and 8% (BFL Class A, 80% BFL Class A + 20% BFL Clean, and 70% BFL Class A + 30% CRG Clean).

Nuclear gauge measured the water content and wet density of the surface layers, and the dry density was calculated accordingly. This test was done three times in October 2016, May 2018, and April 2019. The results showed that the water content did not change significantly for all sections. In addition, dry and wet density values of the surface layers were relatively higher in April 2019.

6.3 DCP Test Results

DCP tests were conducted to determine the shear strength of the surface and subgrade layers. They were conducted in October 2016, November 2016, April 2017, June 2017, May 2018, and April 2019. Moreover, the thickness of the surface layer could be determined, where the cumulative blows versus cumulative depth has a sudden slope shift, and the thickness is considered both in FWD and MASW back-calculation analyses. The cumulative blows, DCPI, and correlated CBR values versus the cumulative depth for all of the testing points of the field sections are presented in figures in this section, based on the time of conducting the tests. In order to evaluate the conditions of the surface and subgrade layers according to their weighted average CBR values, a relative rating system was utilized, in accordance with the “Statewide Urban Design and Specification Design Manual”(SUDAS 2015) and it is shown in Table 19.

Table 19. Relative ratings of subbase and subgrade layers based on CBR values

CBR (%)	Material	Rating
> 80	Subbase	Excellent
50–80	Subbase	Very good
30–50	Subbase	Good
20–30	Subgrade	Very good
10–20	Subgrade	Fair to good
5–10	Subgrade	Poor to fair
<5	Subgrade	Very poor

Source: Statewide Urban Design and Specifications (SUDAS) 2015

Results of the DCP tests showed that the surface thickness for all of the sections was in the range of 7 to 10 in. DCP-CBR values for the subgrade were very close for all the sections (6 to 10%). The mixtures of 80% BFL Class A + 20% BFL Clean and 70% BFL Class A + 30% CRG Clean had, respectively, the highest and lowest DCP-SCR values for the surface layer.

6.3.1 October 2016

The DCP test in October 2016 was performed in order to investigate the as constructed values of the thickness of the surface and the CBR values of the surface and subgrade layers. The results are briefly shown in Table 20, while the cumulative blows, DCPI, and correlated CBR values versus the cumulative depth for the first section is shown in Figure 57.

Table 20. DCP results of thickness for the surface, surface and subgrade CBR, and rating in October 2016

Sections October 2016	Thickness (in.)		CBR (%)		Rating	
	Surface	Subgrade	Surface	Subgrade	Surface	Subgrade
LCF Class A	9	Inf	89	5	Excellent	Very poor
OFD Class A	8	Inf	86	9	Excellent	Poor-fair
BFL Class A	9	Inf	85	8	Excellent	Poor-fair
80% BFL Class A + 20% BFL Clean	5	Inf	99	10	Excellent	Poor-fair
70% BFL Class A + 30% OFD Clean	6	Inf	104	10	Excellent	Poor-fair
70% BFL Class A + 30% LCF Clean	6	Inf	55	8	Very good	Poor-fair
70% BFL Class A + 30% CRG Clean	6	Inf	48	9	Good	Poor-fair

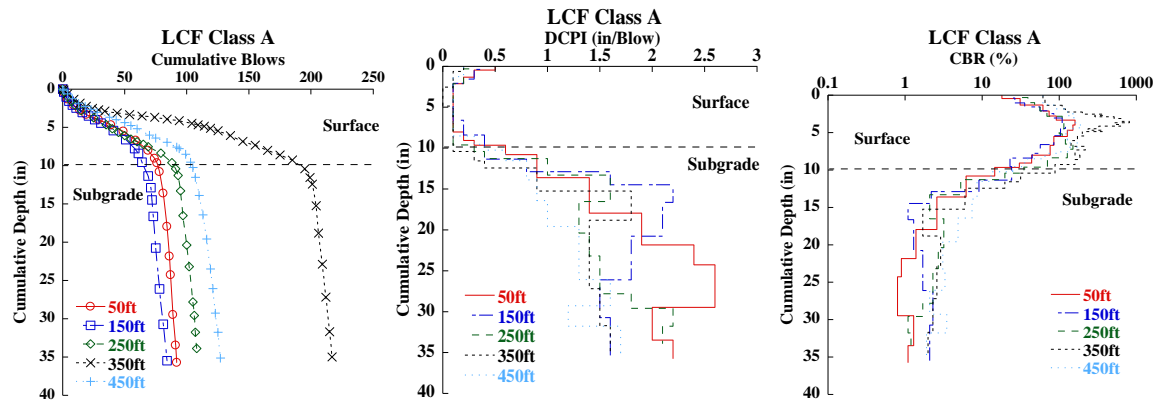


Figure 57. Cumulative blows, DCPI, and correlated CBR versus cumulative depth for the first section

The 70% BFL Class A + 30% LCF Clean and 70% BFL Class A + 30% CRG Clean had the minimum surface DCP-CBR values after construction. According to the SUDAS, all of the surfaces rated excellent except the 70% BFL Class A + 30% LCF Clean and the 70% BFL Class A + 30% CRG Clean, which were rated, respectively, as very good and good. The subgrade DCP-CBR values for all sections were rated poor-to-fair, except the LCF Class A subgrade, which had a rating of very poor.

6.3.2 November 2016

The DCP test in November 2016 was also performed in order to evaluate the changes in the values of the thickness for the surface and the CBR values of the surface and subgrade layers, in the one month since construction. The results of thickness, CBR values, and rating are briefly shown in Table 21, while the cumulative blows, DCPI, and correlated CBR values versus the cumulative depth for all of the testing points are shown in Appendix C.

Table 21. DCP results of thickness for the surface, surface and subgrade CBR and rating in November 2016

Sections November 2016	Thickness (in.)		CBR (%)		Rating	
	Surface	Subgrade	Surface	Subgrade	Surface	Subgrade
LCF Class A	9	Inf	111	5	Excellent	Poor-Fair
OFD Class A	8	Inf	78	8	Very Good	Poor-Fair
BFL Class A	9	Inf	63	6	Very Good	Poor-Fair
80% BFL Class A + 20% BFL Clean	6	Inf	86	6	Excellent	Poor-Fair
70% BFL Class A + 30% OFD Clean	6	Inf	74	7	Very Good	Poor-Fair
70% BFL Class A + 30% LCF Clean	8	Inf	66	6	Very Good	Poor-Fair
70% BFL Class A + 30% CRG Clean	6	Inf	81	9	Excellent	Poor-Fair

The surface DCP-calculated thickness values for all of the sections ranged from 4 in. to 9 in. The surface DCP-calculated thickness values for the 80% BFL Class A + 20% BFL Clean and the 70% BFL Class A + 30% LCF Clean sections increased from October 2016. The increase in the

surface thickness can be due to the increase in the uniformity of the mixture of gravels. The surface DCP-calculated thickness values of other sections did not change significantly.

The maximum and minimum changes in the average values of the surface DCP-CBR were for the 70% BFL Class A + 30% CRG Clean (68%) and the OFD Class A (-9%), respectively.

Table 22 shows the results of surface thickness and CBR between October and November 2016.

Table 22. DCP results of change in surface thickness and subgrade and surface CBR from October 2016

Sections October 2016–November 2016	Surface thickness (%)	CBR (%)	
		Surface	Subgrade
LCF Class A	0.22	25.08	12.12
OFD Class A	-3.42	-8.98	-2.22
BFL Class A	0.23	-26.68	-22.87
80% BFL Class A + 20% BFL Clean	16.01	-12.62	-36.37
70% BFL Class A + 30% OFD Clean	-1.33	-28.53	-28.65
70% BFL Class A + 30% LCF Clean	24.96	19.65	-17.20
70% BFL Class A + 30% CRG Clean	3.39	67.95	6.12

According to the SUDAS, relative rating of the average weighted-CBR values for the 80% BFL Class A + 20% BFL Clean was still excellent. The surface DCP-CBR values of other sections were rated very good and excellent. The changes in the subgrade average weighted-CBR values was the lowest for the OFD Class A (-2%). The CBR values for the subgrade of all other sections were rated poor-to-fair.

6.3.3 April 2017

DCP tests were conducted in April 2017 before the first maintenance, in order to evaluate the changes in the values of the thickness for the surface and the CBR values of the surface and subgrade layers, after the first freeze/thaw season. The results of thickness, CBR values, and rating are briefly shown in Table 23, while the cumulative blows, DCPI, and correlated CBR values versus the cumulative depth for all of the testing points are shown in Appendix C.

Table 23. DCP results of thickness for the surface, surface and subgrade CBR, and rating in April 2017

Sections April 2017	Thickness (in.)		CBR (%)		Rating	
	Surface	Subgrade	Surface	Subgrade	Surface	Subgrade
LCF Class A	10	Inf	85	3	Excellent	Very poor
OFD Class A	9	Inf	73	5	Very good	Poor-fair
BFL Class A	8	Inf	109	6	Excellent	Poor-fair
80% BFL Class A + 20% BFL Clean	6	Inf	116	8	Excellent	Poor-fair
70% BFL Class A + 30% OFD Clean	6	Inf	119	13	Excellent	Fair-good
70% BFL Class A + 30% LCF Clean	7	Inf	116	7	Excellent	Poor-fair
70% BFL Class A + 30% CRG Clean	6	Inf	101	11	Excellent	Fair-good

The thickness of the surface layers ranged from 5 in. to 10 in. The average of the DCP-calculated thickness values of the surface layers for all sections did not change significantly, except the 80% BFL Class A + 20% BFL Clean and the 70% BFL Class A + 30% LCF Clean. The surface thickness values of these two sections increased 14% and 13%, respectively.

The average of the surface DCP-CBR values for the LCF Class A and the OFD Class A sections decreased, while the DCP-CBR values of all other sections increased. The maximum change in the surface DCP-CBR values were observed for the 70% BFL Class A + 30% LCF Clean (110%) and the 70% BFL Class A + 30% CRG Clean (109%).

Table 24 shows the changes in results between October 2016 and April 2017.

Table 24. DCP results of change in thickness for the surface and surface and subgrade CBR between October 2016 and April 2017

Sections October 2016–April 2017	Surface thickness (%)	CBR (%)	
		Surface	Subgrade
LCF Class A	9	-5	-31
OFD Class A	9	-15	-41
BFL Class A	-9	28	-25
80% BFL Class A + 20% BFL Clean	14	18	-21
70% BFL Class A + 30% OFD Clean	-5	15	34
70% BFL Class A + 30% LCF Clean	13	110	-4
70% BFL Class A + 30% CRG Clean	4	109	25

The rating of the average DCP-CBR values for all of the surfaces were excellent with the exception of the OFD Class A, which was very good.

The subgrade average of the DCP-CBR values for all sections decreased except for the subgrade of 70% BFL Class A + 30% OFD Clean and 70% BFL Class A + 30% CRG Clean. The subgrade DCP-CBR values were rated poor-to-fair except for the LCF Class A, which was rated very poor.

6.3.4 June 2017

DCP tests were performed in June 2017 in order to evaluate the changes in the values of the thickness for the surface and the CBR values of the surface and subgrade layers after the second maintenance. The results of thickness, CBR values, and rating are briefly shown in Table 25, while the cumulative blows, DCPI, and correlated CBR values versus the cumulative depth for all of the testing points are shown in Appendix C.

Table 25. DCP results of thickness for the surface, surface and subgrade CBR and rating in June 2017

Sections June 2017	Thickness (in.)		CBR (%)		Rating	
	Surface	Subgrade	Surface	Subgrade	Surface	Subgrade
LCF Class A	9	Inf	190	9	Excellent	Poor-fair
OFD Class A	9	Inf	170	9	Excellent	Poor-fair
BFL Class A	8	Inf	132	9	Excellent	Poor-fair
80% BFL Class A + 20% BFL Clean	7	Inf	169	23	Excellent	Very good
70% BFL Class A + 30% OFD Clean	7	Inf	112	6	Excellent	Poor-fair
70% BFL Class A + 30% LCF Clean	7	Inf	169	7	Excellent	Poor-fair
70% BFL Class A + 30% CRG Clean	7	Inf	135	7	Excellent	Poor-fair

The thickness of the surface layers ranged between 5 in. and 9 in. The average of the DCP-calculated thickness values of the surface layers for all of the sections did not change significantly, except the 80% BFL Class A + 20% BFL Clean, the 70% BFL Class A + 30% OFD Clean, and the 70% BFL Class A + 30% CRG Clean mixtures. The surface thickness values of these mixtures increased 38%, 23%, and 25%, respectively.

Table 26 shows the changes in results between October 2016 and June 2017.

Table 26. DCP results of change in thickness for the surface and surface and subgrade CBR between October 2016 and June 2017

Sections October 2016–June 2017	Surface thickness (%)	CBR (%)	
		Surface	Subgrade
LCF Class A	-1	115	94
OFD Class A	2	98	11
BFL Class A	-8	54	11
80% BFL Class A + 20% BFL Clean	38	71	139
70% BFL Class A + 30% OFD Clean	23	8	-34
70% BFL Class A + 30% LCF Clean	10	206	-8
70% BFL Class A + 30% CRG Clean	25	180	-16

The average of the surface DCP-CBR values for all of the sections increased after maintenance. According to the SUDAS, rating of the average DCP-CBR values for all of the surfaces were excellent. The subgrade average of the DCP-CBR values for all of the sections increased except

for the subgrade of the 70% BFL Class A + 30% OFD Clean, the 70% BFL Class A + 30% LCF Clean, and the 70% BFL Class A + 30% CRG Clean sections. The subgrade DCP-CBR values were rated poor-to-fair except for the subgrade of the 80% BFL Class A + 20% BFL Clean, which was rated very good.

6.3.5 May 2018

DCP tests were performed in May 2018, in order to evaluate the changes in the values of the thickness for the surface and the CBR values of the surface and subgrade layers after the second freeze and thaw season (right before the second maintenance). The results of thickness, CBR values, and rating are briefly shown in Table 27, while the cumulative blows, DCPI, and correlated CBR values versus the cumulative depth for all of the testing points are shown in Appendix C.

Table 27. DCP results of thickness for the surface, surface and subgrade CBR, and rating in May 2018

Sections October 2016–May 2018	Thickness (in.)		CBR (%)		Rating	
	Surface	Subgrade	Surface	Subgrade	Surface	Subgrade
LCF Class A	11	Inf	82	3	Excellent	Very poor
OFD Class A	9	Inf	73	6	Very good	Poor-fair
BFL Class A	8	Inf	123	13	Excellent	Fair-good
80% BFL Class A + 20% BFL Clean	8	Inf	142	8	Excellent	Poor-fair
70% BFL Class A + 30% OFD Clean	9	Inf	102	6	Excellent	Poor-fair
70% BFL Class A + 30% LCF Clean	9	Inf	67	4	Very good	Very poor
70% BFL Class A + 30% CRG Clean	8	Inf	79	6	Very good	Poor-fair

The thickness of the surface layers ranges from 5 in. to 11 in. The average of the DCP-calculated thickness values of the surface layers for all of the sections increased (1% to 52%), except for the BFL Class A (-8%). The average of the surface DCP-CBR values decreased for the LCF Class A (8%), OFD Class A (15%), and the 70% BFL Class A + 30% OFD Clean (2%), while these values increased for the BFL Class A (44%), 80% BFL Class A + 20% BFL Clean (44%), 70% BFL Class A + 30% LCF Clean (21%), and 70% BFL Class A + 30% CRG Clean (65%).

Table 28 shows the changes in results between October 2016 and May 2018.

Table 28. DCP results of change in thickness for the surface and surface and subgrade CBR between October 2016 and May 2018

Sections May 2018	Surface thickness (%)	CBR (%)	
		Surface	Subgrade
LCF Class A	20	-8	-38
OFD Class A	4	-15	-31
BFL Class A	-8	44	58
80% BFL Class A + 20% BFL Clean	52	44	-21
70% BFL Class A + 30% OFD Clean	41	-2	-40
70% BFL Class A + 30% LCF Clean	46	21	-45
70% BFL Class A + 30% CRG Clean	28	65	-34

According to the SUDAS, the relative rating of LCF Class A, BFL Class A, 80% BFL Class A + 20% BFL Clean, and 70% BFL Class A + 30% OFD Clean were excellent. OFD Class A, 70% BFL Class A + 30% LCF Clean, and 70% BFL Class A + 30% CRG Clean were rated as very good. The subgrade average of the DCP-CBR values for all sections decreased (21% to 58%), except the BFL Class A, which increased 58%. The subgrade DCP-CBR values for LCF Class A and 70% BFL Class A + 30% LCF Clean were rated very poor. OFD Class A, 80% BFL Class A + 20% BFL Clean, and 70% BFL Class A + 30% OFD Clean were rated poor-to-fair and BFL Class A was rated fair-to-good.

6.3.6 April 2019

DCP tests were performed for the last time in April 2019 in order to evaluate the changes in the values of the thickness for the surface and the CBR values of the surface and subgrade layers after the third freeze and thaw period (before the third maintenance). The results of thickness, CBR values, and rating are detailed in Table 29, while the cumulative blows, DCPI, and correlated CBR values versus the cumulative depth for all testing points are shown in Appendix C.

Table 29. DCP results of thickness for the surface, surface and subgrade CBR, and rating in April 2019

Sections April 2019	Thickness (in.)		CBR (%)		Rating	
	Surface	Subgrade	Surface	Subgrade	Surface	Subgrade
LCF Class A	10	Inf	97	4	Excellent	Very poor
OFD Class A	7	Inf	64	5	Very good	Very poor
BFL Class A	9	Inf	108	6	Excellent	Poor-fair
80% BFL Class A + 20% BFL Clean	8	Inf	107	5	Excellent	Very poor
70% BFL Class A + 30% OFD Clean	8	Inf	91	4	Excellent	Very poor
70% BFL Class A + 30% LCF Clean	8	Inf	97	2	Excellent	Very poor
70% BFL Class A + 30% CRG Clean	6	Inf	81	4	Excellent	Poor-fair

The thickness of the surface layers ranged from 5 in. to 10 in. The average of the DCP-calculated thickness values of the surface layers for all sections increased (3% to 18%) for all sections except the 70% BFL Class A + 30% OFD Clean (-5%) and the BFL Class A (-9%).

The average surface DCP-CBR values decreased for LCF Class A (4%), OFD Class A (17%), and control section (48%), while these values increased for BFL Class A (38%), 80% BFL Class A + 20% BFL Clean (21%), 70% BFL Class A + 30% OFD Clean (21%), 70% BFL Class A + 30% LCF Clean (92%), and 70% BFL Class A + 30% CRG Clean (65%).

Table 30 shows the changes in results between October 2016 and April 2019.

Table 30. DCP results of change in thickness for the surface and surface and subgrade CBR between October 2016 and April 2019

Sections October 2016–April 2019	Surface thickness (%)	CBR (%)	
		Surface	Subgrade
LCF Class A	9	-4	-27
OFD Class A	9	-17	-42
BFL Class A	-9	38	-33
80% BFL Class A + 20% BFL Clean	12	21	-33
70% BFL Class A + 30% OFD Clean	-5	21	48
70% BFL Class A + 30% LCF Clean	11	92	-4
70% BFL Class A + 30% CRG Clean	4	65	23

According to the SUDAS, the relative rating of all sections were rated excellent, while OFD Class A was rated very good. The subgrade average of the DCP-CBR values for all of the sections decreased for all sections (4% to 42%), while the values increased for 70% BFL Class A + 30% OFD Clean (45%) and 70% BFL Class A + 30% CRG Clean (23%). The subgrade DCP-CBR values for all sections was rated as very poor, except the subgrades of the BFL Class A and 70% BFL Class A + 30% CRG Clean, which were rated poor-to-fair.

Figure 58 shows the LCF Class A and 80% BFL Class A + 20% BFL Clean had the excellent rating according to the SUDAS for the surface DCP-CBR values.

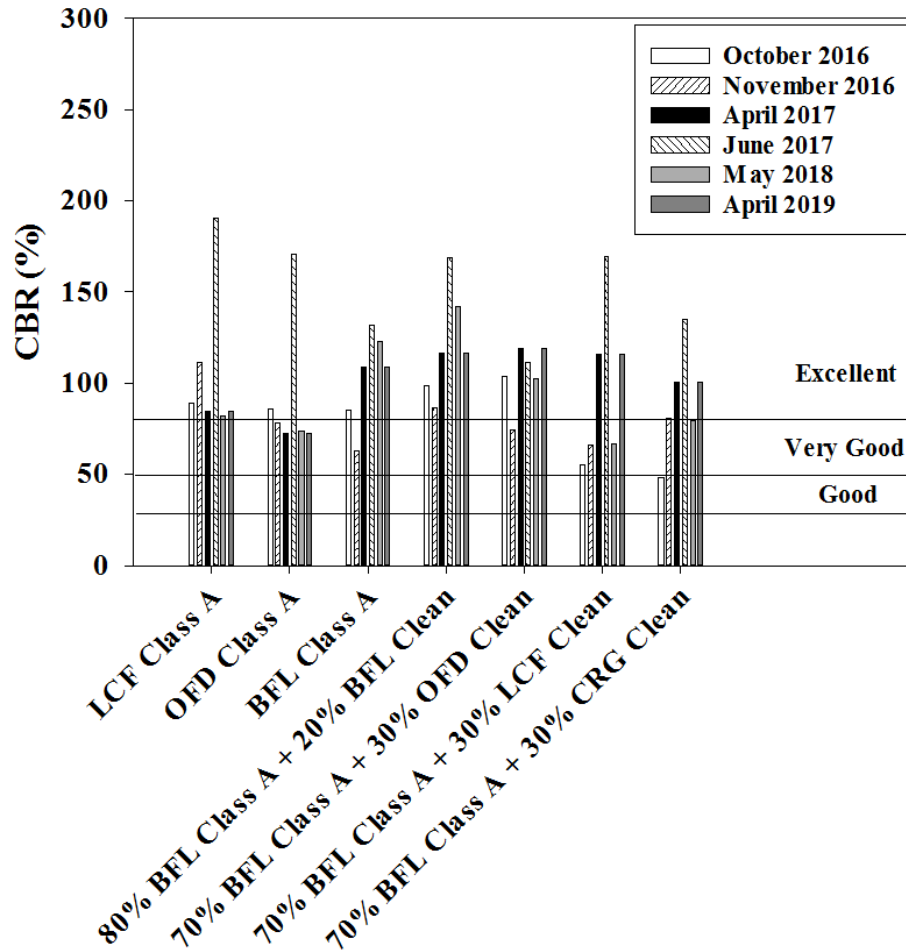


Figure 58. Surface DCP-CBR results over the course of the project

OFD Class A DCP-CBR rating for surface was excellent in October 2016 and June 2017, after construction and maintenance, but it was rated very good for other times of testing. BFL Class A and 70% BFL Class A + 30% OFD Clean DCP-CBR rating for surface was always excellent, except for the November 2016 testing. The surface DCP-CBR of 70% BFL Class A + 30% LCF Clean was rated very good for all testing periods (except April 2017, June 2017, and April 2019, which were excellent). The surface DCP-CBR for 70% BFL Class A + 30% CRG Clean was rated good in October 2016, and the values of DCP-CBR increased over time, and it was rated excellent in June 2017. However, the DCP-CBR value for this section decreased, and it was rated very good in May 2018 (after the second freeze/thaw season) and again increased to excellent in April 2019.

Figure 59 shows that the subgrade of LCF Class A DCP-CBR values were always rated very poor according to the SUDAS, except November 2016 (one month after construction) and June 2017 (after maintenance), where it was poor-to-fair.

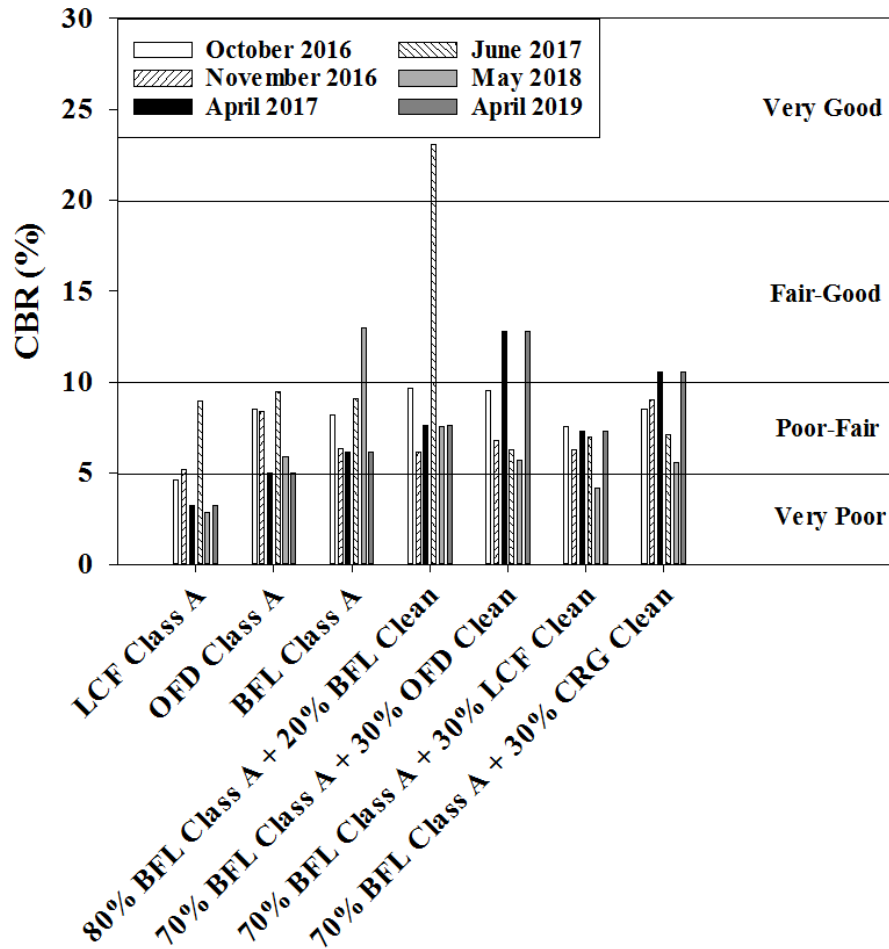


Figure 59. Subgrade DCP-CBR results for different times

Subgrade DCP-CBR values of OFD Class A had poor-to-fair relative rating. DCP-CBR values of BFL Class A was rated poor-to-fair, except May 2018, where it was fair-to-good. The 80% BFL Class A + 20% OFD Clean subgrade DCP-CBR values was rated always poor-to-fair, except June 2017 (after maintenance) and April 2019, where it was rated very good. The subgrade DCP-CBR values of 70% BFL Class A + 30% LCF Clean were always rated poor-to-fair, except May 2018, when it was rated very poor. The subgrade DCP-CBR of 70% BFL Class A + 30% CRG Clean was rated poor-to-fair for all tests, except April 2017 (before maintenance) and April 2019, when it was rated fair-to-good.

6.4 MASW Test Results

The multichannel analysis of surface waves (MASW) test is a non-destructive, wave-propagation-based geophysical test, which was conducted with two different active sources (small and large hammers). MASW tests were performed three times throughout the course of the project in October 2016, April 2017, and May 2018 to evaluate the possibility of performing geophysical tests on granular roads. Results of the MASW tests were compared for surface and subgrade moduli to those calculated from FWD tests. MASW analysis was performed on a two-

layered system consisting of surface and subgrade with an infinite subgrade thickness. The thickness of the surface layer was calculated by DCP tests. The density of each test section was collected from the nuclear gauge density tests. Poisson's ratio of the surface and subgrade were assumed at 0.4, and 0.3, respectively. The same values of the thickness, density, and Poisson's ratio were considered also in the FWD back-calculation. The results of modulus for surface and subgrade layers for small and large hammers are presented in Figures 60–67.

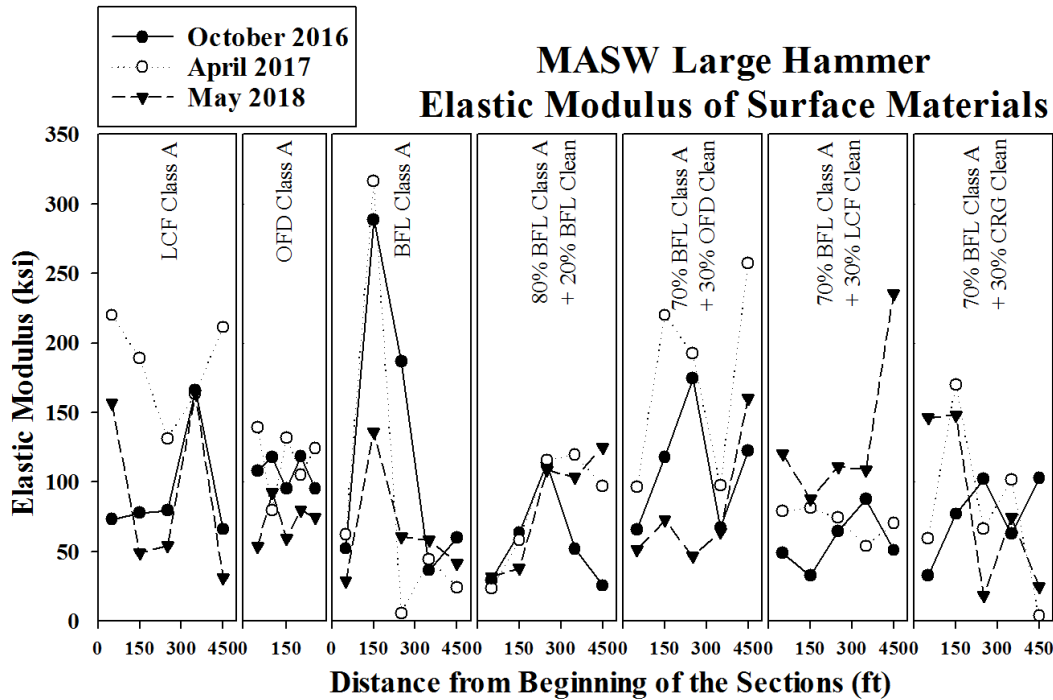


Figure 60. Surface elastic modulus of MASW–large hammer

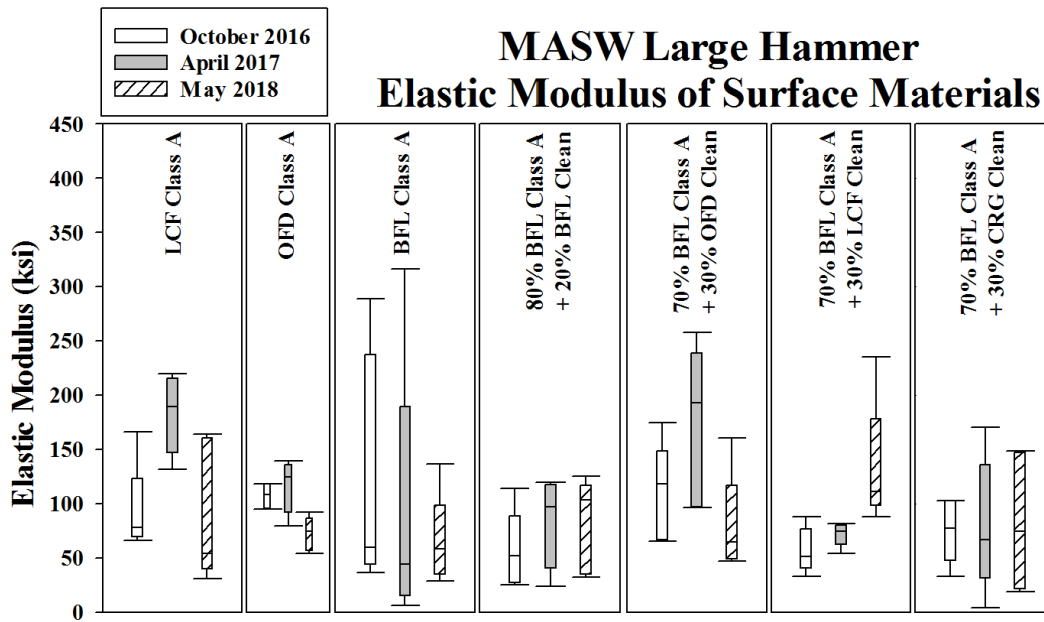


Figure 61. Surface elastic modulus ranges of MASW–large hammer

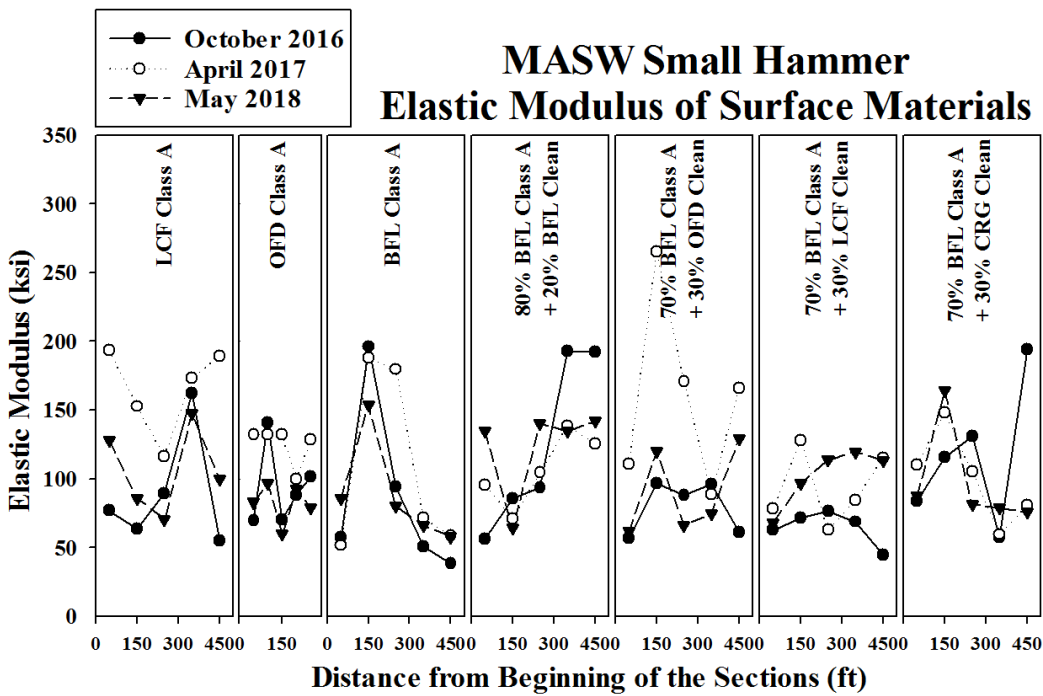


Figure 62. Surface elastic modulus of MASW–small hammer

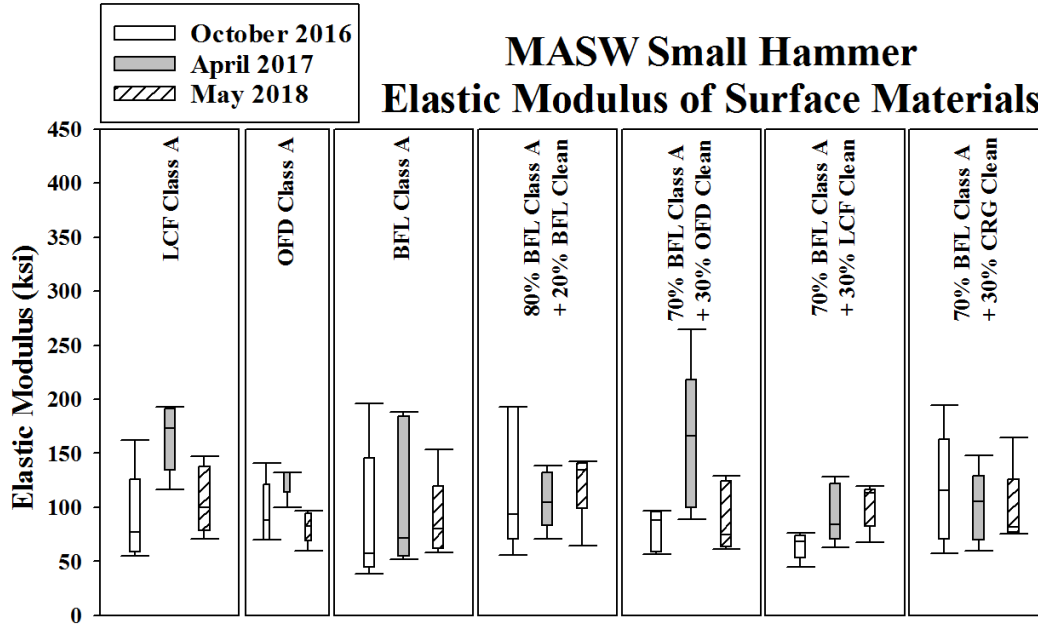


Figure 63. Surface elastic modulus ranges of MASW–small hammer

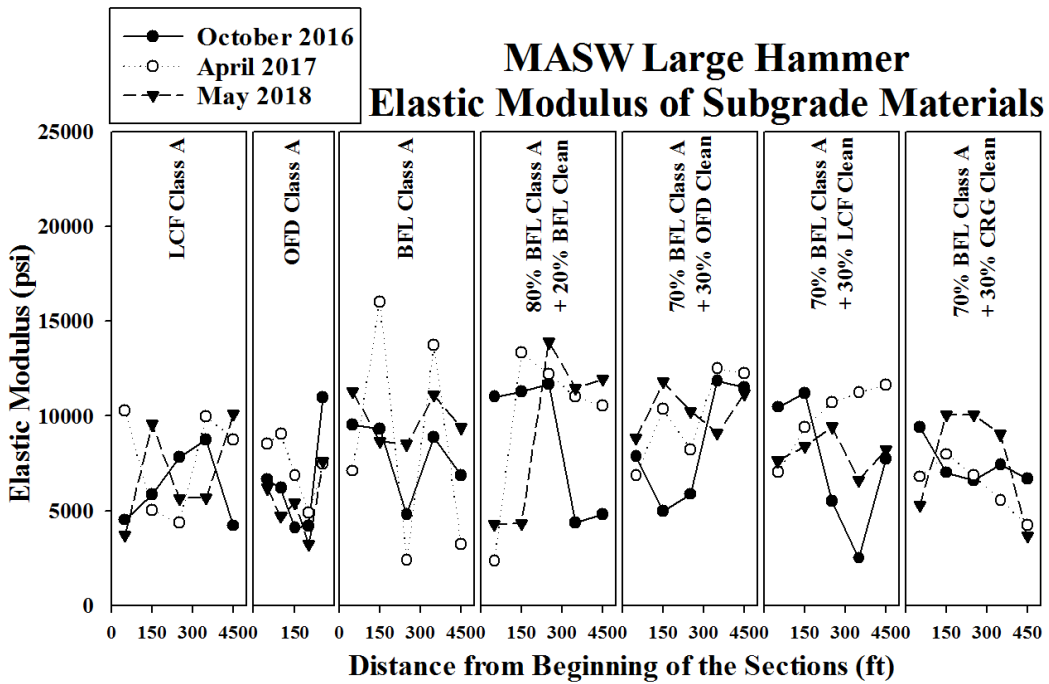


Figure 64. Subgrade elastic modulus of MASW–large hammer

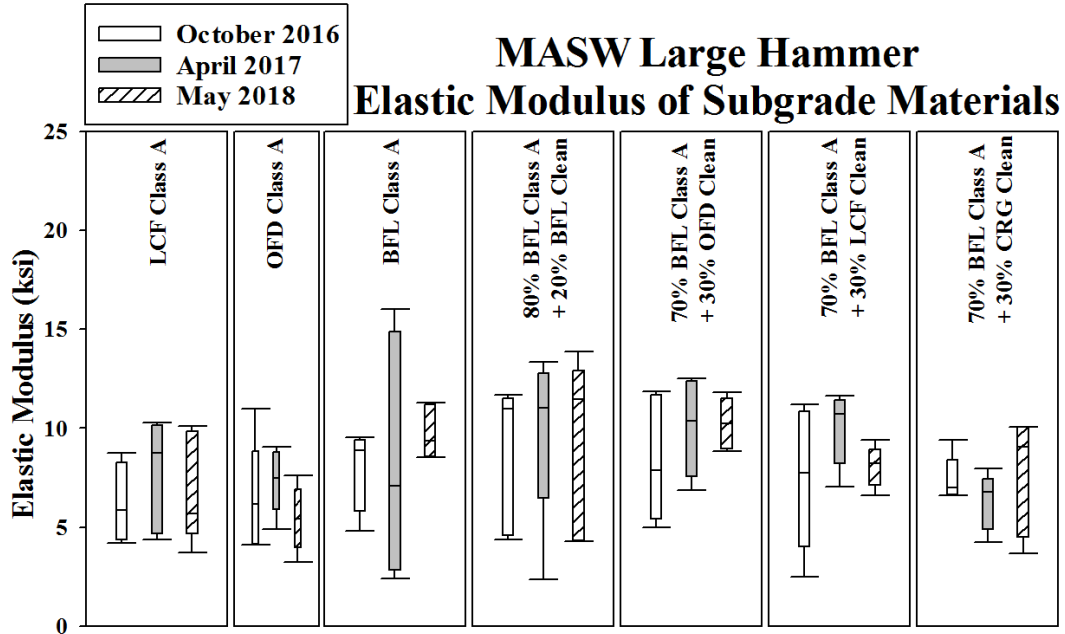


Figure 65. Subgrade elastic modulus ranges of MASW–large hammer

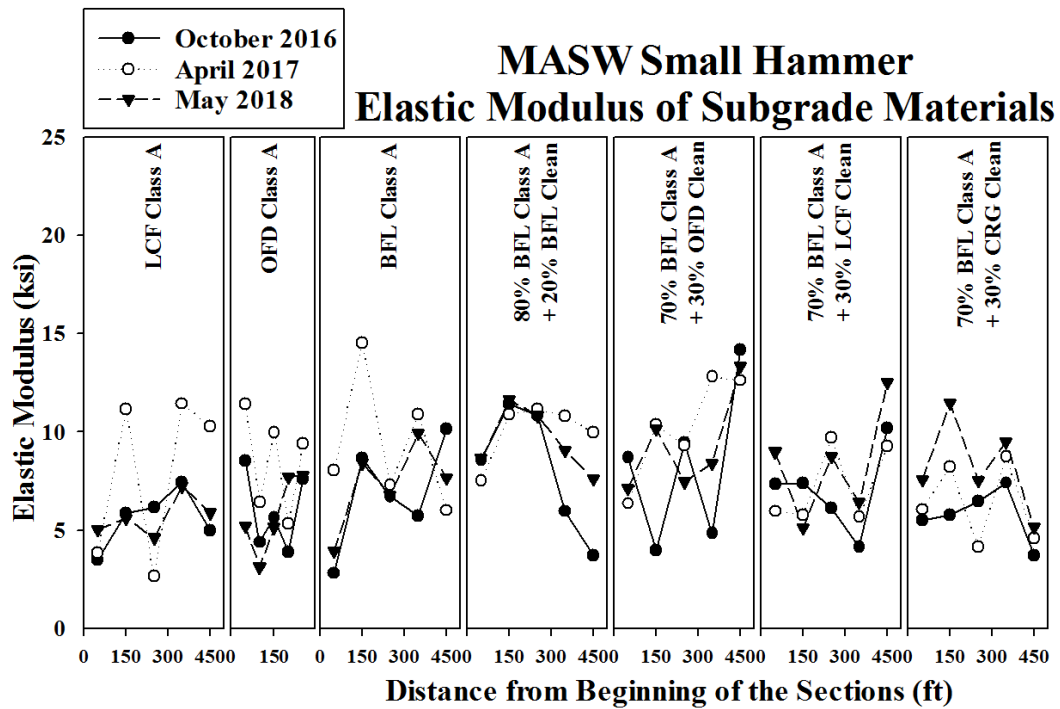


Figure 66. Subgrade elastic modulus of MASW–small hammer

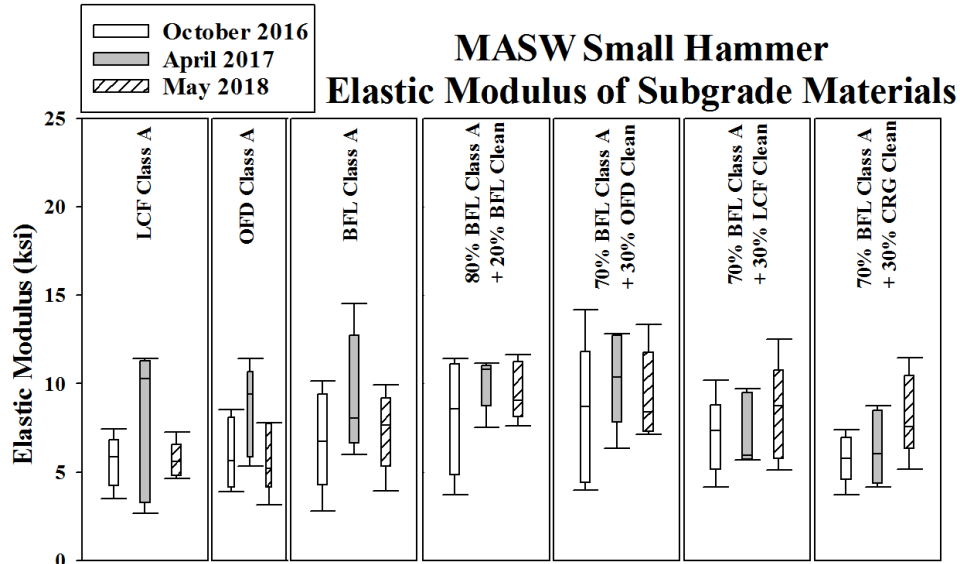


Figure 67. Subgrade elastic modulus ranges of MASW–small hammer

Subgrade elastic modulus values from the small and large hammer had better agreement compared to the surface elastic modulus values attained by the small and large hammer. Moreover, the large hammer showed higher ranges of surface and subgrade elastic modulus values, while the surface and subgrade elastic modulus values for small hammer were closer. BFL Class A, LCF Class A, and 70% BFL Class A + 30% LCF Clean had the highest, and 80% BFL Class A + 20% BFL Clean, 70% BFL Class A + 30% LCF Clean, and BFL Class A had the lowest surface elastic modulus values in October 2016, April 2017, and May 2018. On the other hand, subgrade elastic modulus values for all of the sections were in a close range.

6.4.1 October 2016

The first set of MASW tests was performed in October 2016, one month after the completion of construction. Tables 31 and 32 show the mean, minimum, maximum, and ranges of the surface and subgrade elastic moduli of both surface and subgrade soils calculated for small and large hammers.

Table 31. Surface elastic modulus of MASW small and large hammer tests in October 2016

Surface Sections	Large hammer modulus (ksi)				Small hammer modulus (ksi)			
	E _{Mean}	E _{Max}	E _{Min}	Range	E _{Mean}	E _{Max}	E _{Min}	Range
LCF Class A	93	166	66	100	88	162	55	107
OFD Class A	107	118	95	23	92	141	58	83
BFL Class A	125	289	36	252	87	196	38	158
80% BFL Class A + 20% BFL Clean	57	114	25	88	124	193	57	136
70% BFL Class A + 30% OFD Clean	110	174	66	109	81	97	61	35
70% BFL Class A + 30% LCF Clean	57	88	33	55	69	84	45	39
70% BFL Class A + 30% CRG Clean	76	103	33	70	132	194	58	137

Table 32. Subgrade elastic modulus of MASW small and large hammer tests in October 2016

Subgrade Sections	Large hammer modulus (ksi)				Small hammer modulus (ksi)			
	E _{Mean}	E _{Max}	E _{Min}	Range	E _{Mean}	E _{Max}	E _{Min}	Range
LCF Class A	7	9	4	5	7	9	5	4
OFD Class A	7	11	4	7	5	8	3	5
BFL Class A	8	11	5	6	8	10	6	4
80% BFL Class A + 20% BFL Clean	8	12	4	7	8	11	4	8
70% BFL Class A + 30% OFD Clean	9	12	5	7	8	14	4	10
70% BFL Class A + 30% LCF Clean	7	11	3	9	7	10	4	6
70% BFL Class A + 30% CRG Clean	8	10	7	3	7	10	4	6

Based on the results of MASW with the large hammer, 80% BFL Class A + 20% BFL Clean had the minimum mean value of the surface elastic modulus. Moreover, the highest elastic modulus among the test sections was determined to be BFL Class A. On the other hand, the results of MASW surface elastic modulus with the small hammer showed that BFL Class A had the maximum and the 70% BFL Class A + 30% LCF Clean had the minimum surface modulus. The subgrade elastic modulus for both methods of MASW (small and large hammer) were in a better agreement than the surface elastic modulus, and it was in the range of 7 to 9 ksi for the large hammer and 5 to 8 ksi for the small hammer. The results of MASW–large hammer mean the subgrade elastic modulus for all test sections are in a better agreement for those calculated for the large hammer. This could be due to the higher energy applied through the large hammer. Therefore, the waves would be able to pass through a greater depth into the subgrade layer.

6.4.2 April 2017

In order to monitor the effects of the freeze and thaw, the second set of MASW tests was performed on the test sections in April 2017. The mean value, maximum, minimum, and range of change in the elastic modulus of the surface and subgrade layers are shown in Tables 33 and 34.

Table 33. Surface elastic modulus of MASW small and large hammer tests in April 2017

Surface Sections	Large hammer modulus (ksi)				Small hammer modulus (ksi)			
	E _{Mean}	E _{Max}	E _{Min}	Range	E _{Mean}	E _{Max}	E _{Min}	Range
LCF Class A	183	220	131	89	153	189	116	73
OFD Class A	116	139	80	60	109	132	52	80
BFL Class A	91	316	6	311	119	188	58	129
80% BFL Class A + 20% BFL Clean	83	120	24	96	110	138	71	68
70% BFL Class A + 30% OFD Clean	173	257	96	161	154	265	78	187
70% BFL Class A + 30% LCF Clean	72	81	54	27	100	128	63	65
70% BFL Class A + 30% CRG Clean	80	170	4	166	102	148	60	88

Table 34. Subgrade elastic modulus of MASW small and large hammer tests in April 2017

Subgrade Sections	Large hammer modulus (ksi)				Small hammer modulus (ksi)			
	E _{Mean}	E _{Max}	E _{Min}	Range	E _{Mean}	E _{Max}	E _{Min}	Range
LCF Class A	7	10	4	6	9	11	3	9
OFD Class A	7	9	5	4	8	10	5	5
BFL Class A	8	16	2	14	9	15	6	9
80% BFL Class A + 20% BFL Clean	11	13	7	6	10	11	6	5
70% BFL Class A + 30% OFD Clean	10	13	7	5	10	13	6	7
70% BFL Class A + 30% LCF Clean	10	12	7	5	7	10	6	4
70% BFL Class A + 30% CRG Clean	7	8	4	4	7	9	4	5

The mean value of the MASW–large hammer surface elastic modulus of almost all sections increased since October 2016, with the exception of BFL Class A. Likewise, the results of the modulus for MASW–small hammer increased except the following sections: 80% BFL Class A + 20% BFL Clean and 70% BFL Class A + 30% CRG Clean. On the other hand, the subgrade elastic modulus calculated with both small and large hammers did not change significantly except the subgrade of the 70% BFL Class A + 30% LCF Clean section (large hammer) and OFD Class A (small hammer). The reason of for the increase in the elastic modulus for both surface and subgrade could be the presence of the frozen zone and/or compaction due to the traffic load (which may have caused stronger bonding between the aggregate materials and better gravel packing).

6.4.3 May 2018

The third set of MASW tests was conducted in May 2018 after the second freeze/thaw season. Aggregate materials were placed on the aggregate section in May 2017 after the first maintenance. Elastic moduli of the majority of sections decreased in the surface since the construction (MASW–large hammer). The maximum decrease in elastic modulus was observed for the BFL Class A. However, the surface elastic modulus for the 80% BFL Class A + 20% BFL Clean, 70% BFL Class A + 30% LCF Clean, and 70% BFL Class A + 30% CRG Clean increased and the maximum increase in elastic modulus was observed for the 70% BFL Class A + 30% LCF Clean. On the other hand, the surface elastic moduli of sections determined via MASW–small hammer did not change significantly except the 70% BFL Class A + 30% LCF Clean section, which experienced a 54% increase in the surface elastic modulus. Therefore, it can be concluded that the mixture of the BFL Class A and LCF Clean tends to get stiffer even after deterioration. The subgrade elastic modulus for both MASW–small and –large hammers did not change significantly since construction (October 2016).

The surface and the subgrade results from the May 2018 tests are shown in Table 35 and 36.

Table 35. Surface elastic modulus of MASW small and large hammer tests in May 2018

Surface Sections	Large hammer modulus (ksi)				Small hammer modulus (ksi)			
	E _{Mean}	E _{Max}	E _{Min}	Range	E _{Mean}	E _{Max}	E _{Min}	Range
LCF Class A	91	164	31	133	97	147	71	77
OFD Class A	72	92	54	38	83	97	60	37
BFL Class A	65	136	29	107	98	154	58	96
80% BFL Class A + 20% BFL Clean	81	125	32	93	108	142	62	81
70% BFL Class A + 30% OFD Clean	79	161	47	114	92	129	66	63
70% BFL Class A + 30% LCF Clean	133	236	88	148	106	120	87	32
70% BFL Class A + 30% CRG Clean	82	148	18	130	93	164	64	100

Table 36. Subgrade elastic modulus of MASW small and large hammer tests in May 2018

Subgrade Sections	Large hammer modulus (ksi)				Small hammer modulus (ksi)			
	E _{Mean}	E _{Max}	E _{Min}	Range	E _{Mean}	E _{Max}	E _{Min}	Range
LCF Class A	7	10	6	4	6	7	5	3
OFD Class A	6	11	3	8	6	8	3	5
BFL Class A	8	11	4	7	8	10	7	3
80% BFL Class A + 20% BFL Clean	10	14	4	10	9	12	7	5
70% BFL Class A + 30% OFD Clean	10	12	8	4	10	13	7	6
70% BFL Class A + 30% LCF Clean	8	9	5	4	8	13	5	7
70% BFL Class A + 30% CRG Clean	8	10	4	6	8	11	5	6

6.5 FWD Test Results

FWD tests were conducted in this project on five points of each test section in October 2016 (after construction), May 2017 (after maintenance), June 2017, May 2018, and May 2019. The FWD is the most common test that is used to simulate the traffic load and evaluate the elastic modulus of the road layers. The two-layered system assumption was considered for the back-calculation of FWD and the back-calculated elastic modulus were compared with MASW results, in order to come up with a trend in the in situ elastic modulus variation for a wide range of stress and strain levels. The surface layer thicknesses are the same as calculated from DCP data. Moreover, density values are measured by nuclear gauge test data. Poisson's ratios of surface and subgrade layers were assumed 0.4 and 0.3, respectively (the same as MASW). The FWD moduli results for surface and subgrade layers are shown in Figures 68–71.

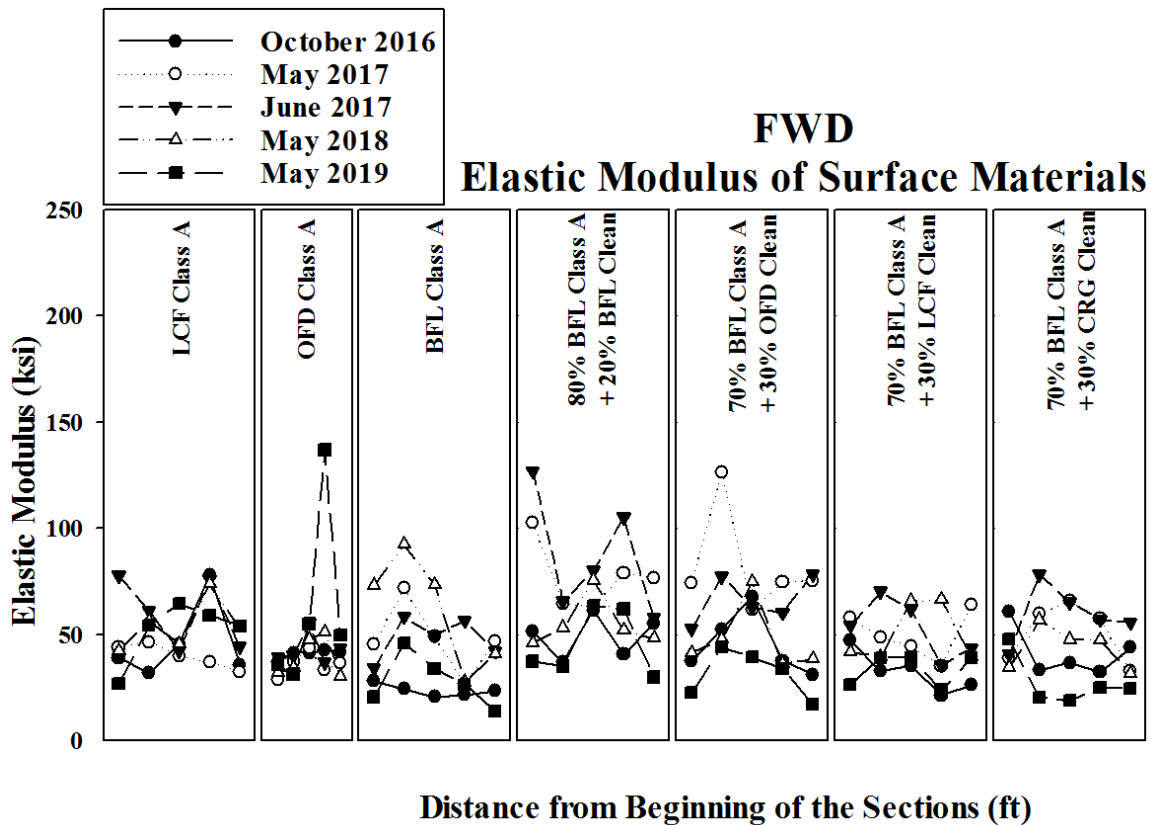


Figure 68. Surface elastic modulus of FWD

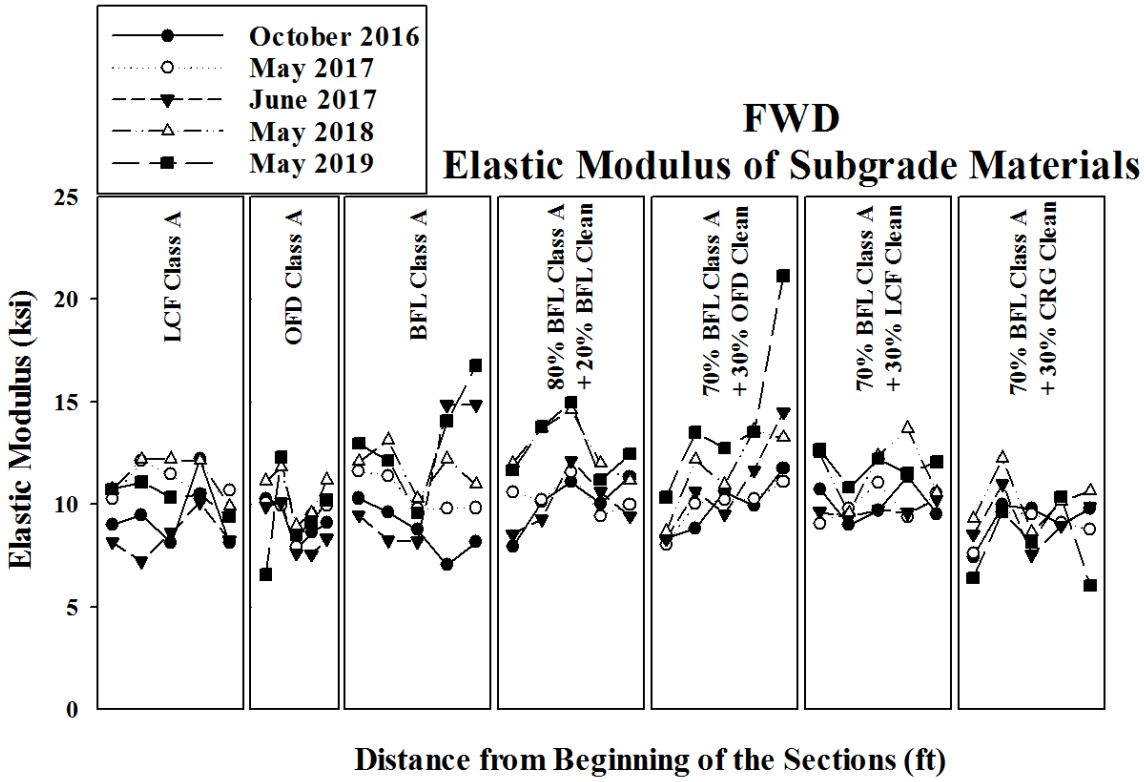


Figure 69. Subgrade elastic modulus of FWD

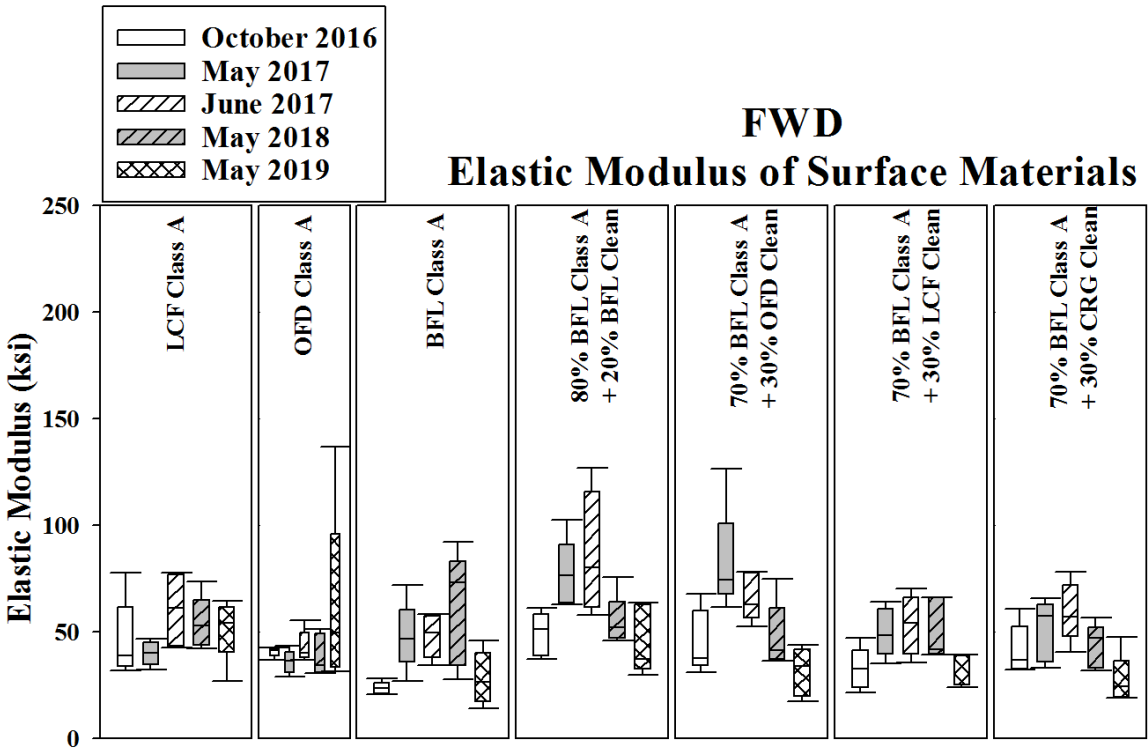


Figure 70. Surface elastic modulus ranges of FWD

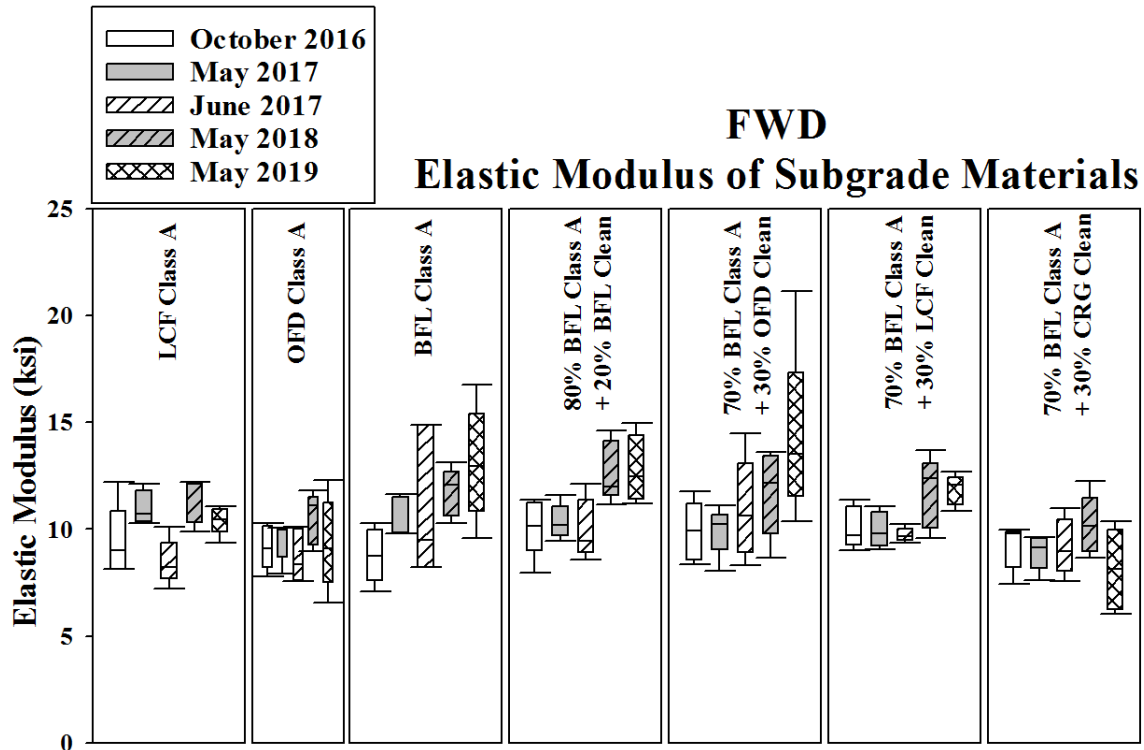


Figure 71. Subgrade elastic modulus ranges of FWD

Back-calculation of the FWD results in October 2016, May 2017, June 2017, May 2018, and May 2019 showed that 80% BFL Class A + 20% BFL Clean (49 ksi - October 2016), 70% BFL Class A + 30% OFD Clean (82 ksi - May 2017), 80% BFL Class A + 20% BFL Clean (87 ksi - June 2017), BFL Class A (62 ksi - May 2018), OFD Class A (62 ksi - May 2019) had maximum surface elastic modulus values, and BFL Class A (24 ksi - October 2016), OFD Class A (36 ksi - May 2017), OFD Class A (43 ksi - June 2017), OFD Class A (39 ksi - May 2018), 70% BFL Class A + 30% CRG Clean (27 ksi - May 2019) had minimum surface elastic modulus values. Back-calculated subgrade elastic modulus for all of the sections were generally constant in the range of 8 to 14 ksi. The 80% BFL Class A + 20% BFL Clean (63 ksi) and BFL Class A (42 ksi), respectively, had the maximum and minimum surface elastic modulus values. However, OFD Class A, 70% BFL Class A + 30% LCF Clean, and 70% BFL Class A + 30% CRG Clean had almost the same surface elastic modulus values (44 ksi).

6.5.1 October 2016

The first set of FWD tests was conducted after the construction of test sections in October 2016. The mean, minimum, maximum, standard deviation, and range of the surface and subgrade elastic moduli are summarized in Tables 37 and 38.

Table 37. Surface elastic modulus of FWD test in October 2016

Sections	Surface elastic modulus (ksi)				
	E _{Mean}	E _{Max}	E _{Min}	SD	Range
LCF Class A	46	78	32	18	46
OFD Class A	41	43	37	2	6
BFL Class A	24	28	21	3	8
80% BFL Class A + 20% BFL Clean	49	61	37	10	24
70% BFL Class A + 30% OFD Clean	45	68	31	15	36
70% BFL Class A + 30% LCF Clean	33	47	21	10	26
70% BFL Class A + 30% CRG Clean	41	61	32	12	29

Table 38. Subgrade elastic modulus of FWD test in October 2016

Sections	Subgrade elastic modulus (ksi)				
	E _{Mean}	E _{Max}	E _{Min}	SD	Range
LCF Class A	10	12	8	2	4
OFD Class A	9	10	8	1	3
BFL Class A	8	10	7	1	3
80% BFL Class A + 20% BFL Clean	10	11	8	1	3
70% BFL Class A + 30% OFD Clean	10	12	9	1	3
70% BFL Class A + 30% LCF Clean	9	11	7	1	4
70% BFL Class A + 30% CRG Clean	10	10	9	1	1

The surface elastic modulus for the sections ranged from 24 ksi for the BFL Class A to 50 ksi for the 80% BFL Class A + 20% BFL Clean. Table 37 shows that the addition of clean aggregates certainly increased the elastic modulus of the surface layer. The maximum elastic modulus variation within the five points of each section was observed for the LCF Class A section. The maximum standard deviation and the ranges of back-calculated subgrade elastic moduli were observed for the subgrade of the LCF Class A (Table 38).

6.5.2 May 2017

The second set of FWD tests was conducted after the first maintenance of all sections in May 2017. Tables 39 and 40 show the mean, minimum, maximum, standard deviation, and the ranges of the surface and subgrade elastic moduli of all sections.

Table 39. Surface elastic modulus of FWD test in May 2017

Sections	Surface elastic modulus (ksi)					
	E _{Mean}	E _{Max}	E _{Min}	SD	Range	Change (%)
LCF Class A	40	47	32	6	14	40
OFD Class A	36	44	29	5	15	36
BFL Class A	48	72	27	16	45	48
80% BFL Class A + 20% BFL Clean	77	103	63	16	40	77
70% BFL Class A + 30% OFD Clean	82	127	62	25	65	82
70% BFL Class A + 30% LCF Clean	50	64	35	11	29	50
70% BFL Class A + 30% CRG Clean	51	66	33	14	33	51

Table 40. Subgrade elastic modulus of FWD test in May 2017

Sections	Subgrade elastic modulus (ksi)					
	E _{Mean}	E _{Max}	E _{Min}	SD	Range	Change (%)
LCF Class A	11	12	10	1	2	11
OFD Class A	10	12	8	1	4	10
BFL Class A	10	11	10	1	2	10
80% BFL Class A + 20% BFL Clean	10	12	8	1	4	10
70% BFL Class A + 30% OFD Clean	10	11	9	1	2	10
70% BFL Class A + 30% LCF Clean	10	11	8	1	3	10
70% BFL Class A + 30% CRG Clean	9	10	9	1	1	9

The mean surface elastic modulus ranged from 36 ksi (OFD Class A) to 82 ksi (70% BFL Class A + 30% OFD Clean). The addition of clean aggregates to BFL Class A (local material) resulted in a higher elastic moduli than those of only Class A aggregates. Moreover, all sections except the LCF Class A and the OFD Class A had higher surface elastic moduli than those measured after construction. The BFL Class A section had the highest increase in the surface elastic modulus (102%) after the first freeze/thaw cycle. The 70% BFL Class A + 30% OFD Clean mixture had the highest elastic modulus in May 2017. The maximum standard deviations for the surface elastic modulus was found to be for 70% BFL Class A + 30% OFD Clean mixture, where the ranges of the elastic moduli for this section's five points were wider than those observed within points in other sections. On the other hand, the subgrade elastic moduli of all sections did not experience any significant change over this period, and the maximum change in the mean value of subgrade elastic modulus since October 2016 was observed for Class A sections (7 to 24%). Moreover, the 70% BFL Class A + 30% OFD Clean section's subgrade had the highest ranges of change for the subgrade elastic moduli. The more scattered data for the surface and subgrade elastic moduli could be due to the differences in the compaction levels for testing points.

6.5.3 June 2017

The third set of FWD tests was performed one month after the first maintenance of the sections, in June 2017. The mean, minimum, maximum, standard deviation, and the range of the surface and subgrade values of elastic moduli are summarized in Tables 41 and 42.

Table 41. Surface elastic modulus of FWD test in June 2017

Sections	Surface elastic modulus (ksi)					
	E _{Mean}	E _{Max}	E _{Min}	SD	Range	Change (%)
LCF Class A	60	78	42	17	35	60
OFD Class A	43	56	37	7	19	43
BFL Class A	48	58	34	10	24	48
80% BFL Class A + 20% BFL Clean	87	127	58	29	69	87
70% BFL Class A + 30% OFD Clean	66	78	53	11	26	66
70% BFL Class A + 30% LCF Clean	53	70	36	14	35	53
70% BFL Class A + 30% CRG Clean	59	78	41	14	38	59

Table 42. Subgrade elastic modulus of FWD test in June 2017

Sections	Subgrade elastic modulus (ksi)					
	E _{Mean}	E _{Max}	E _{Min}	SD	Range	Change (%)
LCF Class A	9	10	7	1	3	9
OFD Class A	9	10	8	1	3	9
BFL Class A	11	15	8	3	7	11
80% BFL Class A + 20% BFL Clean	10	12	8	1	4	10
70% BFL Class A + 30% OFD Clean	11	15	10	2	5	11
70% BFL Class A + 30% LCF Clean	10	10	9	0	2	10
70% BFL Class A + 30% CRG Clean	9	11	8	1	3	9

The maximum mean value of surface elastic moduli ranged from 43 ksi (OFD Class A) to 87 ksi (80% BFL Class A + 20% BFL Clean). All sections resulted in a stiffer surface than those observed after construction (from 5% for OFD Class A to 103% for BFL Class A). Subgrade elastic modulus values ranged from 9 to 11 ksi. The significance of the change in the back-calculated subgrade elastic moduli from October 2016 was negligible (1%–9%) for all the sections except the BFL Class A section (32%), which also had the highest surface elastic modulus increase.

6.5.4 May 2018

The fourth set of FWD tests was performed after the second freeze/thaw cycle, in May 2018. The mean, minimum, maximum, standard deviation and the ranges of the surface and subgrade elastic moduli are summarized in Tables 43 and 44.

Table 43. Surface elastic modulus of FWD test in May 2018

Sections	Surface elastic modulus (ksi)					
	E _{Mean}	E _{Max}	E _{Min}	SD	Range	Change (%)
LCF Class A	54	74	42	12	31	54
OFD Class A	39	51	30	10	21	39
BFL Class A	62	92	28	27	65	62
80% BFL Class A + 20% BFL Clean	55	76	46	12	29	55
70% BFL Class A + 30% OFD Clean	48	75	36	16	38	48
70% BFL Class A + 30% LCF Clean	51	66	40	14	27	51
70% BFL Class A + 30% CRG Clean	44	57	32	10	25	44

Table 44. Subgrade elastic modulus of FWD test in May 2018

Sections	Subgrade elastic modulus (ksi)					
	E _{Mean}	E _{Max}	E _{Min}	SD	Range	Change (%)
LCF Class A	11	12	10	1	2	11
OFD Class A	11	12	9	1	3	11
BFL Class A	12	13	10	1	3	12
80% BFL Class A + 20% BFL Clean	13	15	11	1	3	13
70% BFL Class A + 30% OFD Clean	12	14	9	2	5	12
70% BFL Class A + 30% LCF Clean	12	14	10	2	4	12
70% BFL Class A + 30% CRG Clean	10	12	9	1	4	10

The maximum mean value of surface elastic modulus among the aggregate sections was BFL Class A (62 ksi) and the minimum was OFD Class A (39 ksi). All sections were stiffer than their initial condition measured in October 2016 after construction, except OFD Class A section, which experienced a 4% decrease in two years. The BFL Class A section experienced the highest stiffness increase since construction (70%), while 70% BFL Class A + 30% LCF Clean experienced the second highest increase (55%). The mean subgrade elastic moduli stayed almost unchanged for all sections (10 to 13 ksi).

6.5.5 May 2019

The last set of FWD tests was performed after the third freeze/thaw cycle, in May 2019. The mean, minimum, maximum, standard deviation, and the ranges of the surface and subgrade of elastic moduli are shown in Tables 45 and 46.

Table 45. Surface elastic modulus of FWD test in May 2019

Sections	Surface elastic modulus (ksi)					
	E _{Mean}	E _{Max}	E _{Min}	SD	Range	Change (%)
LCF Class A	52	65	27	14	37	52
OFD Class A	62	137	31	43	106	62
BFL Class A	28	46	14	12	32	28
80% BFL Class A + 20% BFL Clean	46	64	30	16	34	46
70% BFL Class A + 30% OFD Clean	31	44	17	11	27	31
70% BFL Class A + 30% LCF Clean	34	40	24	8	16	34
70% BFL Class A + 30% CRG Clean	27	48	19	12	29	27

Table 46. Subgrade elastic modulus of FWD test in May 2019

Sections	Subgrade elastic modulus (ksi)					
	E _{Mean}	E _{Max}	E _{Min}	SD	Range	Change (%)
LCF Class A	10	11	9	1	2	10
OFD Class A	9	12	7	2	6	9
BFL Class A	13	17	10	3	7	13
80% BFL Class A + 20% BFL Clean	13	15	11	2	4	13
70% BFL Class A + 30% OFD Clean	14	21	10	4	11	14
70% BFL Class A + 30% LCF Clean	12	13	11	1	2	12
70% BFL Class A + 30% CRG Clean	8	10	6	2	4	8

The maximum mean value of surface elastic modulus among the aggregate sections was determined to be OFD Class A section (62 ksi), while the minimum surface elastic modulus was calculated for the 70% BFL Class A + 30% CRG Clean section (27 ksi). All sections except BFL Class A/BFL Clean, BFL Class A/OFD Clean, and BFL Class A/CRG Clean were stiffer than those measured in October 2016, after construction. The maximum increase in the mean surface elastic modulus value was for the OFD Class A. The mean values of subgrade elastic moduli were almost the same for all sections and ranged from 10 ksi to 13 ksi.

6.6 APLT Results

APLT tests were conducted in order to perform a preliminary assessment of the differences in support capacities of the different sections in relation to the different aggregate sources utilized in the surface layer in October 2016. Tests were conducted at one location on each section using a target cyclic stress of 90 psi for 1,000 cycles at each test point. The support capacities were evaluated by determining the composite resilient modulus (M_r) values and permanent deformation (δ_p) characteristics.

Figure 72 presents the in situ M_{r-Comp} results with cycles at each test point.

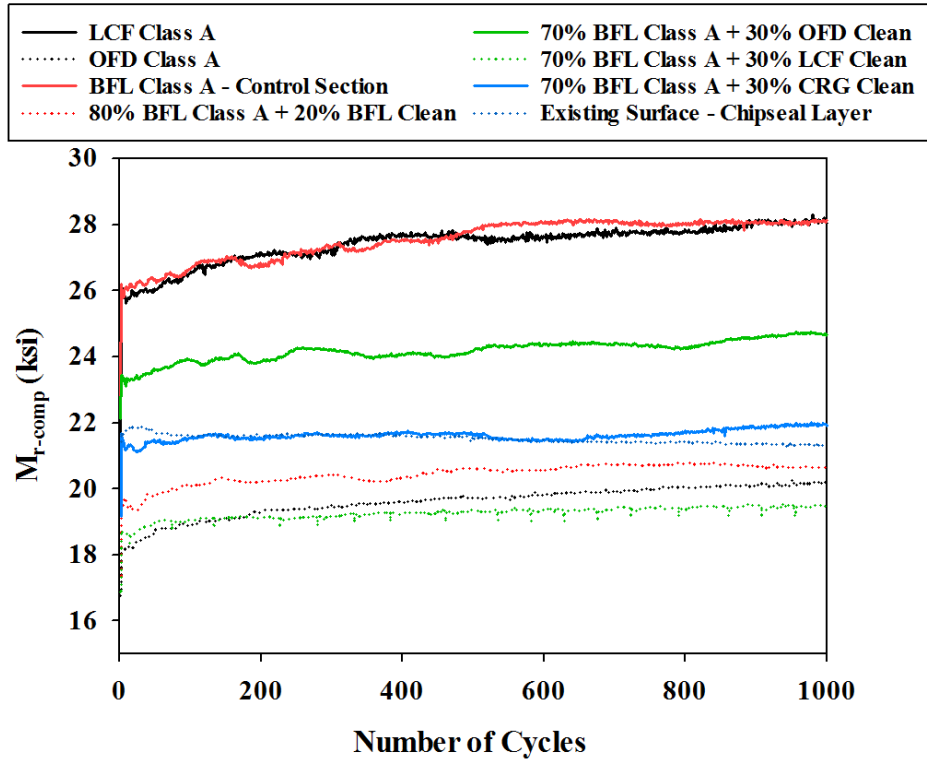


Figure 72. In situ M_{r-Comp} results at each test point

Similarly, results of δ_p are presented in Figure 73.

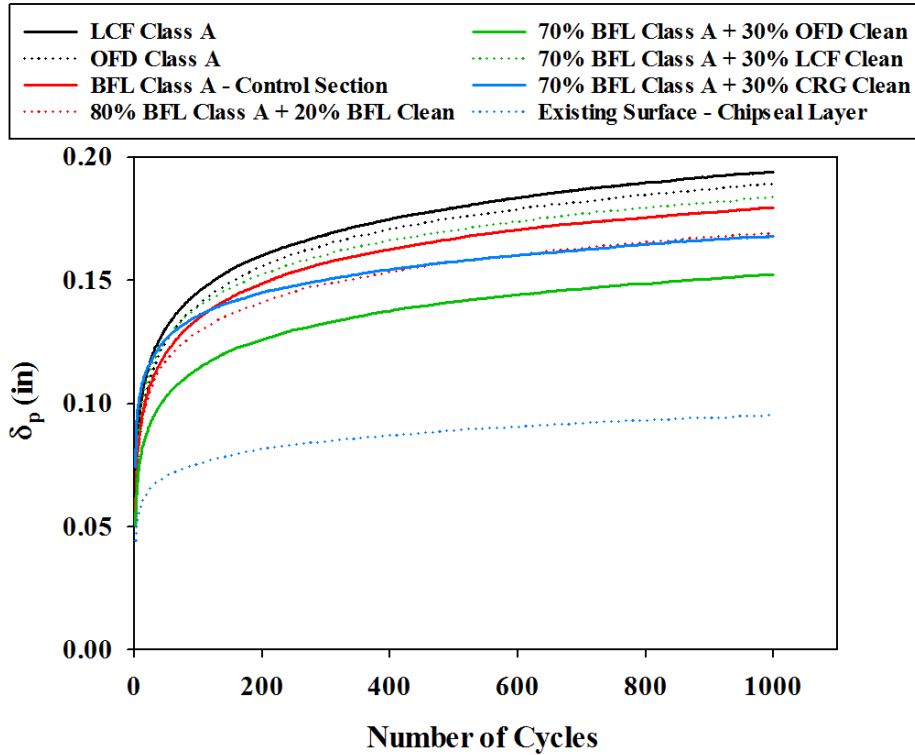


Figure 73. Permanent deformation (δ_p) results at each test point

The results of each test section are provided in Appendix D.

Table 47 summarizes the average in situ M_{r-comp} values for the last 50 loading cycles and δ_p at the end of the test.

Table 47. Comparison of in situ M_{r-comp} and δ_p at the end of the test results (cyclic stress = 90 psi)

Aggregate source	M_{r-comp} (ksi)	δ_p (in.)
LCF Class A	28.12	0.19
OFD Class A	20.17	0.19
BFL Class A	28.09	0.18
80% BFL Class A + 20% BFL Clean	20.66	0.17
70% BFL Class A + 30% OF Clean	24.7	0.15
70% BFL Class A + 30% LCF Clean	19.49	0.18
70% BFL Class A + 30% CRG Clean	21.94	0.17

The lowest M_{r-Comp} of about 19.5 ksi was measured for the 70% BFL Class A + 30% OFD Clean test section, and the highest M_{r-Comp} (28.1 ksi) was measured in LCF Class A. No significant differences in δ_p were found between test sections.

Table 48 summarizes C and d parameters for comparisons between N^* , δ_p at N^* , and adjusted δ_p at N^* (δ_p at N^* minus C), and N to reach $\delta_p = 0.5$ in. The N^* value represents the number of cycles to reach a near-linear elastic deformation state.

Table 48. Summary of permanent deformation prediction parameters (cyclic stress = 90 psi)

Aggregate source	C	d	R²	N* at $\Delta\delta = 10^{-6}$ in./cycle	δ_p (in.) at N*	Adj. δ_p (in.) at N*	N at $\delta_p = 0.5$ in.
LCF Class A	28,118	0.19	0.98	46,320	0.34	0.26	837,404
OFD Class A	20,174	0.19	0.98	50,871	0.35	0.28	628,416
BFL Class A	28,090	0.18	0.98	42,966	0.31	0.24	1,369,689
80% BFL Class A + 20% BFL Clean	20,659	0.17	0.98	35,539	0.27	0.2	3,694,398
70% BFL Class A + 30% OFD Clean	24,703	0.15	0.99	34,275	0.25	0.19	5,335,089
70% BFL Class A + 30% LCF Clean	19,486	0.18	0.99	39,963	0.3	0.23	1,779,304
70% BFL Class A + 30% CRG Clean	21,943	0.17	0.99	22,354	0.23	0.14	>>10 ⁷

Based on the power model parameters, 70% BFL Class A + 30% Clean produced the lowest N^* value (22.3k cycles) and OFD Class A produced the highest N^* value (50.9k cycles). The lowest number of cycles required to achieve a $\delta_p = 0.5$ in. was OFD Class A with approximately 628k cycles.

The results presented herein demonstrated the response of the composite foundation system (aggregate layer + underlying subgrade) to cyclic loading at the different test points. The differences observed among the test points can be attributed to variations in the following:

- Underlying subgrade layer strength/stiffness
- Aggregate layer's material properties
- Aggregate layer's stiffness (because of the differences in material type and compaction)
- Thickness of the aggregate layer

The DCP test results confirmed that variable base and subgrade layer conditions existed between the different sections, and the thickness of the base layer may not have been a constant 4 in. Because of the combined effect of these variables on the overall response, the influence of the material type on the resilient modulus or permanent deformation could be observed accurately.

6.7 IRI Results

In this project, IRI was measured by "Roadroid," an Android-based application. In order to remove any additional movement of the phone while performing the IRI tests, a firm mount was used to connect the phone to the windshield. Moreover, the same truck and mounting location were used each time the test was performed. The calculated IRI (cIRI) with a narrower range of speed between 37 and 50 mph was used, rather than of the estimated IRI (eIRI), which had a broader range of speed between 12 and 62 mph. Therefore, cIRI values provided higher accuracy than eIRI values (41). The cIRI values measured during this study are shown in Figure 74.

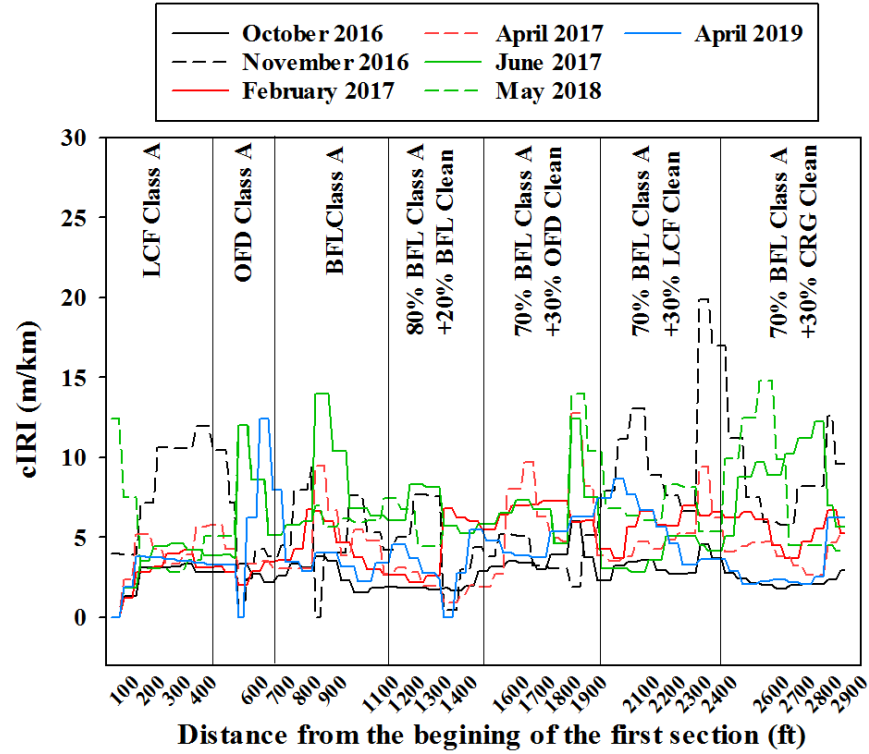


Figure 74. cIRI values over the length of the road

The IRI values are categorized into four different specifications as shown in Table 49.

Table 49. IRI classification

IRI specification	IRI values
Good	<4
Fair	4–6
Poor	6–8
Bad	>8

The average values of each section for different times are presented in Figure 75 and Table 50.

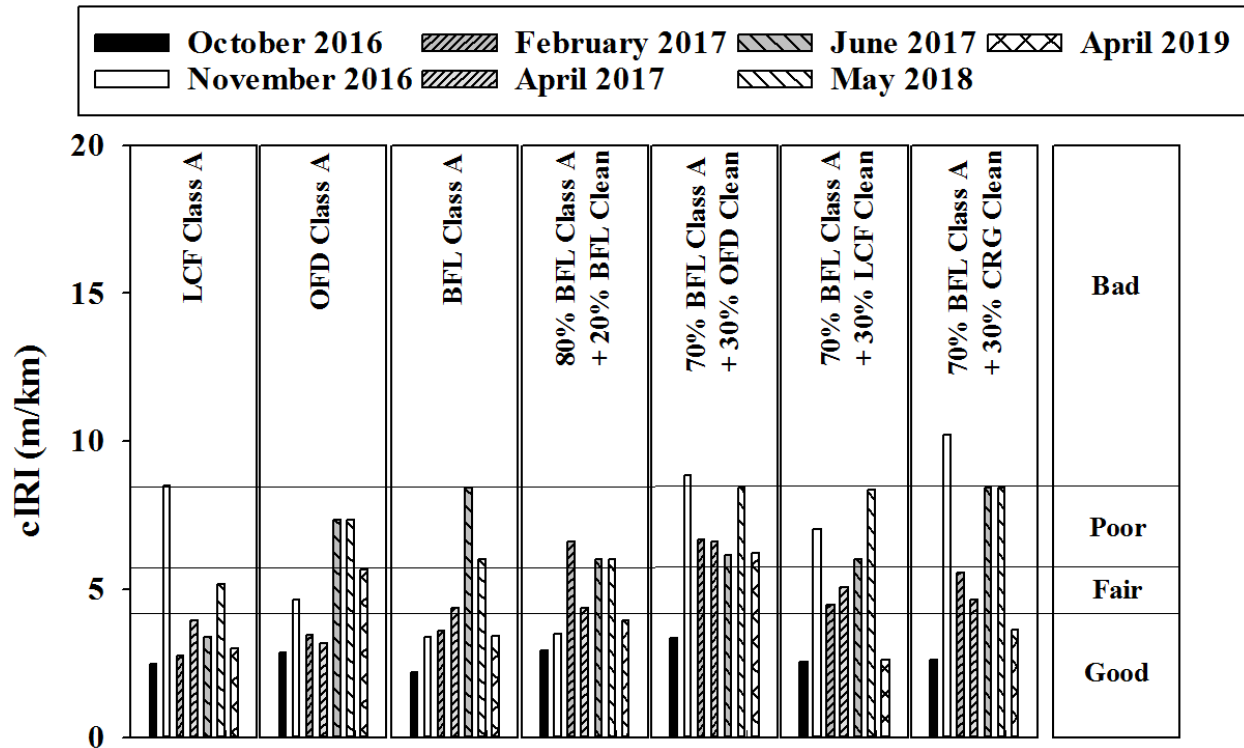


Figure 75. Average values of cIRI for each section over time

Table 50. Average IRI values for each section over time

Sections	Oct 2016	Nov 2016	Feb 2017	Apr 2017	Jun 2017	May 2018	Apr 2019	Average	Condition
LCF Class A	2	9	3	4	3	5	3	4	Fair
OFD Class A	3	5	3	3	7	7	6	5	Fair
BFL Class A	2	3	4	4	8	6	3	4	Fair
80% BFL Class A + 20% BFL Clean	3	3	7	4	6	6	4	5	Fair
70% BFL Class A + 30% OFD Clean	3	9	7	7	6	8	6	7	Poor
70% BFL Class A + 30% LCF Clean	3	7	4	5	6	8	3	5	Fair
70% BFL Class A + 30% CRG Clean	3	10	6	5	8	8	4	6	Poor

The average values of cIRI for all sections had a fair quality of smoothness except the following sections: 70% BFL Class A + 30% OFD Clean and 70% BFL Class A + 30% CRG Clean, which had poor quality of smoothness. The average cIRI values over time showed that LCF Class A and BFL Class A had the best smoothness among the sections.

6.8 LWD Results

LWD tests were performed in October 2016, November 2016, December 2016, February 2017, April 2017, June 2017, May 2018, and April 2019. The objective of this testing program was to assess the composite elastic modulus (E_{Comp}) of each test section. Figure 76 and Table 51 present the in situ E_{Comp} values over time.

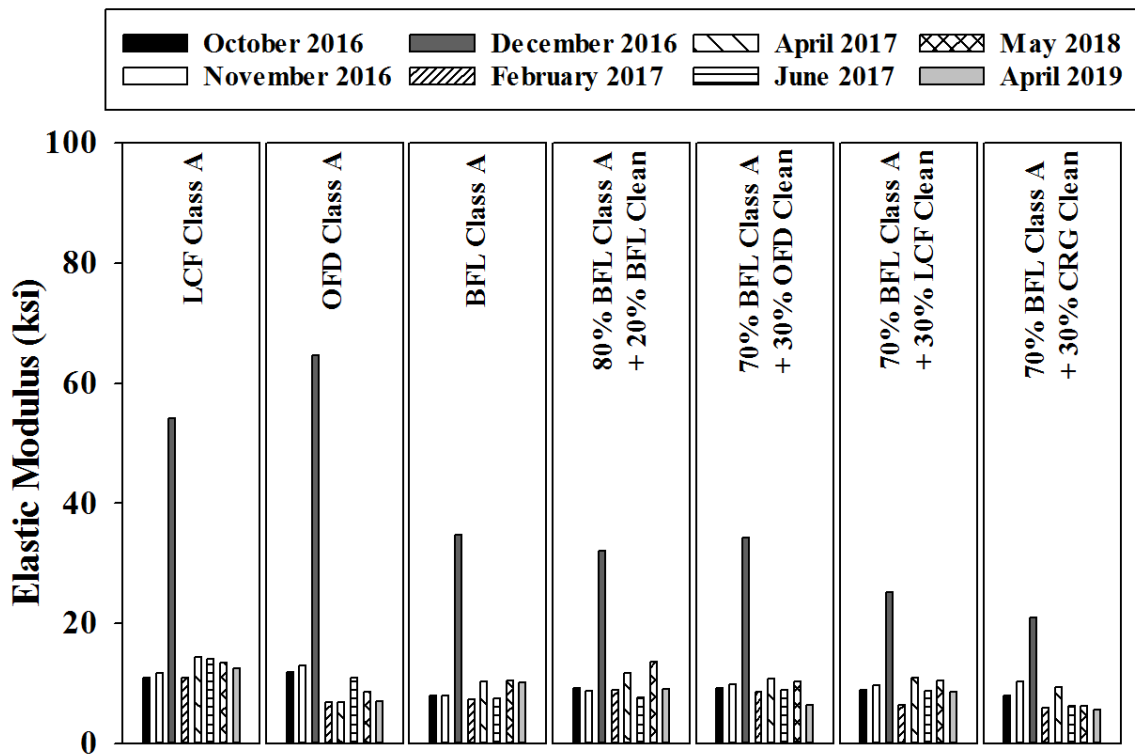


Figure 76. Average LWD composite elastic modulus results for each section over time

Table 51. LWD composite elastic modulus values (ksi) for all sections over time

Sections	Oct 2016	Nov 2016	Dec 2016	Feb 2017	Apr 2017	Jun 2017	May 2018	Apr 2019
LCF Class A	11	12	54	11	14	14	13	12
OFD Class A	12	13	65	7	7	11	9	7
BFL Class A	8	8	35	7	10	7	10	10
80% BFL Class A + 20% BFL Clean	9	9	32	9	12	8	14	9
70% BFL Class A + 30% OFD Clean	9	10	34	8	11	9	10	6
70% BFL Class A + 30% LCF Clean	9	10	25	6	11	9	10	8
70% BFL Class A + 30% CRG Clean	8	10	21	6	9	6	6	6

The results of the E_{Comp} and the change of E_{Comp} from the initial results in October 2016 for other times are explained in the following sections.

6.8.1 October 2016

The first set of LWD field testing was conducted in October 2016 (after construction, 36°F). OFD Class A (12 ksi) and BFL Class A (8 ksi) had the minimum and maximum E_{Comp} , respectively. The maximum and minimum standard deviations were observed for OFD Class A (4 ksi) and 70% BFL Class A + 30% CRG Clean (1 ksi), respectively (Table 52).

Table 52. Surface elastic modulus of LWD test in October 2016

Sections	Composite elastic modulus (ksi)				
	E_{Mean}	E_{Min}	E_{Max}	Range	SD
LCF Class A	11	10	11	1	0
OFD Class A	12	7	16	9	4
BFL Class A	8	7	10	4	1
80% BFL Class A + 20% BFL Clean	9	8	11	3	1
70% BFL Class A + 30% OFD Clean	9	8	10	3	1
70% BFL Class A + 30% LCF Clean	9	7	10	3	1
70% BFL Class A + 30% CRG Clean	8	7	9	2	1

6.8.2 November 2016

The second set of LWD field testing was conducted in November 2016 (32°F). The highest and the lowest in situ E_{Comp} were measured in OFD Class A (13 ksi) and BFL Class A (8 ksi), respectively, similar to October 2016. The maximum and minimum standard deviations were for BFL Class A (4 ksi) and 80% BFL Class A + 20% BFL Clean (1 ksi), respectively. The E_{Comp} of BFL Class A did not change from those values observed in October 2016. All sections with the exception of 80% BFL Class A + 20% BFL Clean (-6%) had an increase in their E_{Comp} (3 to 28%) in one month due to the decrease in the initial void ratio and compaction (Table 53).

Table 53. Surface elastic modulus of FWD test in November 2016

Sections	Composite elastic modulus (ksi)					
	E_{Mean}	E_{Min}	E_{Max}	Range	SD	Change (%)
LCF Class A	12	10	15	5	2	12
OFD Class A	13	9	17	7	3	13
BFL Class A	8	7	10	4	1	8
80% BFL Class A + 20% BFL Clean	9	8	10	2	1	9
70% BFL Class A + 30% OFD Clean	10	8	12	4	2	10
70% BFL Class A + 30% LCF Clean	10	8	11	3	1	10
70% BFL Class A + 30% CRG Clean	10	8	13	5	2	10

6.8.3 December 2016

The third set of LWD field testing was conducted in December 2016 (-16°F). All sections had a significant increase in their E_{Comp} due to the frozen ground conditions (123% to 445%). The highest E_{Comp} was measured for the OFD Class A (65 ksi), and the lowest E_{Comp} was measured for the 70% BFL Class A + 30% CRG Clean (21 ksi) section. OFD Class A and LCF Class A had the maximum standard deviations (54 ~ 56ksi), while the rest of the sections' standard deviations ranged from 2 to 7 ksi (Table 54).

Table 54. Surface elastic modulus of FWD test in December 2016

Sections	Composite elastic modulus (ksi)					
	E_{Mean}	E_{Min}	E_{Max}	Range	SD	Change (%)
LCF Class A	54	23	153	130	56	54
OFD Class A	65	32	160	127	54	65
BFL Class A	35	31	40	9	4	35
80% BFL Class A + 20% BFL Clean	32	22	43	20	7	32
70% BFL Class A + 30% OFD Clean	34	25	39	14	6	34
70% BFL Class A + 30% LCF Clean	25	17	31	13	5	25
70% BFL Class A + 30% CRG Clean	21	14	29	15	6	21

6.8.4 February 2017

The fourth set of LWD tests was conducted in February 2017 (30°F). E_{Comp} values decreased for all sections due to the initial thawing after winter, from 3% (80% BFL Class A + 20% BFL Clean) to 42% (OFD Class A), except the LCF Class A with an almost 1% increase in E_{Comp} . LCF Class A had the maximum (11 ksi) stiffness. Table 55 shows that the 80% BFL Class A + 20% BFL Clean and 70% BFL Class A + 30% OFD Clean sections had the highest stiffness among the mixture sections.

Table 55. Surface elastic modulus of FWD test in February 2017

Sections	Composite elastic modulus (ksi)					
	E_{Mean}	E_{Min}	E_{Max}	Range	SD	Change (%)
LCF Class A	11	10	12	2	1	11
OFD Class A	7	6	8	2	1	7
BFL Class A	7	2	9	7	3	7
80% BFL Class A + 20% BFL Clean	9	8	10	2	1	9
70% BFL Class A + 30% OFD Clean	8	7	10	3	2	8
70% BFL Class A + 30% LCF Clean	6	4	10	5	2	6
70% BFL Class A + 30% CRG Clean	6	4	8	4	2	6

6.8.5 April 2017

The fifth set of LWD field testing was conducted in April 2017 (70°F), after the freezing and thawing season. The maximum and minimum E_{Comp} were observed for LCF Class A (14 ksi) and OFD Class A section (7 ksi). The LCF Class A and OFD Class A sections also had the highest and lowest standard deviations (3 and 2.3 ksi, respectively). E_{Comp} values increased for all sections from 16 ksi (70% BFL Class A + 30% CRG Clean) to 32 ksi (LCF Class A), except for OFD Class A (Table 56).

Table 56. Surface elastic modulus of FWD test in April 2017

Sections	Composite elastic modulus (ksi)					
	E_{Mean}	E_{Min}	E_{Max}	Range	SD	Change (%)
LCF Class A	14	12	19	7	3	14
OFD Class A	7	6	8	2	1	7
BFL Class A	10	8	14	6	2	10
80% BFL Class A + 20% BFL Clean	12	8	14	6	2	12
70% BFL Class A + 30% OFD Clean	11	9	12	3	1	11
70% BFL Class A + 30% LCF Clean	11	9	12	3	1	11
70% BFL Class A + 30% CRG Clean	9	8	11	3	1	9

6.8.6 June 2017

The sixth set of LWD field testing was conducted in June 2017, after maintenance (106°F). The highest E_{Comp} was observed for LCF Class A (14 ksi), and the lowest E_{Comp} was observed for the 70% BFL Class A + 30% CRG Clean (6.2 ksi), similar to April 2017. Except LCF Class A, which had a 29% increase in the E_{Comp} , all of the other sections experienced decreases in their E_{Comp} , from 2% (70% BFL Class A + 30% LCF Clean) to 23% (70% BFL Class A + 30% CRG Clean). The 70% BFL Class A + 30% OFD Clean and 70% BFL Class A + 30% LCF Clean yielded the highest E_{Comp} among the mixture sections (Table 57).

Table 57. Surface elastic modulus of FWD test in June 2017

Sections	Composite elastic modulus (ksi)					
	E_{Mean}	E_{Min}	E_{Max}	Range	SD	Change (%)
LCF Class A	14	10	24	14	6	14
OFD Class A	11	8	18	11	4	11
BFL Class A	7	5	9	4	2	7
80% BFL Class A + 20% BFL Clean	8	6	9	4	1	8
70% BFL Class A + 30% OFD Clean	9	8	10	2	1	9
70% BFL Class A + 30% LCF Clean	9	7	10	3	1	9
70% BFL Class A + 30% CRG Clean	6	4	9	4	2	6

6.8.7 May 2018

The seventh set of LWD field testing was conducted in May 2018 (43°F), after the second freeze/thaw period. E_{Comp} values increased for all sections except OFD Class A (-28%) and 70% BFL Class A + 30% CRG Clean (-23%) sections. The highest E_{Comp} was observed for 80% BFL Class A + 20% BFL Clean (14 ksi), and the lowest E_{Comp} was observed for 70% BFL Class A + 30% CRG Clean (6 ksi). OFD Class A had the minimum standard deviation (~1 ksi), and 70% BFL Class A + 30% OFD Clean and 70% BFL Class A + 30% LCF Clean had the maximum standard deviations (2 ksi) (Table 58).

Table 58. Surface elastic modulus of FWD test in May 2018

Sections	Composite elastic modulus (ksi)					
	E_{Mean}	E_{Min}	E_{Max}	Range	SD	Change (%)
LCF Class A	13	11	16	5	2	13
OFD Class A	9	8	9	1	1	9
BFL Class A	10	9	13	3	1	10
80% BFL Class A + 20% BFL Clean	14	13	15	2	1	14
70% BFL Class A + 30% OFD Clean	10	8	13	5	2	10
70% BFL Class A + 30% LCF Clean	10	8	12	5	2	10
70% BFL Class A + 30% CRG Clean	6	4	9	4	2	6

6.8.8 April 2019

The last set of LWD field testing was conducted in April 2019 (46°F), after the third freeze/thaw period. E_{Comp} values increased for all sections except LCF Class A (27%). The highest E_{Comp} was observed for 80% BFL Class A + 20% BFL Clean (14 ksi), and the lowest E_{Comp} was observed for 70% BFL Class A + 30% CRG Clean (6 ksi). Standard deviations of all sections were below 1 ksi except for OFD Class A and BFL Class A (~ 1 ksi) and 70% BFL Class A + 30% LCF Clean (3 ksi) (Table 59).

Table 59. Surface elastic modulus of FWD test in April 2019

Sections	Composite elastic modulus (ksi)					
	E _{Mean}	E _{Min}	E _{Max}	Range	SD	Change (%)
LCF Class A	14	13	14	2	1	14
OFD Class A	7	6	8	2	1	7
BFL Class A	11	10	12	3	1	11
80% BFL Class A + 20% BFL Clean	9	9	10	1	0	9
70% BFL Class A + 30% OFD Clean	6	5	6	1	1	6
70% BFL Class A + 30% LCF Clean	9	7	13	6	3	9
70% BFL Class A + 30% CRG Clean	6	5	7	2	1	6

In order to compare the stiffness of the road sections over time, the average results and the standard deviations of the E_{Comp} values from the LWD tests are shown in Table 60.

Table 60. LWD composite elastic modulus mean values and the standard deviations for each section

Sections	E _{Comp-avg} (ksi)	SD (ksi)
LCF Class A	13	1
OFD Class A	9	3
BFL Class A	9	1
80% BFL Class A + 20% BFL Clean	10	2
70% BFL Class A + 30% OFD Clean	9	1
70% BFL Class A + 30% LCF Clean	9	2
70% BFL Class A + 30% CRG Clean	7	2

The E_{Comp} results for December 2016 are excluded from the average values since those measurement were taken when the ground was frozen.

Table 60 shows that LCF Class A had the highest (12 ksi) E_{Comp} values over time. OFD Class A, had higher standard deviations (3 ksi) compared to the other sections with standard deviations equal to and below 2 ksi.

6.9 Dustometer Test Results

In order to evaluate the dust production of each test section in relation to the different aggregate sources utilized in the surface layers, the dustometer tests were performed in October and December 2016; February, April, and June 2017; May 2018; and April 2019. Figure 77 and Table 61 show the results of dust production (lb/mile) during the three years of the project for all seven test sections.

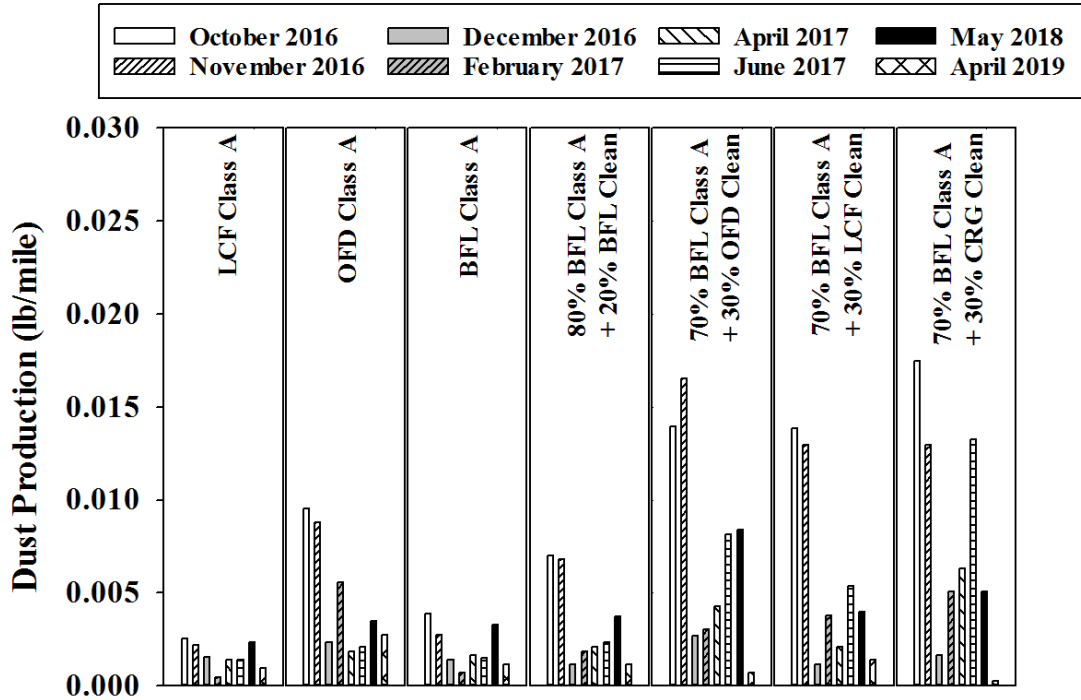


Figure 77. Dustometer results for each section over time

Table 61. Dust production (E-03 lb/mile) for all sections over time

Sections	Oct 2016	Nov 2016	Dec 2016	Feb 2017	Apr 2017	Jun 2017	May 2018	Apr 2019
LCF Class A	3	2	2	0.5	1	1	2	1
OFD Class A	10	9	2	6	2	2	3	3
BFL Class A	4	3	1	1	2	2	3	1
80% BFL Class A + 20% BFL Clean	7	7	1	2	2	2	4	1
70% BFL Class A + 30% OFD Clean	14	17	3	3	4	8	8	1
70% BFL Class A + 30% LCF Clean	14	13	1	4	2	5	4	1
70% BFL Class A + 30% CRG Clean	17	13	2	5	6	13	5	0.2

6.9.1 October 2016

The first dustometer test was conducted in October 2016 (after construction). The lowest dust production of about 3 E-03 lb/mile was measured in the LCF Class A, and the highest dust production of about 18 E-03 lb/mile was measured in 70% BFL Class A + 30% CRG Clean.

6.9.2 November 2016

The second dustometer test was conducted in November 2016. The lowest dust production of about 2 E-03 lb/mile was measured in the LCF Class A, and the highest dust production of about 17 E-03 lb/mile was measured in 70% BFL Class A + 30% OFD Clean.

6.9.3 December 2016

The third set of dustometer tests was conducted in December 2016, during the freezing season. All of the test sections showed a significant decrease in their dust production, especially the 70% BFL Class A + 30% OFD Clean. The BFL Class A, 80% BFL Class A + 20% BFL Clean, and 70% BFL Class A + 30% LCF Clean sections had the lowest dust production (1 E-03 lb/mile), while the maximum dust production was for 70% BFL Class A + 30% OFD Clean (3 E-03 lb/mile).

6.9.4 February 2017

The fourth set of dustometer tests was conducted in February 2017, at the end of the freezing season. The change in the dust production was not significant for all sections. The highest dust production was observed in OFD Class A (6 E-03 lb/mile), while the lowest dust production was for BFL Class A (1 E-03 lb/mile).

6.9.5 April 2017

The fifth set of dustometer tests was conducted in April 2017, during the thawing season. Almost all of the sections had a low dust production (1 to 6 E-03 lb/mile) because of wet surfaces due to thawing. Nevertheless, the highest dust production was observed for 70% BFL Class A + 30% CRG Clean (6 E-03 lb/mile), and the lowest dust production was for LCF Class A (1 E-03 lb/mile).

6.9.6 June 2017

The sixth set of dustometer field testing was conducted in June 2017. An insignificant change in dust production was observed for all sections compared to April 2017, except for 70% BFL Class A + 30% CRG Clean, where the highest dust production was observed (13 E-03 lb/mile). The lowest dust production was observed for LCF Class A (1 E-03 lb/mile).

6.9.7 May 2018

The seventh set of dustometer field testing was conducted in May 2018, after the second freeze/thaw period. The highest dust production was observed for 70% BFL Class A + 30% OFD Clean (8 E-03 lb/mile), and the lowest dust production was observed for LCF Class A (2 E-03 lb/mile).

6.9.8 April 2019

The last set of dustometer field testing was conducted in April 2019, after the third freeze/thaw period. The amount of dust for all sections was lower than other times (<3 E-03 lb/mile). The

highest dust production was observed for OFD Class A (3 E-03 lb/mile), and the lowest dust production was observed for 70% BFL Class A + 30% CRG Clean (0.2 E-03 lb/mile).

Table 62 shows the average results of dust production for each of the sections for the different times of performing the dustometer test.

Table 62. Average dust production for each section

Sections	Average dust production (E-03 lb/mile)
LCF Class A	2
OFD Class A	5
BFL Class A	2
80% BFL Class A + 20% BFL Clean	3
70% BFL Class A + 30% OFD Clean	7
70% BFL Class A + 30% LCF Clean	6
70% BFL Class A + 30% CRG Clean	8

The table shows that the 70% BFL Class A + 30% CRG Clean section had the maximum dust production, equal to 7.75 E-3 lb/mile, and LCF Class A had the lowest dust production value, which was 1.60 E-3 lb/mile.

6.10 Ground Temperature Monitoring Results

In order to monitor the change in the temperature at different depths, eight thermocouples were installed in the center and at the shoulder of the LCF Class A section, on November 10, 2016. The first two thermocouples were placed at a depth of 6 in. and 1 ft below the ground surface. The spacing between the other thermocouples was 1 ft, and the last thermocouple was placed 7 ft below the ground surface. All thermocouples were connected to two data loggers, which were placed in a pelican case on top of a wooden table on the shoulder of the road (Figure 78).



Figure 78. Data loggers to record the temperature changes

Figure 79 shows a sketch of the thermocouples.

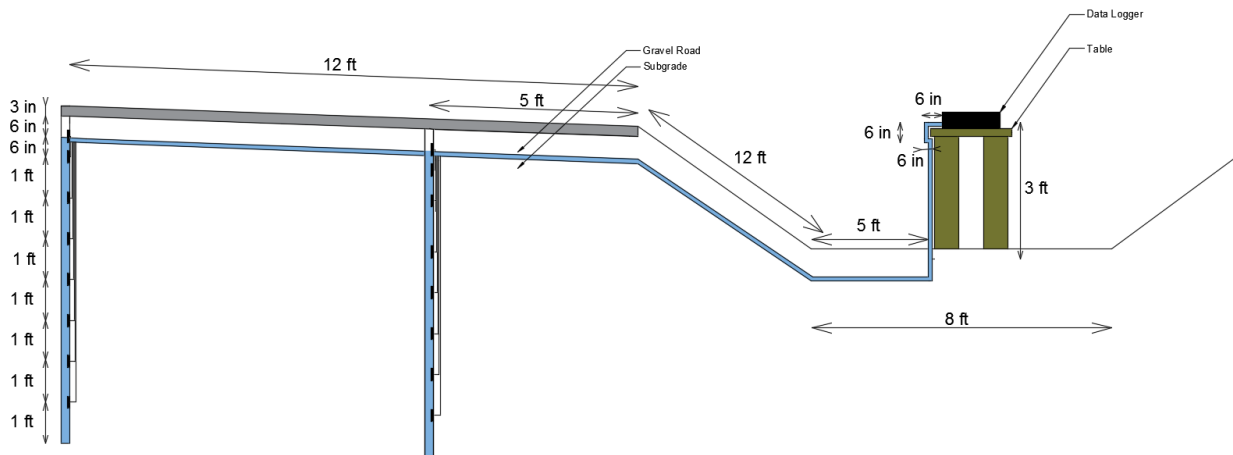


Figure 79. Sketch details of the center and shoulder thermocouples and the data loggers

In addition, photographs of the step-by-step installation are provided in Appendix E.

Figure 80 shows the temperature values at the different depths for the center of the road.

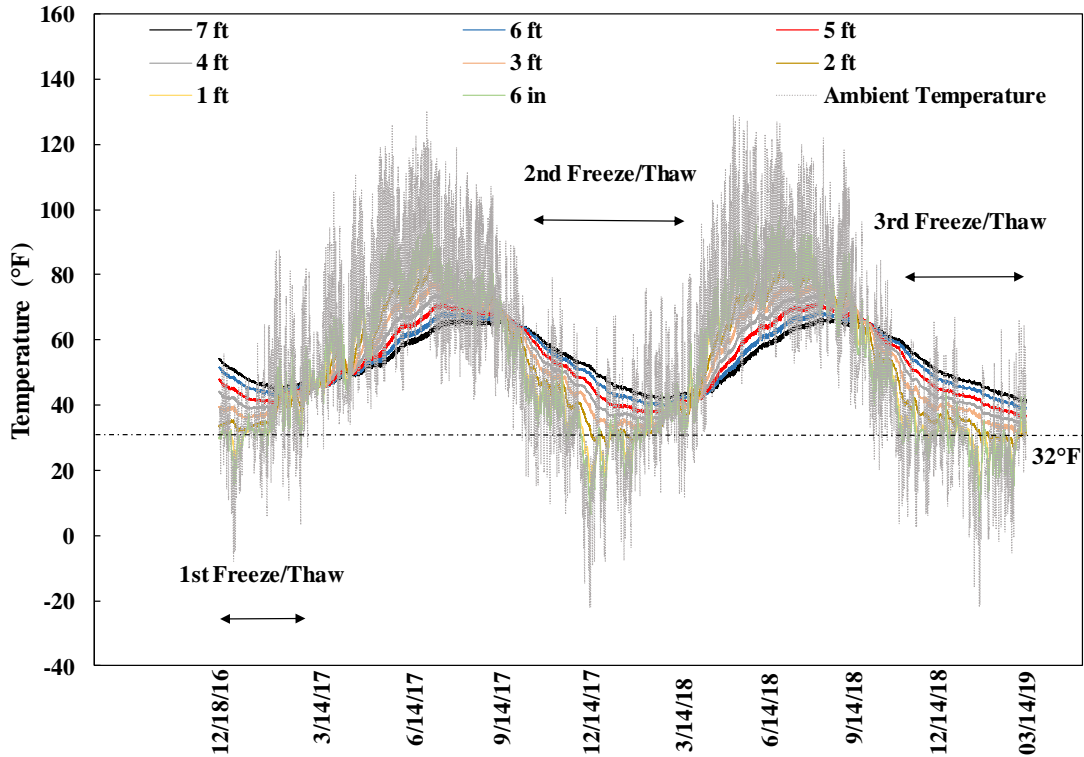


Figure 80. Temperature variations recorded for the center of the road

The thermocouples at the center recorded the temperatures between December 22, 2016 and March 18, 2019. The center thermocouples showed the hottest and coldest surface temperature as 96°F on July 21 and 22, 2017, and 6°F on January 1, 2018, respectively. In addition, the ambient temperature at the center of the road ranged between -22 and 130°F. Based on the results of the temperature obtained from the thermocouples at the center of the road, three freeze/thaw periods were observed between December 22, 2016 and April 7, 2017; October 28, 2017 and April 19, 2018; and November 10, 2018 and March 16, 2019.

Figure 81 shows the temperature values at the different depths for the shoulder of the road.

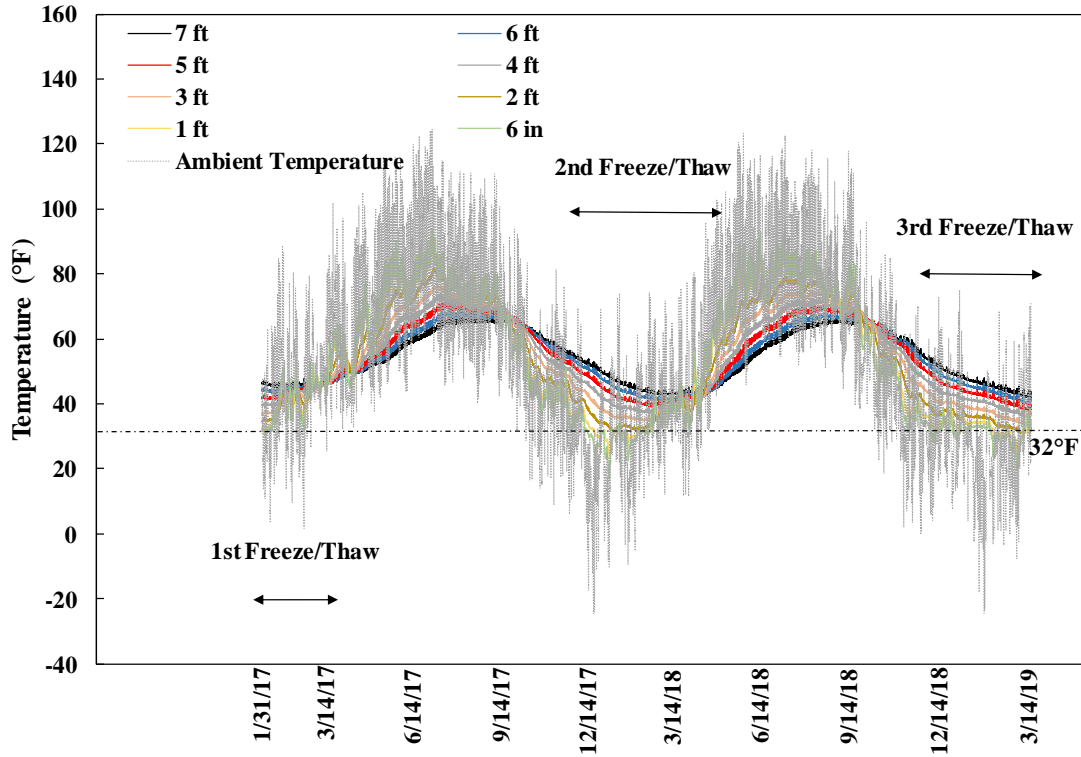


Figure 81. Temperature variations recorded for the shoulder of the road

The thermocouples at the shoulder of the road recorded the temperature between January 31, 2017 and March 18, 2019. The hottest and coldest surface temperature were measured as 94°F on July 22, 2017, and 17°F on January 17, 2018, respectively. In addition, the ambient temperature at the shoulder of the road ranged between -25 to 125°F. Three freeze/thaw periods were observed between January 31, 2017 and March 16, 2017; November 6, 2017 and April 20, 2018; and November 14, 2018 and March 16, 2019.

Figures 82 and 83 show that the variation of the temperature decreased with the increase in depth.

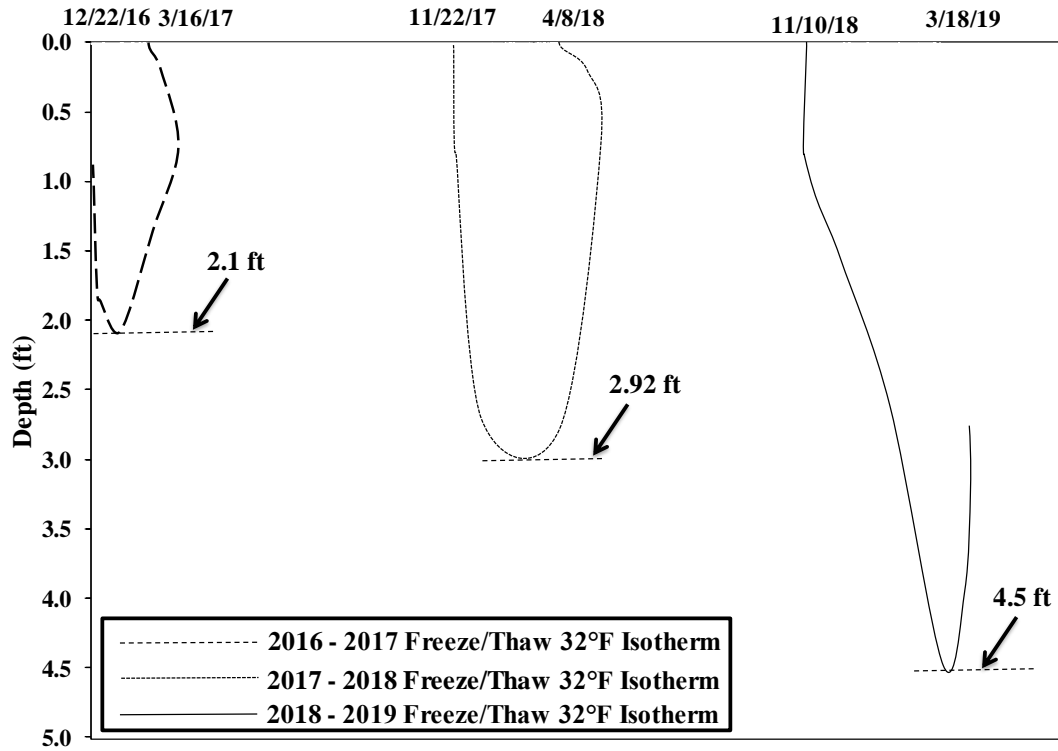


Figure 82. Freeze/thaw periods for three consecutive years, recorded at the center of the road

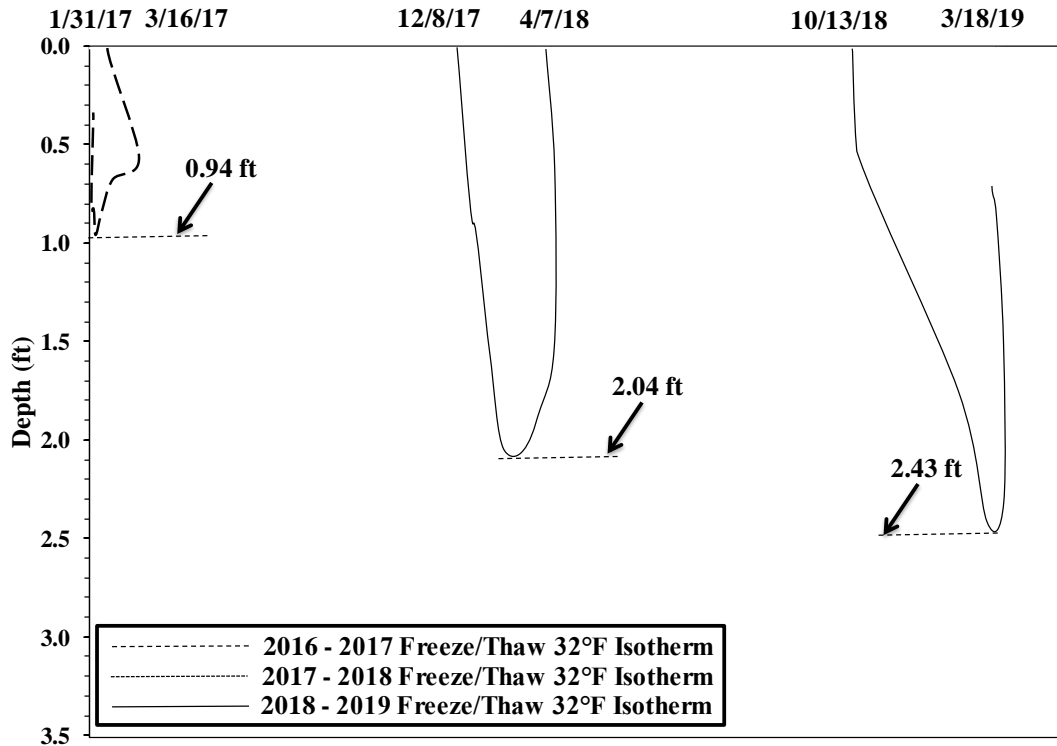


Figure 83. Freeze/thaw periods for two consecutive years, recorded at the shoulder of the road

Moreover, the temperature observed for the deeper thermocouples was always higher during the cold season and lower during the hot season, compared to the shallower thermocouples.

Figures 82 and 83 show the depth of the frozen zone for the three freeze/thaw periods observed for the length of the project. The results for both center and shoulder thermocouples show that the depth of the frozen zone for the second freeze/thaw period was higher than the first, and the third freeze/thaw period was deeper than the second. Therefore, the ground was frozen for a longer period of time compared to the first freeze/thaw period. The frost depth at the center was always deeper than the shoulder because the snow plowed to the shoulder acts as insulation, which caused a lower frost depth and higher ground temperature.

The number of the freeze/thaw cycles can be measured by the number of times that the temperature went below and above 32°F. The number of the freeze/thaw cycles also were depth dependent. Table 63 shows how many of the freeze/thaw cycles the different depths experienced.

Table 63. The number of the freeze/thaw periods that each layer experienced

Depth (ft)	Shoulder			Center		
	1st F/T	2nd F/T	3rd F/T	1st F/T	2nd F/T	3rd F/T
0.5	4	12	7	8	25	24
1	0	5	7	15	7	17
2	0	2	5	0	17	1
3	0	0	0	0	0	9
5	0	0	0	0	0	0
6	0	0	0	0	0	0
7	0	0	0	0	0	0

CHAPTER 7. COST ANALYSIS

Granular road surface aggregate materials were hauled from different quarries as shown in Figure 84.

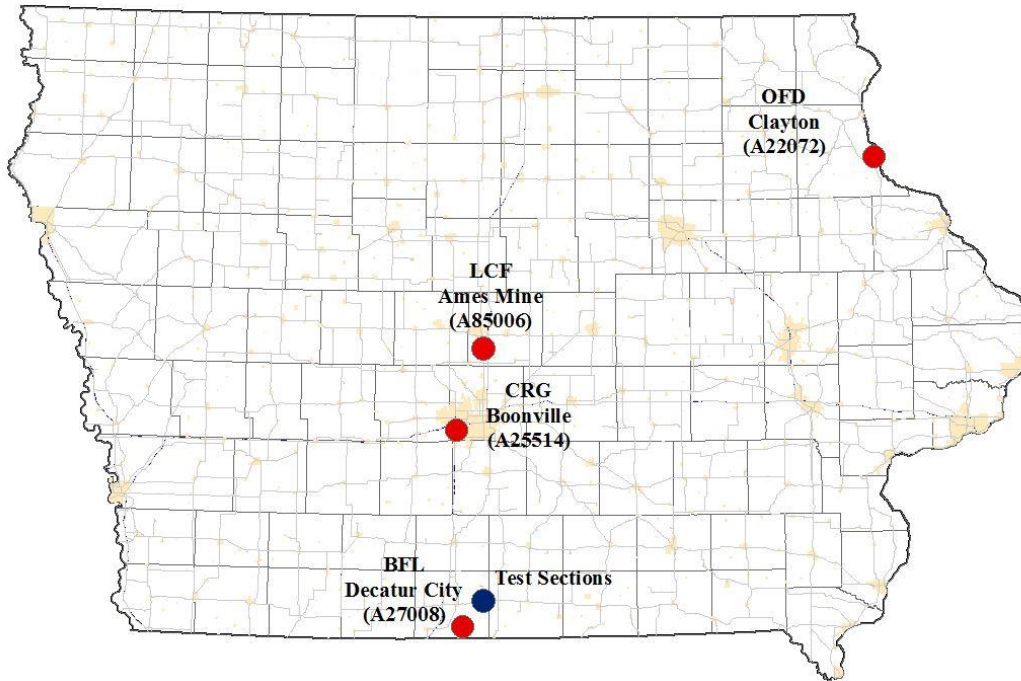


Figure 84. Locations of the aggregate resources and the site in Iowa

The haul time (min), material and cost (/ton), and the delivered prices for each of the aggregate types are summarized in Table 64.

Table 64. Aggregate and hauling time costs for each material

Source	Aggregate cost (\$/ton)	Haul time (min)	Labor haul cost (\$/truck)	Labor haul cost (\$/ton)	Delivered price (\$/ton)
BFL Class A	10.80	32	15.73	1.05	11.85
BFL Clean	13.45	32	15.73	1.05	14.50
CRG Clean	18.00	102	50.15	3.34	21.34
LCF Class A	9.55	182	89.48	5.97	15.52
LCF Clean	13.45	182	89.48	5.97	19.42
OFD Class A	3.35	612	300.75	20.05	23.40
OFD Clean	3.35	612	300.75	20.05	23.40

The labor haul rate was considered to be \$29.50/hr per 15 ton tandem-dump truck. Haul times were estimated based on Google Maps for round-trip travel. The costs of the OFD materials

(Class A and Clean) were lower than those of other materials. However, the longer haul time caused these materials' costs to be more expensive than the others.

The construction procedure required utilizing road construction equipment such as a motor grader, tandem- and belly-dump trucks, loader, tractor, and drum roller. The labor cost and the costs of the equipment per hour are presented in Table 65.

Table 65. Labor and equipment unit costs

Category	Unit cost per hour
On-site labor	\$30.40
Grader	\$69.11
Bottom-dump truck	\$76.64
Tandem-dump truck	\$49.37
Loader	\$47.29
Tractor	\$76.64
Drum roller	\$59.41

7.1 Construction Costs

The total granular road surface aggregate material tonnages and costs required for the construction based on the tonnage required for each section are summarized in Table 66.

Table 66. Weight of the surface aggregate materials required for each section for construction

Sections	BFL Class A (ton)	BFL Clean (ton)	CRG Clean (ton)	LCF Class A (ton)	LCF Clean (ton)	OFD Class A (ton)	OFD Clean (ton)	Total cost (\$)	Total cost (\$/ton)
LCF Class A	0	0	0	325	0	0	0	5,043	15.52
OFD Class A	0	0	0	0	0	195	0	4,563	23.40
BFL Class A	325	0	0	0	0	0	0	3,851	11.85
80% BFL Class A + 20% BFL Clean	210	55	0	0	0	0	0	3,286	12.40
70% BFL Class A + 30% OFD Clean	130	0	0	0	0	0	65	3,061	15.70
70% BFL Class A + 30% LCF Clean	140	0	0	0	72	0	0	3,057	14.42
70% BFL Class A + 30% CRG Clean	145	0	70	0	0	0	0	3,212	14.94

The costs in Table 66 include the labor costs for hauling and the costs of the aggregate materials.

Table 67 shows the separated costs of labor for hauling and aggregate.

Table 67. Gravel and labor cost of hauling the gravel for each section for construction

Sections	Gravel (\$)	Labor hauling (\$)
LCF Class A	3,104	1,939
OFD Class A	1,047	3,516
BFL Class A	3,510	341
80% BFL Class A + 20% BFL Clean	3,008	278
70% BFL Class A + 30% OFD Clean	1,753	1,308
70% BFL Class A + 30% LCF Clean	2,480	576
70% BFL Class A + 30% CRG Clean	2,826	386

The hours for labor and equipment for construction of the test sites are presented in Table 68.

Table 68. Labor and equipment required times for construction

Sections	Labor (hr)	Grader (hr)	Tandem dump (hr)	Bottom dump (hr)	Drum roller (hr)
LCF Class A	66	16	21	7	5
OFD Class A	46	11	15	5	4
BFL Class A	66	16	21	7	5
80% BFL Class A + 20% BFL Clean	66	16	21	7	5
70% BFL Class A + 30% OFD Clean	66	16	21	7	5
70% BFL Class A + 30% LCF Clean	66	16	21	7	5
70% BFL Class A + 30% CRG Clean	66	16	21	7	5

The labor and equipment time required for all sections were the same except for OFD Class A, due to the shorter length of this section.

Tables 69 and 70 show the calculated costs of the equipment and labor during test sites' construction, respectively. The labor costs included the costs for the construction and the cost of hauling labor.

Table 69. Equipment costs for each section for construction

Sections	Tandem dump (\$)	Bottom dump (\$)	Grader (\$)	Drum roller (\$)	Total (\$)
LCF Class A	1,037	536	1,106	297	2,976
OFD Class A	741	383	760	238	2,122
BFL Class A	1,037	536	1,106	297	2,976
80% BFL Class A + 20% BFL Clean	1,037	536	1,106	297	2,976
70% BFL Class A + 30% OFD Clean	1,037	536	1,106	297	2,976
70% BFL Class A + 30% LCF Clean	1,037	536	1,106	297	2,976
70% BFL Class A + 30% CRG Clean	1,037	536	1,106	297	2,976

Table 70. Labor costs of the sections for construction

Sections	On-site (\$)	Hauling (\$)	Total (\$)
LCF Class A	2,006	1,939	3,945
OFD Class A	1,398	3,516	4,914
BFL Class A	2,006	341	2,347
80% BFL Class A + 20% BFL Clean	2,006	278	2,284
70% BFL Class A + 30% OFD Clean	2,006	1,308	3,315
70% BFL Class A + 30% LCF Clean	2,006	576	2,583
70% BFL Class A + 30% CRG Clean	2,006	386	2,393

Table 71 summarizes the final construction costs based on the labor, equipment, and aggregate costs for each of the sections.

Table 71. Equipment, gravel, and labor total costs for each section per square yard

Sections	Equipment (\$/yd ²)	Gravel (\$/yd ²)	Labor (\$/yd ²)	Total (\$/yd ²)
LCF Class A	1.80	1.88	2.39	6.08
OFD Class A	2.14	1.06	4.96	8.16
BFL Class A	1.80	2.13	1.42	5.35
80% BFL Class A + 20% BFL Clean	1.80	1.82	1.38	5.01
70% BFL Class A + 30% OFD Clean	1.80	1.06	2.01	4.88
70% BFL Class A + 30% LCF Clean	1.80	1.50	1.57	4.87
70% BFL Class A + 30% CRG Clean	1.80	1.71	1.45	4.97

The equipment costs for all sections were the same except for OFD Class A, which was shorter. The surface aggregate cost for BFL Class A was higher than the other sections (\$2.13/yd²). The labor cost in Table 71 is the sum of the labor costs for hauling and the costs of the labor hours spent on-site. Due to the longer distance between the OFD quarry and the test sites, the labor cost

for hauling was much higher than those of other sections (\$4.96/yd²). Table 71 shows that test sections built with clean aggregates had lower total costs.

7.2 Maintenance Costs

Based on the field survey and material collection in April 2017, it was decided to add more surface aggregate materials in order to get the particle-size distribution curve as close as possible to the initial construction gradation. The minimum aggregate materials (by weight) were dumped on the OFD Class A section and the maximum were added to the 70% BFL Class A + 30% OFD Clean section. The total surface aggregate material tonnages and costs required for the maintenance based on the tonnage required for each section are summarized in Table 72.

Table 72. Weight of the surface gravel materials required for each section for maintenance

Sections	BFL Class A (ton)	BFL Clean (ton)	CRG Clean (ton)	LCF Class A (ton)	LCF Clean (ton)	OFD Class A (ton)	OFD Clean (ton)	Total Cost (\$)	Total Cost (\$/ton)
LCF Class A	0	0	0	60	0	0	0	931	15.52
OFD Class A	0	0	0	0	0	20	0	468	23.40
BFL Class A	80	0	0	0	0	0	0	948	11.85
80% BFL Class A + 20% BFL Clean	75	10	0	0	0	0	0	1034	12.16
70% BFL Class A + 30% OFD Clean	75	0	0	0	0	0	30	1591	15.15
70% BFL Class A + 30% LCF Clean	45	0	0	0	20	0	0	922	14.18
70% BFL Class A + 30% CRG Clean	45	0	20	0	0	0	0	960	14.77

This cost includes the labor costs for material hauling and the costs of the aggregate materials. Table 73 shows the separated labor cost for hauling and aggregate cost.

Table 73. Aggregate and labor cost of hauling the gravel for each section for maintenance

Sections	Aggregate (\$)	Labor hauling (\$)
LCF Class A	573	358
OFD Class A	107	361
BFL Class A	864	84
80% BFL Class A + 20% BFL Clean	945	89
70% BFL Class A + 30% OFD Clean	971	620
70% BFL Class A + 30% LCF Clean	755	167
70% BFL Class A + 30% CRG Clean	846	114

The hours for labor and equipment for maintenance of the test sites are presented in Table 74.

Table 74. Labor and equipment required times for maintenance

Sections	Labor (hr)	Grader (hr)	Tandem dump (hr)	Loader (hr)
LCF Class A	10	3	6	2
OFD Class A	7	2	4	2
BFL Class A	10	3	6	2
80% BFL Class A + 20% BFL Clean	10	3	6	2
70% BFL Class A + 30% OFD Clean	10	3	6	2
70% BFL Class A + 30% LCF Clean	10	3	6	2
70% BFL Class A + 30% CRG Clean	10	3	6	2

The belly-dump truck and drum roller were not used during maintenance. The surface compaction was done by tire compaction with a motor grader and loader.

Tables 75 and 76 present the calculated costs of the equipment and labor for the maintenance, respectively.

Table 75. Equipment costs for each sections for maintenance

Sections	Tandem dump (\$)	Grader (\$)	Loader (\$)	Total (\$)
LCF Class A	1,037	1,106	94.58	598
OFD Class A	741	760	47.29	383
BFL Class A	1,037	1,106	94.58	598
80% BFL Class A + 20% BFL Clean	1,037	1,106	94.58	598
70% BFL Class A + 30% OFD Clean	1,037	1,106	94.58	598
70% BFL Class A + 30% LCF Clean	1,037	1,106	94.58	598
70% BFL Class A + 30% CRG Clean	1,037	1,106	94.58	598

Table 76. Labor costs for each section for maintenance

Sections	On-Site (\$)	Hauling (\$)	Total (\$)
LCF Class A	304	358	662
OFD Class A	213	361	573
BFL Class A	304	84	388
80% BFL Class A + 20% BFL Clean	304	89	393
70% BFL Class A + 30% OFD Clean	304	620	924
70% BFL Class A + 30% LCF Clean	304	167	471
70% BFL Class A + 30% CRG Clean	304	114	418

Table 77 summarizes the final maintenance costs including the labor, equipment, and aggregate costs for each section.

Table 77. Equipment, gravel, and labor total costs for each section per square yard

Sections	Equipment (\$/yd²)	Gravel (\$/yd²)	Labor (\$/yd²)	Total (\$/yd²)
LCF Class A	0.36	0.35	0.40	1.11
OFD Class A	0.39	0.11	0.58	1.07
BFL Class A	0.36	0.52	0.24	1.12
80% BFL Class A + 20% BFL Clean	0.36	0.57	0.24	1.17
70% BFL Class A + 30% OFD Clean	0.36	0.59	0.56	1.51
70% BFL Class A + 30% LCF Clean	0.36	0.46	0.29	1.11
70% BFL Class A + 30% CRG Clean	0.36	0.51	0.25	1.13

The equipment costs for all sections were the same except the OFD Class A, which was shorter. The gravel cost for 70% BFL Class A + 30% OFD Clean was higher than those of other sections (\$0.59/yd²), and the OFD Class A had the lowest gravel cost (\$0.11/yd²) because it had the lowest material loss and thickness change. The labor cost in Table 77 is the sum of the labor costs of material hauling and labor hours spent on-site for maintenance. OFD Class A had the

highest cost for labor due to the long distance between the test site and quarry. The maintenance costs per square yard for all sections were almost the same ($\approx \$1/\text{yd}^2$). However, the 70% BFL Class A + 30% OFD Clean section had the most costly maintenance within all sections ($\$1.51/\text{yd}^2$), while the section built with LCF Clean had the lowest maintenance cost.

7.3 Hauling Costs

There are several methods to haul aggregate materials from quarries, including railways and roadways. It is common practice for LCF and OFD aggregates sources to be hauled via railways. All aggregate materials used in this study were hauled via roadways. However, the research team also investigated the costs benefits of material transportation via railways.

Table 78 presents the hauling costs per ton for the Class A and clean materials used in this study. It should be noted that none of the materials were actually transported via railway in this study; however, possible hauling cost via railway were estimated and used in the cost analyses.

Table 78. Comparisons between the labor costs of hauling materials for railway and roadway

Source	Labor haul cost (\$/ton)	
	Truck	Rail
BFL	1.05	-
CRG	3.34	-
LCF	5.97	47.8
OFD	20.05	14.63

The lowest hauling cost is by truck for BFL (Decatur City) materials due to the proximity of the quarry to the construction site. LCF has a higher hauling cost than CRG because of the longer distance from LCF quarry (Ames) than CRG (West Des Moines) to the construction site. OFD materials are from northeast Iowa (Clayton), and the distance between the Clayton quarry and the site is almost 271 miles (based on Google Maps). Therefore, the most expensive truck hauling cost was for the OFD materials.

LCF and OFD sources also use railways for hauling. The OFD quarry transports the majority of its aggregate materials through its transload location in Clayton by rail. These materials are shipped to the closest transload location, which is Centerville, Iowa. Once the materials are unloaded from railcars, they are reloaded into trucks and transported to the site. The transportation cost of this method is the costs of rail and truck transportation. Therefore, the rail transportation costs for the OFD materials ($\$14.63/\text{ton}$) are cheaper than the truck transportation ($\$20.05/\text{ton}$) as expected. On the other hand, the rail transportation cost for the LCF material ($\$47.80/\text{ton}$) is much more expensive than the truck transportation ($\$5.97/\text{ton}$). For rail transportation, LCF materials are shipped by trucks from the Ferguson quarry to Newton (transload location). The LCF source is served by a single railroad, originating in Newton, and ending in Council Bluffs. Any changes to the route requires an interchange from one railroad to

another, which incurs switching charges and delay. The handling costs for the loading and unloading are also added to the freight rail cost. In addition, there is an additional truck hauling cost from Council Bluffs to the construction site, like with the OFD source hauling. (144 miles).

7.4 Benefit-Cost Analysis

This project collected Class A and clean aggregates from four different quarries. Three sections were built with Class A materials, and four sections were built by mixing local Class A material (BFL) with clean aggregates. Each section has different properties and conditions. The main differences are construction and maintenance costs, durability (gradation change, total breakage), dust production, and engineering properties (stiffness and strength). A benefit-cost analysis (BCA) was performed in order to find the benefits of each section and compared them to each other. In order to conduct a BCA for this project, three main steps were followed: defining the base case and alternatives, determining the benefits, and calculating the current value of costs and benefits. These steps for BCA analyses are discussed in the following sections.

7.5 Base Case and Alternatives

The first step in BCA is to concisely determine the base case. Accordingly, BFL Class A (the local commonly used material) was considered as the base case, and the other sections were selected as alternatives. Table 79 shows the total construction costs of all sections.

Table 79. Total costs of construction for each section

Sections	Total (\$)	Length (mile)	Total (\$/mile)
LCF Class A	10,025	0.09	105,864
OFD Class A	8,083	0.06	142,261
BFL Class A	8,833	0.09	93,280
80% BFL Class A + 20% BFL Clean	8,268	0.09	87,312
70% BFL Class A + 30% OFD Clean	8,044	0.09	84,943
70% BFL Class A + 30% LCF Clean	8,039	0.09	84,894
70% BFL Class A + 30% CRG Clean	8,195	0.09	86,535

Due to the differences in the length of sections, the total construction costs were converted for 1 mile for each section.

7.6 Defining the Benefits

- User Cost Saving: In order to preserve the surface conditions of the road sections, maintenance was performed once during the three years of this study, in May 2017. During the maintenance, traffic will slow down, and it was assumed that this would cause delays to the travel time, which is about two times (6 min) greater than the time to pass the road (3

min) without maintenance. The truck percentage for this road was assumed at 25%, based on the information from subject matter experts (county engineers at the Decatur County Engineer’s Office). Moreover, the total AADT of this road is 80, based on the Iowa DOT Traffic Map. The delay will affect annually the costs of driving on the road. In this regard, the U.S. Bureau of Labor Statistics (BLS) provides access to the data of user cost value for trucks and cars in order to consider the value of time. This value is equal to \$54/hr for trucks and equal to \$25/hr for cars.

- **Maintenance Cost Saving:** Cost saving by decreasing maintenance frequency is another benefit that can have a major impact on the final BCA. In that regard, maintenance can be conducted less frequently, such as once every three years, instead of once every two years. This can happen based on monitoring the performance of each alternative section over the three years of the study. Therefore, assumptions were made to consider the maintenance frequency once in every three to five years, in order to find its effect on the BCA.

7.7 NPV Calculation for Benefit-Cost Calculation

Based on the decisions that were made for the base case consideration and the types of benefits, the annual values of the costs and benefits were calculated. The service life and the discount rate are two of the main factors in net present value (NPV) calculation. Equation 24 shows the formula to calculate the net present value.

$$NPV = \text{Construction Costs} + \sum_{k=1}^n \text{Maintenance Cost}_k \left[\frac{1}{(1+i)^{n_k}} \right] - \text{Salvage Value} \left[\frac{1}{(1+i)^{n_k}} \right] \quad (24)$$

where, i is the discount rate and n is the service life of the project. The salvage value of the road, which represents the value of an investment alternative at the end of the analysis period, is assumed to be zero because it is assumed that there is no remaining life for the surface materials after the service life of the road.

In order to provide a framework for the BCA calculation in this project, an Excel sheet was prepared and attached to this report. A sample calculation of BCA is also in Appendix F. The NPV of the benefits divided by the NPV of the total costs of the project presents the BCR. Moreover, the benefits are divided into two categories: user cost saving and maintenance cost saving. The BCA was conducted with three main variable assumptions: (1) a service life between 20, 30, 40, and 50 years; (2) a discount rate of 3%; and (3) maintenance frequency for the alternative sections for once in three, four, and five years. The results are presented in the following sections.

7.8 Results and Discussion

In a BCA model, so many possible assumptions can be made on input variables such as the costs, benefits, discount rate, and service life, which can result in a range of outputs. Therefore, a sensitivity analysis should be taken into consideration in order to elucidate the effectiveness of

each variable in a BCA model. In this regard, BCA models were prepared for the discount rate equal to 3%; service life of 20, 30, 40, and 50 years; and scenarios could be given to alter the maintenance frequency, due to observing the change in the BCR values, of once in every one, two, or three years for low-performance; two, three, or four years for medium-performance; and three, four, or five years for high-performance alternatives.

Figure 85 shows the costs per mile for aggregates and hauling for different sections, which are used in the BCA.

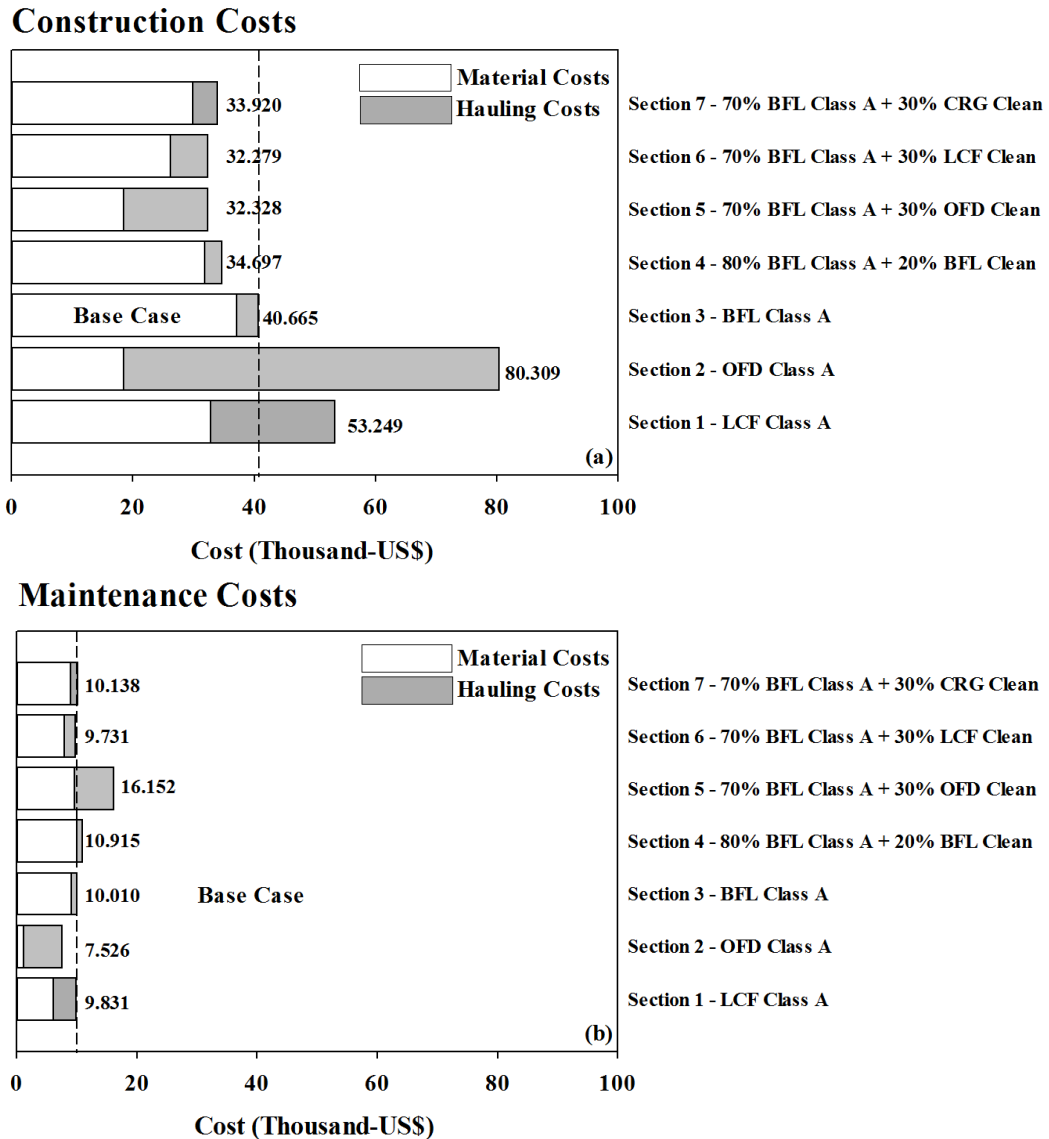


Figure 85. Construction, top, and maintenance, bottom, costs for materials and hauling (truck)

BFL Class A was selected as the control section since it is local material. The construction costs for OFD Class A was higher than those of other sections due to the higher hauling costs of these

materials (~\$8,000). The 70% BFL Class A + 30% OFD Clean and 70% BFL Class A + 30% LCF Clean had lower construction costs (~\$32,000). However, OFD Class A (\$8,000) and 70% BFL Class A + 30% OFD Clean (\$16,000) had, respectively, the minimum and maximum maintenance costs.

When the two hauling options were compared for OFD sources, the hauling cost for the OFD materials could be lower than the hauling costs with truck. Therefore, hauling costs with rail for OFD Class A and 70% BFL Class A + 30% OFD Clean were also considered in the BCA (Table 80).

Table 80. Hauling costs of OFD materials per mile with rail and truck

Sections	Hauling costs (\$) per mile	
	Truck	Rail
OFD Class A	61,882	43,280
70% BFL Class A + 30% OFD Clean	23,021	16,820

The rail hauling option for LCF materials was not considered in the analysis because it was obviously more costly compared to truck hauling.

7.8.1 Material and Thickness Loss

One of the methods to find the benefit of using different aggregate materials is to compare them based on abrasion rates. Figure 86 shows the material loss for each section before performing maintenance.

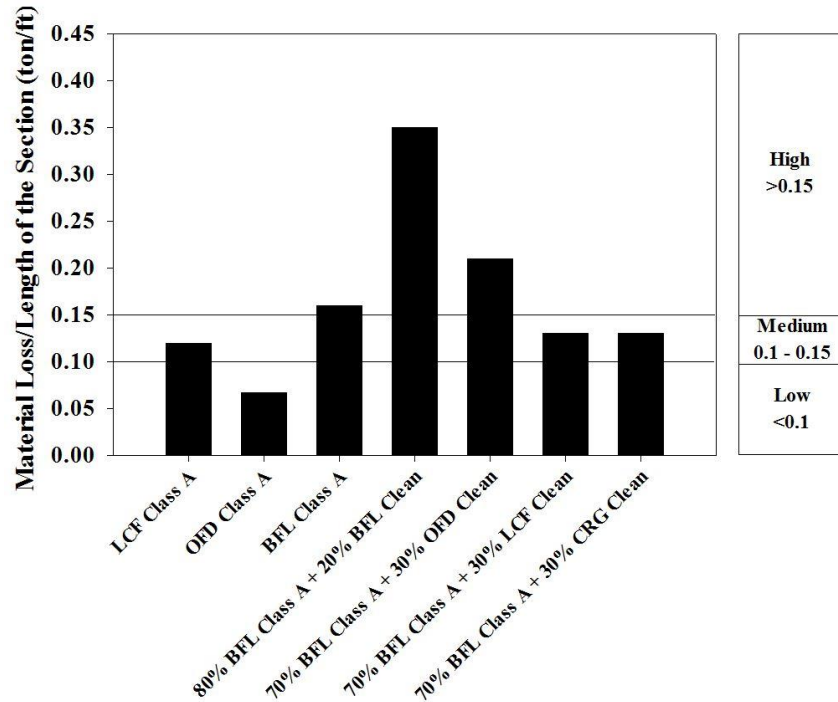


Figure 86. Material loss for each section before maintenance

The materials loss values were calculated by the amount of change in the surface thickness and the required materials to bring the surface thickness to 4 in., and then the values of thickness loss were divided by the length of the sections to normalize the effect of length. Sections then were categorized into three categories of high, medium, and low material loss per length. The sections were categorized as follows: BFL Class A, 80% BFL Class A + 20% BFL Clean, and 70% BFL Class A + 30% OFD Clean had high (>0.15 ton/ft); LCF Class A, 70% BFL Class A + 30% LCF Clean, and 70% BFL Class A + 30% CRG Clean had medium (0.1 to 0.15 ton/ft); and OFD Class A had low (<0.1 ton/ft) material loss per length. These results show that 70% BFL Class A + 30% LCF Clean and 70% BFL Class A + 30% CRG Clean is more durable than local BFL materials (BFL Class A and 80% BFL Class A + 20% BFL Clean) when material loss is considered.

Figure 87 shows the thickness changes in the granular road surface layers for each section before maintenance in May 2017.

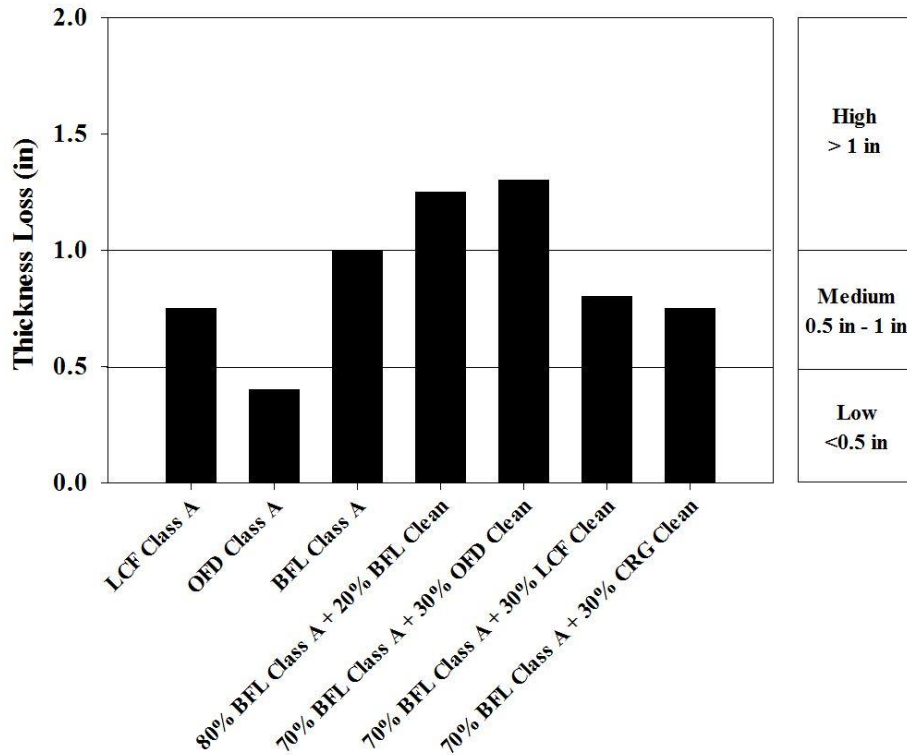


Figure 87. Thickness loss from initial thickness (4 in.) for each section before maintenance

Accordingly, sections were then categorized into three groups of high, medium, and low thickness loss per length. The sections were categorized as follows: BFL Class A, 80% BFL Class A + 20% BFL Clean, and 70% BFL Class A + 30% OFD Clean had high (>1 in.); LCF Class A, 70% BFL Class A + 30% LCF Clean, and 70% BFL Class A + 30% CRG Clean had medium (0.5 to 1 in.); and OFD Class A had low (<0.5 in.) thickness loss per length. Based on these results, it can be concluded that 70% BFL Class A + 30% LCF Clean and 70% BFL Class A + 30% CRG Clean is more durable than local BFL materials (BFL Class A and 80% BFL Class A + 20% BFL Clean) when thickness loss is considered.

Table 81 shows the different scenarios based on the results of thickness and aggregate (material) loss for each section.

Table 81. Scenarios for maintenance frequency based on the thickness and aggregate loss

Sections	Worst case	Most likely	Best case
LCF Class A	2	3	4
OFD Class A	3	4	5
BFL Class A	1	2	3
80% BFL Class A + 20% BFL Clean	1	2	3
70% BFL Class A + 30% OFD Clean	1	2	3
70% BFL Class A + 30% LCF Clean	2	3	4
70% BFL Class A + 30% CRG Clean	2	3	4

Sections were categorized into three groups. Three scenarios were determined for each group and named worst case, when the maintenance needs to be done with a conservative decision; most likely, when the maintenance needs to be performed as a common decision; and best case, when the contractor makes an optimistic decision about the performance of the materials to perform maintenance less often.

For the sections with high material and thickness loss (BFL Class A, 80% BFL Class A + 20% BFL Clean, and 70% BFL Class A + 30% OFD Clean), maintenance could be performed every one, two, or three years. Sections with medium aggregate loss (LCF Class A, 70% BFL Class A + 30% LCF Clean, and 70% BFL Class A + 30% CRG Clean) could have maintenance every two, three, or four years, and OFD Class A with low aggregate loss requires maintenance less often (three, four, or five years).

Figure 88 shows BCA results based on the scenarios from material and thickness loss.

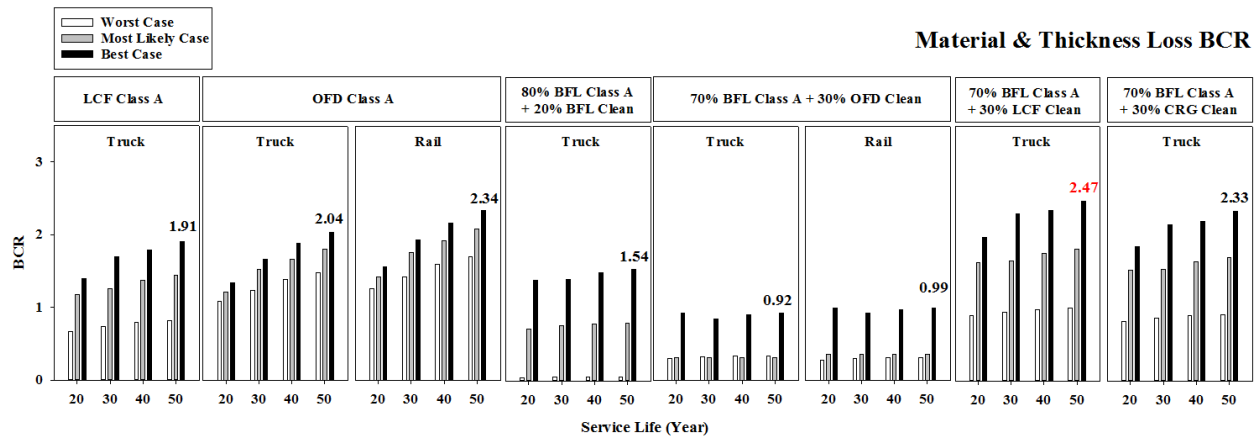


Figure 88. BCR values for material and thickness loss

The BCR for LCF Class A was lower than 1 for worst-case scenarios (maintenance every two years). However, this section had a BCR > 1 for most likely and best-case scenarios (maintenance every three or four years). OFD Class A always proved to be beneficial to use compared to the base case (BFL Class A) by having a BCR higher than 1 for different scenarios and service life values. The BCR values for 80% BFL Class A + 20% BFL Clean were lower than 1 for worst-case and most likely scenarios (maintenance every one or two years), and higher than 1 for the best-case scenario (maintenance every three years). The 70% BFL Class A + 30% OFD Clean had the minimum BCR values (<1) for all scenarios. The BCR values for 70% BFL Class A + 30% LCF Clean were lower than 1 for the worst-case scenario (maintenance every two years) except for 50 years of service life of which it was 1. However, the most likely and best-case scenarios (maintenance every three or four years) showed BCR values higher than 1 for 70% BFL Class A + 30% LCF Clean. The BCR values for 70% BFL Class A + 30% CRG Clean for the worst-case scenario (maintenance every two years) were lower than 1. However, the most likely and best-case scenarios (maintenance every three or four years) showed higher BCR values than 1. The highest BCR value was observed for 70% BFL Class A + 30% LCF Clean

(2.47) and 70% BFL Class A + 30% CRG Clean (2.33) for service life, indicating that the transportation of high-quality clean aggregate materials offer the potential to be more cost-efficient when material and thickness losses are considered.

Figure 88 shows the BCR values for OFD Class A and 70% BFL Class A + 30% OFD Clean increase when hauling materials by rail rather than truck. This increase for OFD Class A is higher (0.3) than 70% BFL Class A + 30% OFD Clean (0.07). However, 70% BFL Class A + 30% OFD Clean was still not cost-effective compared to use of local aggregate materials. Nevertheless, this case caused OFD Class A section to become the second most beneficial (cost-effective) section after 70% BFL Class A + 30% LCF Clean with BCR values higher than 70% BFL Class A + 30% CRG Clean.

7.8.2 Gravel Aggregate Content Loss

Gravel loss (aggregate size > US #4, 0.19 in.) is one of the main degradation indicators on the surface materials of granular roadways. The benefits of using alternative sections compared to the base case section were evaluated by considering the coarse aggregate loss. Figure 89 shows the gravel loss from construction (September 2016) to before maintenance (May 2017).

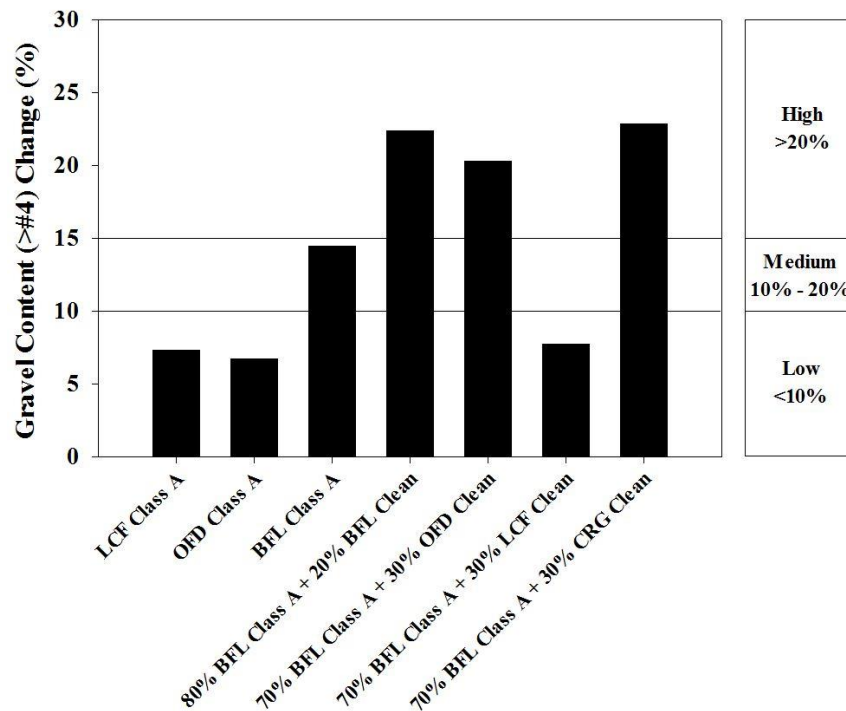


Figure 89. Gravel percentage change from construction to maintenance

Test sections then were categorized into the three categories of high, medium, and low gravel loss. The results were as follows: 80% BFL Class A + 20% BFL Clean, 70% BFL Class A + 30% OFD Clean, and 70% BFL Class A + 30% CRG Clean had high (>20%); BFL Class A had

medium (10 to 20%); and LCF Class A, OFD Class A, and 70% BFL Class A + 30% LCF Clean had low (<10%) gravel loss.

Table 82 shows the different scenarios based on the results of gravel loss for each section.

Table 82. Scenarios for maintenance frequency based on the gravel loss for each section

Sections	Worst case	Most likely	Best case
LCF Class A	3	4	5
OFD Class A	3	4	5
BFL Class A	2	3	4
80% BFL Class A + 20% BFL Clean	1	2	3
70% BFL Class A + 30% OFD Clean	1	2	3
70% BFL Class A + 30% LCF Clean	3	4	5
70% BFL Class A + 30% CRG Clean	1	2	3

For the sections with high gravel loss (80% BFL Class A + 20% BFL Clean, 70% BFL Class A + 30% OFD Clean, and 70% BFL Class A + 30% CRG Clean), maintenance could be performed every one, two, or three years. BFL Class A with medium aggregate loss could have maintenance every two, three, or four years, and the sections with low aggregate loss (LCF Class A, OFD Class A, and 70% BFL Class A + 30% LCF Clean), require maintenance less often (three, four, or five years).

Figure 90 shows BCA results based on the scenarios from gravel loss.

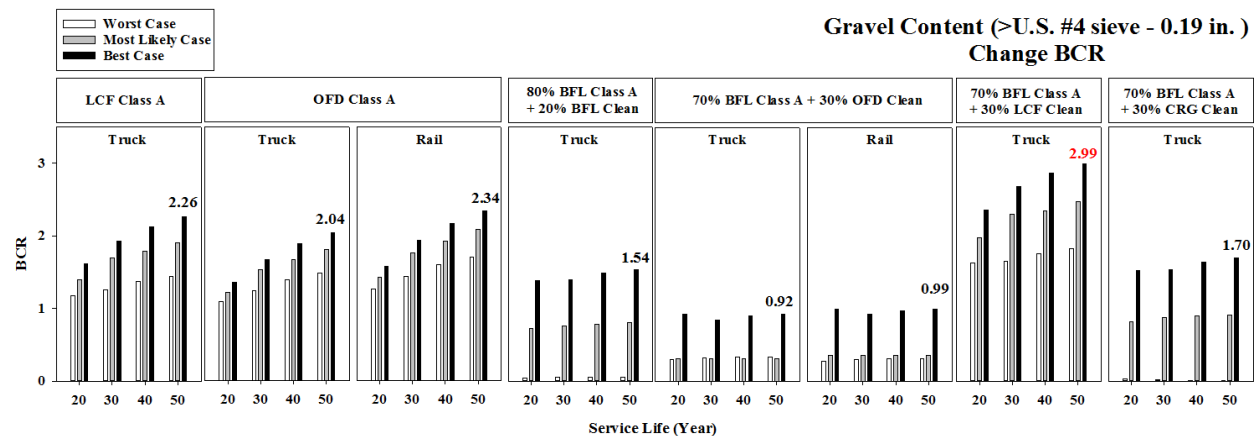


Figure 90. BCR values for gravel loss

LCF Class A, OFD Class A, and 70% BFL Class A + 30% LCF Clean always proved to be beneficial to use compared to the base case (BFL Class A) by having a BCR higher than 1 for different scenarios and service life values. The BCR values for 80% BFL Class A + 20% BFL Clean and 70% BFL Class A + 30% CRG Clean were lower than 1 for worst-case and most likely scenarios (maintenance every one or two years) and higher than 1 for the best-case

scenario (maintenance every three years). The 70% BFL Class A + 30% OFD Clean had the minimum BCR values (<1) for all scenarios. The highest BCR values were observed for 70% BFL Class A + 30% LCF Clean (2.99), LCF Class A (2.26), and OFD Class A (2.04) during their service life when gravel loss was considered.

Figure 90 shows the BCR values for OFD Class A and 70% BFL Class A + 30% OFD Clean increase when hauling materials by rail rather than truck. This increase for OFD Class A was higher (0.3) than that of 70% BFL Class A + 30% OFD Clean (0.07). However, 70% BFL Class A + 30% OFD Clean was still not beneficial. Nevertheless, rail hauling resulted in OFD Class A section being the second most beneficial section after the 70% BFL Class A + 30% LCF Clean section.

7.8.3 Performance-Based Benefit-Cost Analysis

Several different laboratory and field tests including FWD, DCP, Dustometer, IRI, and sieve analyses (total breakage, fines content, and gravel-to-sand ratio) were conducted on each section multiple times during the project timeline. In this study, these results were divided into three different categories based on their degree of importance for maintenance, and a weight of each parameter was considered for each group to come up with an overall value of BCR (Figure 91).

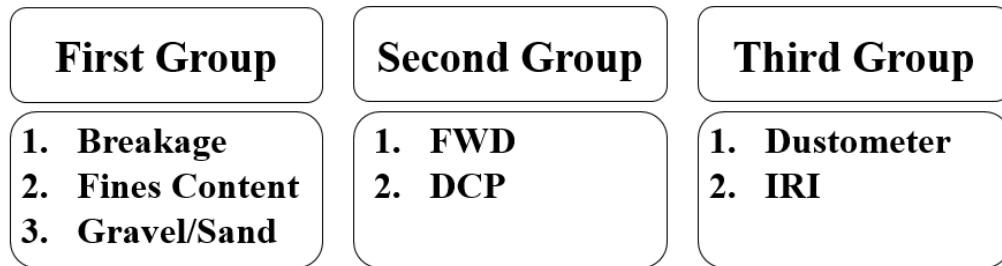


Figure 91. Classification of the laboratory and field results for BCA

The results of sieve analyses (total breakage, fines content, and gravel-to-sand ratio) were placed in the first group due their importance by being representative of the total deterioration of the sections and a weight of 0.75 or 1, depending on the condition, was selected for this group. The FWD and DCP results were categorized as the second group since they provide mechanical properties of each section (stiffness and strength) and a weight of 0.5 was used. Finally, dustometer and IRI tests (dust production and ride quality) were assigned to the third group with a degree of importance of 0.25. Material and thickness loss and gravel content change were also included in weighted models with a weight of 1 while the first, the second, and the third groups were weighted as 0.75, 0.5, and 0.25, respectively. The BCR results for each of the laboratory and field tests are presented in the following sections.

7.8.4 First Group (Sieve Analyses Results)

7.8.4.1 Total Breakage

Total breakage is an indicator of material degradation and is defined as the area between the particle-size distributions curves of materials collected at different times. Figure 92 shows the total breakage of all test sections since construction (September 2016).

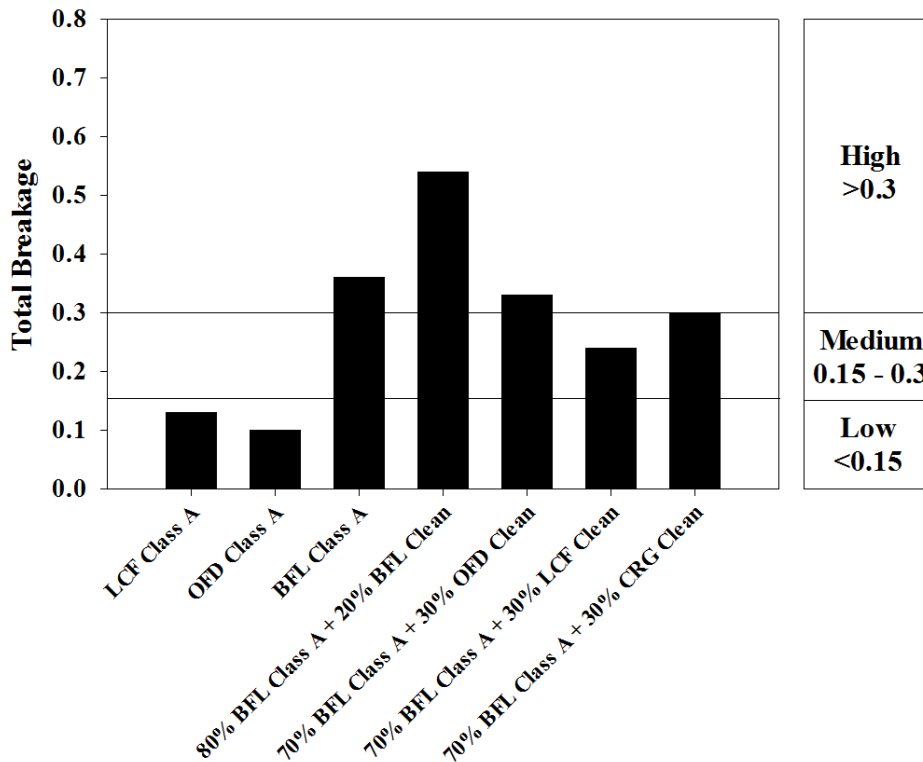


Figure 92. Total breakage average values over the length of project

Test sections were categorized into the three groups, where BFL Class A, 80% BFL Class A + 20% BFL Clean, and 70% BFL Class A + 30% OFD Clean had high (>0.3); 70% BFL Class A + 30% LCF Clean and 70% BFL Class A + 30% CRG Clean had medium (0.15 to 0.3); and LCF Class A and OFD Class A had low (<0.15) total breakage values. The 70% BFL Class A + 30% LCF Clean and 70% BFL Class A + 30% CRG Clean were better than BFL materials.

Table 83 shows the different scenarios based on the results of average total breakage over the maintenance period.

Table 83. Scenarios for maintenance frequency based on the average total breakage

Sections	Worst case	Most likely	Best case
LCF Class A	3	4	5
OFD Class A	3	4	5
BFL Class A	1	2	3
80% BFL Class A + 20% BFL Clean	1	2	3
70% BFL Class A + 30% OFD Clean	1	2	3
70% BFL Class A + 30% LCF Clean	2	3	4
70% BFL Class A + 30% CRG Clean	2	3	4

For the sections with high average total breakage (BFL Class A, 80% BFL Class A + 20% BFL Clean, and 70% BFL Class A + 30% OFD Clean), maintenance could be performed every one, two, or three years. The 70% BFL Class A + 30% LCF Clean and 70% BFL Class A + 30% CRG Clean with medium average total breakage could have maintenance every two, three, or four years, and the sections with low aggregate loss (LCF Class A and OFD Class A), require maintenance less often (three, four, or five years).

Figure 93 shows BCA results based on the scenarios from average total breakage.

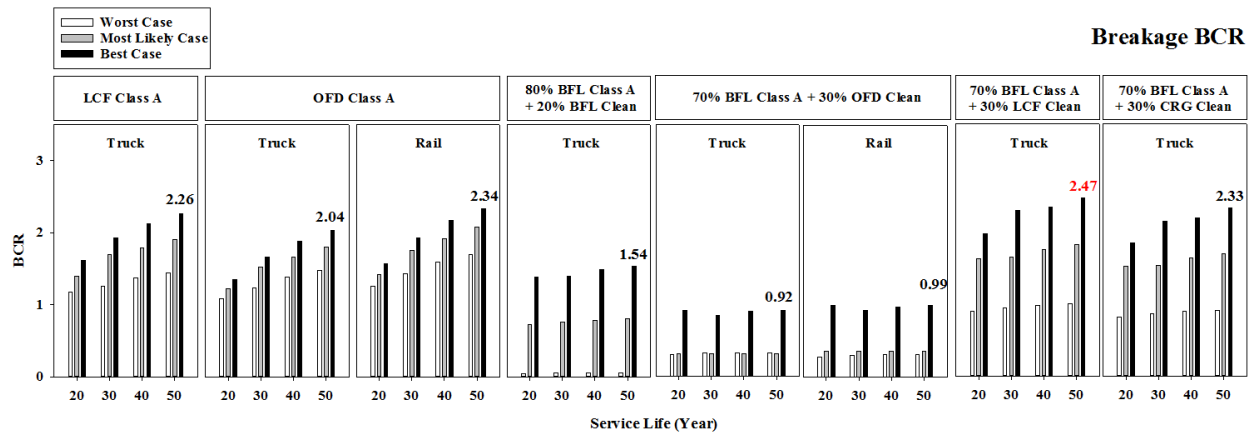


Figure 93. BCR values for average total breakage

LCF Class A and OFD Class A always proved to be beneficial compared to the base case (BFL Class A) by having a BCR higher than 1 for different scenarios and service life values. The BCR values for 80% BFL Class A + 20% BFL Clean were lower than 1 for worst-case and most likely scenarios (maintenance every one or two years) and higher than 1 for the best-case scenario (maintenance every three years). The 70% BFL Class A + 30% OFD Clean was not beneficial to use in any case compared to the base case (BFL Class A) that had BCR values lower than 1 for all scenarios. The BCR values for 70% BFL Class A + 30% LCF Clean and 70% BFL Class A + 30% CRG Clean were lower than 1 for the worst-case scenario (maintenance every two years) and higher than 1 for the most likely and best-case scenarios (maintenance every three or four years). The highest BCR value was observed for 50 years of service life and the best-case

scenario (maintenance every four years) for 70% BFL Class A + 30% LCF Clean (2.47). The lowest BCR value was observed for 20 years of service life and the worst-case scenario (maintenance every one year) for 80% BFL Class A + 20% BFL Clean (0.04).

Figure 93 shows the BCR values for OFD Class A and 70% BFL Class A + 30% OFD Clean increase when hauling materials by rail rather than truck. This increase for OFD Class A was higher (0.3) than 70% BFL Class A + 30% OFD Clean (0.07). However, the 70% BFL Class A + 30% OFD Clean was still not beneficial. Nevertheless, rail hauling resulted in the OFD Class A section being the second most beneficial section after 70% BFL Class A + 30% LCF Clean with BCR values higher than 70% BFL Class A + 30% CRG Clean.

7.8.4.2 Fines Content

Average values of fines content over time could be good for comparing alternative sections to the base case (BFL Class A) since fines content affects dust production and distresses such as rutting and pot holes. Figure 94 shows the average fines content values over the length of the project and test sections, which were categorized into three groups where BFL Class A had high (>20%); 80% BFL Class A + 20% BFL Clean, 70% BFL Class A + 30% OFD Clean, 70% BFL Class A + 30% LCF Clean, and 70% BFL Class A + 30% CRG Clean had medium (15% to 30%); and LCF Class A and OFD Class A had low (<15%) average fines content values.

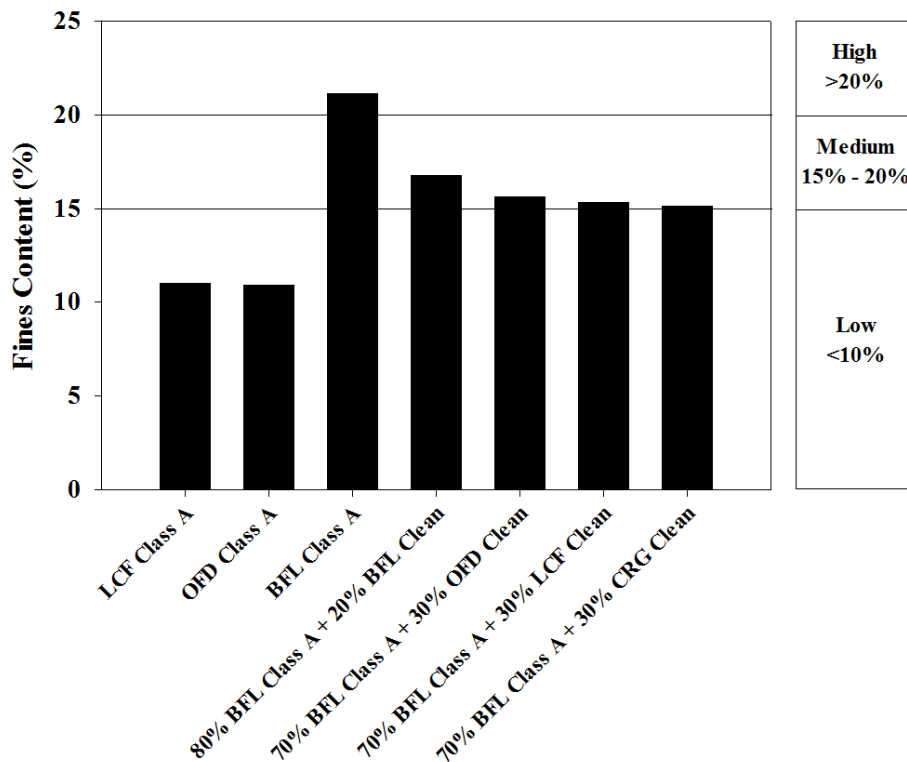


Figure 94. Average fines content values over the length of project

Results showed that the BFL Class A mixed with LCF Clean and CRG Clean were more beneficial than only the local BFL material and mixtures.

Table 84 shows the different scenarios based on the results of average fines content.

Table 84. Scenarios for maintenance frequency based on the average fines content

Sections	Worst case	Most likely	Best case
LCF Class A	3	4	5
OFD Class A	3	4	5
BFL Class A	1	2	3
80% BFL Class A + 20% BFL Clean	2	3	4
70% BFL Class A + 30% OFD Clean	2	3	4
70% BFL Class A + 30% LCF Clean	2	3	4
70% BFL Class A + 30% CRG Clean	2	3	4

BFL Class A with high average fines content could have maintenance performed every one, two, or three years. Sections with medium average fines content (80% BFL Class A + 20% BFL Clean, 70% BFL Class A + 30% OFD Clean, 70% BFL Class A + 30% LCF Clean, and 70% BFL Class A + 30% CRG Clean) could have maintenance every two, three, or four years, and LCF Class A and OFD Class A with low average fines content require maintenance less often (three, four, or five years).

Figure 95 shows BCA results based on the scenarios from average fines content.

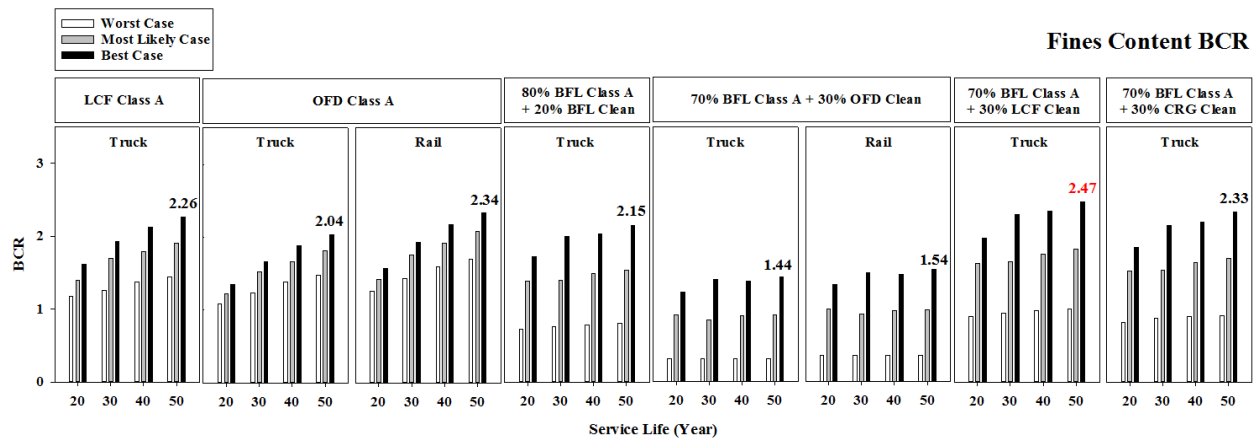


Figure 95. BCR values for average fines content

LCF Class A and OFD Class A always proved to be beneficial compared to the base case (BFL Class A) by having a BCR higher than 1 for different scenarios and service life values. The BCR values for 80% BFL Class A + 20% BFL Clean were lower than 1 for the worst-case (maintenance every two years) and higher than 1 for the most likely and best-case scenarios (maintenance every three or four years). The 70% BFL Class A + 30% OFD Clean was not

beneficial compared to the base case (BFL Class A) that had BCR values lower than 1 for its most likely and worst-case scenarios (maintenance every two or three years). However 70% BFL Class A + 30% OFD Clean had BCR values higher than 1 for the best-case scenario (maintenance every four years). The BCR values for 70% BFL Class A + 30% LCF Clean and 70% BFL Class A + 30% CRG Clean were lower than 1 for the worst-case scenario (maintenance every two years) and higher than 1 for the most likely and best-case scenarios (maintenance every three or four years). The highest BCR value was observed for 20 years of service life and best-case scenario for 70% BFL Class A + 30% LCF Clean (2.47), and the lowest BCR value was observed for 20 years of service life.

Figure 95 shows the BCR values for OFD Class A and 70% BFL Class A + 30% OFD Clean increase when hauling materials by rail rather than truck. The increase for OFD Class A was higher (0.3) than 70% BFL Class A + 30% OFD Clean (0.1). Rail hauling resulted in OFD Class A section being the second most beneficial section after 70% BFL Class A + 30% LCF Clean with BCR values higher than 70% BFL Class A + 30% CRG Clean.

7.8.4.3 Gravel-to-Sand Ratio

Average values of gravel-to-sand ratio over time show the amount of large-size particles (sand and gravel) that became finer materials, and these values could be compared for each alternative section with the base case (BFL Class A). Figure 96 shows the average gravel-to-sand ratio values over the length of the project.

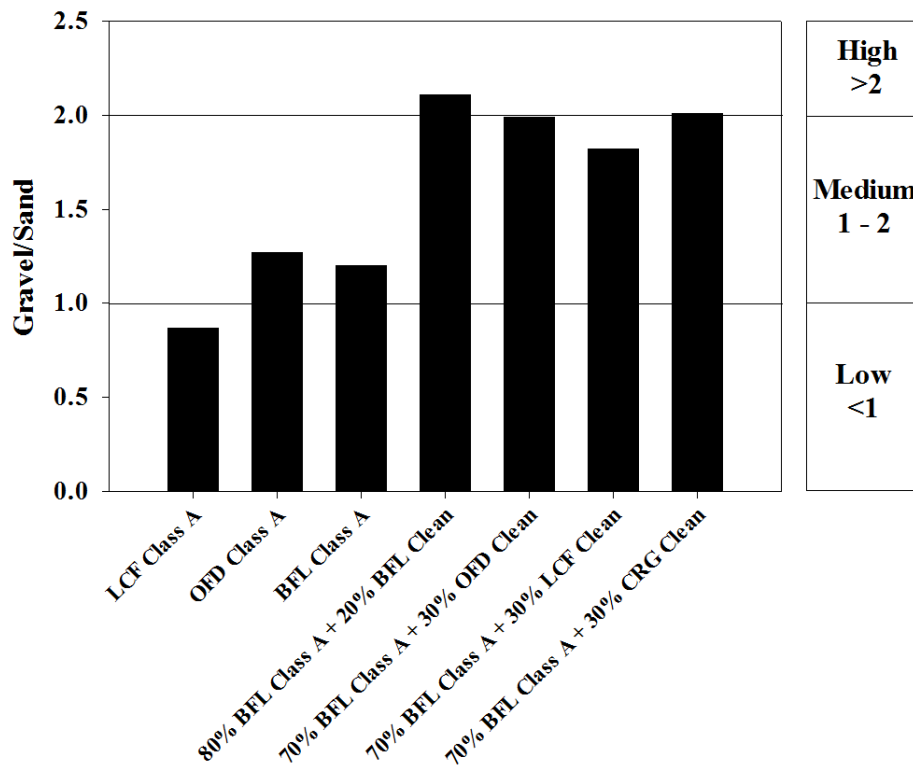


Figure 96. Average gravel-to-sand ratio values over the length of project

The test sections were categorized into three groups, where 80% BFL Class A + 20% BFL Clean and 70% BFL Class A + 30% CRG Clean had high (>2); OFD Class A, BFL Class A, 70% BFL Class A + 30% OFD Clean, and 70% BFL Class A + 30% LCF Clean had medium (1 to 2); and LCF Class A had low (<1) average gravel-to-sand ratio values.

Table 85 shows the different scenarios based on the results of average gravel-to-sand ratio.

Table 85. Scenarios for maintenance frequency based on the average gravel-to-sand ratio

Sections	Worst case	Most likely	Best case
LCF Class A	1	2	3
OFD Class A	2	3	4
BFL Class A	2	3	4
80% BFL Class A + 20% BFL Clean	3	4	5
70% BFL Class A + 30% OFD Clean	2	3	4
70% BFL Class A + 30% LCF Clean	2	3	4
70% BFL Class A + 30% CRG Clean	3	4	5

LCF Class A with low average gravel-to-sand ratio could have maintenance every one, two, or three years. Sections with medium average gravel-to-sand ratio (OFD Class A, BFL Class A, 70% BFL Class A + 30% OFD Clean, and 70% BFL Class A + 30% LCF Clean) could have maintenance every two, three, or four years, and 80% BFL Class A + 20% BFL Clean and 70% BFL Class A + 30% CRG Clean with high average gravel-to-sand ratio require maintenance less often (three, four, or five years).

Figure 97 shows BCA results based on the scenarios from average gravel-to-sand ratio.

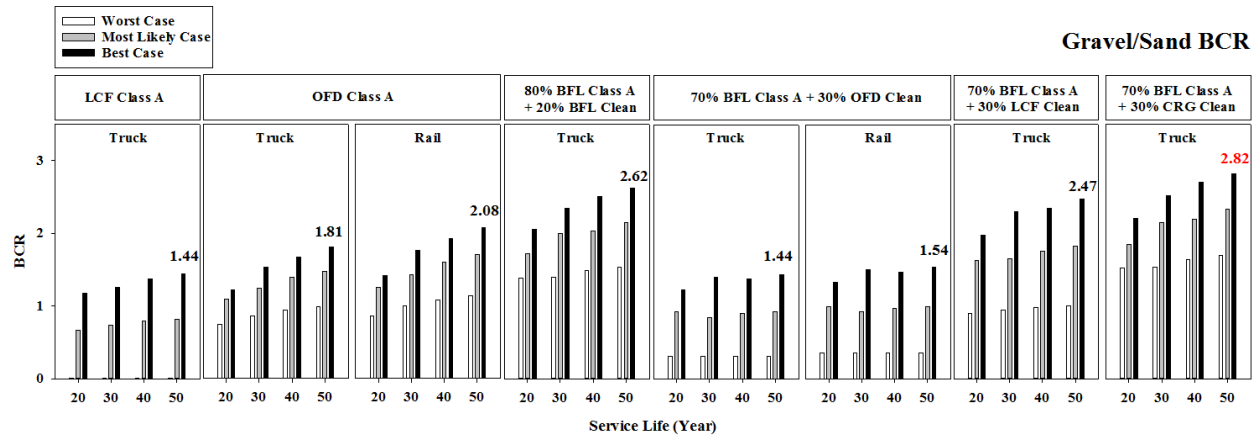


Figure 97. BCR values for average gravel-to-sand ratio

The BCR values for LCF Class A and 70% BFL Class A + 30% OFD Clean were lower than 1 for the worst-case and most likely scenarios (maintenance every one or two years for LCF Class A and two or three years for 70% BFL Class A + 30% OFD Clean) and higher than 1 for the

best-case scenario (maintenance every three years for LCF Class A and four years for 70% BFL Class A + 30% OFD Clean). OFD Class A was not beneficial for the worst-case scenario (maintenance every two years), but it was beneficial for the most likely and best-case scenarios (maintenance every three or four years). The 80% BFL Class A + 20% BFL Clean and 70% BFL Class A + 30% CRG Clean were always beneficial compared to the base case (BFL Class A) by having a BCR higher than 1 for different scenarios and service life values. The BCR values for 70% BFL Class A + 30% LCF Clean were lower than 1 for the worst-case scenario (maintenance every two years) and higher than 1 for the most likely and best-case scenarios (maintenance every three or four years). The highest BCR value was observed for 50 years of service life and the best-case scenario for 70% BFL Class A + 30% CRG Clean (2.82), and the lowest BCR value was observed for the worst-case scenario and all service life values for LCF Class A (0.01) when fines gravel-to-sand ratio was considered.

Figure 97 shows the BCR values for OFD Class A and 70% BFL Class A + 30% OFD Clean increase when hauling materials by rail rather than truck. This increase for OFD Class A is higher (0.27) than 70% BFL Class A + 30% OFD Clean (0.1).

7.8.5 Second Group (Surface Elastic Modulus - FWD, Surface Shear Strength - DCP)

7.8.5.1 Surface Elastic Modulus - FWD

Surface elastic modulus (stiffness) is another factor that was considered in order to investigate the benefits of constructing alternative sections for the base case (BFL Class A). Figure 98 shows the back-calculated surface elastic modulus of each section as a result of the FWD tests.

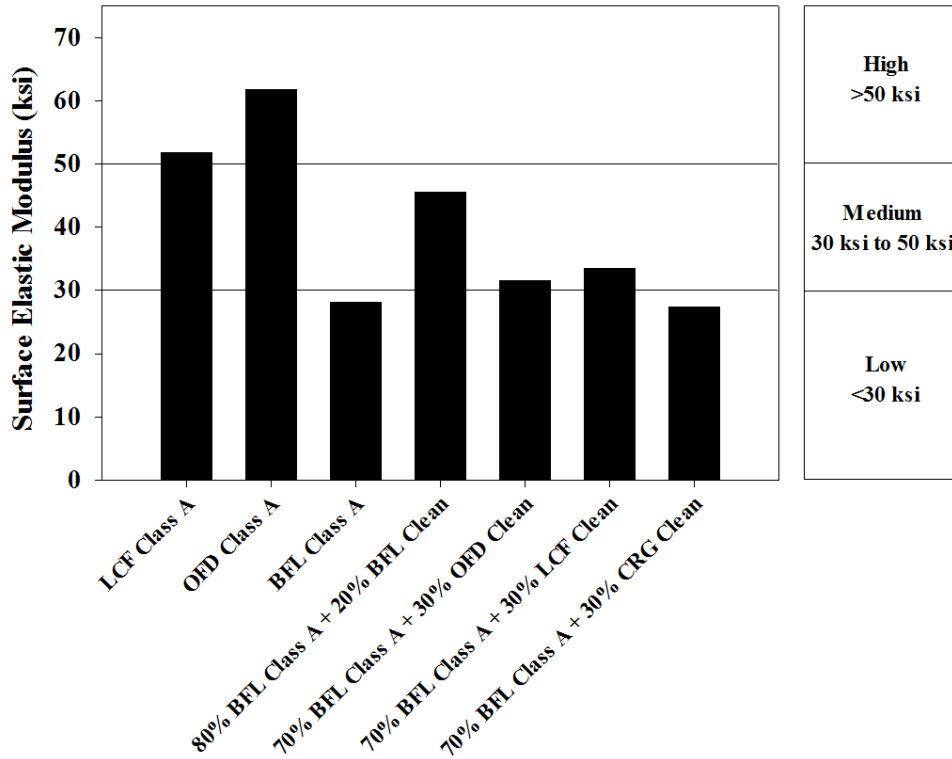


Figure 98. Average back-calculated surface elastic moduli during the project

Test sections then were categorized into three groups, where LCF Class A and OFD Class A had high (>50 ksi); 80% BFL Class A + 20% BFL Clean, 70% BFL Class A + 30% OFD Clean, and 70% BFL Class A + 30% LCF Clean had medium (30 ksi to 50 ksi); and BFL Class A and 70% BFL Class A + 30% CRG Clean had low (<30 ksi) average back-calculated surface elastic modulus values.

Table 86 shows the different scenarios based on the results of average surface elastic modulus.

Table 86. Scenarios for maintenance frequency based on the average surface elastic modulus

Sections	Worst case	Most likely	Best case
LCF Class A	3	4	5
OFD Class A	3	4	5
BFL Class A	1	2	3
80% BFL Class A + 20% BFL Clean	2	3	4
70% BFL Class A + 30% OFD Clean	2	3	4
70% BFL Class A + 30% LCF Clean	2	3	4
70% BFL Class A + 30% CRG Clean	1	2	3

BFL Class A and 70% BFL Class A + 30% CRG Clean with low average surface elastic modulus could have maintenance every one, two, or three years. Sections with medium average surface elastic modulus (80% BFL Class A + 20% BFL Clean, 70% BFL Class A + 30% OFD Clean, and 70% BFL Class A + 30% LCF Clean) could have maintenance every two, three, or four years, and LCF Class A and OFD Class A with high average surface elastic modulus require maintenance less often (three, four, or five years).

Figure 99 shows BCA results based on the scenarios from average back-calculated surface elastic modulus.

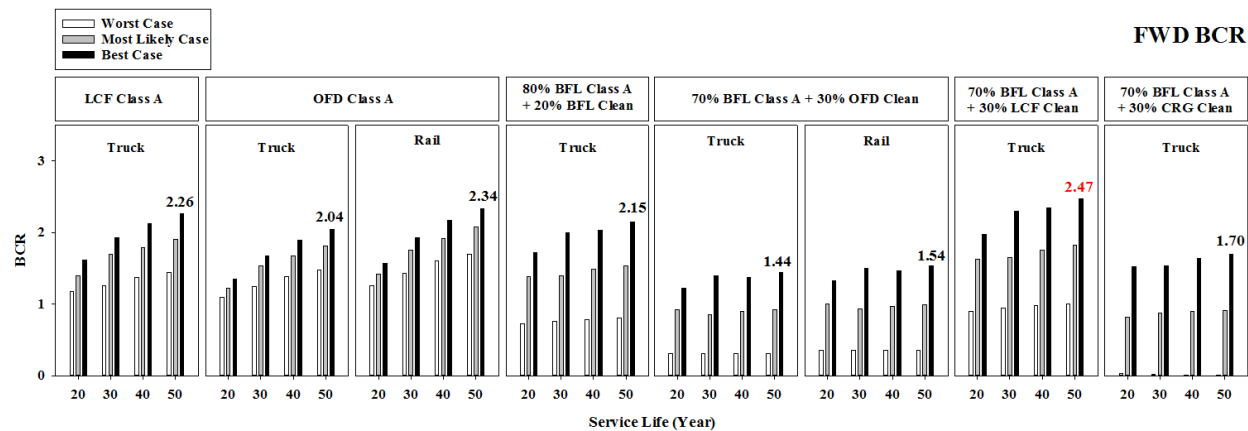


Figure 99. BCR values for average back-calculated surface elastic modulus

LCF Class A and OFD Class A always proved to be beneficial compared to the base case (BFL Class A) by having a BCR higher than 1 for different scenarios and service life values. The BCR values for 80% BFL Class A + 20% BFL Clean were lower than 1 for worst-case (maintenance every two years) and higher than 1 for most likely and best-case scenarios (maintenance every three or four years). The 70% BFL Class A + 30% OFD Clean was not beneficial compared to the base case (BFL Class A) with BCR values lower than 1 for the worst-case and most likely scenarios (maintenance every two or three years). However, 70% BFL Class A + 30% OFD Clean had BCR values higher than 1 for the best-case scenario (maintenance every four years). The BCR values for 70% BFL Class A + 30% LCF Clean were lower than 1 for the worst-case scenario (maintenance every two years) and higher than 1 for the most likely and best-case scenarios (maintenance every three or four years). The BCR values for 70% BFL Class A + 30% CRG Clean for the worst-case and most likely scenarios (maintenance every one or two years) was lower than 1 but for the best case (maintenance every three years) were higher than 1. The highest BCR value was observed for 50 years of service life and the best-case scenario for 70% BFL Class A + 30% LCF Clean (2.47), and the lowest BCR value was observed for 40 and 50 years of service life values and worst-case scenario for 70% BFL Class A + 30% CRG Clean (0.01) when stiffness of the roadways were considered.

Figure 99 shows the BCR values for OFD Class A and 70% BFL Class A + 30% OFD Clean increase when hauling materials by rail rather than truck. This increase for OFD Class A is

higher (0.3) than 70% BFL Class A + 30% OFD Clean (0.1). Rail hauling resulted in OFD Class A section being the second most beneficial section after 70% BFL Class A + 30% LCF Clean section.

7.8.5.2 Surface Shear Strength - DCP

Surface shear strength is another factor that was considered in order to investigate the benefits of constructing alternative sections for the base case (BFL Class A). Figure 100 shows the surface shear strength of all sections as a result of the DCP tests.

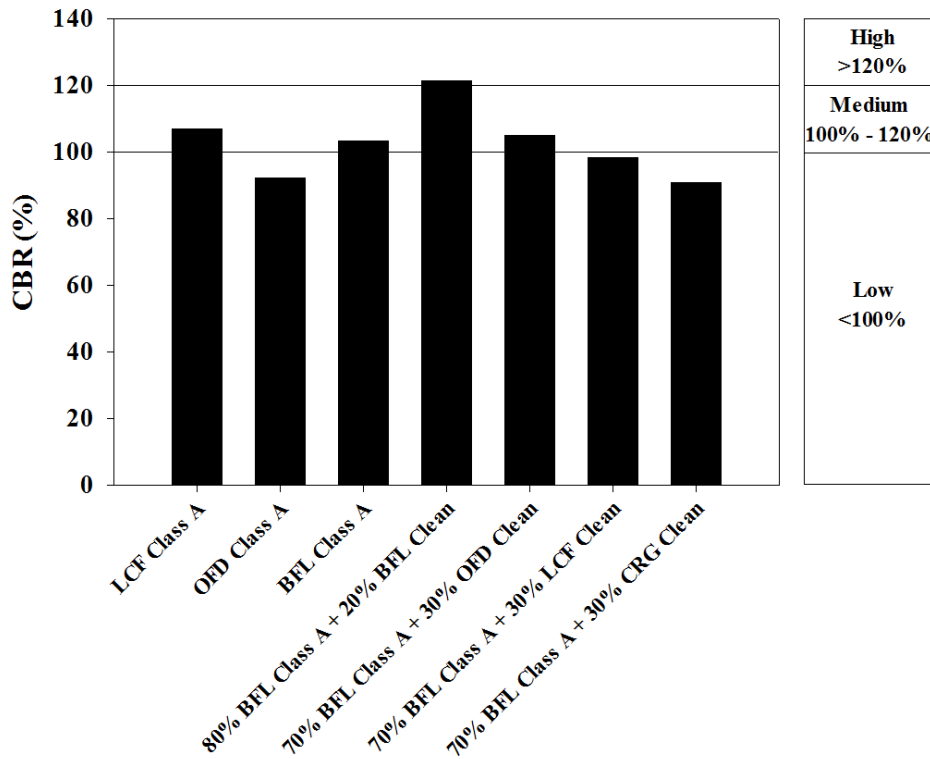


Figure 100. Average surface shear strength values over the length of project

Test sections then were categorized into three groups, where 80% BFL Class A + 20% BFL Clean had high (>120%); LCF Class A, BFL Class A, and 70% BFL Class A + 30% OFD Clean had medium (100% to 120%); and OFD Class A, 70% BFL Class A + 30% LCF Clean, and 70% BFL Class A + 30% CRG Clean had low (<100%) average surface shear strength.

Table 87 shows the different scenarios based on the results of average surface shear strength.

Table 87. Scenarios for maintenance frequency based on the average surface shear strength

Sections	Worst case	Most likely	Best case
LCF Class A	2	3	4
OFD Class A	1	2	3
BFL Class A	2	3	4
80% BFL Class A + 20% BFL Clean	3	4	5
70% BFL Class A + 30% OFD Clean	2	3	4
70% BFL Class A + 30% LCF Clean	1	2	3
70% BFL Class A + 30% CRG Clean	1	2	3

OFD Class A, 70% BFL Class A + 30% LCF Clean, and 70% BFL Class A + 30% CRG Clean with low average surface shear strength could have maintenance every one, two, or three years. LCF Class A, BFL Class A, and 70% BFL Class A + 30% OFD Clean with medium average surface shear strength could have maintenance every two, three, or four years, and 80% BFL Class A + 20% BFL Clean with high average surface shear strength require maintenance less often (three, four, or five years).

Figure 101 shows BCA results based on the scenarios from average surface shear strength.

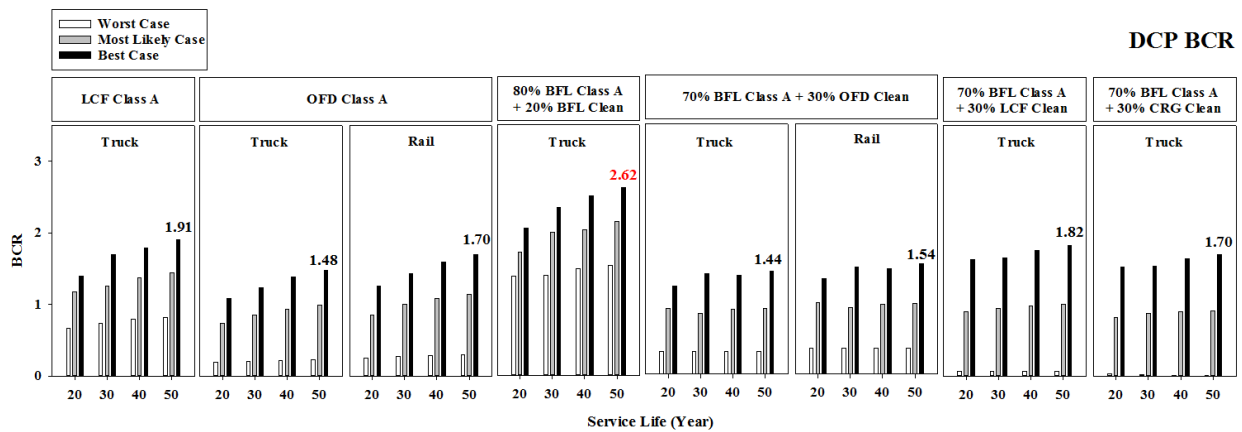


Figure 101. BCR values for average surface shear strength

The BCR values for LCF Class A were lower than 1 for worst-case (maintenance every two years) and higher than 1 for most likely and best-case scenarios (maintenance every three or four years). OFD Class A, 70% BFL Class A + 30% LCF Clean, and 70% BFL Class A + 30% CRG Clean were not beneficial compared to the base case (BFL Class A) with BCR values lower than 1 for worst-case and most likely scenarios (maintenance every one or two years). However, the aforementioned three sections had BCR values higher than 1 for the best-case scenario (maintenance every three years). The 80% BFL Class A + 20% BFL Clean always proved to be beneficial compared to the base case (BFL Class A) by having a BCR higher than 1 for different scenarios and service life values. The 70% BFL Class A + OFD Clean was not beneficial compared to the base case (BFL Class A) with BCR values lower than 1 for worst-case and most

likely scenarios (maintenance every two or three years). However, 70% BFL Class A + OFD Clean had BCR values higher than 1 for the best-case scenario (maintenance every four years). The highest BCR value was observed for 50 years of service life and the best-case scenario for 80% BFL Class A + 20% BFL Clean (2.62), and the lowest BCR value was observed for 40 and 50 years of service life values and worst-case scenario for 70% BFL Class A + 30% CRG Clean (0.01).

Figure 101 shows the BCR values for OFD Class A and 70% BFL Class A + 30% OFD Clean increase when hauling materials by rail rather than truck. This increase for OFD Class A is higher (0.22) than for 70% BFL Class A + 30% OFD Clean (0.1).

7.8.6 Third Group (Dust Production - Dustometer, Surface Roughness-IRI)

7.8.6.1 Dust Production-Dustometer

Dust production is one of the main problems with granular roadways, and it would be beneficial to find the best alternative section with lower dust production. Figure 102 shows the average dust production of all sections as a result of dustometer tests.

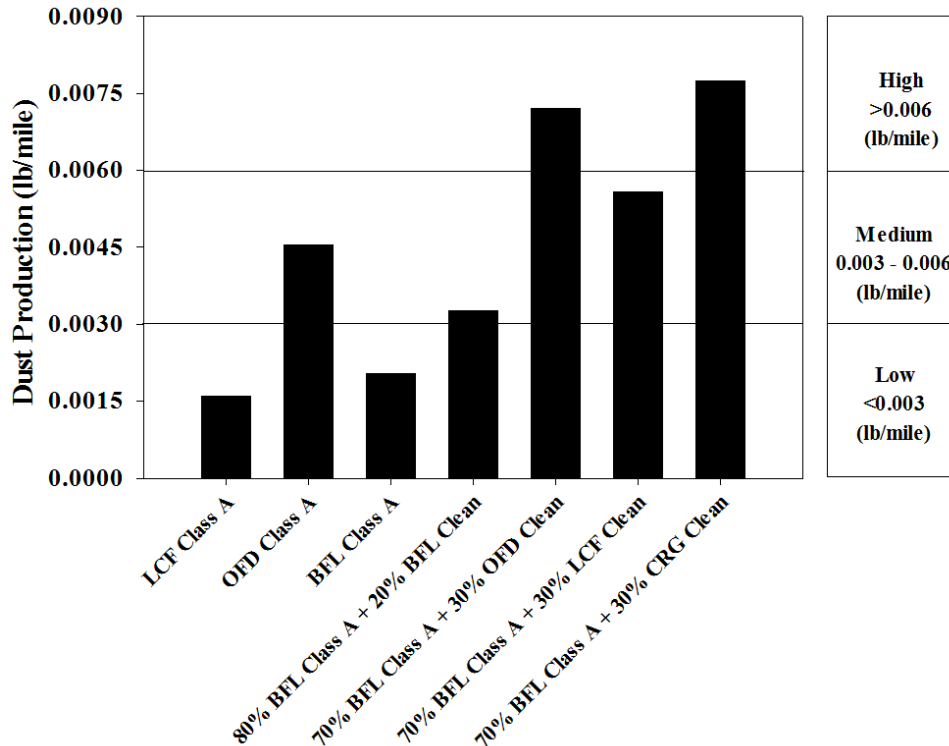


Figure 102. Average dust production over the length of project

Test sections were categorized into three groups, where 70% BFL Class A + 30% OFD Clean and 70% BFL Class A + 30% CRG Clean had high (>0.006 lb/mile); OFD Class A, 80% BFL

Class A + 20% BFL Clean, and 70% BFL Class A + 30% LCF Clean had medium (0.003 to 0.006 lb/mile); and LCF Class A and BFL Class A had low (<0.003 lb/mile) average dust production.

Table 88 shows the different scenarios based on the results of average dust production.

Table 88. Scenarios for maintenance frequency based on the average dust production

Sections	Worst case	Most likely	Best case
LCF Class A	3	4	5
OFD Class A	2	3	4
BFL Class A	3	4	5
80% BFL Class A + 20% BFL Clean	2	3	4
70% BFL Class A + 30% OFD Clean	1	2	3
70% BFL Class A + 30% LCF Clean	2	3	4
70% BFL Class A + 30% CRG Clean	1	2	3

LCF Class A and BFL Class A with low average dust production could have maintenance every three, four, or five years. OFD Class A, 80% BFL Class A + 20% BFL Clean, and 70% BFL Class A + 30% LCF Clean with medium average dust production could have maintenance every two, three, or four years, and 70% BFL Class A + 30% OFD Clean and 70% BFL Class A + 30% CRG Clean with high average dust production require maintenance more often (one, two, or three years).

Figure 103 shows BCA results based on the scenarios from average dust production.

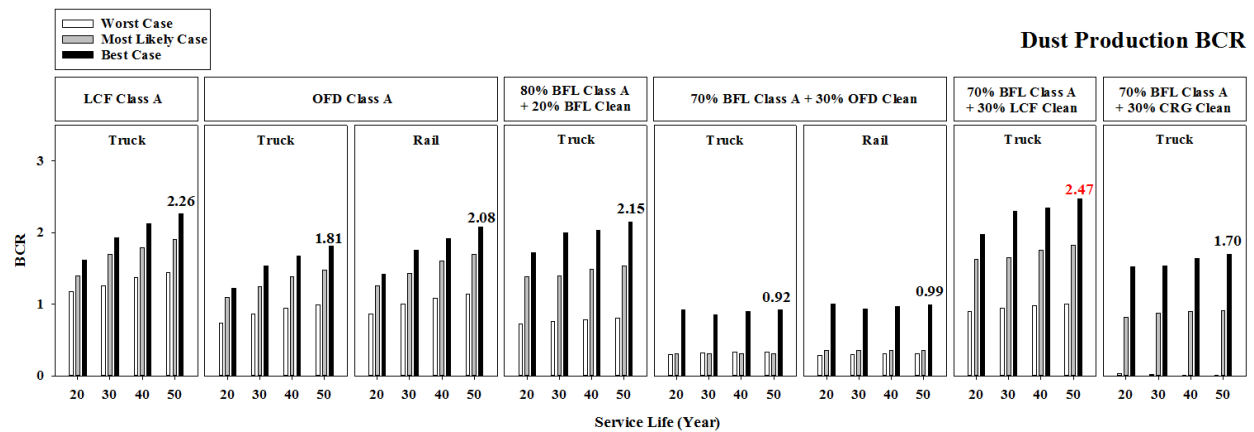


Figure 103. BCR values for average dust production

LCF Class A always proved to be beneficial compared to the base case (BFL Class A) by having a BCR higher than 1 for different scenarios and service life values. The BCR values for OFD Class A were lower than 1 for worst-case (maintenance every two years) and higher than 1 for

most likely and best-case scenarios (maintenance every three or four years). The 80% BFL Class A + 20% BFL Clean and 70% BFL Class A + 30% LCF Clean were not beneficial to use compared to the base case (BFL Class A) with BCR values lower than 1 for the worst-case scenario (maintenance every two years). However these two sections had BCR values higher than 1 for the most likely and best-case scenarios (maintenance every three or four years). The 70% BFL Class A + 30% OFD Clean, and 70% BFL Class A + 30% CRG Clean were not beneficial compared to the base case (BFL Class A) with BCR values lower than 1 for worst-case and most likely scenarios (maintenance every one or two years). However, the aforementioned two sections had BCR values higher than 1 for the best-case scenario (maintenance every three years). The highest BCR value was observed for 50 years of service life and the best-case scenario for 70% BFL Class A + 30% LCF Clean (2.47), and the lowest BCR value was observed for 40 and 50 years of service life values and worst-case scenario for 70% BFL Class A + 30% CRG Clean (0.01) when dust production was considered.

Figure 103 shows the BCR values for OFD Class A and 70% BFL Class A + 30% OFD Clean increase when hauling materials by rail rather than truck. This increase for OFD Class A is higher (0.27) than 70% BFL Class A + 30% OFD Clean (0.07).

7.8.6.2 Surface Roughness–IRI

Surface roughness is one of the important factors in the serviceability of roadways. This factor has been investigated in this study by conducting IRI tests and reported as cIRI as mentioned previously. Figure 104 shows the average cIRI values of all sections.

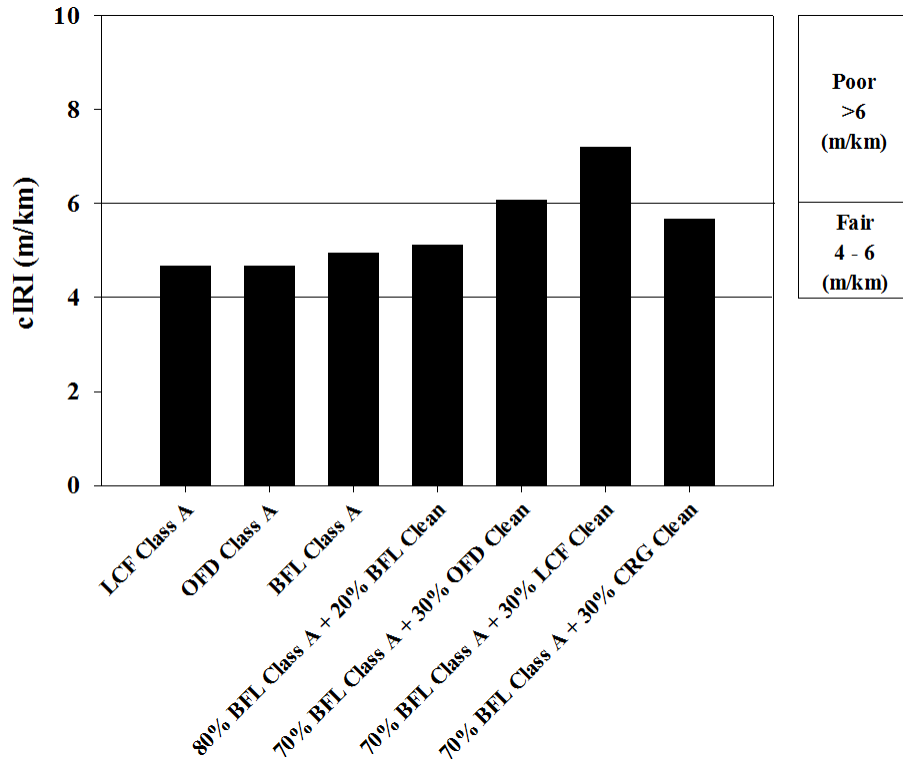


Figure 104. Average surface roughness (cIRI) over the length of project

Test sections were categorized into two groups, where 70% BFL Class A + 30% OFD Clean and 70% BFL Class A + 30% LCF Clean had poor (>6 m/km), and the rest of the sections had fair (4 to 6 m/km) conditions.

Table 89 shows the different scenarios based on the results of average surface roughness.

Table 89. Scenarios for maintenance frequency based on the average surface roughness

Sections	Worst case	Most likely	Best case
LCF Class A	2	3	4
OFD Class A	2	3	4
BFL Class A	2	3	4
80% BFL Class A + 20% BFL Clean	2	3	4
70% BFL Class A + 30% OFD Clean	1	2	3
70% BFL Class A + 30% LCF Clean	1	2	3
70% BFL Class A + 30% CRG Clean	2	3	4

The 70% BFL Class A + 30% OFD Clean A and 70% BFL Class A + 30% LCF Clean with poor average surface roughness conditions could have maintenance every one, two, or three years. LCF Class A, OFD Class A, BFL Class A, 80% BFL Class A + 20% BFL Clean, and 70% BFL

Class A + 30% CRG Clean with fair average surface roughness condition could have maintenance every two, three, or four years.

Figure 105 shows BCA results based on the scenarios from average surface roughness conditions.

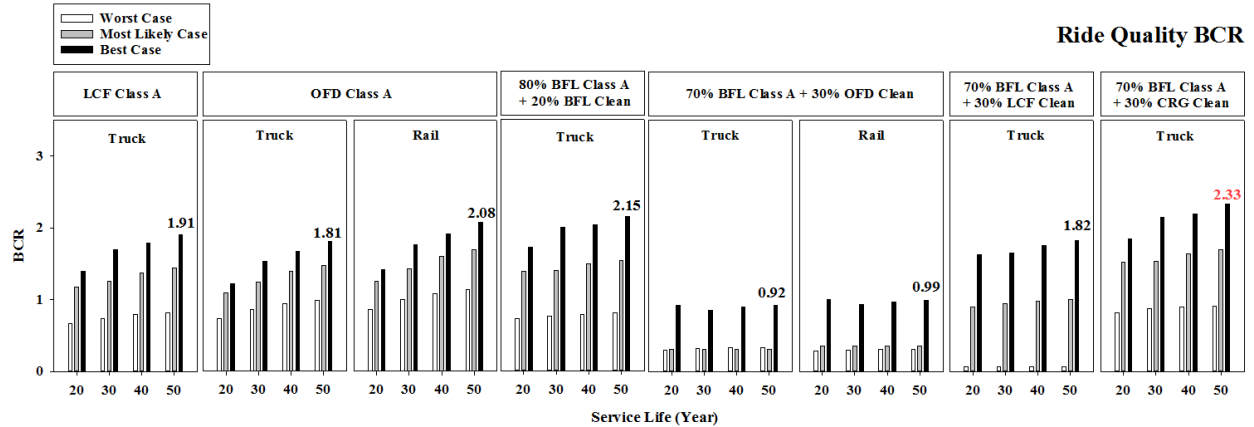


Figure 105. BCR values for average surface roughness conditions

The BCR values for LCF Class A, OFD Class A, 80% BFL Class A + 20% BFL Clean, and 70% BFL Class A + 30% CRG Clean were lower than 1 for worst-case (maintenance every two years) and higher than 1 for most likely and best-case scenarios (maintenance every three or four years). The 70% BFL Class A + 30% OFD Clean and 70% BFL Class A + 30% LCF Clean were not beneficial compared to the base case (BFL Class A) with BCR values lower than 1 for the worst-case and most likely scenarios (maintenance every one or two years). However, the aforementioned two sections had BCR values higher than 1 for the best-case scenario (maintenance every three years). The highest BCR value was observed for 50 years of service life and the best-case scenario for 70% BFL Class A + 30% CRG Clean (2.33), and the lowest BCR value was observed for 30, 40, and 50 years of service life values and the worst-case scenario for 70% BFL Class A + 30% LCF Clean (0.06) when ride quality was considered.

Figure 105 shows the BCR values for OFD Class A and 70% BFL Class A + 30% OFD Clean increase when hauling materials by rail rather than truck. This increase for OFD Class A is higher (0.27) than 70% BFL Class A + 30% OFD Clean (0.07). The 70% BFL Class A + 30% OFD Clean still will not be beneficial even if the OFD materials were hauled by train. Nevertheless, rail hauling resulted in the OFD Class A section being the third most beneficial section after 70% BFL Class A + 30% CRG Clean and 80% BFL Class A + 20% BFL Clean sections.

7.8.7 Overall Performance-Based BCR Values

7.8.7.1 First Condition

For this analysis, the first group (total breakage, fines content, and gravel-to-sand ratio) was weighted as 1, the second group (FWD and DCP) was weighted as 0.5, and the third group (dustometer and IRI) was weighted as 0.25 (Figure 106).

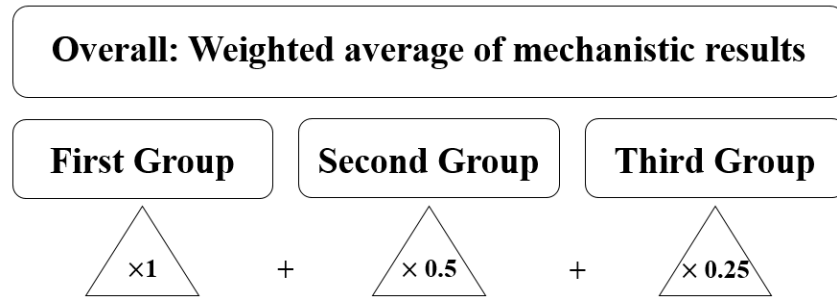


Figure 106. Weighted average of the BCR values based on the mechanical properties

Figure 107 shows the average weighted value of the BCR values for different scenarios and service life parameters.

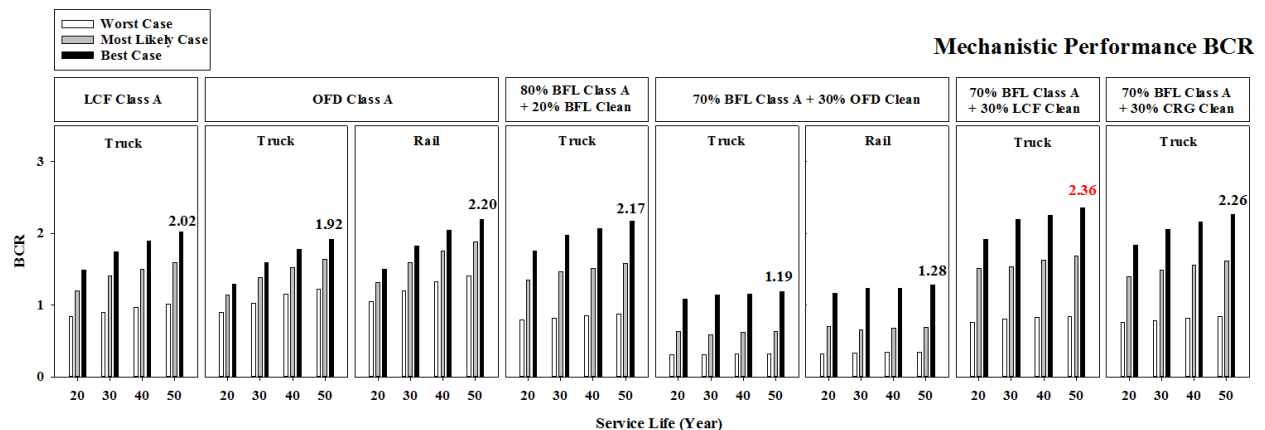


Figure 107. BCR values for weighted performance measures

The BCR values for LCF Class A, 80% BFL Class A + 20% BFL Clean, 70% BFL Class A + 30% LCF Clean, and 70% BFL Class A + 30% CRG Clean were lower than 1 for worst-case and higher than 1 for most likely and best-case scenarios. However, LCF Class A had a BCR higher than 1 (1.02) for the worst-case scenario, when the service life was 50 years. OFD Class A always had BCR values higher than 1 for all the scenarios and service life values except for 20 years of service life at the worst-case scenario. The 70% BFL Class A + 30% OFD Clean was not beneficial compared to the base case (BFL Class A) with BCR values lower than 1 for worst-case and most likely scenarios. However, this section had BCR values higher than 1 for the best-case scenario. The highest BCR value was observed for 50 years of service life and the best-case

scenario for 70% BFL Class A + 30% LCF Clean (2.36), and the lowest BCR value was observed for 20 and 30 years of service life values and the worst-case scenario for 70% BFL Class A + 30% OFD Clean (0.31).

Figure 107 shows the BCR values for OFD Class A and 70% BFL Class A + 30% OFD Clean increase when hauling materials by rail rather than truck. This increase for OFD Class A was higher (0.28) than 70% BFL Class A + 30% OFD Clean (0.09). Hauling OFD materials by train resulted in the OFD Class A section being the third most beneficial section after 70% BFL Class A + 30% LCF Clean and 70% BFL Class A + 30% CRG Clean with BCR values higher than 80% BFL Class A + 20% BFL Clean.

7.8.7.2 Second Condition

For this analysis, the material and surface thickness loss was weighted as 1, the first group (total breakage, fines content, and gravel-to-sand ratio) was weighted as 0.75, the second group (FWD and DCP) was weighted as 0.5, and the third group (dustometer and IRI) was weighted as 0.25 (Figure 108).

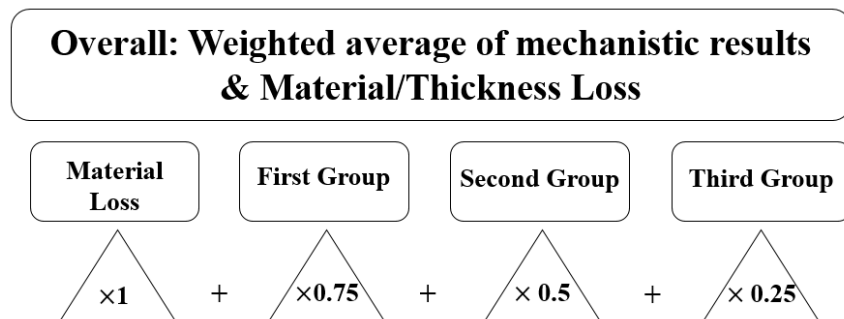


Figure 108. Weighted average of the BCR values based on the mechanical properties and material/thickness loss

Figure 109 shows the average weighted values of the BCR for different scenarios and service life values.

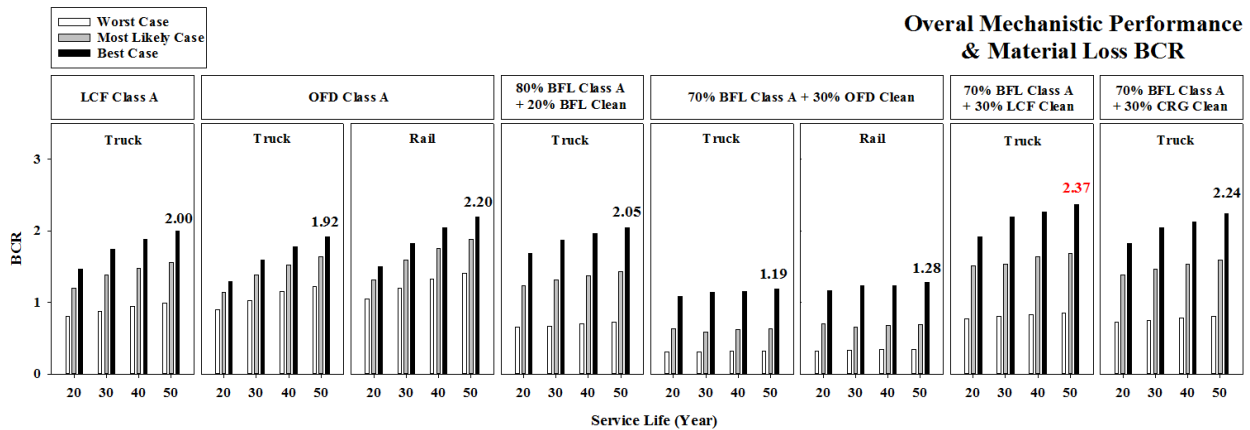


Figure 109. BCR values for weighted performance measures and material/thickness loss

The BCR values for LCF Class A, 80% BFL Class A + 20% BFL Clean, 70% BFL Class A + 30% LCF Clean, and 70% BFL Class A + 30% CRG Clean were lower than 1 for worst-case and higher than 1 for most likely and best-case scenarios. OFD Class A always had BCR values higher than 1 for all the scenarios and service life values except for 20 years of service life at the worst-case scenario. The 70% BFL Class A + 30% OFD Clean was not beneficial to construct compared to the base case (BFL Class A) with BCR values lower than 1 for the worst-case and most likely scenarios. However, this section had BCR values higher than 1 for the best-case scenario. The highest BCR value was observed for 50 years of service life and the best-case scenario for 70% BFL Class A + 30% LCF Clean (2.37), and the lowest BCR value was observed for 20 and 30 years of service life values and the worst-case scenario for 70% BFL Class A + 30% OFD Clean (0.31).

Figure 109 shows the BCR values for OFD Class A and 70% BFL Class A + 30% OFD Clean increase with hauling materials with rail rather than truck. This increase for OFD Class A was higher (0.28) than 70% BFL Class A + 30% OFD Clean (0.09). Rail hauling of OFD materials resulted in the OFD Class A section being the third most beneficial section after 70% BFL Class A + 30% LCF Clean and 70% BFL Class A + 30% CRG Clean with BCR values higher than LCF Class A.

7.8.7.3 Third Condition

For this analysis, the gravel content change was weighted as 1, the first group (total breakage, fines content, and gravel-to-sand ratio) was weighted as 0.75, the second group (FWD and DCP) was weighted as 0.5, and the third group (dustometer and IRI) was weighted as 0.25 (Figure 110).

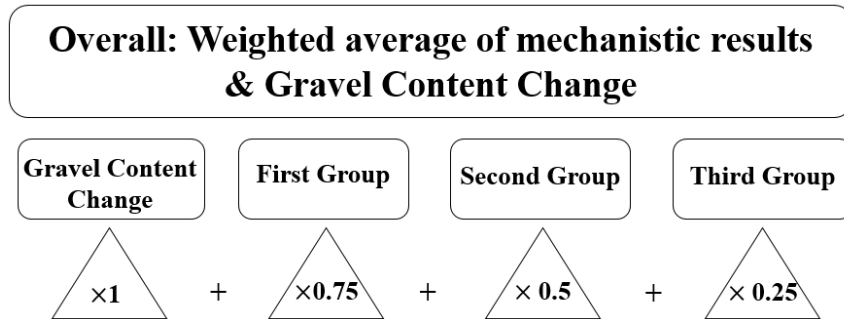


Figure 110. Weighted average of the BCR values based on the mechanical properties and gravel loss

Figure 111 shows the average weighted values of the BCR for different scenarios and service life values.

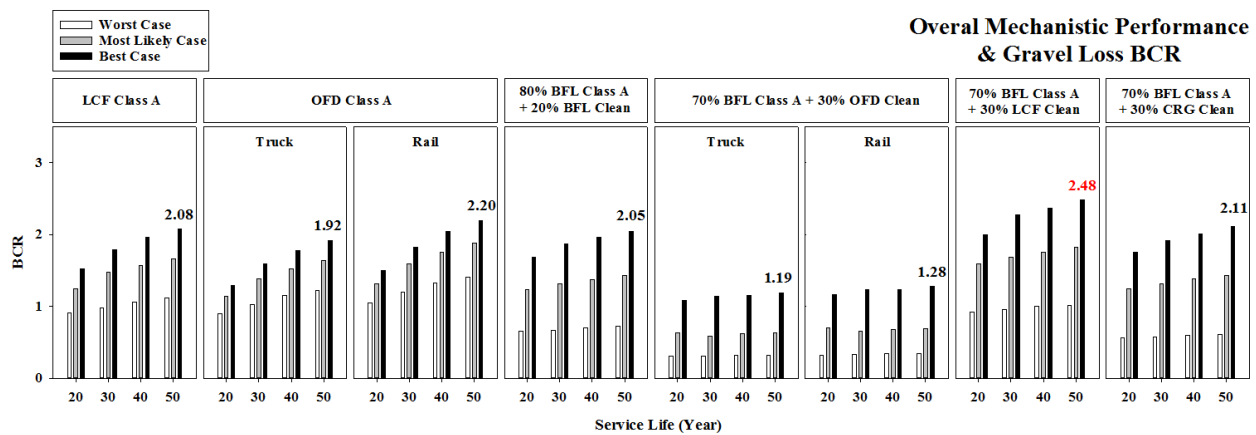


Figure 111. BCR values for weighted performance measures and gravel loss

LCF Class A and 70% BFL Class A + 30% LCF Clean always had BCR values higher than 1 except for 20 and 30 years of service life values for the worst-case scenario. OFD Class A always had BCR values higher than 1 for all the scenarios and service life values except for the 20 years of service life at the worst-case scenario. The BCR values for 80% BFL Class A + 20% BFL Clean and 70% BFL Class A + 30% CRG Clean were lower than 1 for the worst-case and higher than 1 for the most likely and best-case scenarios. The 70% BFL Class A + 30% OFD Clean was not beneficial to construct compared to the base case (BFL Class A) with BCR values lower than 1 for the worst-case and most likely scenarios. However, this section had BCR values higher than 1 for the best-case scenario. The highest BCR value was observed for 50 years of service life and the best-case scenario for 70% BFL Class A + 30% LCF Clean (2.48), and the lowest BCR value was observed for 20 and 30 years of service life values and the worst-case scenario for 70% BFL Class A + 30% OFD Clean (0.31).

The BCR values for OFD Class A and 70% BFL Class A + 30% OFD Clean increase when hauling materials by rail rather than truck. This increase for OFD Class A was higher (0.28) than

70% BFL Class A + 30% OFD Clean (0.09). Rail hauling of OFD materials resulted in the OFD Class A section being the second most beneficial section after 70% BFL Class A + 30% LCF Clean with BCR values higher than that of 70% BFL Class A + 30% CRG Clean.

CHAPTER 8. CONCLUSIONS AND RECOMMENDATIONS

This chapter briefly summarizes the results of the laboratory and field tests, temperature readings, and cost analysis for the test sections. In addition, recommendations for future studies are provided.

The results of this study showed that mixing clean and Class A aggregates could be an efficient way to reduce costs, because clean aggregate materials are larger in size and lower amounts (tonnage) of materials are required to achieve a specific thickness. Therefore, the total amount of materials for the sections with the mixture of Class A and clean materials will be lower than sections with only Class A materials. This results in a decrease in the costs of aggregates and hauling.

8.1 Field Observations

Based on the observations throughout construction and maintenance, it was concluded that the two sections consisting of mixtures of 70% BFL Class A + 30% LCF Clean and 70% BFL Class A + 30% CRG Clean had the best overall performance. The 70% BFL Class A + 30% CRG Clean section was more difficult to maintain due to the high angularity of the aggregate materials. However, this section performed well for a long period of time and became stiff after each blading occurrence. Blading was more time-consuming for the OFD Class A, 80% BFL Class A + 20% BFL Clean, and 70% BFL Class A + 30% OFD Clean sections relative to the other test sections. OFD Class A required blading more often than other sections; however, the amount of aggregate material and thickness loss for this section was lower than the other sections. The OFD Class A and 70% BFL Class A + 30% OFD Clean sections had more potholes compared to the other sections.

8.2 Laboratory Test Results

Extensive laboratory testing including sieve and hydrometer analysis, Atterberg limits, compaction, abrasion, and C-Freeze tests were conducted on surface and subgrade materials from each section. Results include the following:

- According to the USCS and AASHTO classification systems, all of the surface aggregate materials were classified as well-graded gravel (GW), or A-1-a, while the subgrade was classified as sandy lean clay (CL), or A-6. The plasticity index (PI) values of the surface aggregates ranged from non-plastic (OFD Class A) to 5 (80% BFL Class A + 20% BFL Clean). These results showed that the surface aggregates were all non-plastic to slightly plastic. The plasticity index of the subgrade material was 12.
- The results of the CBR tests showed that the difference in the values of the stress on the piston for different surface aggregate materials increased with an increase in the penetration depth. OFD Class A had the maximum unsoaked CBR, and BFL Class A had the maximum soaked CBR value. The difference between soaked and unsoaked CBR values for the subgrade were negligible.

- Abrasion losses ranging from 11 to 49% were observed for the three Class A materials alone (LCF, OFD, and BFL), with BFL Class A giving the highest abrasion loss. The mixtures of BFL Class A with the four different clean aggregates all exhibited similar abrasion losses of 33 to 43%. The existence of the lower quality BFL Class A, therefore, significantly decreases the resistance of the surface aggregate mixtures against abrasion, as the higher strength materials accelerate the degradation of the weaker ones in the mixture.
- The LCF Class A and OFD Class A aggregates showed the minimum percent loss in C-Freeze tests. These results also indicated that the presence of BFL Class A in the surface aggregate mixtures will increase the material losses during freeze/thaw cycles.

8.3 Field Test Results

In order to evaluate the performance of the different surface aggregate materials, the changes in the properties of the aggregate materials (fines content, gravel-to-sand ratio, and breakage indices), as well as the stiffness, strength, dust production, and ride quality of each section were monitored on several occasions throughout the project duration. The results include the following:

- The BFL Class A material exhibited the highest initial fines content. In addition, the largest changes in the fines content were observed for the sections built with BFL Class A. Among them, the largest change in fines content was observed for the 80% BFL Class A + 20% BFL Clean section, which was consistent with the laboratory abrasion test results.
- The 80% BFL Class A + 20% BFL Clean had the highest average gravel-to-sand ratio values, as well as the largest standard deviations of the gravel-to-sand ratios. OFD Class A had the lowest standard deviations for both gravel-to-sand ratio and fines content.
- The 70% BFL Class A + 30% CRG Clean and 70% BFL Class A + 30% LCF Clean sections had the lowest breakage potentials and total breakage values, while the 80% BFL Class A + 20% BFL Clean had the lowest breakage potential, average total breakage values, and variations over time.
- All of the surface course DCP-CBR average values were rated as excellent based on the SUDAS classification system. All of the subgrade DCP-CBR values were rated poor to fair, except for the subgrade under the LCF Class A (very poor) and the 80% BFL Class A + 20% BFL Clean (fair to good) sections. Results of the DCP tests showed that the surface thicknesses for all sections were in the range of 7 to 10 in. DCP-CBR values for the subgrade was in a narrow range of 6 to 10% for all sections. The surface courses of the 80% BFL Class A + 20% BFL Clean and 70% BFL Class A + 30% CRG Clean had the highest and lowest DCP-CBR values, respectively.
- The various stiffness test results did not provide any clear or consistent correlations with the index properties of any of the test sections.
- The average values of IRI (ride quality) for all sections corresponded to a fair quality of smoothness except for 70% BFL Class A + 30% OFD Clean and 70% BFL Class A + 30% CRG Clean, which had poor smoothness quality. The average IRI values over time showed that LCF Class A and BFL Class A had the best smoothness among all sections.
- The LWD test results showed that LCF Class A had the maximum and 70% BFL Class A + 30% CRG Clean had the minimum composite (surface and subgrade) elastic modulus values.

Composite elastic modulus values of all sections were generally consistent for different seasons, except in December 2016 when tests were performed on frozen ground.

- Dustometer test results showed that the 70% BFL Class A + 30% CRG Clean section had the maximum dust production and LCF Class A had the lowest dust production.
- Temperature data recorded at the center and shoulder of the road showed that the maximum frost depths increased each year between 2016 and 2019. Results showed that the frost depth at the center of the road was always higher than that at the shoulder. The proposed reason for this trend was the existence of snow cover and vegetation on the shoulders, which insulates the ground somewhat against the effects of harsh weather.

8.4 Cost Analysis Results

A BCA was performed based on performance measures including material and thickness loss, gravel (>US #4 sieve, 0.19 in.) loss, fines content, gravel-to-sand ratio, total breakage, and results of the FWD, DCP, dustometer, and surface ride quality tests, to find the most cost-effective materials. Service life values of 20, 30, 40, and 50 years were examined. Finally, overall BCR values were calculated by assigning weighting factors to the BCR values based on the relative importance of each of the performance measures.

BCA results include the following:

- OFD Class A had the highest construction costs per mile due to the greater haul distance of OFD materials from project site. The mixture of 80% BFL Class A + 20% BFL Clean had the lowest construction costs due to the proximity of the materials of this section to the site and the smaller amount of aggregates required to build this section.
- OFD Class A required a smaller amount of aggregate materials for maintenance, and consequently was the least expensive section to maintain. The 70% BFL Class A + 30% OFD Clean required the most aggregate materials for maintenance and was, therefore, the most expensive section to maintain.
- The 70% BFL Class A + 30% LCF Clean had the highest BCR values for material and thickness loss, gravel content change, total breakage, fines content, FWD modulus, and dust production. However, 70% BFL Class A + 30% CRG Clean had the highest BCR values for gravel-to-sand ratio and ride quality. After applying the weighting factors, the overall performance-based BCR values were highest for the 70% BFL Class A + 30% LCF Clean and 70% BFL Class A + 30% CRG Clean mixtures.
- Using rail hauling over truck hauling would be beneficial, especially for OFD Class A and 70% BFL Class A + 30% OFD Clean sections. However, the analysis showed that rail hauling did not increase the BCR of these sections significantly. For the hauling distances involved in this particular study, using local aggregates was, therefore, more cost-effective than using OFD aggregates from farther away. Similar rail hauling benefit-cost analyses were conducted for the LCF aggregates. However, rail hauling of LCF was more costly than truck hauling due to the routes of the specific railways owned by the quarry used in this study.

8.5 Recommendations

Based on the observations and results of this research, the following future research activities and developments are recommended:

- Building new test sections in different regions to examine a wider range of local quarry materials, traffic loads, and subgrade conditions
- Increasing the test section lengths from 500 ft to ¼ mile (at least) and conduct BCAs on longer granular roadway network that has been built with Class A-clean aggregate mixtures
- Developing a new method of back-calculation to increase accuracy of modulus values from FWD data
- Performing BCA on construction and maintenance of low-volume roads with different materials, stabilization methods, or other conditions

In this study, four different clean aggregates were mixed with local Class A materials. However, it would also be useful to investigate the effectiveness of using other aggregate options in the construction of longer test sections, and monitor their performance over time similar to the present study. Longer sections (>0.25 mile) with sufficient lengths of gaps in between would make maintenance of the sections easier and better represent the performance of actual roads constructed with the same materials. In this case, mixing of materials from adjacent sections will be reduced, and the number of testing points can be increased to capture clearer evaluations of the test section performance.

The FWD is a relatively expensive test, and several back-calculation methods exist such as Modulus 7, BAKFAA, and combined Boussinesq and Odemark's theory, to calculate the surface and subgrade elastic moduli. The back-calculation methods are different in their error minimization procedures and assumptions, which results in different non-unique results for elastic modulus. It would be helpful to collect a sufficient database of back-calculated elastic modulus values with corresponding measurements of surface thickness, temperature, density, and Poisson's ratios to build a neural network model to better predict the elastic moduli.

In performing the BCA, it was challenging to determine the benefits of using several aggregate options. Loss of materials and surface thickness is the most important aspect in the cost analysis of granular roadways, because this is the cause of several other problems such as surface distresses (potholes, rutting, etc.), dust production, and higher surface roughness. Moreover, the only consideration for performing maintenance and adding new aggregates to the sections was by measuring the thickness loss. Therefore, maintenance costs are directly associated with material and surface thickness loss of the granular roads. However, several other changes in the material properties were considered in the BCA model including gravel loss, fines content, gravel-to-sand ratio, and total breakage, along with other performance measures including surface stiffness and strength, dust production, and ride quality. These considerations enabled comparisons between the BCR values of the alternative sections and the control section. The results showed that mixing LCF and CRG Clean materials with BFL Class A is the most cost-effective option. Hauling high-quality materials (such as OFD) for the longer distances used in this particular study would not be cost-effective due to the high hauling costs, even though the

aggregate prices were lower than the other aggregate options. Although rail hauling could help reduce hauling costs compared to truck hauling, it would not be sufficient to make OFD the most cost-effective option for the quarry and test site locations in this study.

REFERENCES

- AASHTO. 1960. *Road User Benefit Analyses for Highway Improvements*. American Association of State Highway Officials. Committee on Planning and Design Policies, Washington, DC.
- . 1993. *AASHTO Guide for the Design of Pavement Structures*. American Association of State Highway and Transportation Officials, Washington, DC.
- Akbariyeh, N. 2015. A New Technique for the Estimation of the Elastic Moduli of Pavement Layers from Light Weight Deflectometer Data. Master's thesis. The University of Texas at Arlington, TX.
- Akinmade, O. D., K. Z. Cinfwat, A. I. Ibrahim, and G. N. Omange. 2017. The Use of Roadroid Application and Smart Phones for Road Condition Monitoring in Developing Countries. 8th Africa Transportation Technology Transfer Conference—Linking Africa Through Sustainable Transport Infrastructure Development, May 8–10, Livingstone, Zambia.
- Alzubaidi, H. and R. Magnusson. 2002. Deterioration and Rating of Gravel Roads: State of the Art. *Road Materials and Pavement Design*, Vol. 3, No. 3, pp. 235–60.
- Appea, A. K. 2003. Validation of FWD Testing Results at the Virginia Smart Road: Theoretically and by Instrument Responses. PhD dissertation. Virginia Polytechnic Institute and State University, Blacksburg, VA.
- Boussinesq, J. 1885. *Application Dès Potentiels a L'étude de L'équilibre et Du Mouvement Des Solides Élastiques*. Gauthier-Villars, unknown location.
- Bozorgzad, A. and H. “D.” Lee. 2017. Consistent Distribution of Air Voids and Asphalt and Random Orientation of Aggregates by Flipping Specimens during Gyrotory Compaction Process. *Construction and Building Materials*, Vol. 132, pp. 376–382.
- Brown, S. F., W. S. Tam, and J. M. Brunton. 1987. Structural Evaluation and Overlay Design: Analysis and Implementation. Sixth International Conference: Structural Design of Asphalt Pavements, July 13–17, Ann Arbor, MI.
- Carlsson, F., O. Johansson-Stenman, and P. K. Nam. 2015. Funding a New Bridge in Rural Vietnam: A Field Experiment on Social Influence and Default Contributions. *Oxford Economic Papers*, Vol. 67, No. 4, pp. 987–1014.
- Ceylan, H., A. Guclu, E. Tutumluer, and M. R. Thompson. 2005. Backcalculation of Full-Depth Asphalt Pavement Layer Moduli Considering Nonlinear Stress-Dependent Subgrade Behavior. *International Journal of Pavement Engineering*, Vol. 6, No. 3, pp. 171–182.
- Chang, D.-W., Y. V. Kang, J. M. Roesset, and K. Stokoe II. 1992a. Effect of Depth to Bedrock on Deflection Basins Obtained with Dynaflect and Falling Weight Deflectometer Tests. *Transportation Research Record: Journal of the Transportation Research Board*, No. 1335, pp. 8–16.
- Chang, D.-W., J. M. Roesset, and K. H. Stokoe II. 1992b. Nonlinear Effects in Falling Weight Deflectometer Tests. *Transportation Research Record: Journal of the Transportation Research Board*, No. 1355, pp. 1–7.
- DelRio-Prat, M., A. Vega-Zamanillo, D. Castro-Fresno, and M. Á. Calzada-Pérez. 2011. Energy Consumption during Compaction with a Gyrotory Intensive Compactor Tester. Estimation Models. *Construction and Building Materials*, Vol. 25, No. 2, pp. 979–986.
- Dharmadhikari, N., E. Lee, and P. Kayabas. 2016. The Lifecycle Benefit–Cost Analysis for a Rural Bridge Construction to Support Energy Transportation. *Infrastructures*, Vol. 1, No. 2, pp. 1–14.

- Dobson, E. F. and L. J. Postill. 1983. Classification of Unpaved Roads in Ontario. *Transportation Research Record: Journal of the Transportation Research Board*, No. 898, pp. 36–47.
- Fathi, A., C. Tirado, M. Mazari, and S. Nazarian. 2019. Models for Estimation of Lightweight Deflectometer Moduli for Unbound Materials. Eighth International Conference on Case Histories in Geotechnical Engineering, March 24–27, Philadelphia, PA.
- Ghadimi, B., A. Nega, and H. Nikraz. 2015. Simulation of Shakedown Behavior in Pavement’s Granular Layer. *International Journal of Engineering and Technology*, Vol. 7, No. 3, pp. 198–203.
- Ghasemi, P., J. Podolsky, R. C. Williams, and E. Dave. 2016. Performance Evaluation of Coarse-Graded Field Mixtures Using Dynamic Modulus Results Gained from Testing in the Indirect Tension Mode. International Conference on Transportation and Development 2016, June 26–29, Houston, TX. pp. 1111–1121.
- Ghasemi, P., M. Aslani, D. K. Rollins, R.C. Williams, and V. R. Schaefer. 2018. Modeling Rutting Susceptibility of Asphalt Pavement Using Principal Component Pseudo Inputs in Regression and Neural Networks. *International Journal of Pavement Research and Technology*. pp. 1–12.
- Gheibi, A. and A. Hedayat. 2018. Ultrasonic Investigation of Granular Materials Subjected to Compression and Crushing. *Ultrasonics*, Vol. 87, pp. 112–125.
- Gibson, B. and C. Y. Wallace. 2016. *Cost Benefit Analysis: Applications and Future Opportunities*. Kentucky Transportation Center, University of Kentucky, Lexington, KY.
- Grasmick, J. G. 2013. Using the Light Weight Deflectometer with Radial Offset Sensors on Two-Layer Systems for Construction Quality Control/Quality Assurance of Reclaimed and Stabilized Materials. Master’s thesis. Colorado School of Mines, Golden, CO.
- Grasmick, J. G., M. A. Mooney, R. W. Surdahl, M. Voth, and C. Senseney. 2014. Capturing a Layer Response during the Curing of Stabilized Earthwork Using a Multiple Sensor Lightweight Deflectometer. *Journal of Materials in Civil Engineering*, Vol. 27, No. 6, pp. 1–12.
- Hadidi, R. and N. Gucunski. 2010. Comparative Study of Static and Dynamic Falling Weight Deflectometer Back-Calculations Using Probabilistic Approach. *Journal of Transportation Engineering*, Vol. 136, No. 3, pp. 196–204.
- Hardin, B. O. 1985. Crushing of Soil Particles. *Journal of Geotechnical Engineering*, Vol. 111, No. 10, pp. 1177–1192.
- Heisey, J. S., K. H. Stokoe II, and A. H. Meyer. 1982a. Moduli of Pavement Systems from Spectral Analysis of Surface Waves. *Transportation Research Record: Journal of the Transportation Research Board*, No. 852, pp. 22–31.
- Heisey, J. S., K. H. Stokoe, W. R. Hudson, and A. H. Meyer. 1982b. *Determination of In Situ Shear Wave Velocities from Spectral Analysis of Surface Waves*. Center for Transportation Research, The University of Texas at Austin, TX.
- Heukelom, W. and C. R. Foster. 1962. Dynamic Testing of Pavements. *Transactions of the American Society of Civil Engineers*, Vol. 127, No. 1, pp. 425–450.
- Hudson, W. R. 1997. *Infrastructure Management*. McGraw- Hill, Inc., New York, NY.
- Iowa DOT. 2012. County Annual Average Daily Traffic (AADT) Maps. Retrieved <https://iowadot.gov/maps/msp/traffic/2016/counties/DECATUR.pdf>.

- Iowa DOT. 2018. *Aggregate Instruction Text: Technical Training and Certification Program 2018–2019*. Iowa Department of Transportation, Ames, IA.
https://iowadot.gov/training/ttcp/training_manuals/Aggregate.pdf.
- Iowa Geological Survey. 2002. *Bedrock Geology of South-Central Iowa, June 2002*. Prepared by J. P. Pope, B. J. Witzkey, R. R. Anderson, G. A. Ludvigson, B. J. Bunker, and S. Greeney, Iowa Department of Natural Resources, Des Moines, IA.
<http://publications.iowa.gov/26198/1/ofm-2002-1.pdf>.
- Isemo, A. and J. Johansson. 1976. Relationship Between Different Factors in Gravel Road Maintenance. Thesis. KTH Royal Institute of Technology, Stockholm, Sweden.
- Jia, X., B. Huang, D. Zhu, Q. Dong, and M. Woods. 2018. Influence of Measurement Variability of International Roughness Index on Uncertainty of Network-Level Pavement Evaluation. *Journal of Transportation Engineering Part B: Pavements*, Vol. 144, No. 2, pp. 1–9.
- Jones, H., F. Moura, and T. Domingos. 2014. Transport Infrastructure Project Evaluation Using Cost-Benefit Analysis. *Procedia – Social and Behavioral Sciences*, Vol. 111, pp. 400–409.
- Jones, R. 1955. A Vibration Method for Measuring the Thickness of Concrete Road Slabs in Situ. *Magazine of Concrete Research*, Vol. 7, No. 20, pp. 97–102.
- . 1958. In-Situ Measurement of the Dynamic Properties of Soil by Vibration Methods. *Geotechnique*, Vol. 8, No. 1, pp. 1–21.
- . 1962. Surface Wave Technique for Measuring the Elastic Properties and Thickness of Roads: Theoretical Development. *British Journal of Applied Physics*, Vol. 13, No. 1, pp. 21–29.
- Kuo, C.-M., C.-C. Lin, C.-H. Huang, and Y.-C. Lai. 2016. Issues in Simulating Falling Weight Deflectometer Test on Concrete Pavements. *KSCIE Journal of Civil Engineering*, Vol. 20, No. 2, pp. 702–708.
- Lade, P. V., J. A. Yamamuro, and P. A. Bopp. 1996. Significance of Particle Crushing in Granular Materials. *Journal of Geotechnical Engineering*, Vol. 122, No. 4, pp. 309–316.
- Layard, R. and S. Glaister, editors. 1994. *Cost-Benefit Analysis*. Second Edition Cambridge University Press, Cambridge, England.
- Lees, G. and C. K. Kennedy. 1975. Quality, Shape and Degradation of Aggregates. *Quarterly Journal of Engineering Geology*, Vol. 8, No. 3, pp. 193–209.
- Li, C., J. Ashlock, D. White, and P. Vennapusa. 2015. *Low-Cost Rural Surface Alternatives: Demonstration Project*. Institute for Transportation, Iowa State University, Ames, IA.
https://intrans.iastate.edu/app/uploads/2018/03/low-cost_rural_surface_alternatives_demo_w_cvr.pdf.
- Li, C., D. J. White, and P. Vennapusa. 2015b. Moisture-Density-Strength-Energy Relationships for Gyrotory Compacted Geomaterials. *Geotechnical Testing Journal*, Vol. 38, No. 4, pp. 461–473.
- Li, C., J. C. Ashlock, S. Lin, and P. K. R. Vennapusa. 2017a. Layered Elastic Moduli of Stabilized Unpaved Roads by Multichannel Analysis of Surface Waves and Falling Weight Deflectometer Tests. 96th Annual Meeting of the Transportation Research Board, January 8–12, Washington, DC.

- Li, C., J. C. Ashlock, D. J. White, C. T. Jahren, and B. Cetin. 2017b. Gyrotory Abrasion with 2D Image Analysis Test Method for Evaluation of Mechanical Degradation and Changes in Morphology and Shear Strength of Compacted Granular Materials. *Construction and Building Materials*, Vol. 152, pp. 547–557.
- Li, C., J. C. Ashlock, D. J. White, and P. K. R. Vennapusa. 2018a. Mechanistic-Based Comparisons of Stabilised Base and Granular Surface Layers of Low-Volume Roads. *International Journal of Pavement Engineering*, Vol. 20, No. 1, pp. 1–13.
- Li, C., J. Ashlock, B. Cetin, and C. Jahren. 2018b. *Feasibility of Granular Road and Shoulder Recycling*. Institute for Transportation, Iowa State University, Ames, IA. https://intrans.iastate.edu/app/uploads/2018/07/granular_rd_and-shoulder_recycling_feasibility_w_cvr.pdf.
- Li, C., J. C. Ashlock, S. Lin, and P. K. R. Vennapusa. 2018c. In Situ Modulus Reduction Characteristics of Stabilized Pavement Foundations by Multichannel Analysis of Surface Waves and Falling Weight Deflectometer Tests. *Construction and Building Materials*, Vol. 188, pp. 809–819.
- Lin, S. 2014. Advancements in Active Surface Wave Methods Modeling, Testing, and Inversion. PhD dissertation. Geotechnical Engineering, Iowa State University, Ames, IA.
- Lin, S. and J. C. Ashlock. 2012. A Study on Issues Relating to Testing of Soils and Pavements by Surface Wave Methods. *AIP Conference Proceedings*, Vol. 1430, No. 31, pp. 1532–1539.
- . 2015. Comparison of MASW and MSOR for Surface Wave Testing of Pavements. *Journal of Environmental & Engineering Geophysics*, Vol. 20, No. 4, pp. 277–85.
- Lin, S., J. C. Ashlock, and R. C. Williams. 2016. Nondestructive Quality Assessment of Asphalt Pavements Based on Dynamic Modulus. *Construction and Building Materials*, Vol. 112, pp. 836–847.
- Mahvelati, S. and J. T. Coe. 2018. Effects of Reductions in Number of Channels on Rayleigh and Love Wave Dispersion Images Acquired Using the Multichannel Analysis of Surface Waves (MASW) Method. *Symposium on the Application of Geophysics to Engineering and Environmental Problems 2018 Proceedings*, pp. 295–299.
- Marsal, R. J. 1967. Large-Scale Testing of Rockfill Materials. *Journal of the Soil Mechanics and Foundations Division*, Vol. 93, No. 2, pp. 27–43.
- Mereu, R. F., R. J. Uffen, and A. E. Beck. 1963. The Use of a Coupler in the Conversion of Impact Energy into Seismic Energy. *Geophysics*, Vol. 28, No. 4, pp. 531–546.
- Nahvi, A., S. M. S. Sadati, K. S. Cetin, H. Ceylan, A. Sassani, and S. Kim. 2018. Towards Resilient Infrastructure Systems for Winter Weather Events: Integrated Stochastic Economic Evaluation of Electrically Conductive Heated Airfield Pavements. *Sustainable Cities and Society*, Vol. 41, pp. 195–204.
- Nazarian, S. 1983. Use of Spectral Analysis of Surface Waves Method for Determination of Moduli and Thicknesses of Pavement Systems. *Transportation Research Record: Journal of the Transportation Research Board*, No. 930, pp. 38–45.
- Nazarian, S. and K. H. Stokoe II. 1985. *In Situ Determination of Elastic Moduli of Pavement Systems by Spectral Analysis of Surface Waves Method (Practical Aspects)*. Center for Transportation Research, The University of Texas at Austin, TX.
- Nega, A., H. Nikraz, and I. L. Al-Qadi. 2016. Dynamic Analysis of Falling Weight Deflectometer. *Journal of Traffic and Transportation Engineering (English Edition)*, Vol. 3, No. 5, pp. 427–437.

- Notani, M. A., A. Arabzadeh, H. Ceylan, S. Kim, and K. Gopalakrishnan. 2019. Effect of Carbon-Fiber Properties on Volumetrics and Ohmic Heating of Electrically Conductive Asphalt Concrete. *Journal of Materials in Civil Engineering*, Vol. 31, No. 9.
- Nurmikolu, Antti. 2005. Degradation and Frost Susceptibility of Crushed Rock Aggregates Used in Structural Layers of Railway Track. DTech thesis. Tampere University of Technology, Finland.
- Odemark, N. 1949. Investigations as to the Elastic Properties of Soils and Design of Pavements According to the Theory of Elasticity. The National Road Research Institute (Statens Vaginstitut), Stockholm, Sweden.
- Oloo, S. Y., D. G. Fredlund, and J. K.-M. Gan. 1997. Bearing Capacity of Unpaved Roads. *Canadian Geotechnical Journal*, Vol. 34, No. 3, pp. 398–407.
- Park, C. B. 1995. *Characterization of Geotechnical Sites by Multi-Channel Analysis of Surface Waves (MCASW)*. Kansas Geological Survey, The University of Kansas, Lawrence, KS.
- Park, C. B., R. D. Miller, and J. Xia. 1999a. Multichannel Analysis of Surface Waves. *Geophysics*, Vol. 64, No. 13, pp. 800–808.
- . 1999b. Multichannel Analysis of Surface Waves. *Geophysics*, Vol. 64, No. 3, pp. 800–806.
- Park, C. B., J. Ivanov, R. D. Miller, J. Xia, and N. Ryden. 2001. Seismic Investigation of Pavements by MASW Method – Geophone Approach. *Symposium on the Application of Geophysics to Engineering and Environmental Problems 2001 Proceedings*.
- Paterson, W. D. O. 1987. *Road Deterioration and Maintenance Effects: Models for Planning and Management*. The Johns Hopkins University Press, Baltimore, MD.
- . 1991. Deterioration and Maintenance of Unpaved Roads: Models of Roughness and Material Loss. *Transportation Research Record: Journal of the Transportation Research Board*, No. 1291, pp. 143–156.
- Prest, A. R. and R. Turvey. 1965. Cost-Benefit Analysis: A Survey. *The Economic Journal*, Vol. 75, No. 300, pp. 683–735.
- Provencher, Y. 1995. Optimizing Road Maintenance Intervals. *Sixth Interantional Conference on Low-Volume Roads Proceedings*, June 25–29, Minneapolis, MN, pp. 199–207.
- Rix, G. J., K. H. Stokoe, II, and J. M. Roesset 1991. *Experimental Study of Factors Affecting the Spectral-Analysis-of-Surface-Waves Method*. Center for Transportation Research, The University of Texas at Austin, TX.
- Ryden, N. 2009. Surface Wave Testing of Pavements. *The Journal of the Acoustical Society of America*, Vol. 125, No. 4.
- Saltan, M., V. E. Uz, and B. Aktas. 2013. Artificial Neural Networks-Based Backcalculation of the Structural Properties of a Typical Flexible Pavement. *Neural Computing and Applications*, Vol. 23, No. 6, pp. 1703–1710.
- Sebaaly, B. E., M. S. Mamlouk, and T. G. Davies. 1986. Dynamic Analysis of Falling Weight Deflectometer Data. *Transportation Research Record: Journal of the Transportation Research Board*, No. 1070, pp. 63–68.
- Stokoe, K. H., II, S. G. Wright, J. A. Bay, and J. M. Roesset. 1994. Characterization of Geotechnical Sites by SASW Method. Unknown journal, pp. 15–25.
- Strombom, R. D. 1987. *Maintenance of Aggregate and Earth Roads*. Washington State Transportation Center, University of Washington, Seattle, WA.

- SUDAS. 2015. Chapter 6: Geotechnical in *SUDAS Design Manual*. Iowa Statewide Urban Design and Specifications (SUDAS), Iowa State University, Ames, IA.
<https://iowasudas.org/manuals/design-manual/#chapter-6-geotechnical>.
- Tarefder, R. A. and M. U. Ahmed. 2013. Consistency and Accuracy of Selected FWD Backcalculation Software for Computing Layer Modulus of Airport Pavements. *International Journal of Geotechnical Engineering*, Vol. 7, No. 1, pp. 21–35.
- Tirado, C., K. Y. Gamez-Rios, A. Fathi, M. Mazari, and S. Nazarian. 2017. Simulation of Lightweight Deflectometer Measurements Considering Nonlinear Behavior of Geomaterials. *Transportation Research Record: Journal of the Transportation Research Board*, No. 2641, pp. 58–65.
- Uddin, W. 2000. Simulation of Falling Weight Deflectometer for In Situ Material Characterization of Highway and Airport Pavements. *Proceedings of 6th International LS-DYNA Users Conference*, April 9–11, Dearborn, MI, pp. 21–32.
- Uddin, W., A. H. Meyer, and W. R. Hudson. 1985. Rigid Bottom Considerations for Nondestructive Evaluation of Pavements. *Transportation Research Record: Journal of the Transportation Research Board*, No. 1070, pp. 21–29.
- Ullidtz, P. 1987. *Pavement Analysis: Developments in Civil Engineering*, Vol. 19. Elsevier, Amsterdam, Netherlands
- . 1998. *Modelling Flexible Pavement Response and Performance*. Polyteknisk Forlag, Lyngby, Denmark.
- Vallejo, L. E., S. Lobo-Guerrero, and K. Hammer. 2006. Degradation of a Granular Base under a Flexible Pavement: DEM Simulation. *International Journal of Geomechanics*, Vol. 6, No. 6, pp. 435–439.
- Van der Poel, C. 1951. Dynamic Testing of Road Constructions. *Journal of Applied Chemistry*, Vol. 1, No. 7, pp. 281–290.
- Vennapusa, P. K. R. and D. J. White. 2009. Comparison of Light Weight Deflectometer Measurements for Pavement Foundation Materials. *Geotechnical Testing Journal*, Vol. 32, No. 3, pp. 239–251.
- Vidale, R. F. 1964. The Dispersion of Stress Waves in Layered Media Overlaying a Half Space of Lesser Acoustic Rigidity. PhD dissertation, University of Wisconsin, Madison, WI.
- Vosoughi, P., S. Tritsch, H. Ceylan, and P. Taylor. 2017. *Lifecycle Cost Analysis of Internally Cured Jointed Plain Concrete Pavement*. National Concrete Pavement Technology Center, Iowa State University, Ames, IA.
https://intrans.iastate.edu/app/uploads/2018/07/lifecycle_cost_analysis_of_IC_JPCP_w_cv.pdf.
- Walls III, J. and M. R. Smith. 1998. *Life-Cycle Cost Analysis in Pavement Design-Interim Technical Bulletin*. Federal Highway Administration Office of Engineering, Washington, DC.
- White, D. and P. Vennapusa. 2013. *Low-Cost Rural Surface Alternatives: Literature Review and Recommendations*. National Concrete Pavement Technology Center and Center for Earthworks Engineering, Iowa State University, Ames, IA.
https://intrans.iastate.edu/app/uploads/2018/03/rural_surface_alternatives_w_cv2.pdf.
- White, D. J. and P. Vennapusa. 2014a. Rapid In Situ Measurement of Hydraulic Conductivity for Granular Pavement Foundations. *Geo-Congress 2014 Technical Papers*, February 23–26, Atlanta, GA, pp. 3005–3014.

- White, D. and P. Vennapusa. 2014b. *Optimizing Pavement Base, Subbase, and Subgrade Layers for Cost and Performance of Local Roads*. National Concrete Pavement Technology Center and Center for Earthworks Engineering, Iowa State University, Ames, IA. https://intrans.iastate.edu/app/uploads/2018/03/local_rd_pvmt_optimization_w_cvr.pdf.
- White, D. J. and P. K. R. Vennapusa. 2017. In Situ Resilient Modulus for Geogrid-Stabilized Aggregate Layer: A Case Study Using Automated Plate Load Testing. *Transportation Geotechnics*, Vol. 11, pp. 120–312.
- White, D. J., P. Vennapusa, and C. T. Jahren. 2004. *Determination of the Optimum Base Characteristics for Pavements*. Center for Transportation Research and Education, Iowa State University, Ames, IA. <https://intrans.iastate.edu/app/uploads/2018/03/tr482.pdf>.
- Wilde, W. J., S. Waalkes, and R. Harrison. 1999. *Life Cycle Cost Analysis of Portland Cement Concrete Pavements*. Center for Transportation Research, University of Texas at Austin, TX.
- Xiao, Y., E. Tutumluer, Y. Qian, and J. A. Siekmeier. 2012. Gradation Effects Influencing Mechanical Properties of Aggregate Base–Granular Subbase Materials in Minnesota. *Transportation Research Record: Journal of the Transportation Research Board*, No. 2267, pp. 14–26.
- Xu, B., S. R. Ranjithan, and Y. R. Kim. 2002a. New Condition Assessment Procedure for Asphalt Pavement Layers, Using Falling Weight Deflectometer Deflections. *Transportation Research Record: Journal of the Transportation Research Board*, No. 1806, pp. 57–69.
- . 2002b. New Relationships between Falling Weight Deflectometer Deflections and Asphalt Pavement Layer Condition Indicators. *Transportation Research Record: Journal of the Transportation Research Board*, No. 1806, pp. 48–56.
- Yusoff, N. I. M., S. Hardwiyono, N. N. Ismail, M. R. Taha, S. A. P. Rosyidi, and K. A. M. Nayan. 2015. Measurements of the Elastic Modulus of Pavement Subgrade Layers Using the SASW and FWD Test Methods. *The Baltic Journal of Road and Bridge Engineering*, Vol. 10, No. 2, pp. 174–181.
- Zeghal, M.. 2009. The Impact of Grain Crushing on Road Performance. *Geotechnical and Geological Engineering*, Vol. 27, No. 4, pp. 549.

**APPENDIX A. IMAGE LOG OF GRAVEL ROAD IN DECATUR COUNTY, IOWA—
CONSTRUCTION, MAINTENANCE, AND FIELD SURVEYING**

Equipment



Figure A.1. Subgrade elastic modulus of FWD test in May 2017



Figure A.2. Drum roller used to compact the shaped surfaces



Figure A.3. Loader

Section 1. LCF Class A



Figure A.4. First section before construction



Figure A.5. Materials dumped for the first sections



Figure A.6. Compacted surface of the first section after construction

Section 2. OFD Class A



Figure A.7. OFD Class A materials dumped on the second section



Figure A.8. Second section during the construction



Figure A.9. Wheel compacted OFD Class A materials in second section



Figure A.10. Second section during drum roller compaction

Section 3. BFL Class A



Figure A.11. BFL Class A materials on the third section



Figure A.12. Wheel compacted surface of the third section



Figure A.13. Final compacted surface of the third section

Section 4. 80% BFL Class A + 20% BFL Clean



Figure A.14. The mixture of the BFL Class A and Clean on the fourth section



Figure A.15. Compacted surface of the fourth section

Section 5. 70% BFL Class A + 30% OFD Clean



Figure A.16. Scraped surface of the fifth section before construction during drum roller compaction



Figure A.17. OFD Clean



Figure A.18. BFL Class A



Figure A.19. Compacted surface of the fifth section

Section 6. 70% BFL Class A + 30% LCF Clean



Figure A.20. LCF Clean



Figure A.21. BFL Class A and LCF Clean mixture



Figure A.22. 70% BFL Class A + 30% LCF Clean under compaction

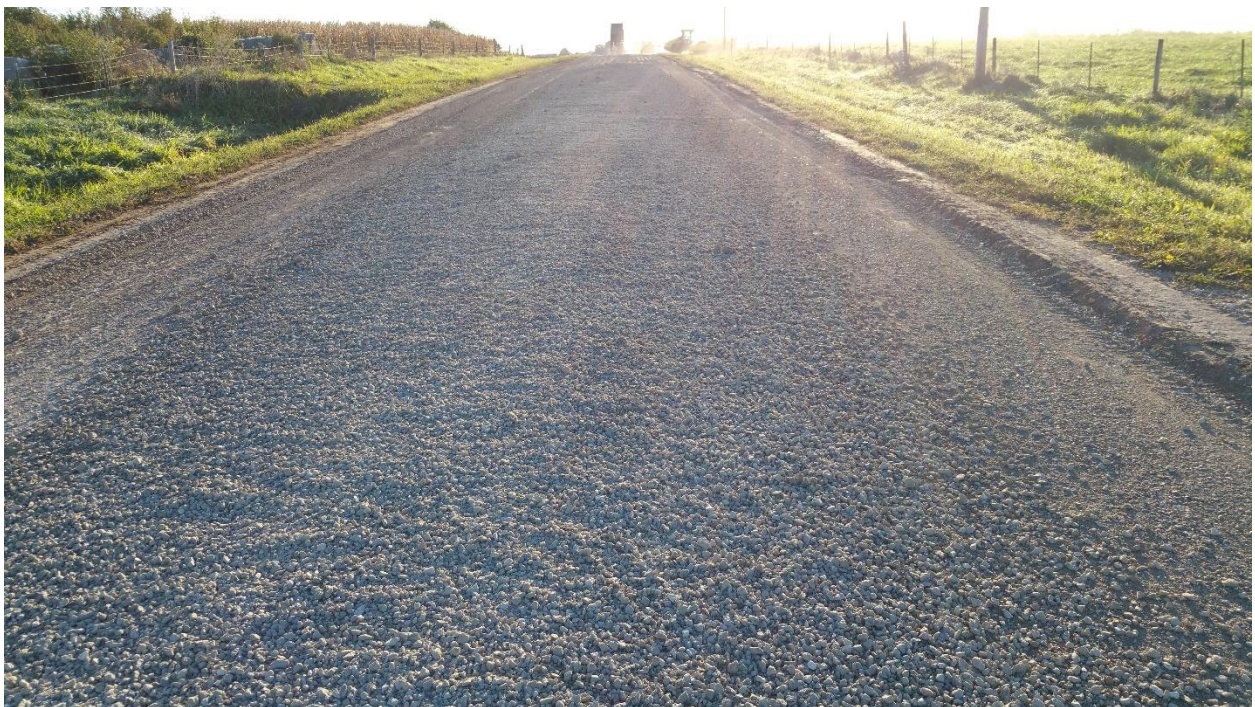


Figure A.23. Wheel compacted surface of 70% BFL Class A + 30% LCF Clean



Figure A.24. Prepared surface of 70% BFL Class A + 30% LCF Clean

Section 7. 70% BFL Class A + 30% CRG Clean



Figure A.25. Round shape CRG Clean materials



Figure A.26. CRG Clean materials on the surface



Figure A.27. Compacted surface of 70% BFL Class A + 30% CRG Clean



Figure A.28. Shaped and compacted surface of 70% BFL Class A + 30% CRG Clean

Image Log of Gravel Road in Decatur County, Iowa–December 2016



Figure A.29. LCF Class A



Figure A.30. OFD Class A



Figure A.31. BFL Class A



Figure A.32. 80% BFL Class A + 20% BFL Clean



Figure A.33. 70% BFL Class A + 30% OFD Clean



Figure A.34. 70% BFL Class A + LCF Class A



Figure A.35. 70% BFL Class A + CRG Clean

Image Log of Gravel Road in Decatur County, Iowa–February 2017



Figure A.36. LCF Class A



Figure A.37. OFD Class A



Figure A.38. BFL Class A



Figure A.39. 80% BFL Class A + 20% BFL Clean



Figure A.40. 70% BFL Class A + 30% OFD Clean



Figure A.41. 70% BFL Class A + 30% LCF Clean



Figure A.42. 70% BFL Class A + 30% CRG Clean

Image Log of Gravel Road in Decatur County, Iowa–August 2017



Figure A.43. LCF Class A



Figure A.44. OFD Class A



Figure A.45. BFL Class A



Figure A.46. 80% BFL Class A + 20% BFL Clean



Figure A.47. 70% BFL Class A + 30% OFD Clean



Figure A.48. 70% BFL Class A + 30% LCF Clean



Figure A.49. 70% BFL Class A + 30% CRG Clean

Image Log of Gravel Road in Decatur County, Iowa–January 2018



Figure A.50. LCF Class A



Figure A.51. OFD Class A



Figure A.52. BFL Class A



Figure A.53. 80% BFL Class A + 20% BFL Clean



Figure A.54. 70% BFL Class A + 30% OFD Clean



Figure A.55. 70% BFL Class A + 30% LCF Clean



Figure A.56. 70% BFL Class A + 30% CRG Clean

Image Log of Gravel Road in Decatur County, Iowa–February 2018



Figure A.57. LCF Class A



Figure A.58. OFD Class A



Figure A.59. BFL Class A



Figure A.60. 80% BFL Class A + 20% BFL Clean



Figure A.61. 70% BFL Class A + 30% OFD Clean



Figure A.62. 70% BFL Class A + 30% LCF Clean



Figure A.63. 70% BFL Class A + 30% CRG Clean

Image Log of Gravel Road in Decatur County, Iowa–April 2018



Figure A.64. LCF Class A



Figure A.65. OFD Class A



Figure A.66. BFL Class A



Figure A.67. 80% BFL Class A + 20% BFL Clean



Figure A.68. 70% BFL Class A + 30% OFD Clean



Figure A.69. 70% BFL Class A + 30% LCF Clean



Figure A.70. 70% BFL Class A + 30% CRG Clean

Image Log of Gravel Road in Decatur County, Iowa–May 2018



Figure A.71. LCF Class A



Figure A.72. OFD Class A



Figure A.73. BFL Class A



Figure A.74. 80% BFL Class A + 20% BFL Clean



Figure A.75. 70% BFL Class A + 30% OFD Clean



Figure A.76. 70% BFL Class A + 30% LCF Clean



Figure A.77. 70% BFL Class A + 30% CRG Clean

Image Log of Gravel Road in Decatur County, Iowa–April 2019



Figure A.78. LCF Class A



Figure A.79. OFD Class A



Figure A.80. BFL Class A



Figure A.81. 80% BFL Class A + 20% BFL Clean



Figure A.82. 70% BFL Class A + 30% OFD Clean



Figure A.83. 70% BFL Class A + 30% LCF Clean



Figure A.84. 70% BFL Class A + 30% CRG Clean

APPENDIX B. PARTICLE-SIZE ANALYSIS RESULTS

LCF Class A

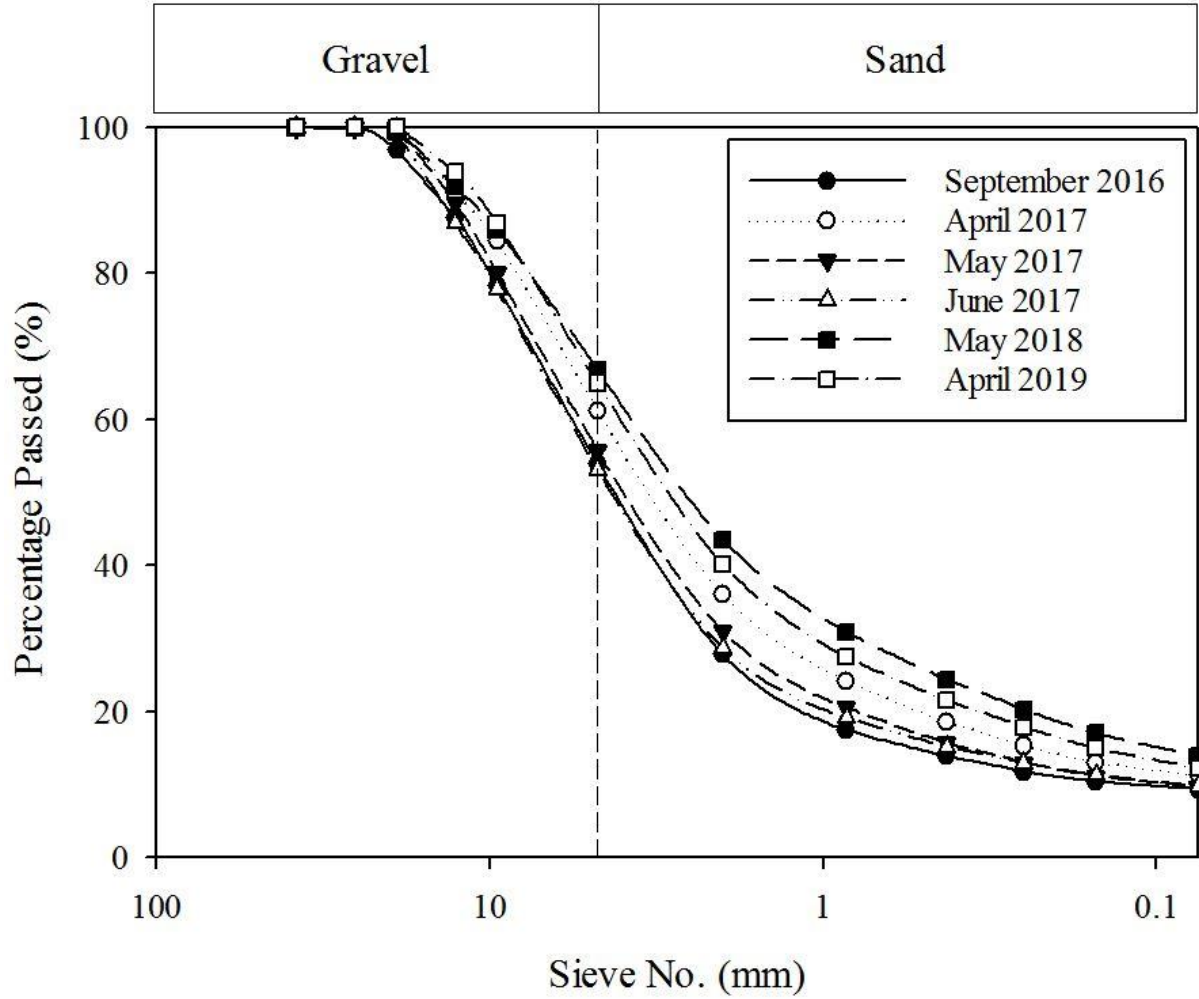


Figure B.1. Particle-size distributions of the first section over time

OFD Class A

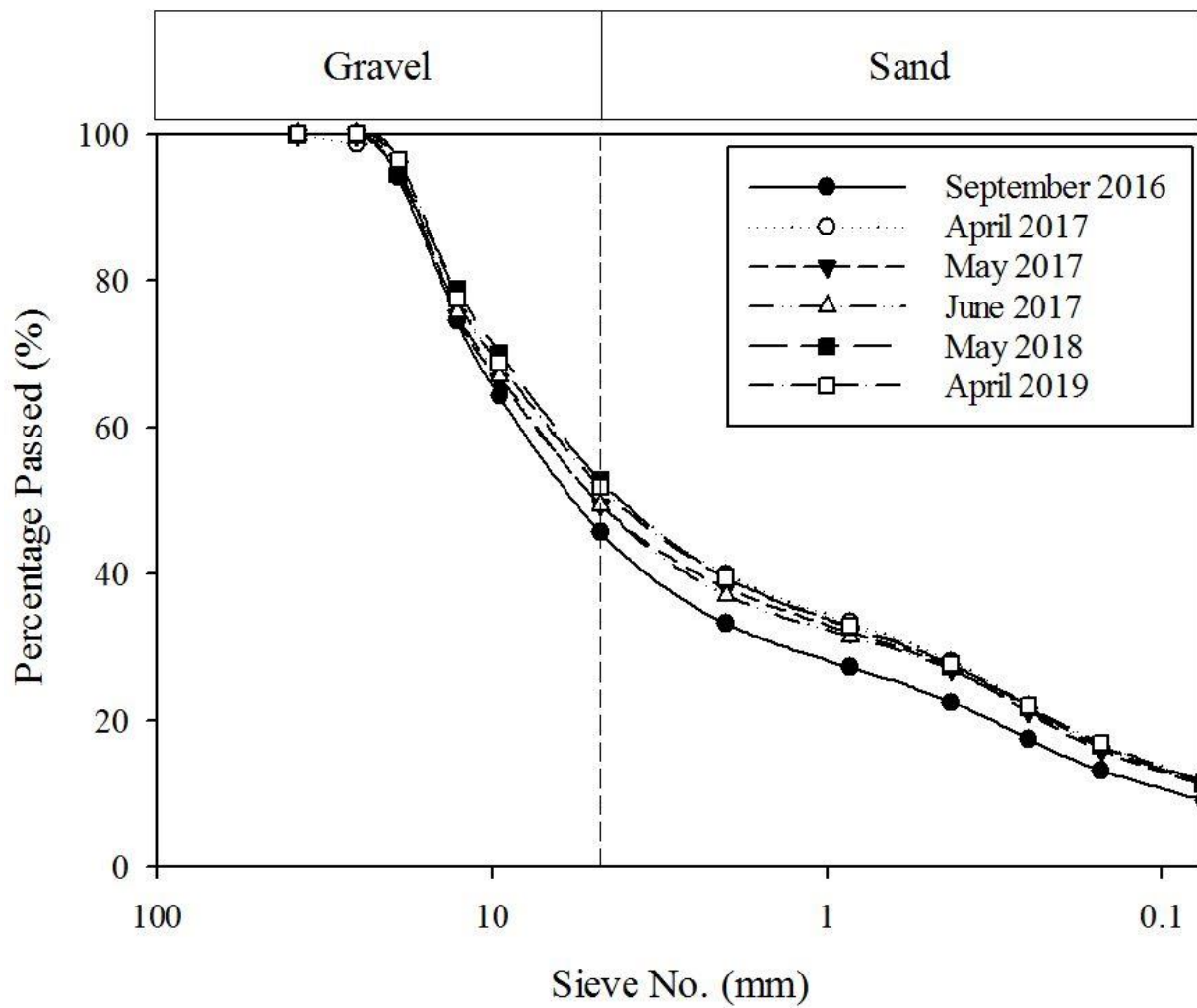


Figure B.2. Particle-size distributions of the second section over time

BFL Class A

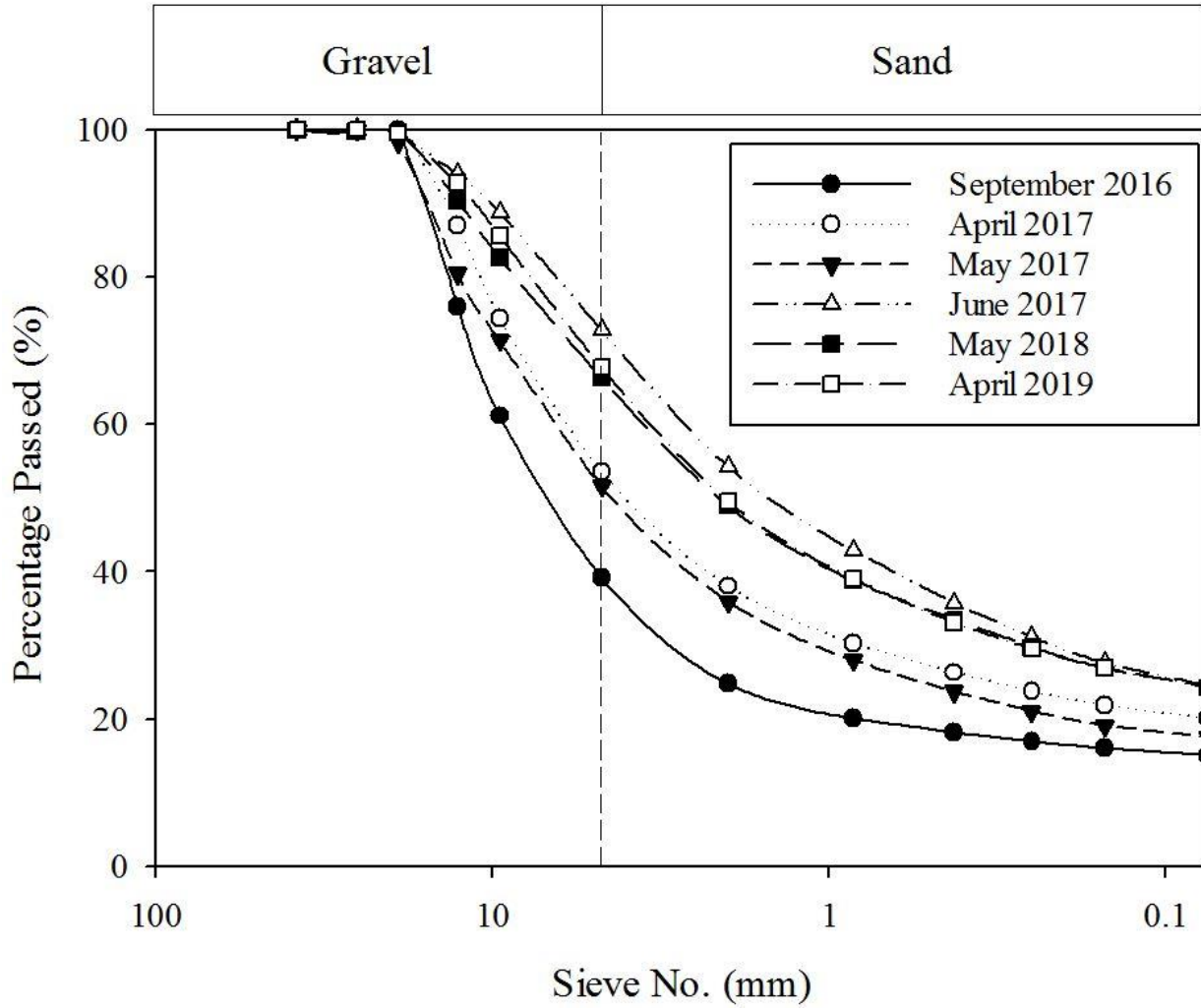


Figure B.3. Particle-size distributions of the third section over time

80% BFL Class A + 20% BFL Clean

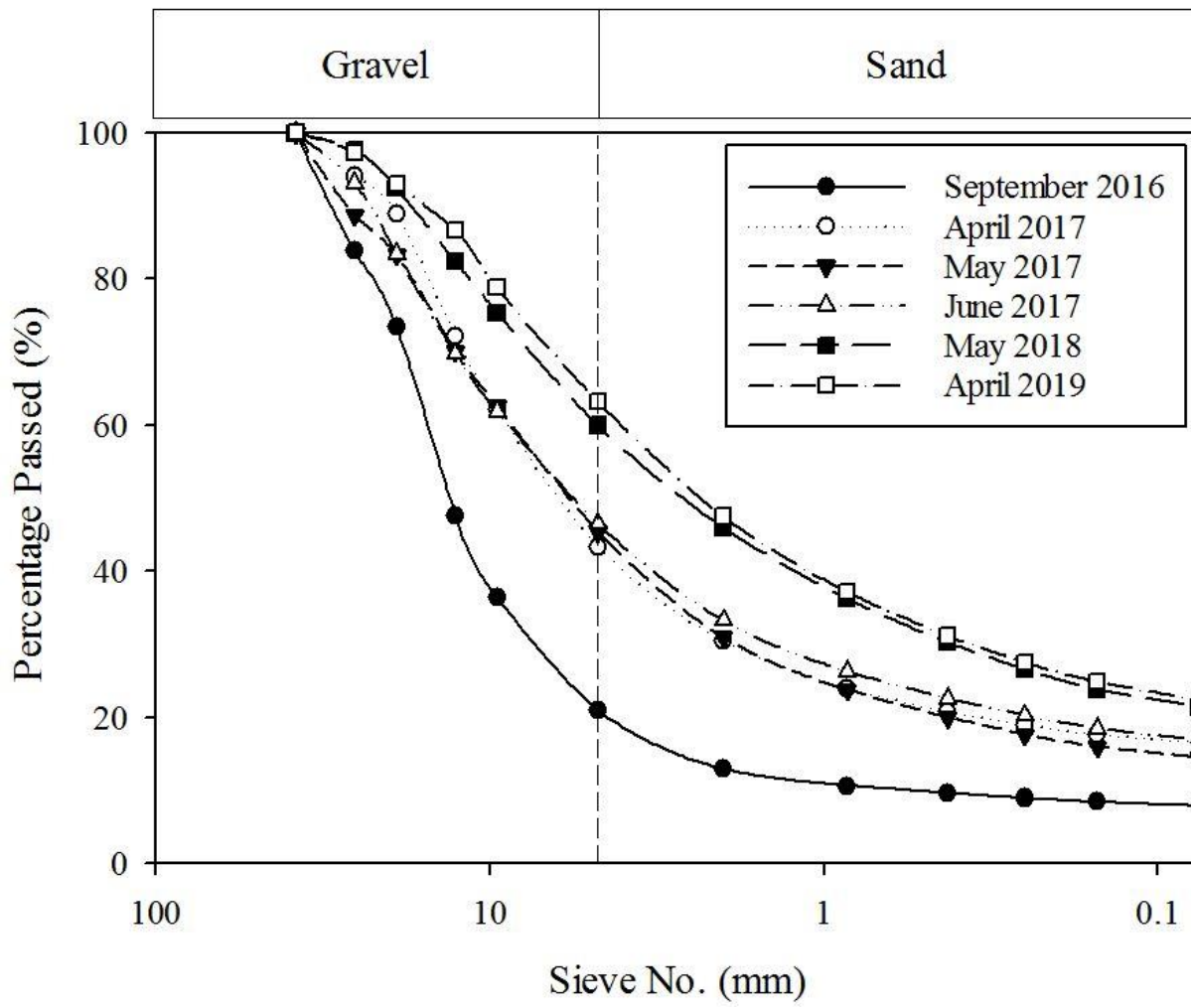


Figure B.4. Particle-size distributions of the fourth section over time

70% BFL Class A + 30% OFD Clean

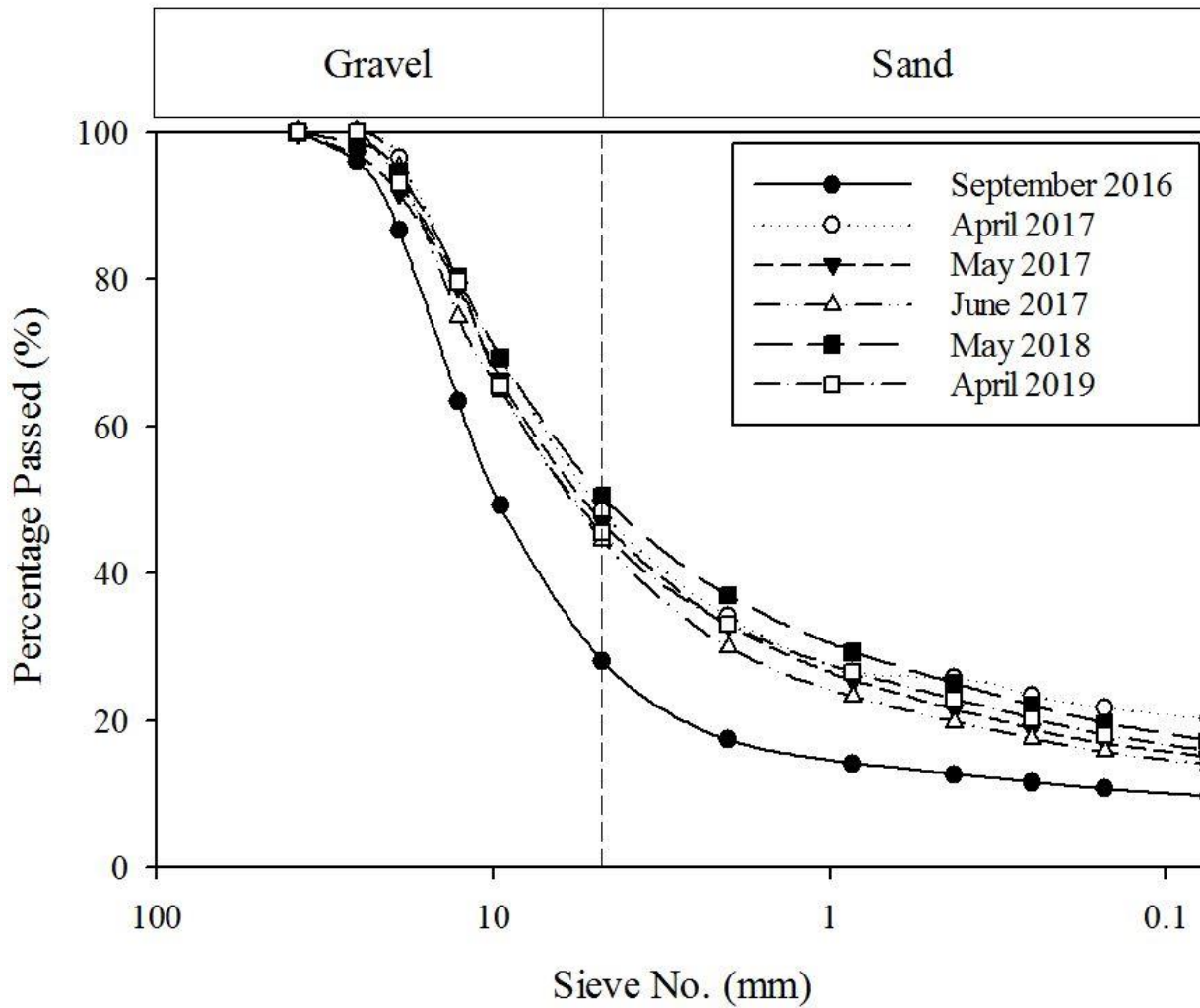


Figure B.5. Particle-size distributions of the fifth section over time

70% BFL Class A + 30% LCF Clean

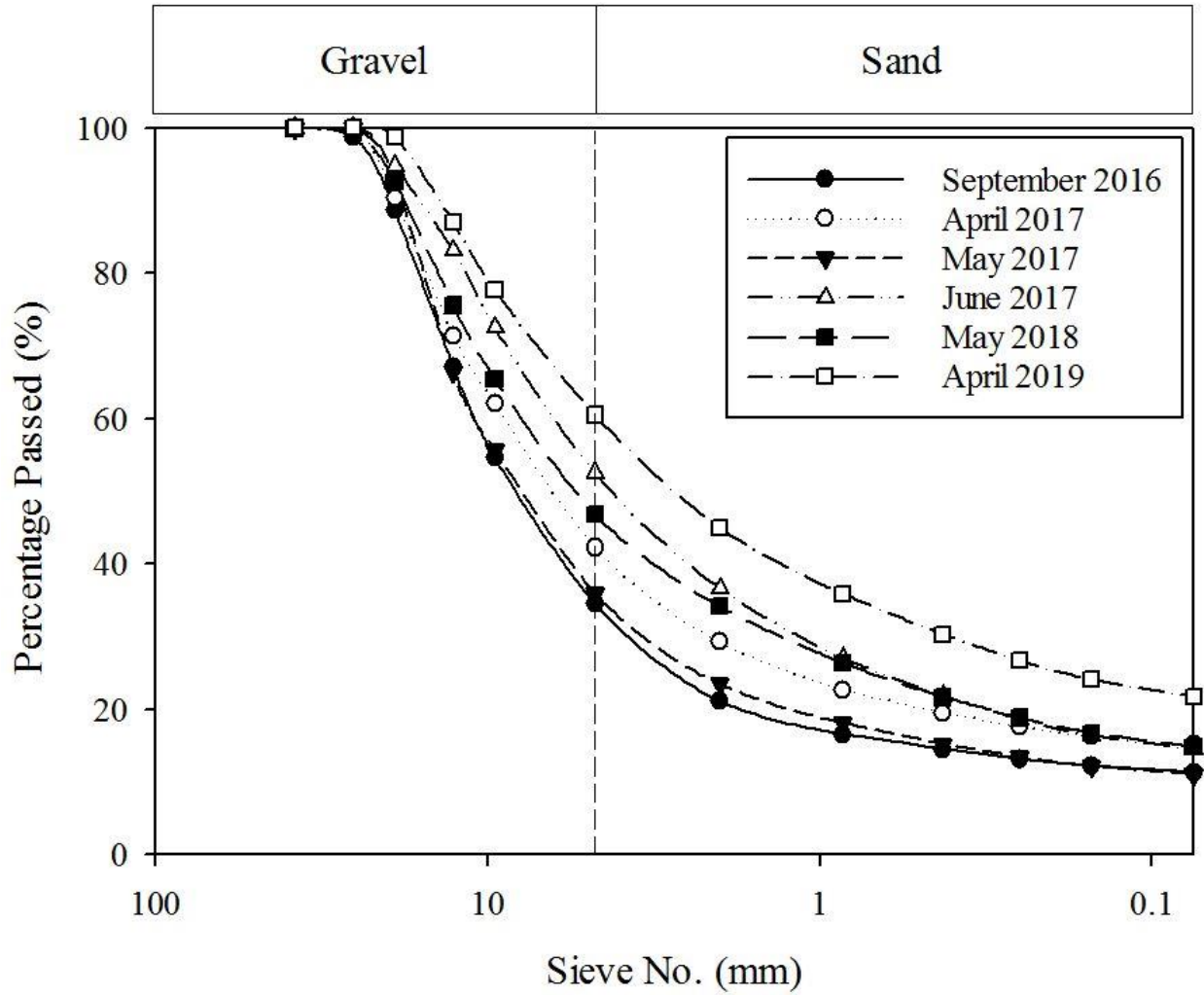


Figure B.6. Particle-size distributions of the sixth section over time

70% BFL Class A + 30% CRG Clean

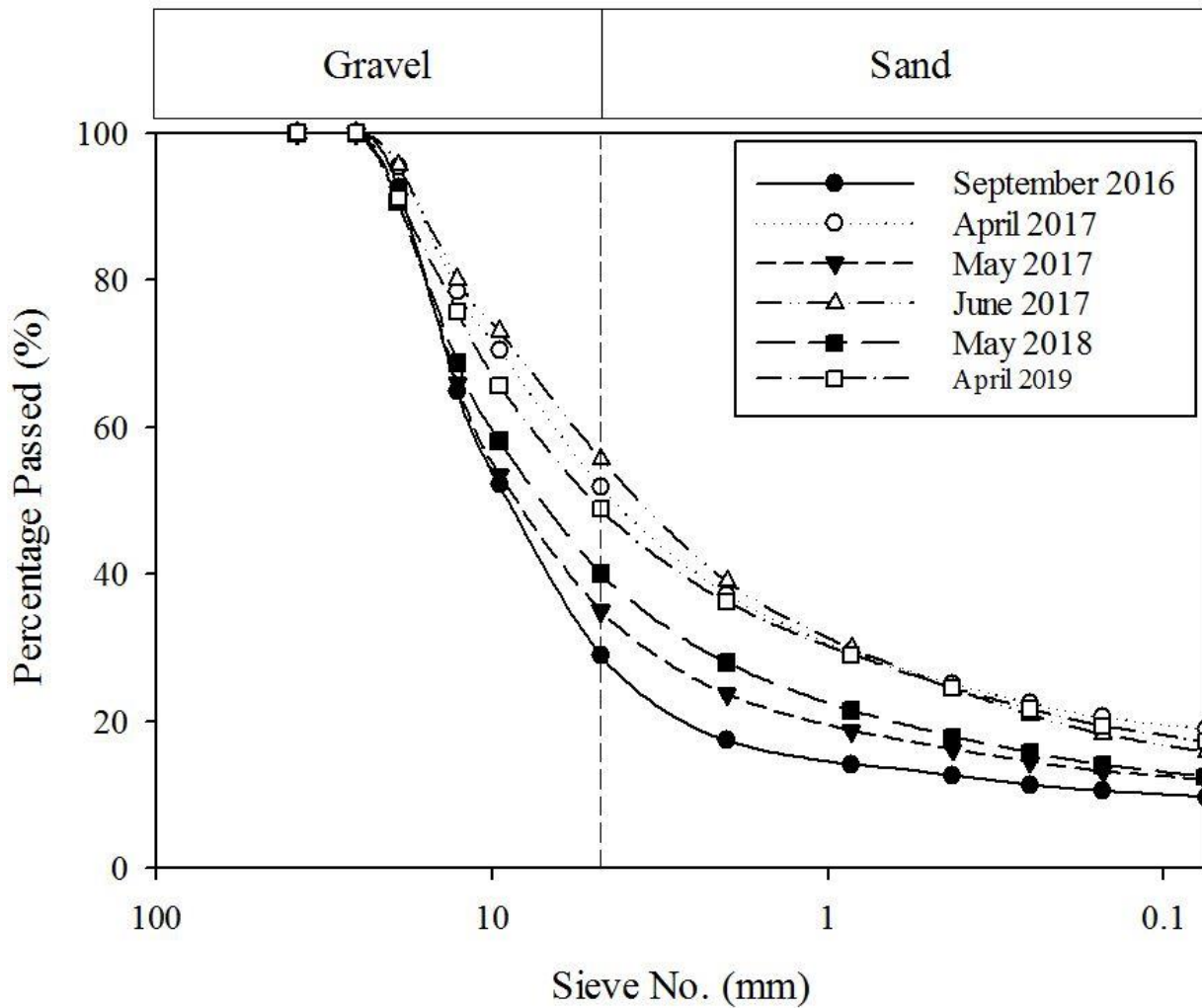


Figure B.7. Particle-size distributions of the seventh section over time

Table B.1. Percentage of change in fines content (%)

Sections	Apr 2017	May 2017	Jun 2017	Apr 2018	May 2018	Apr 2019
LCF Class A	21	3	4	14	49	31
OFD Class A	29	23	23	10	24	27
BFL Class A	33	16	62	47	61	61
80% BFL Class A + 20% BFL Clean	109	83	113	124	170	183
70% BFL Class A + 30% OFD Clean	109	56	44	80	79	64
70% BFL Class A + 30% LCF Clean	33	-3	28	64	30	91
70% BFL Class A + 30% CRG Clean	95	24	62	105	28	78

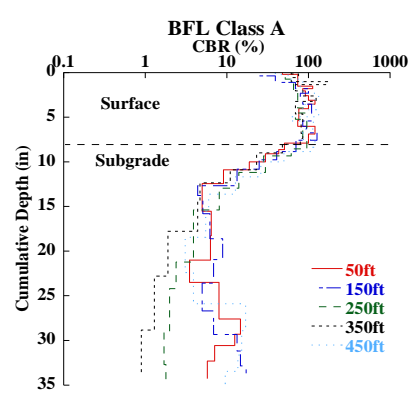
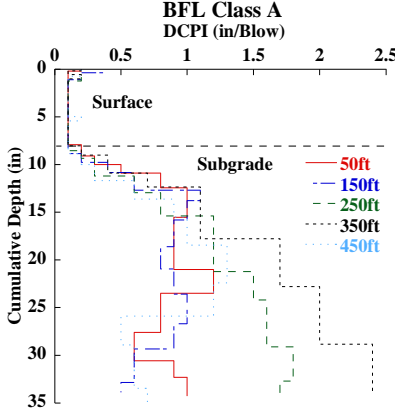
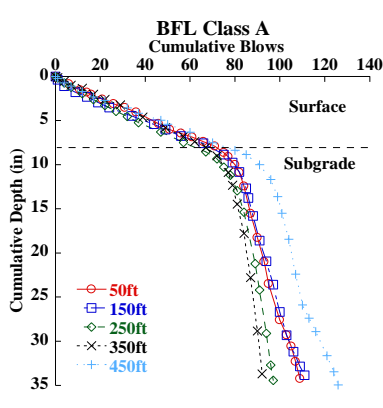
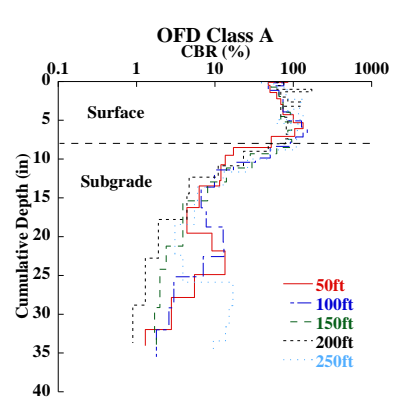
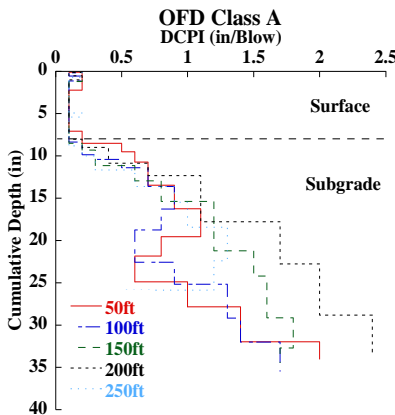
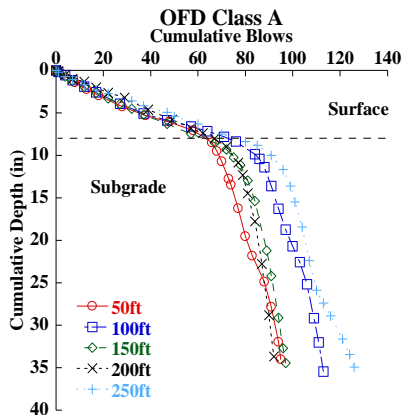
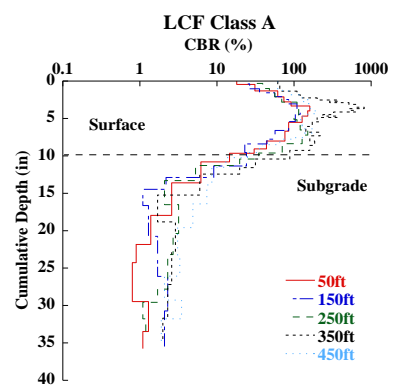
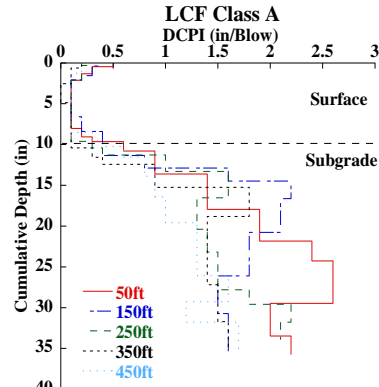
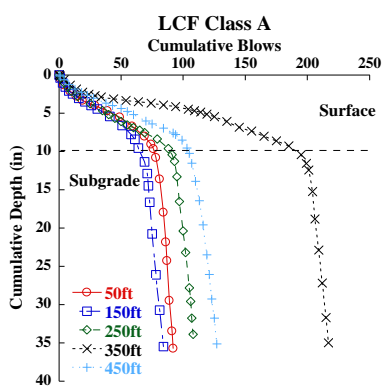
Table B.2. Percentage of change in gravel-to-sand ratio (%)

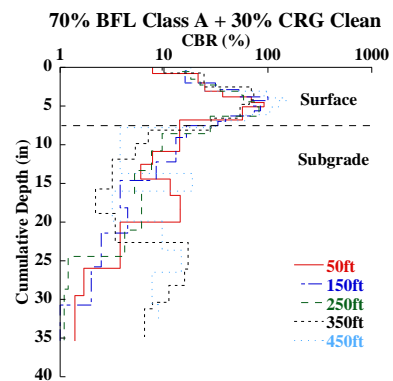
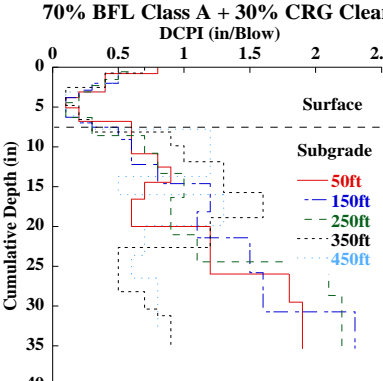
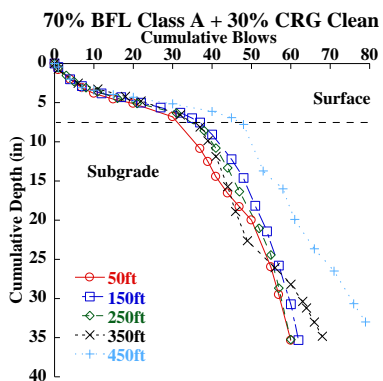
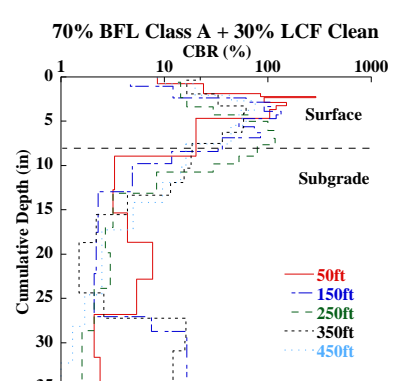
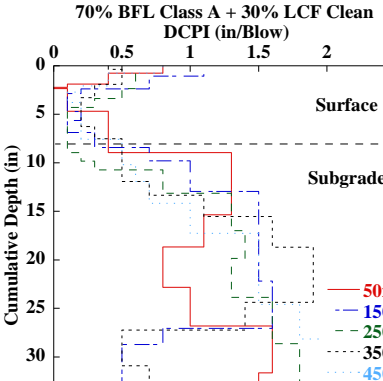
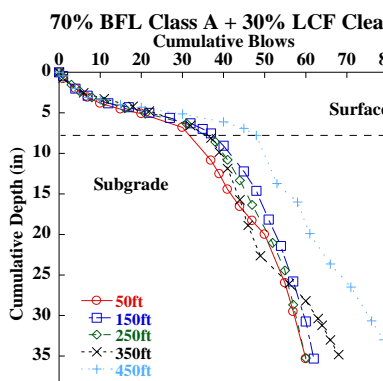
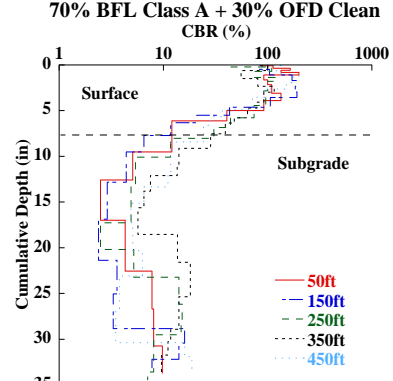
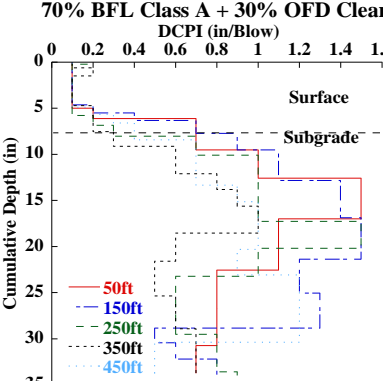
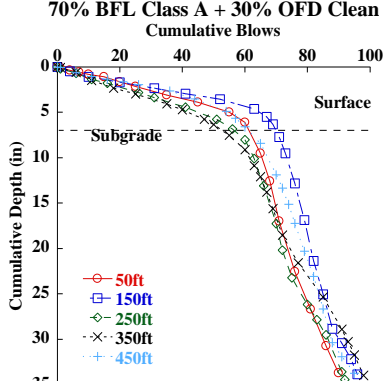
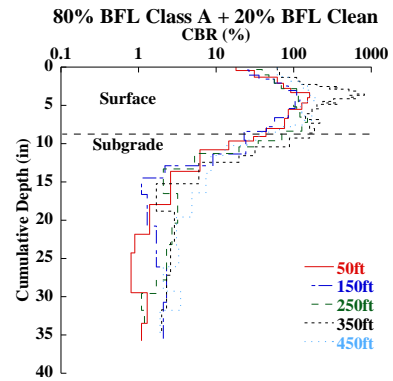
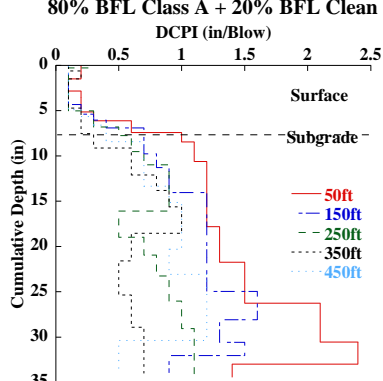
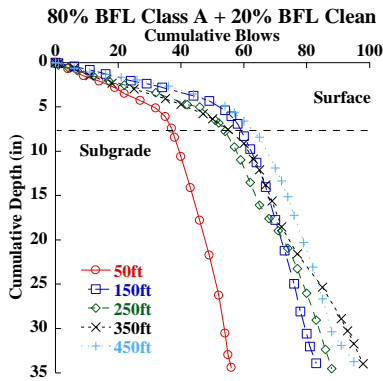
Sections	Apr 2017	May 2017	Jun 2017	Apr 2018	May 2018	Apr 2019
LCF Class A	-24	-7	5	-11	-39	-36
OFD Class A	-21	-11	-11	-19	-23	-19
BFL Class A	-45	-44	-78	-62	-68	-71
80% BFL Class A + 20% BFL Clean	-65	-71	-70	-82	-83	-85
70% BFL Class A + 30% OFD Clean	-53	-58	-54	-63	-62	-53
70% BFL Class A + 30% LCF Clean	-25	-9	-56	-55	-41	-64
70% BFL Class A + 30% CRG Clean	-61	-24	-70	-68	-41	-56

Table B.3. Percentage of change in breakage potential (%)

Sections	Apr 2017	May 2017	Jun 2017	Apr 2018	May 2018	Apr 2019
LCF Class A	-8	-3	-1	-6	-15	-13
OFD Class A	-8	-6	-5	-5	-8	-8
BFL Class A	-15	-10	-31	-21	-26	-27
80% BFL Class A + 20% BFL Clean	-21	-20	-22	-30	-35	-37
70% BFL Class A + 30% OFD Clean	-20	-16	-14	-21	-20	-17
70% BFL Class A + 30% LCF Clean	-8	-2	-16	-20	-13	-26
70% BFL Class A + 30% CRG Clean	-20	-5	-21	-26	-9	-18

APPENDIX C. DCP TEST RESULTS





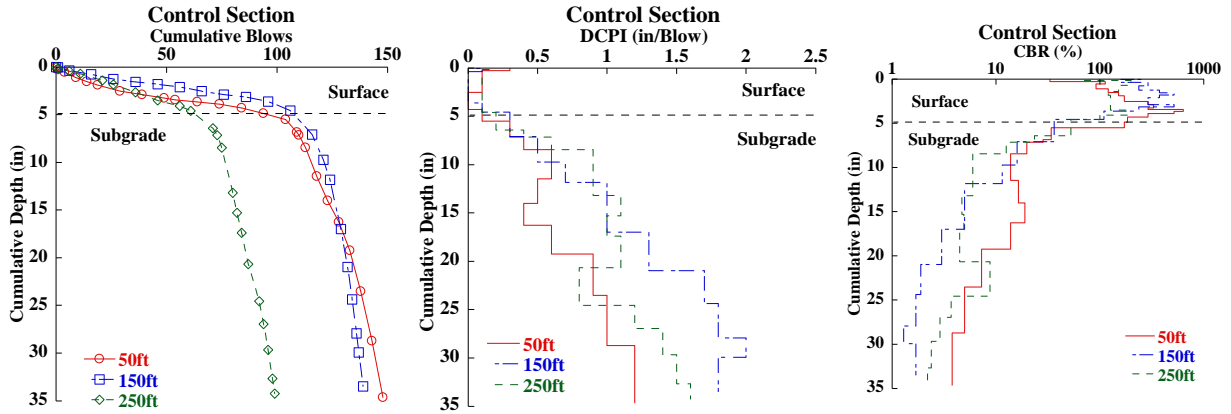
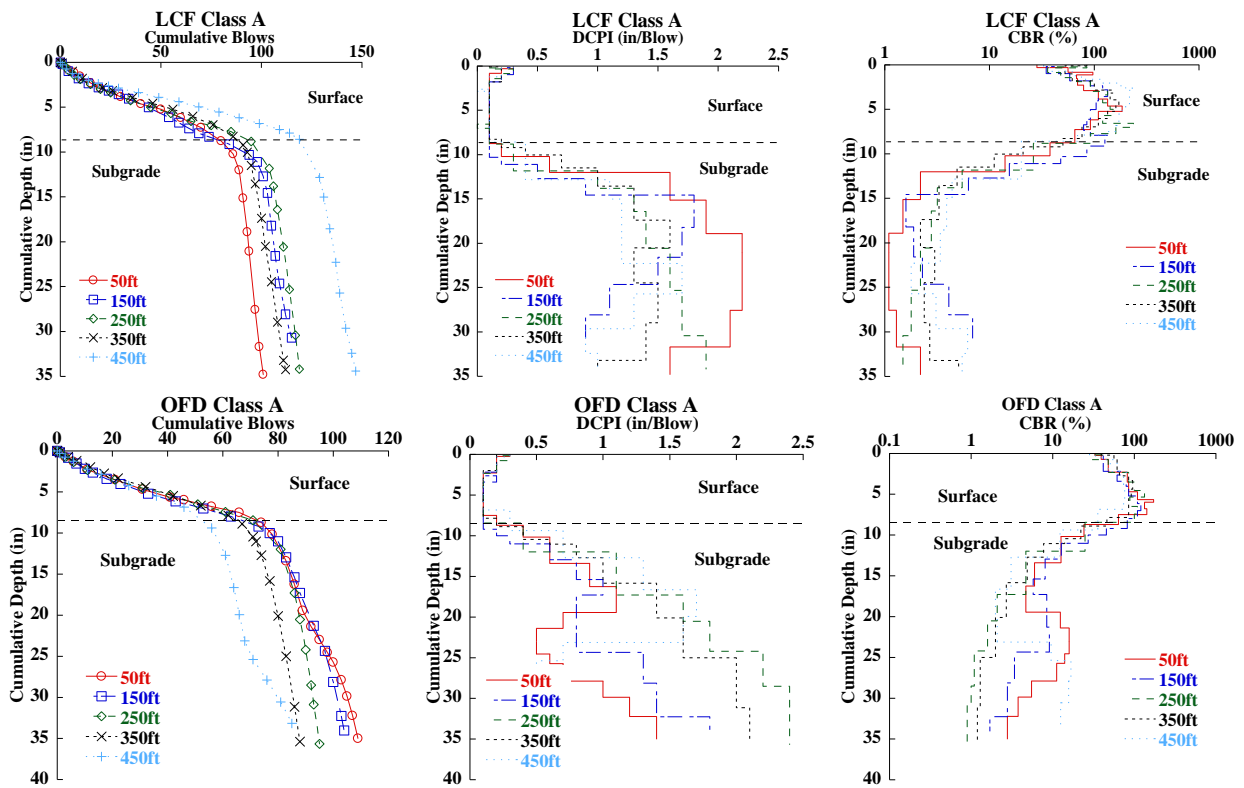
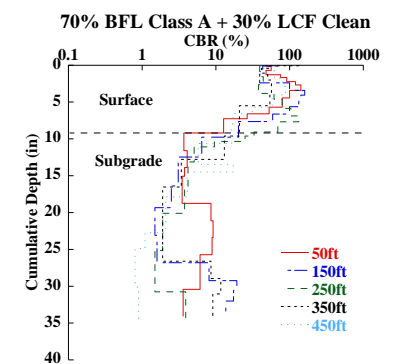
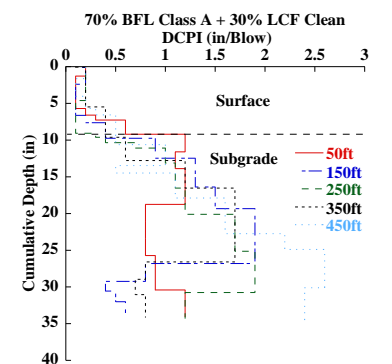
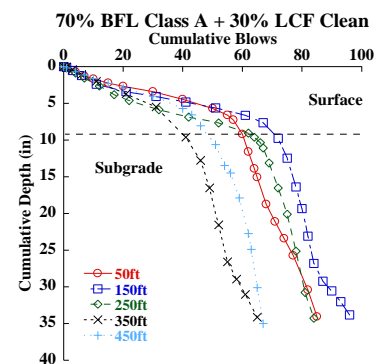
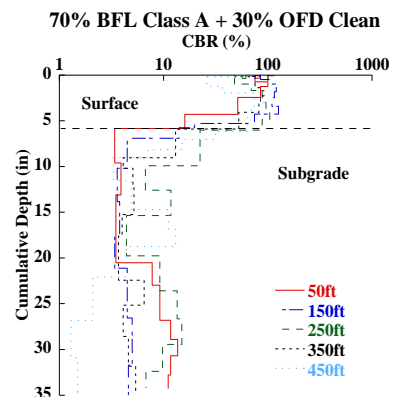
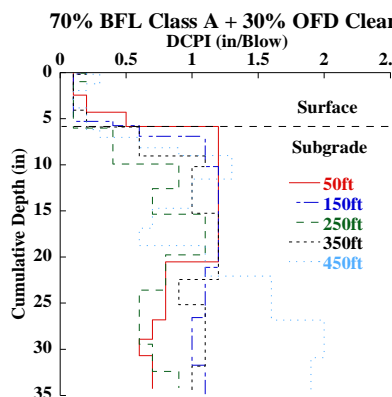
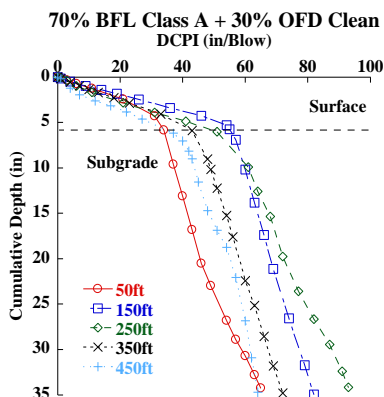
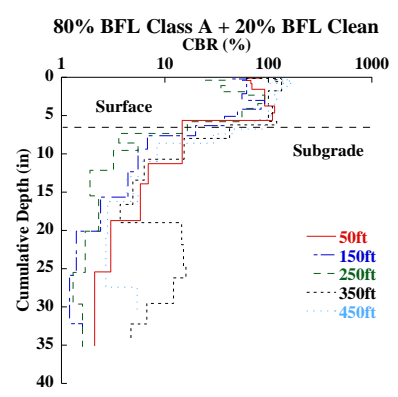
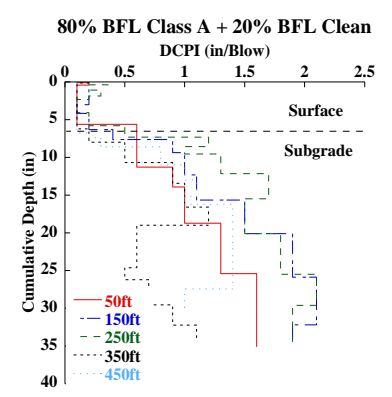
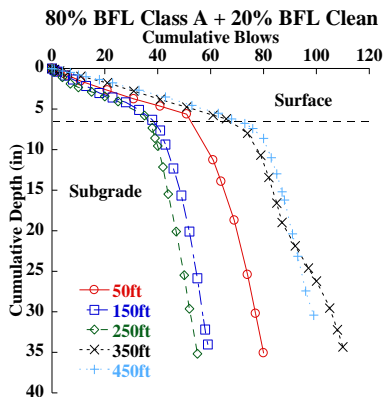
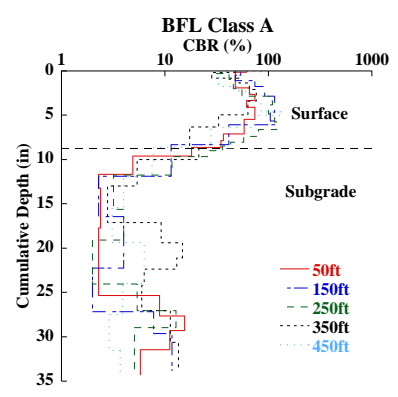
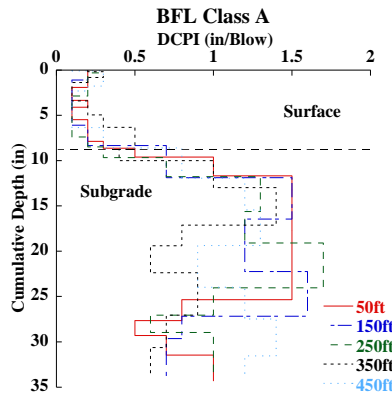
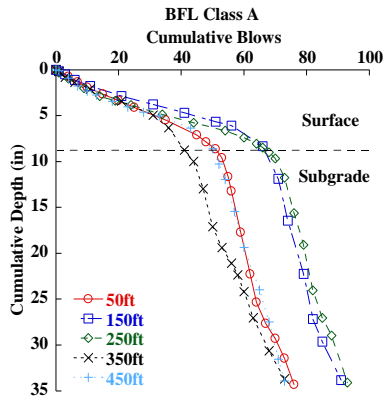


Figure C.1. DCP results for changes in the blows, DCPI, and DCP-CBR with cumulative depth for October 2016





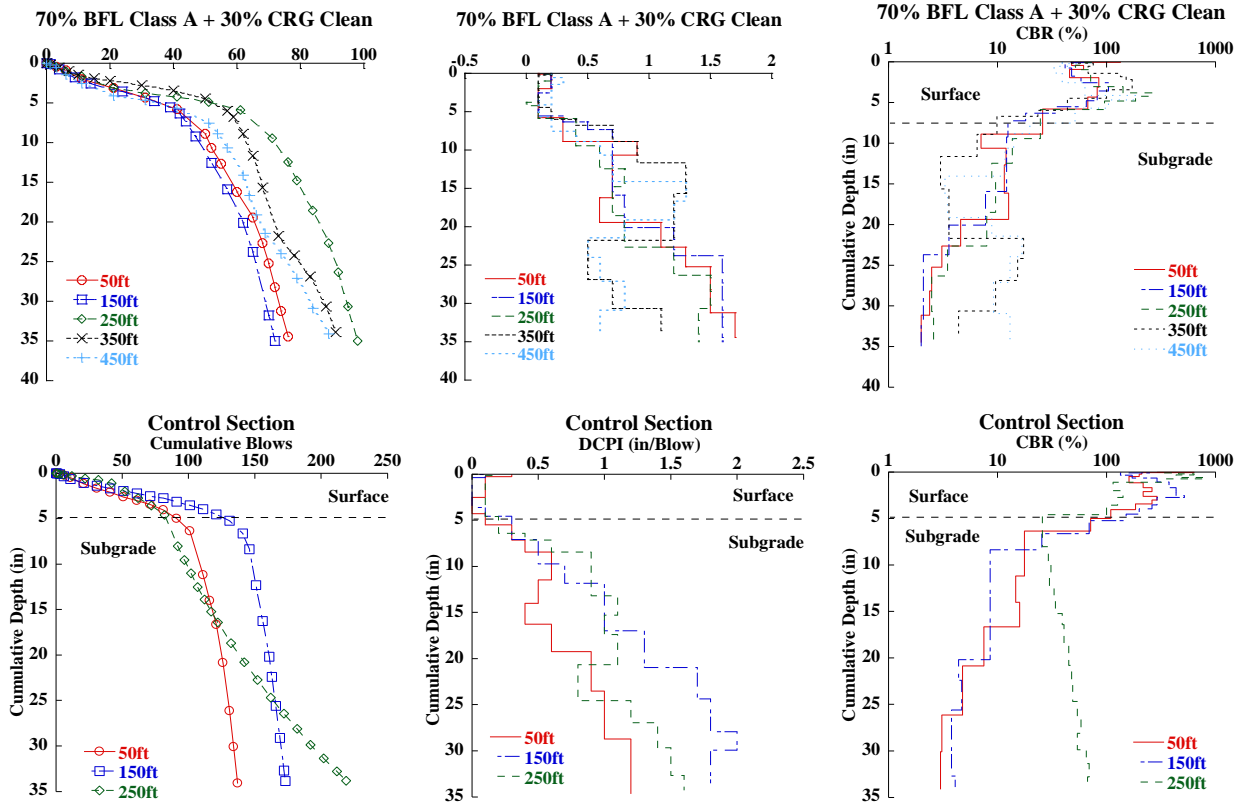
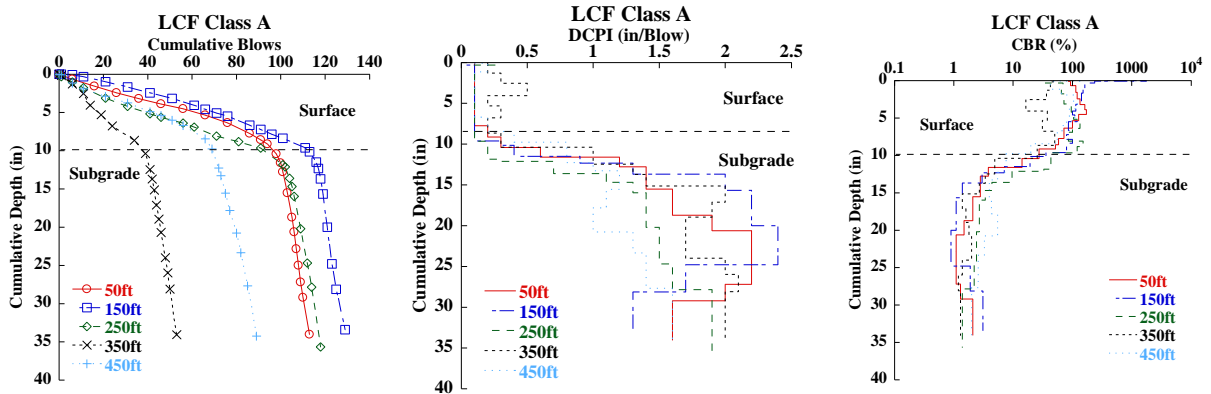
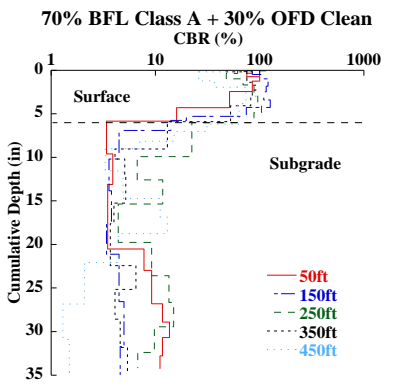
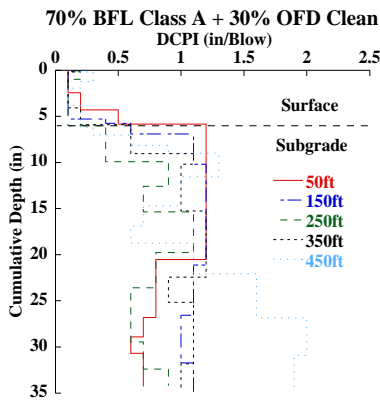
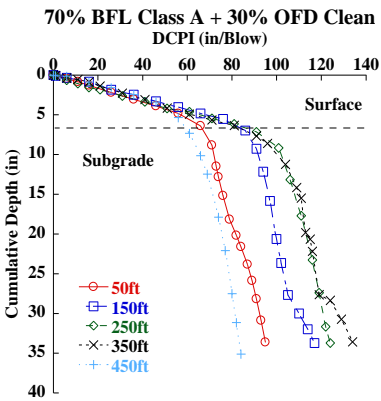
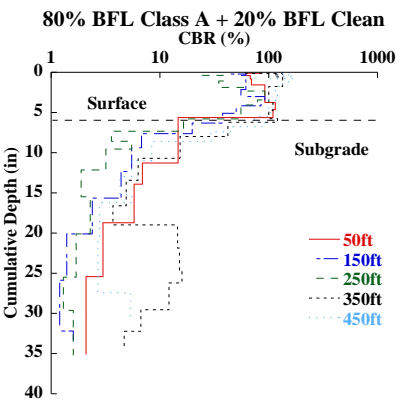
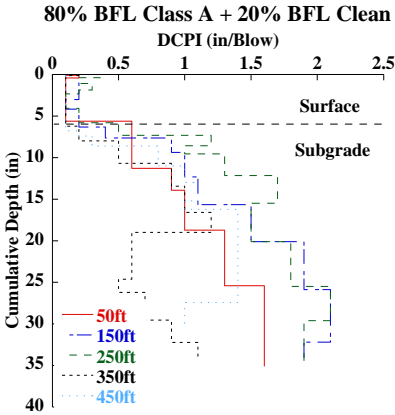
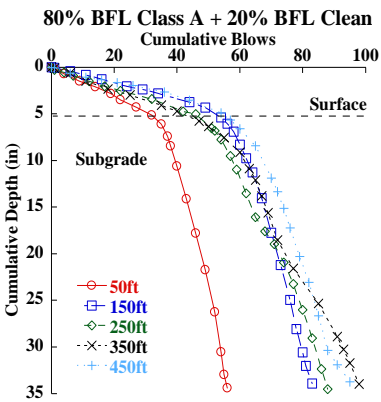
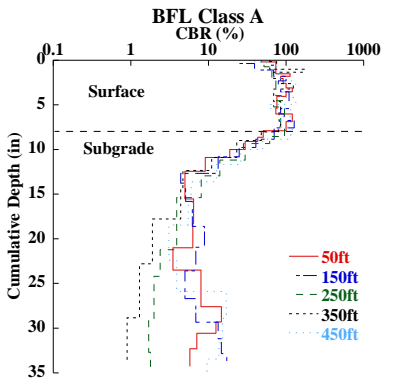
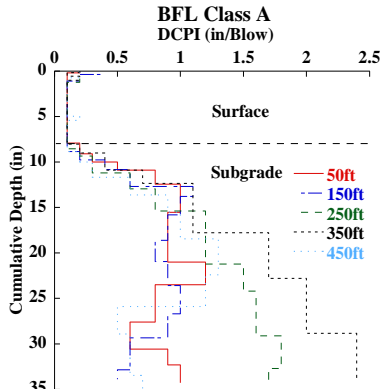
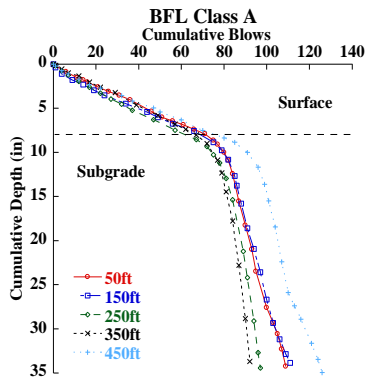
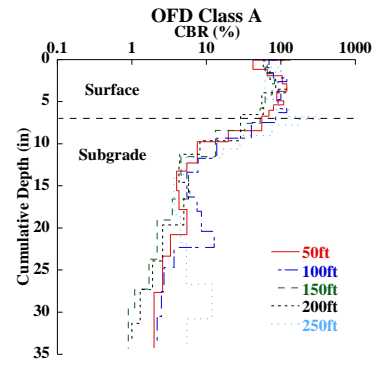
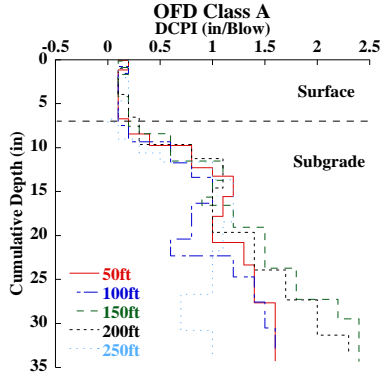
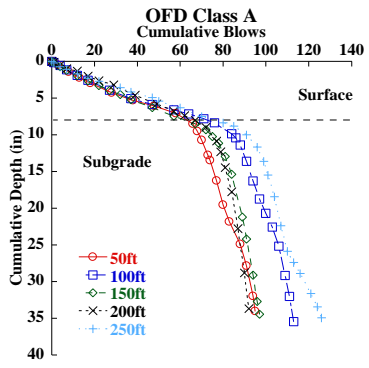


Figure C.2. DCP results for changes in the blows, DCPI, and DCP-CBR with cumulative depth for November 2016





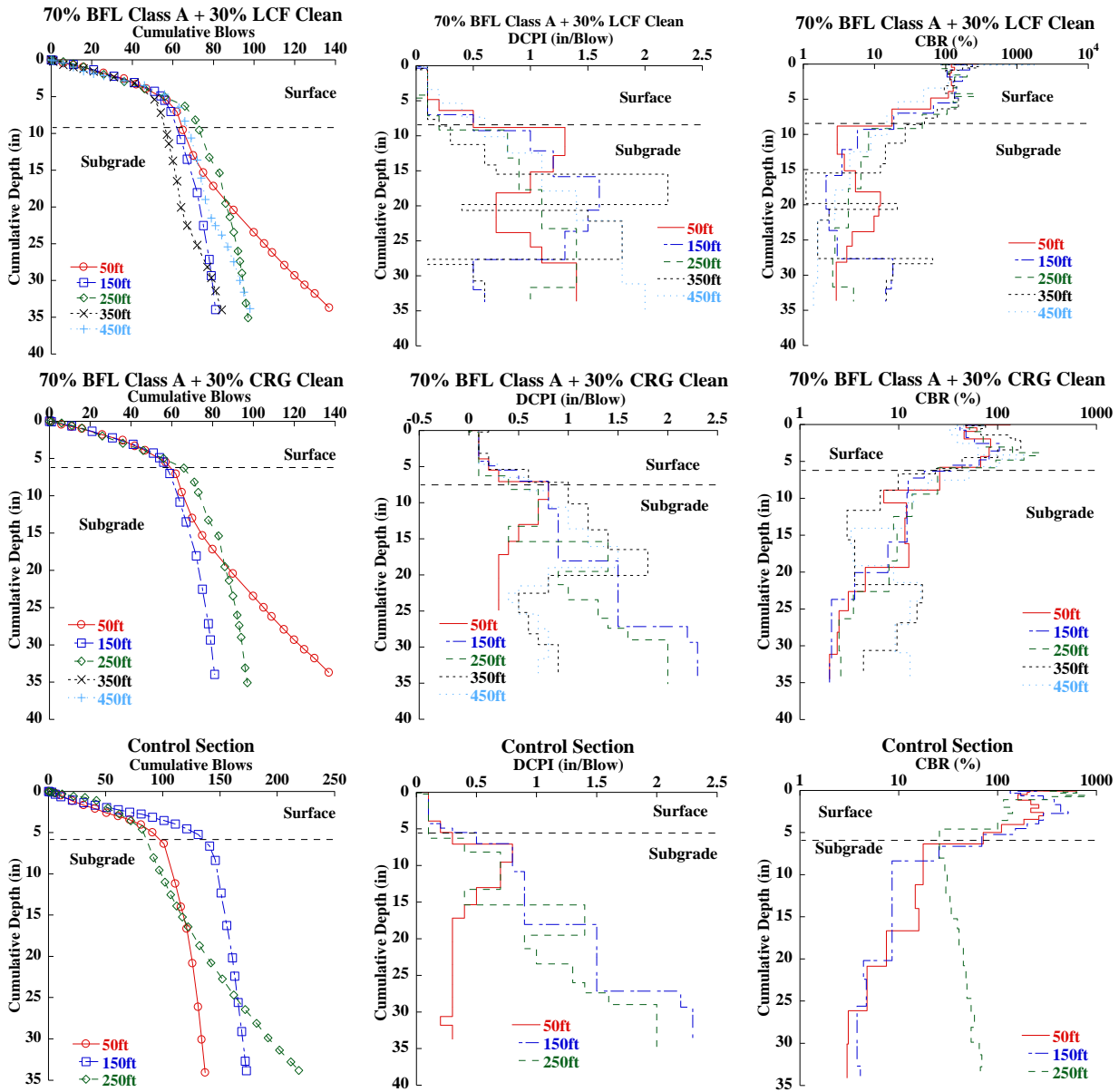
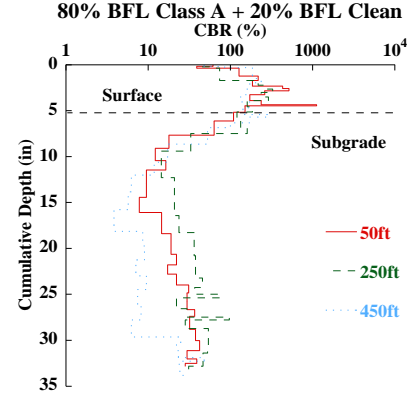
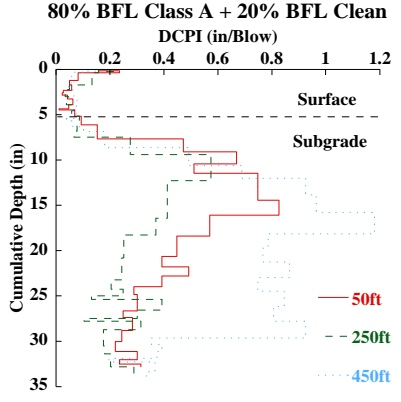
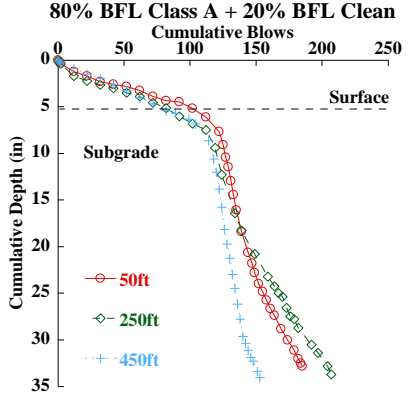
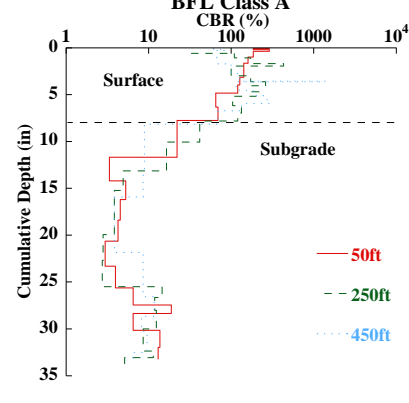
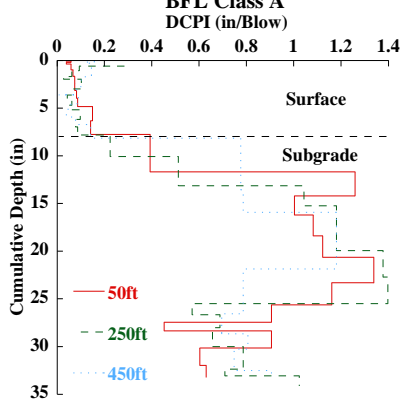
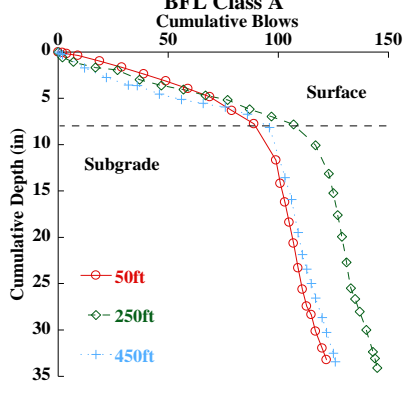
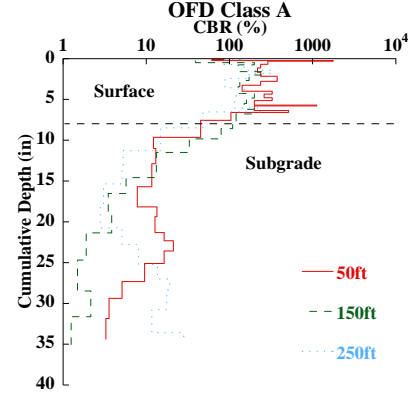
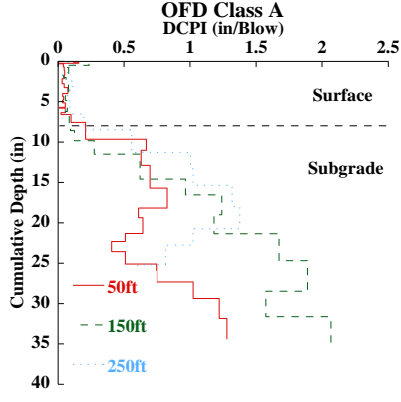
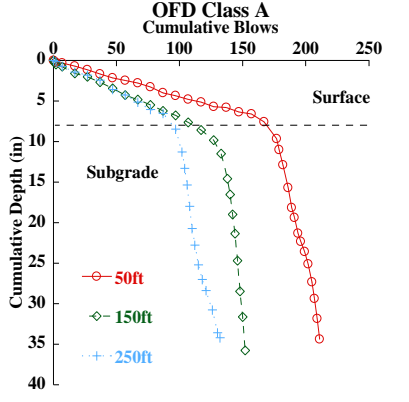
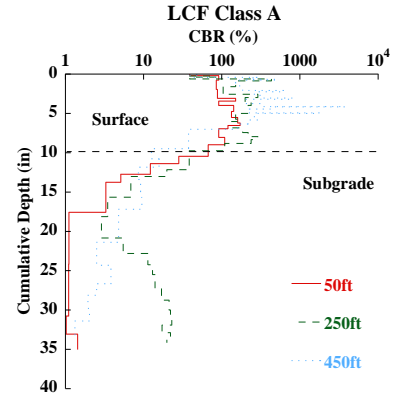
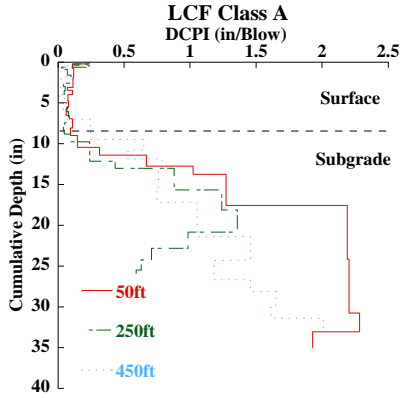
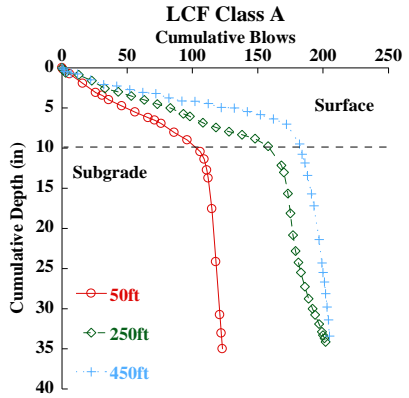


Figure C.3. DCP results for changes in the blows, DCPI, and DCP-CBR with cumulative depth for April 2017



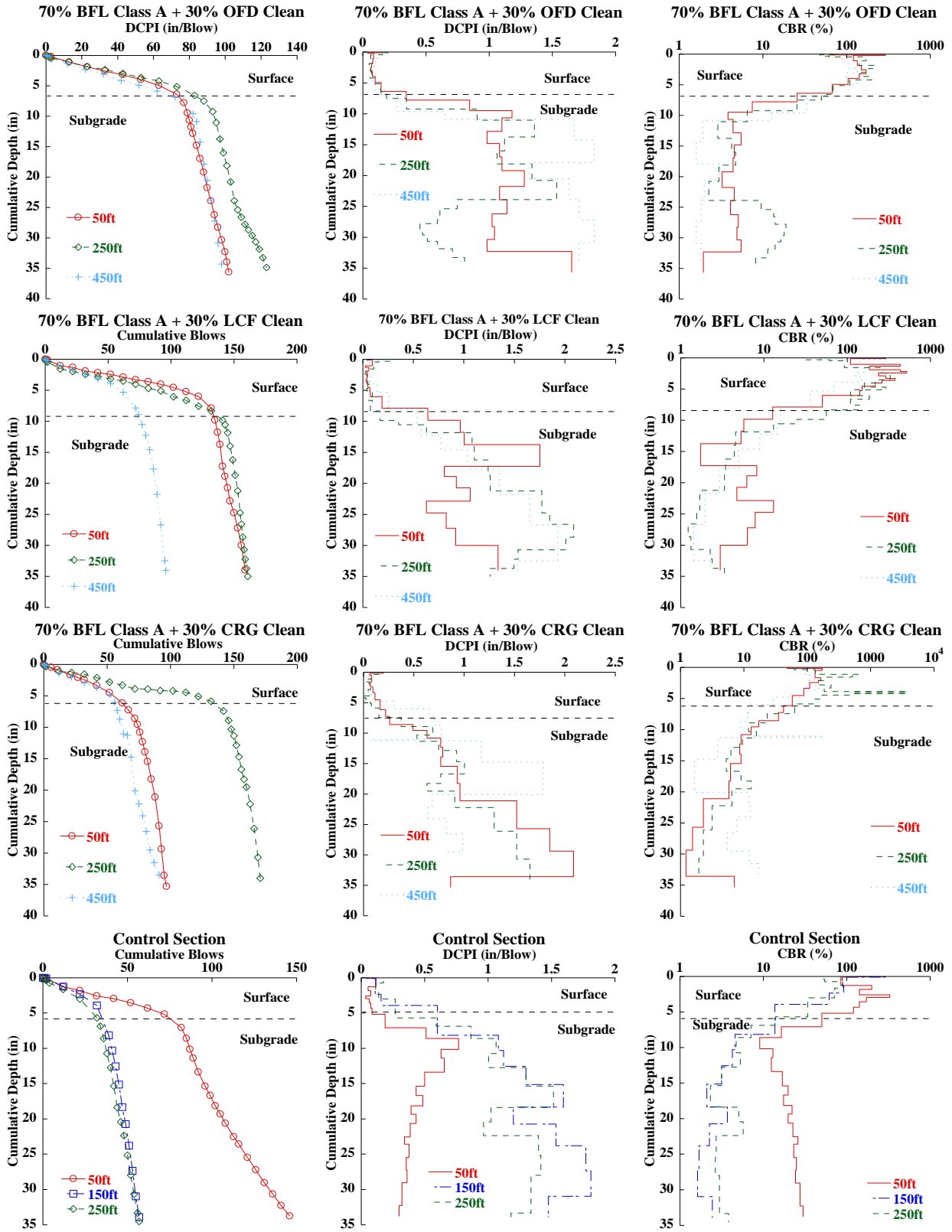
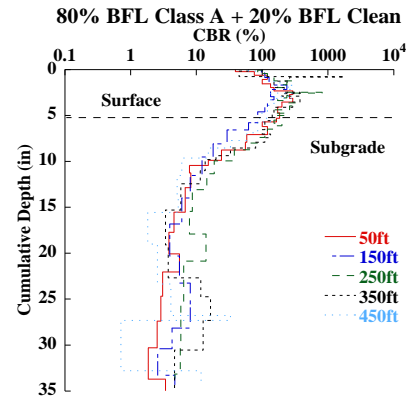
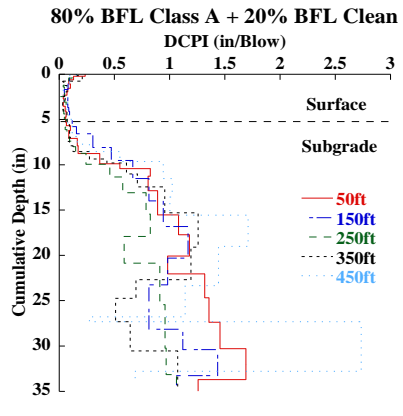
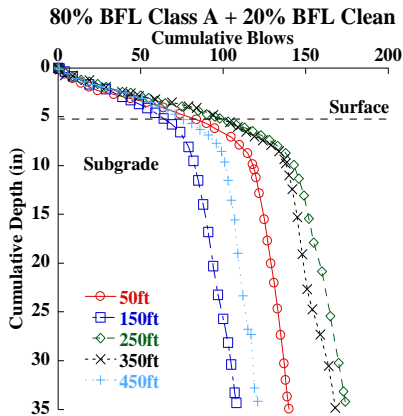
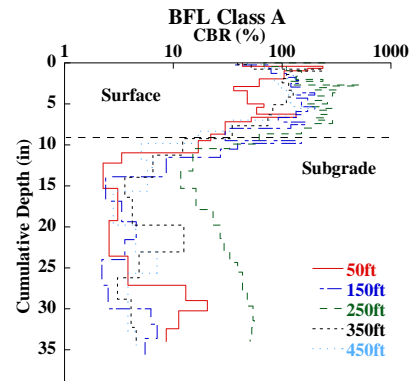
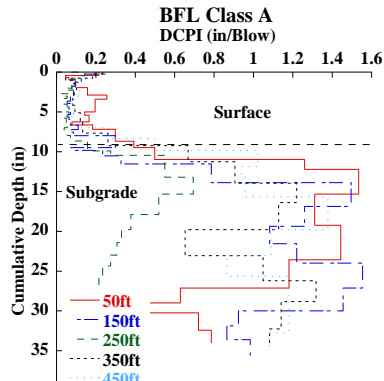
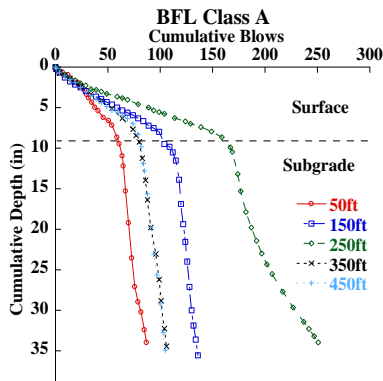
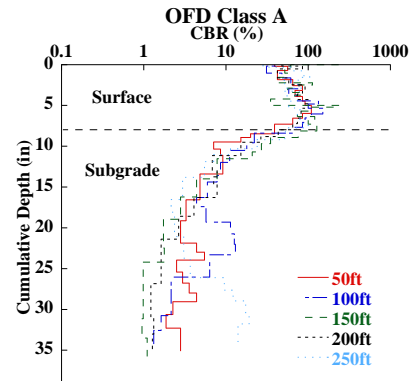
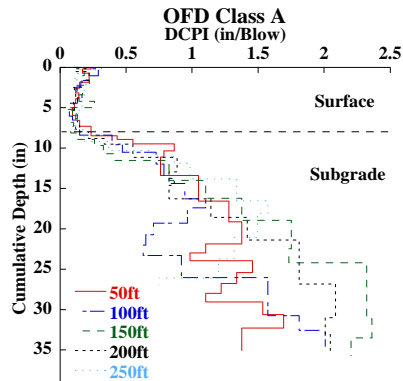
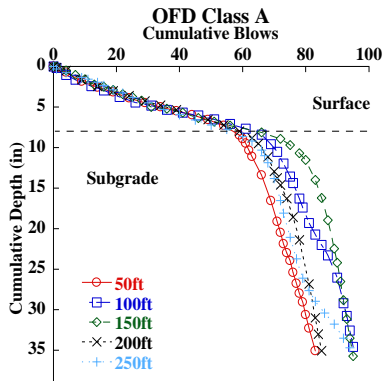
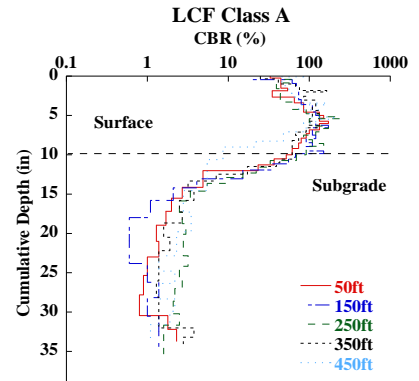
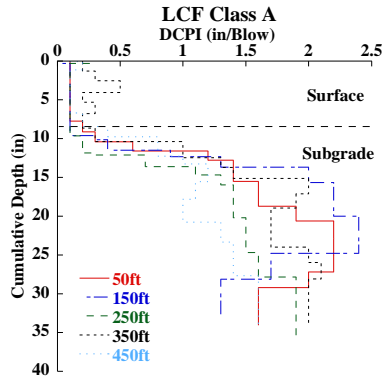
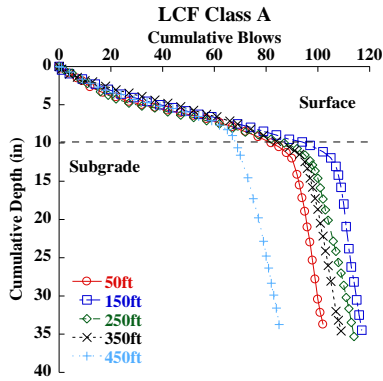


Figure C.4. DCP results for changes in the blows, DCPI, and DCP-CBR with cumulative depth for June 2017



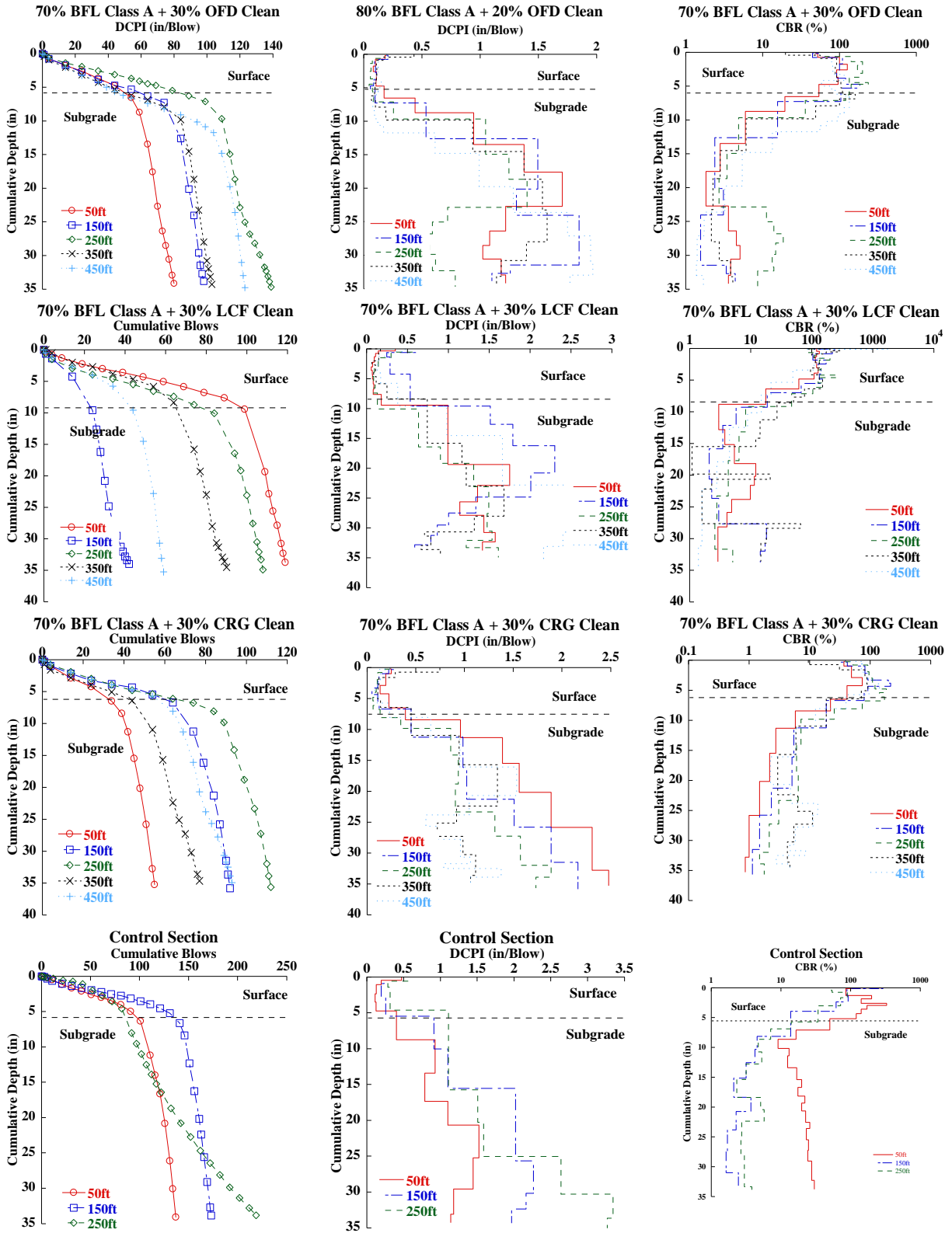
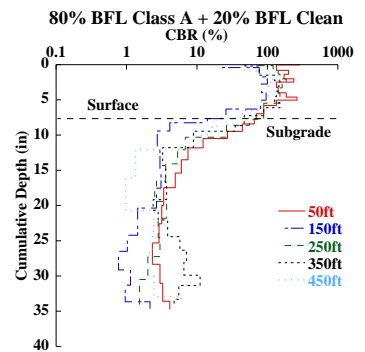
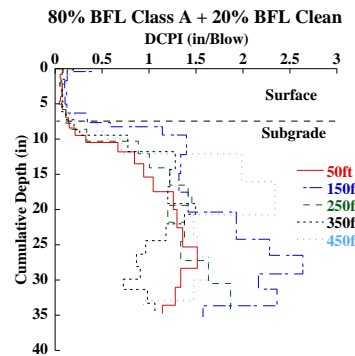
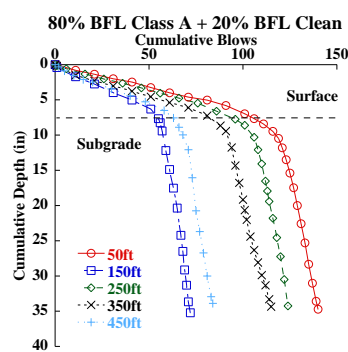
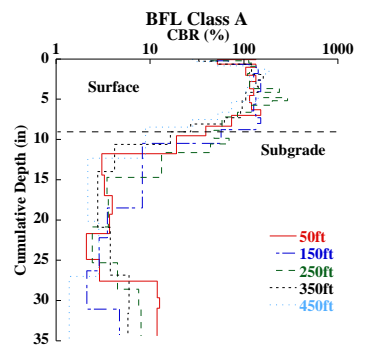
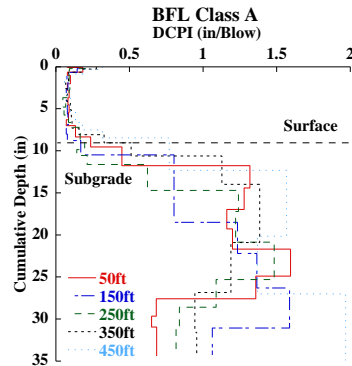
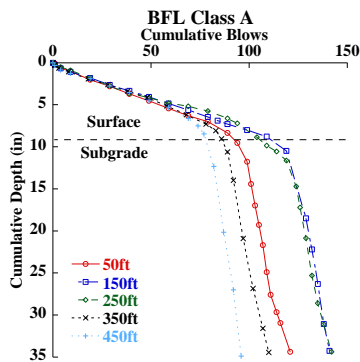
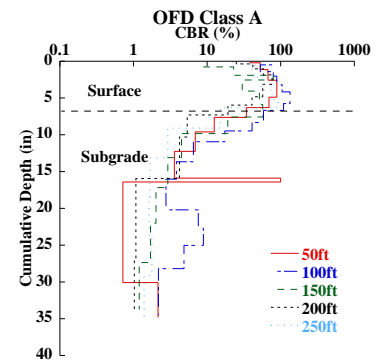
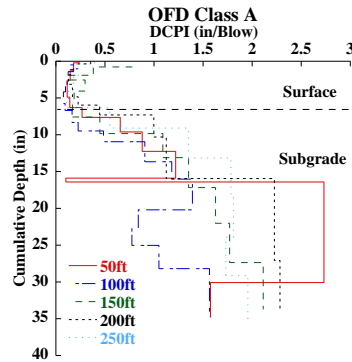
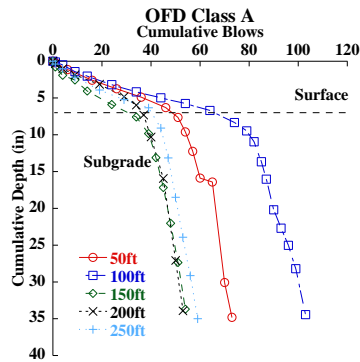
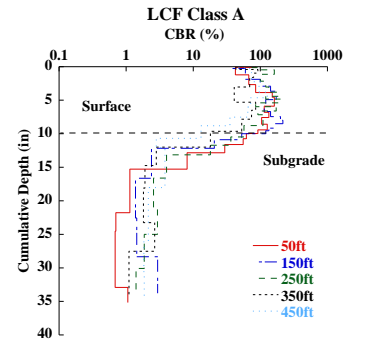
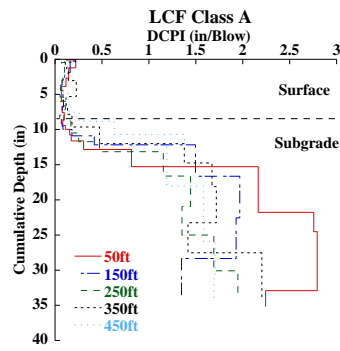
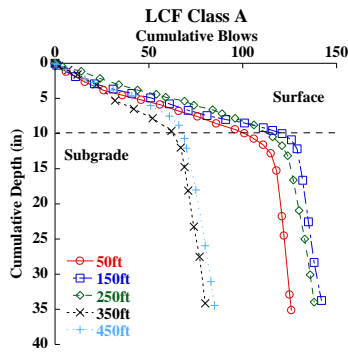


Figure C.5. DCP results for changes in the blows, DCPI, and DCP-CBR with cumulative depth for May 2018



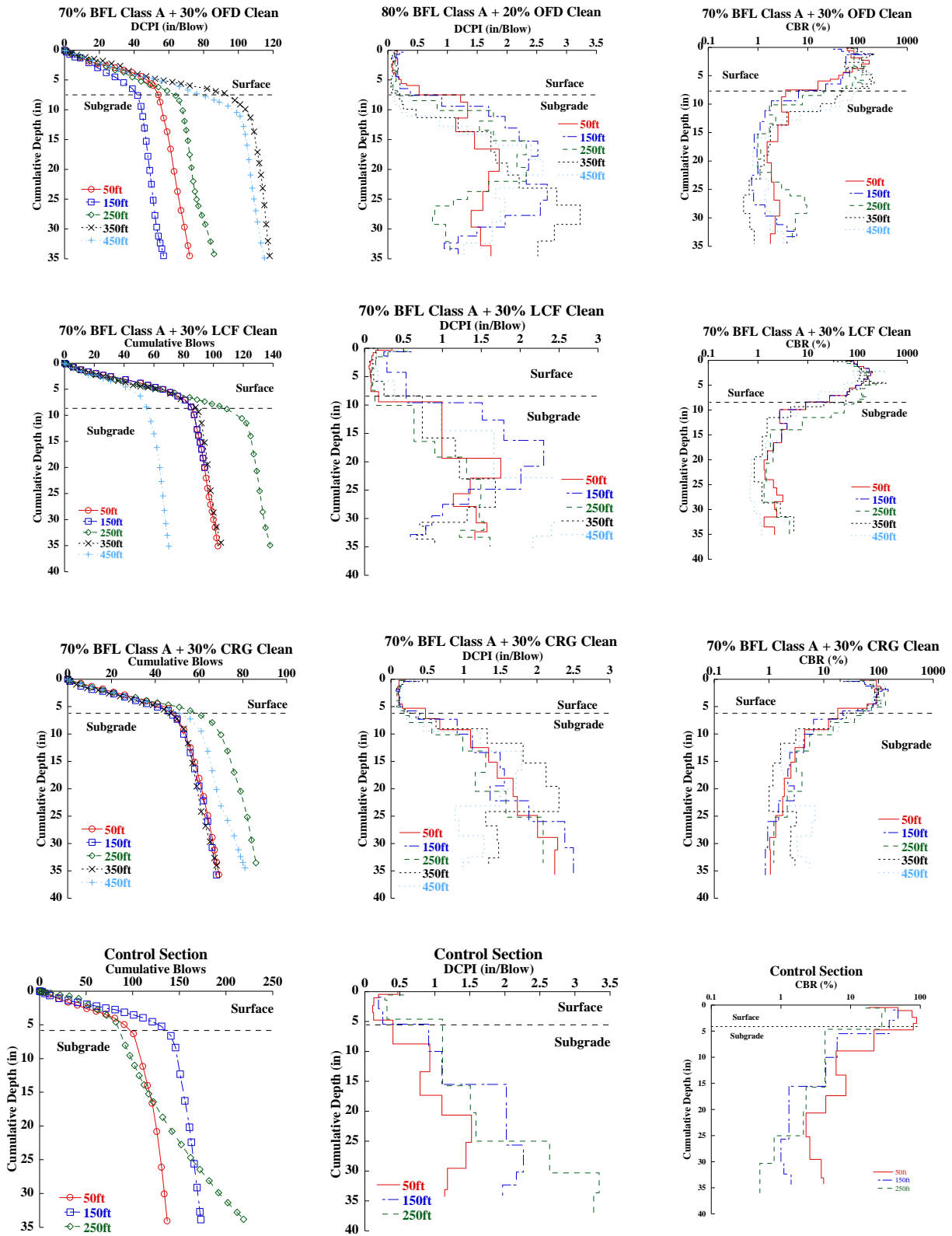


Figure C.6. DCP results for changes in the blows, DCPI, and DCP-CBR with cumulative depth for April 2019

APPENDIX D. AUTOMATED PLATE LOAD TEST (APLT) RESULTS

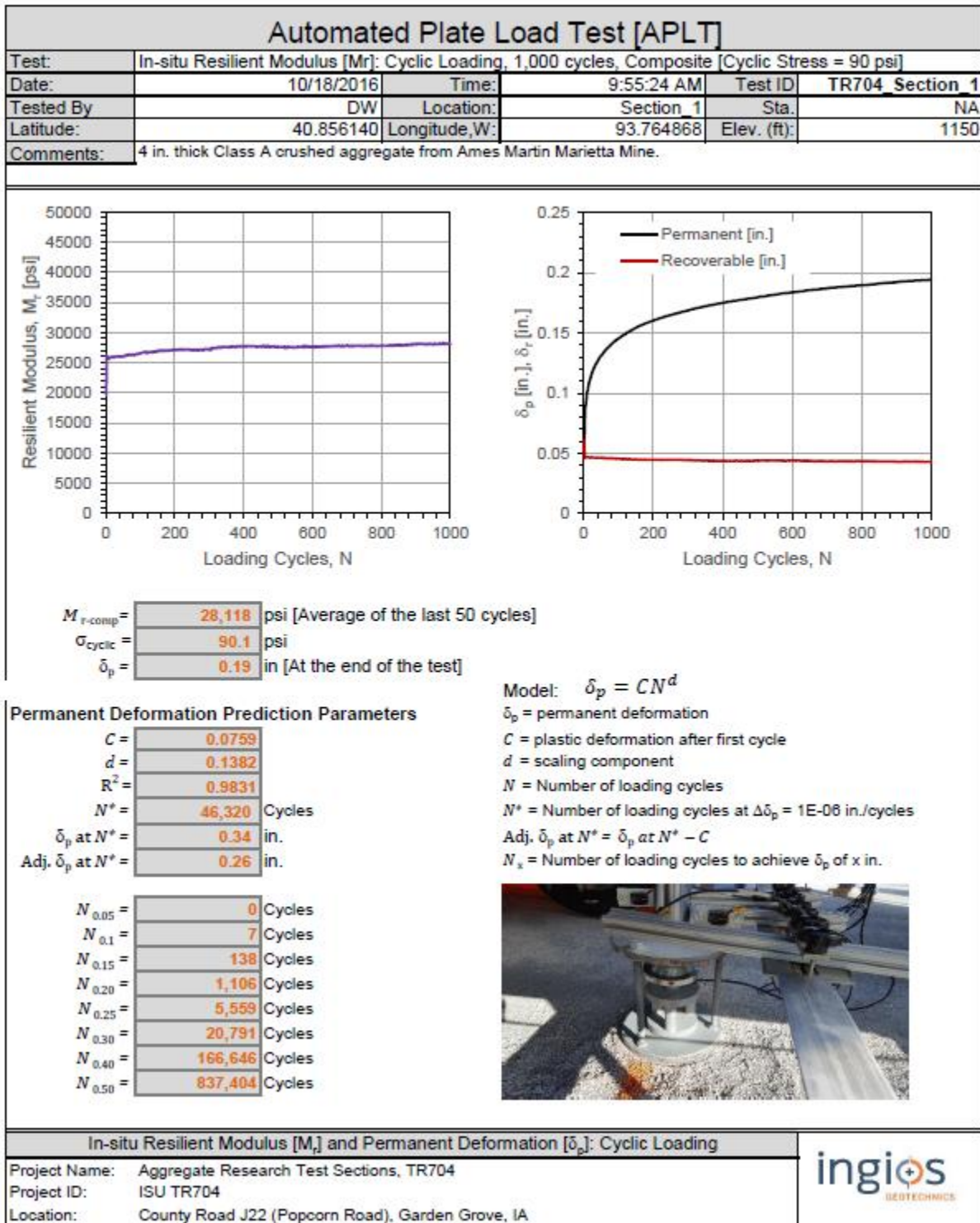


Figure D.1. APLT test results for the first section

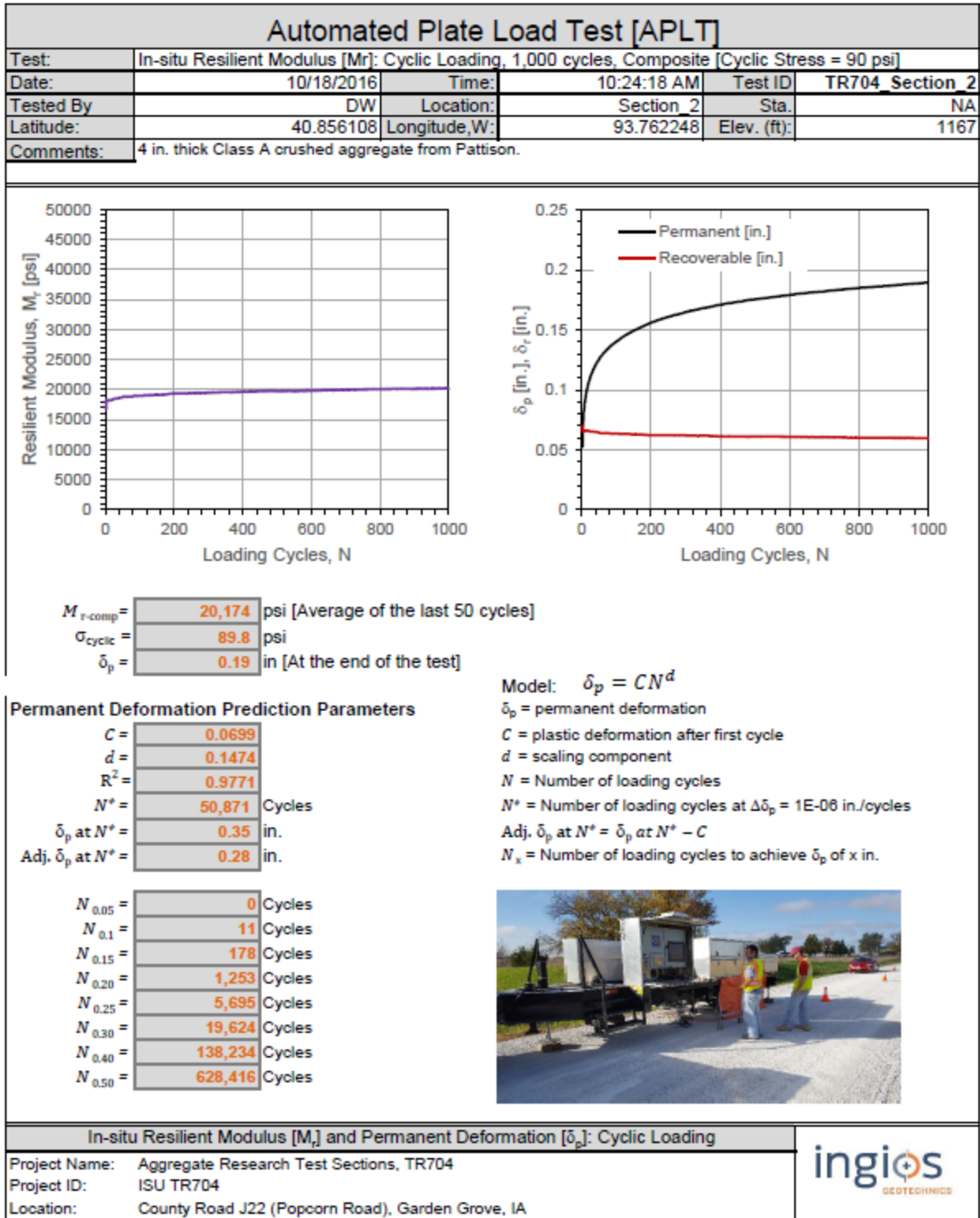


Figure D.2. APLT test results for the second section

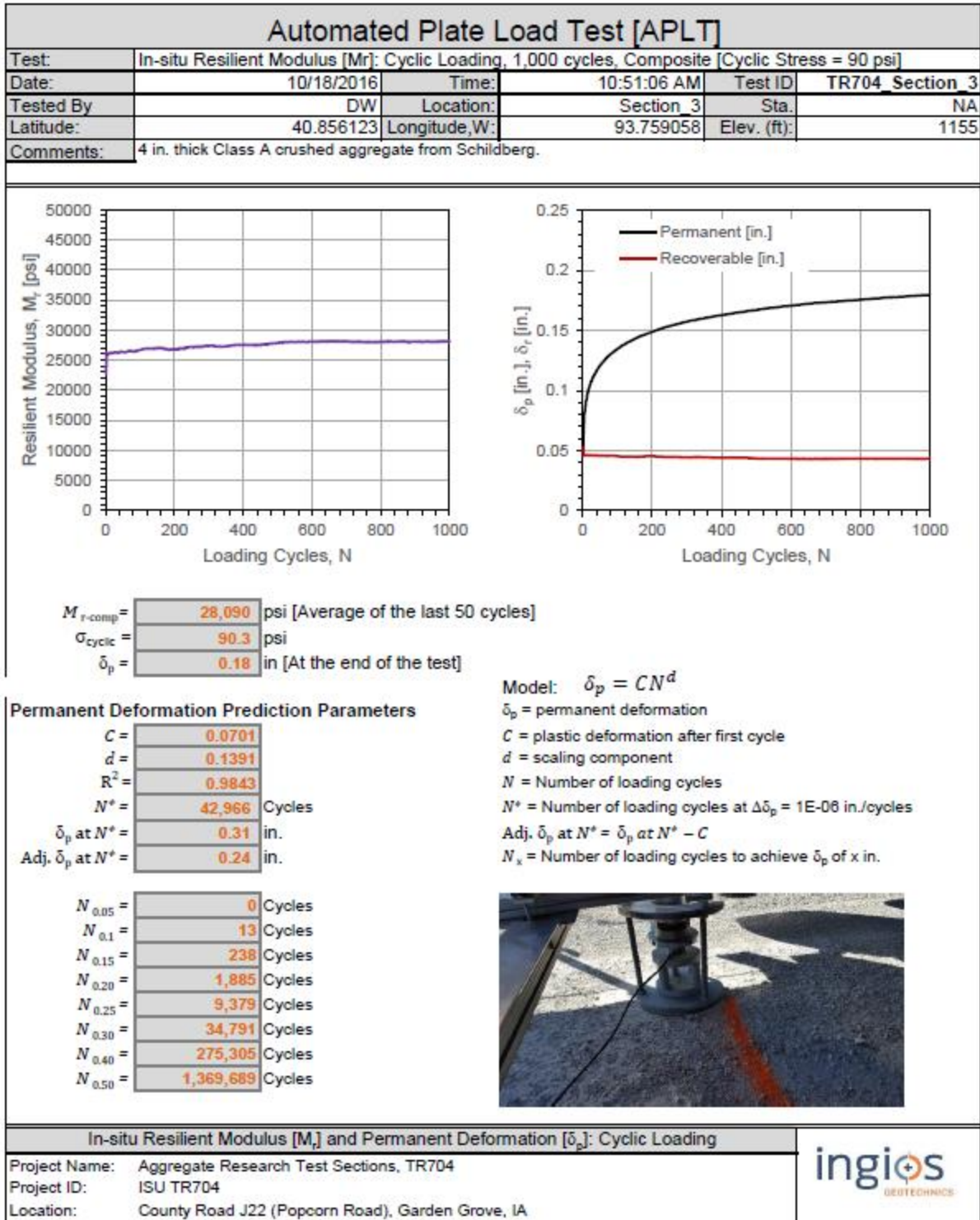


Figure D.3. APLT test results for the third section

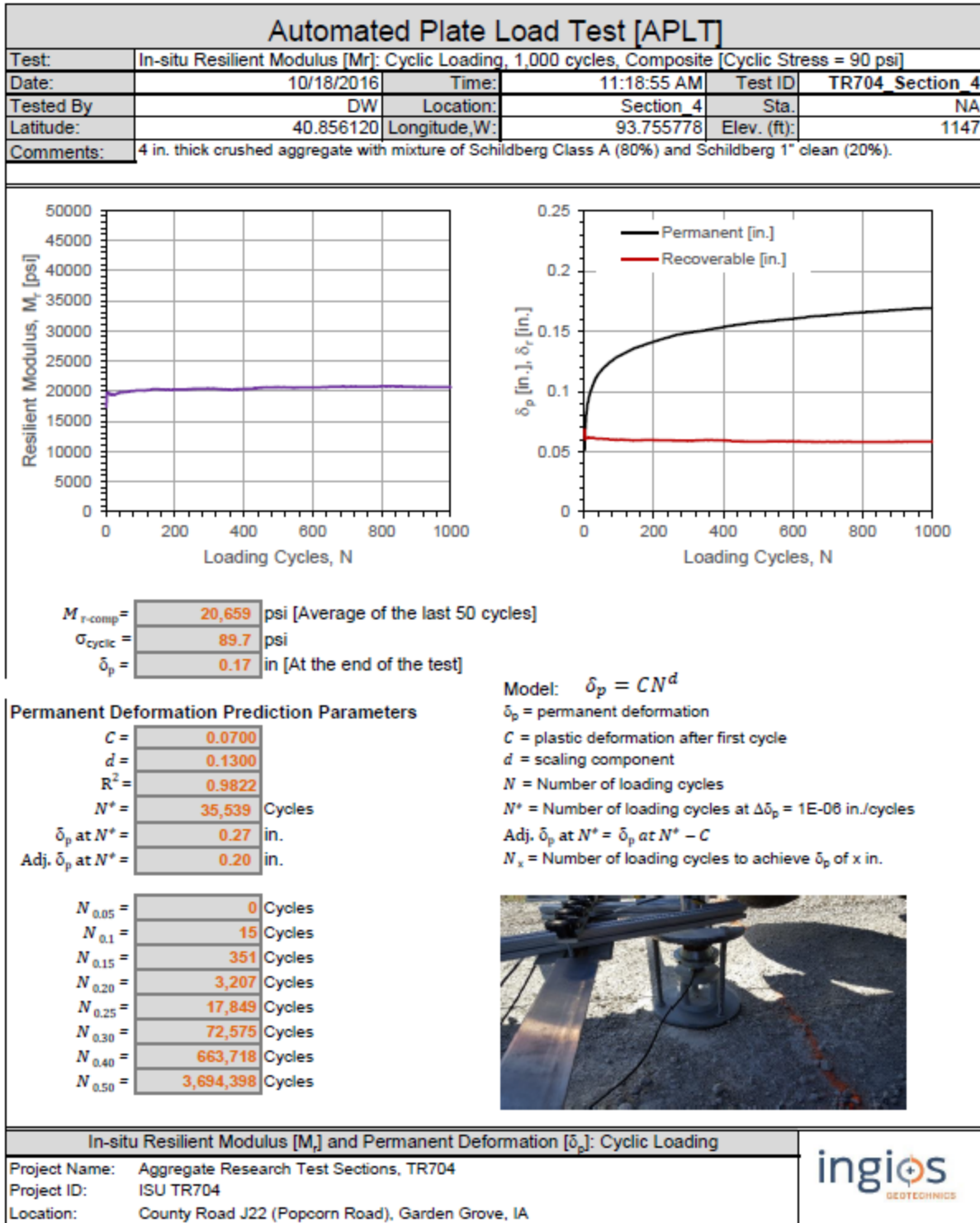


Figure D.4. APLT test results for the fourth section

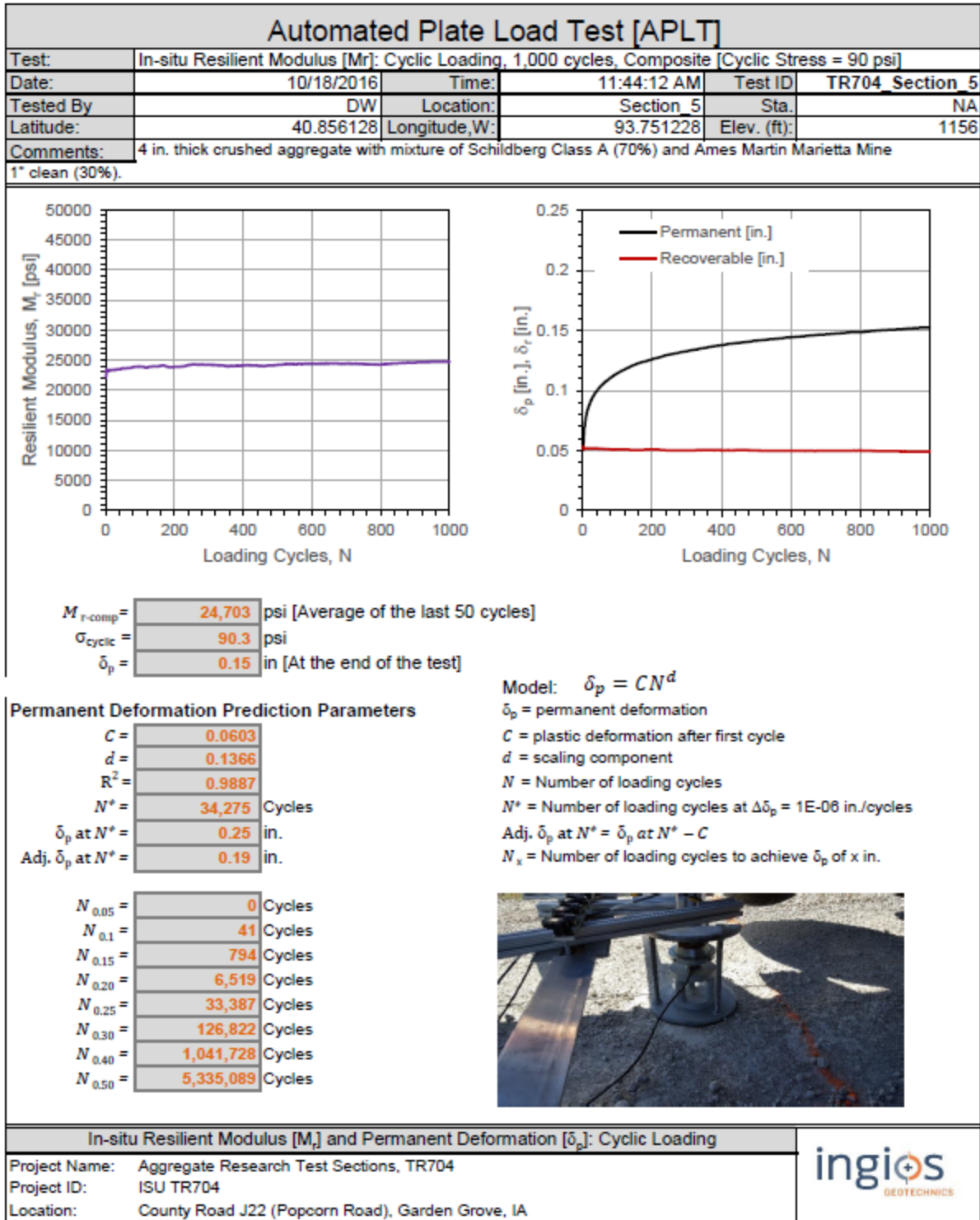


Figure D.5. APLT test results for the fifth section

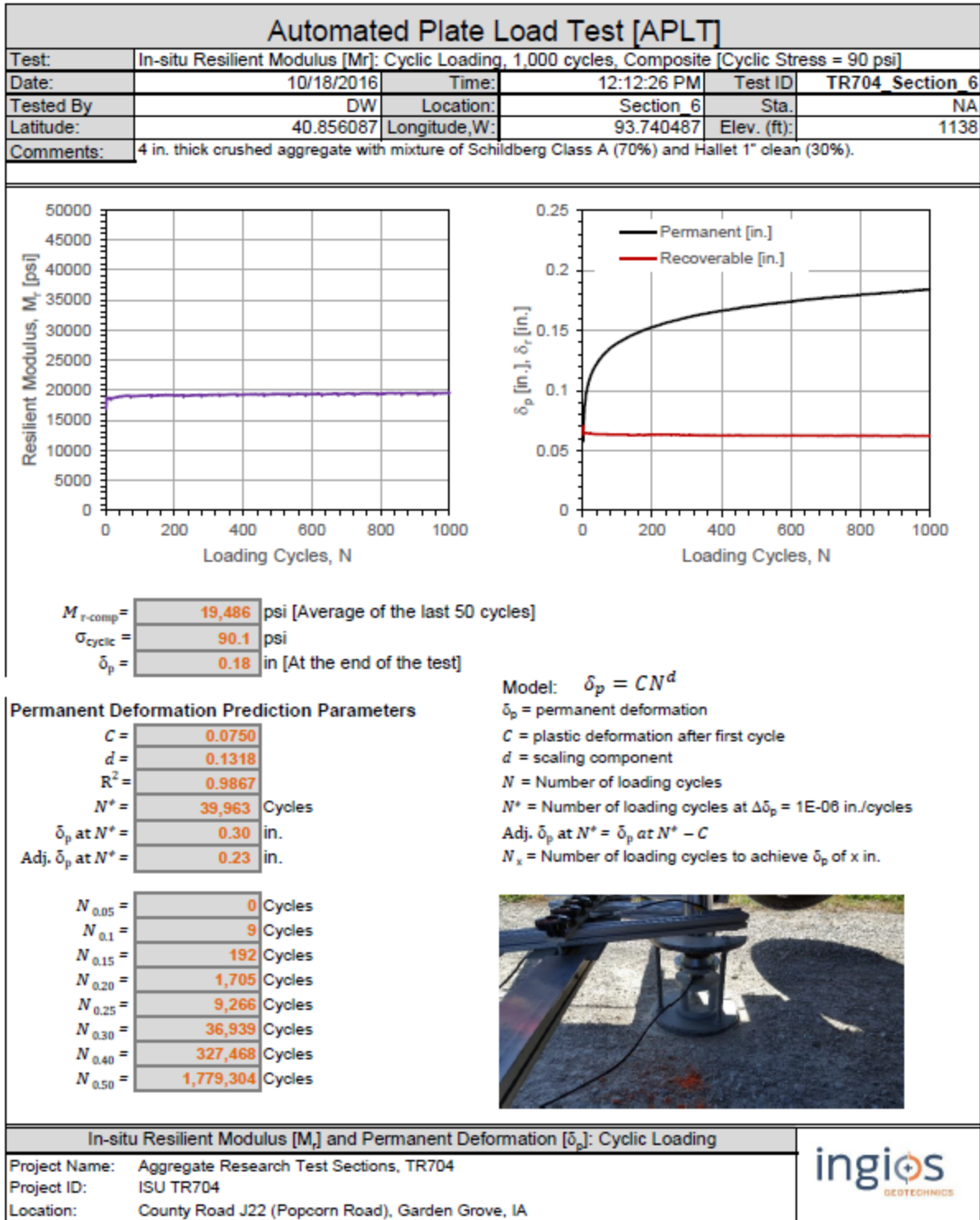


Figure D.6. APLT test results for the sixth section

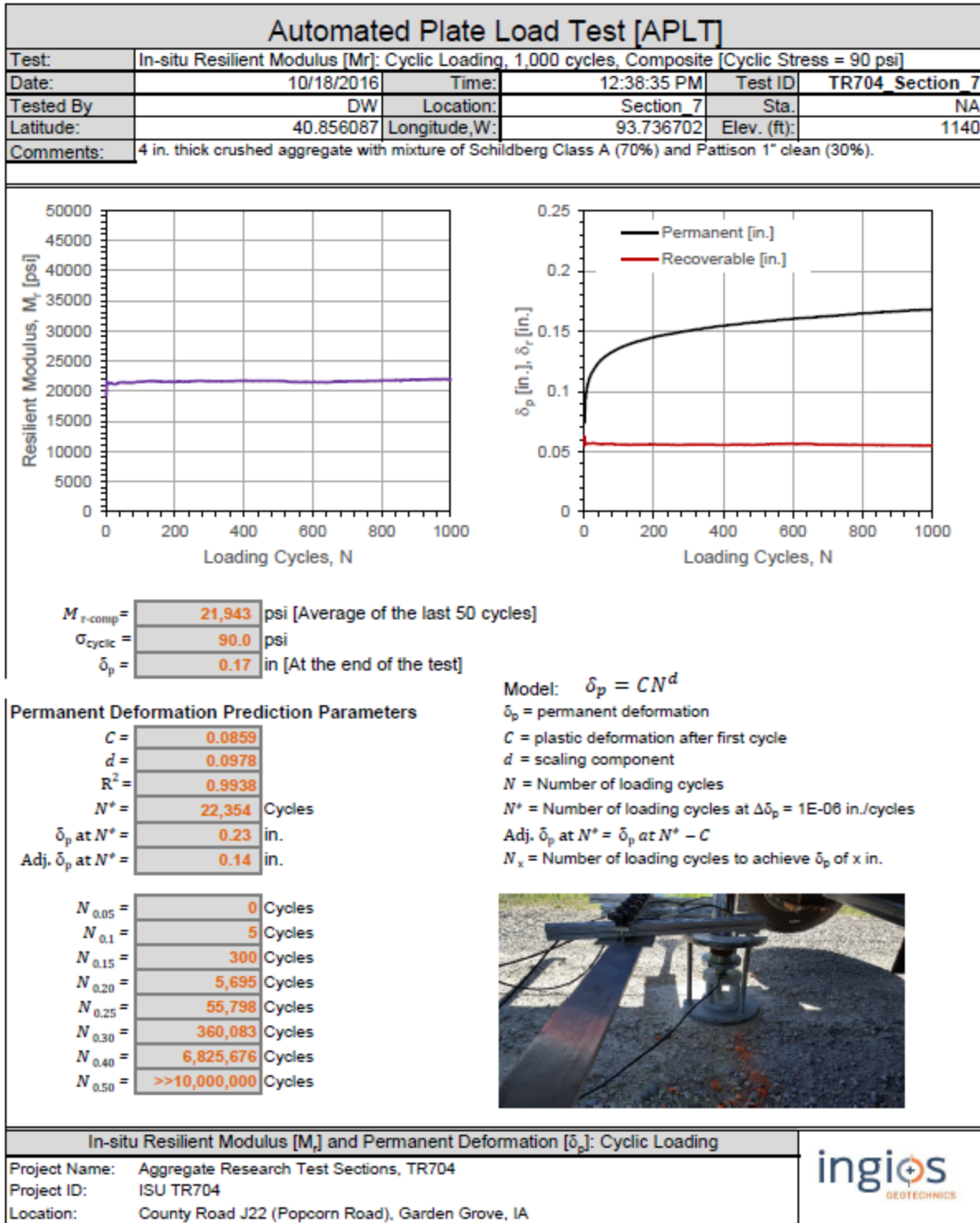


Figure D.7. APLT test results for the seventh section

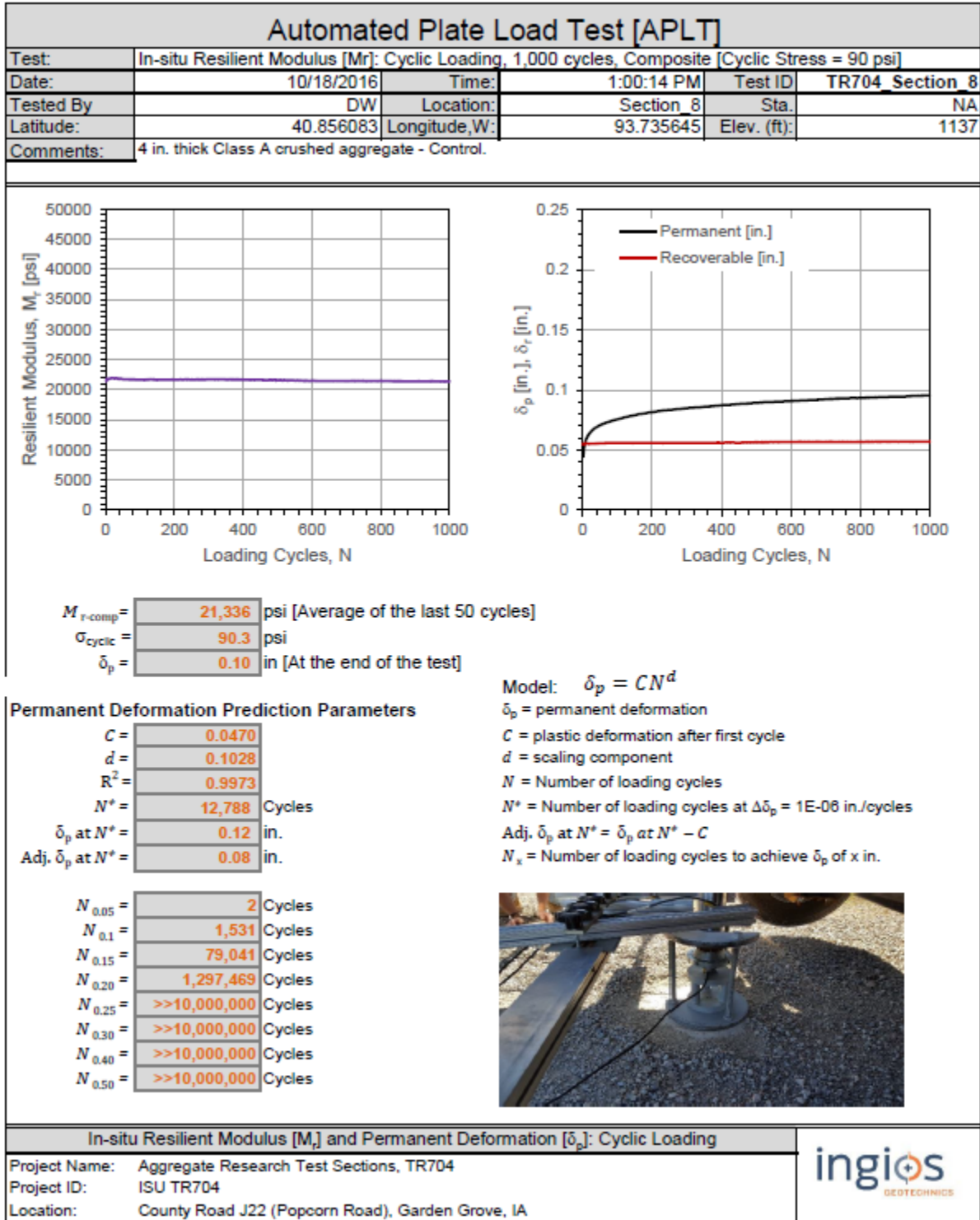


Figure D.8. APLT test results for the control section

APPENDIX E. THERMOCOUPLE INSTALLATION



Figure E.1. Borehole digging with auger at center and shoulder of the road



Figure E.2. Painting the thermocouple path



Figure E.3. Digging the thermocouple path with auger



Figure E.4. Digging the surface for the thermocouple installation



Figure E.5. Thermocouples at PVC tubes



Figure E.6. Connecting the thermocouples to the data logger



Figure E.7. Locking the data loggers

APPENDIX F. BENEFIT-COST ANALYSIS SPREADSHEET

Summary		
BCR	398.80	Calculation
User cost saving	\$4,033.52	Calculation
Maintenace cost saving	\$16,280.07	Calculation
Car damage saving	\$0.00	Calculation
Road Info		
Service life	20	
Initial cost	84894	
Discount rate	5%	
AADT	80	IDOT AADT Map
Truck traffic percentage	25%	Subject Matter Expert
Calculations		
Costs		
Increase in initial cost	0%	
Benefits		
User cost saving		
Actual driving time (min)	3	
Detour time (min)	9	
Road closure (hour)	8	
User cost value, cars	25	Bureau of Labor Statistics (BLS)
User cost value, truck	54	Bureau of Labor Statistics (BLS)
Annual user cost saving	2064	Calculation
Maintenance cost saving		
New maintenace frequency	3	
Conventional maintenace frequency	2	
Conventional maintenace cost	18258	
New maintenace cost	25323	
Conventional NPV	\$105,707.33	Calculation
New NPV	\$89,427.26	Calculation
Car damage saving		
Current car damage per mile	\$0.40	
Current truck damage per mile	\$0.50	
New car damage rate per mile	\$0.40	
New truck damage rate per mile	\$0.50	
Annual saving	\$0.00	Calculation

Figure F.1. BCR calculator Excel sheet

**THE INSTITUTE FOR TRANSPORTATION IS THE FOCAL POINT FOR TRANSPORTATION
AT IOWA STATE UNIVERSITY.**

InTrans centers and programs perform transportation research and provide technology transfer services for government agencies and private companies;

InTrans contributes to Iowa State University and the College of Engineering's educational programs for transportation students and provides K–12 outreach; and

InTrans conducts local, regional, and national transportation services and continuing education programs.



**IOWA STATE
UNIVERSITY**

Visit InTrans.iastate.edu for color pdfs of this and other research reports.